UNIVERSITA' DELLA CALABRIA

UNIVERSITA'DELLA CALABRIA

Department of Environmental and Chemical Engineering - DIATIC

Scienze e Ingegneria dell'Ambiente, delle Costruzioni e dell'Energia - SIACE

CICLO

XXIX

INNOVATIVE UV-LED POLYMERISED BICONTINUOUS MICROEMULSION COATING FOR MEMBRANES WITH SPECIAL EMPHASIS ON MBRs

PhD Thesis

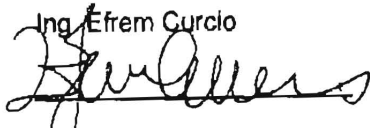Settore Scientifico Disciplinare CHIM/07 – Fondamenti chimici delle tecnologie
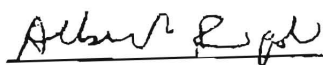
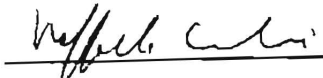**Coordinatore:**

Ch.mo Prof. Pietro Pantano

Supervisori:

Ing. Efrem Curcio

Prof. Bartolo Gabriele

Dott. Alberto Figoli

Prof. Jan Hoinkis

Prof. Raffaele Molinari
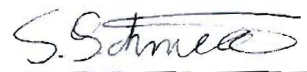
Candidato:

Stefan-André Schmidt

Summary

The main objective of this work is the preparation of polymerisable bicontinuous microemulsion (PBM) coatings applied onto commercial membranes for improving the anti-fouling properties and performance, in terms of water flux and foulants rejection.

Microstructured and nanostructured materials obtained by PBM have been widely investigated in the course of the last 30 years. The interest in microemulsion lies mainly in the possibility of dissolving larger amounts of oil and water by using polymerisable and non-polymerisable surfactants. By polymerising the bicontinuous microemulsion it is possible to produce transparent porous polymeric solids [Gan et al. (1995), Gan and Chew (1997)].

This thesis represents the follow-up of the work done by Galiano et al. (2015) and Deowan et al. (2016). Galiano et al. (2015) developed the PBM composition that based on a non-polymerisable surfactant (DTAB) and another polymerisable surfactant (AUTEAB). In their work the PBM was polymerised by redox initiators leading to a process that is very difficult to up-scale for a commercial application. Critical issues were, the polymerisation time (at least 20 minutes), and the reproducibility of the coating.

Therefore, it is the aim of this work to develop another polymerisation technique that increases the polymerisation speed and allows the easy reproduction of membranes with defined properties. The polymerisation by photoinitiators excited by UV-light represents a promising possibility for this requirement as it has the potential of decreasing the polymerisation time down to a few seconds.

Several photoinitiators were selected for their compatibility with the PBM, and studied for their conversion rate efficiency (section 5.1.5). As there is a wide range of potential UV-light sources available, several technologies are studied for their coating performance (section 5.1.3). Subsequent to that, experiments were done in order to define the ideal photoinitiator type and concentration while polymerising onto glass plates. The coating onto commercial membranes is studied deeply for e.g. different casting knife thickness or ambient temperature (section 5.2.2).

As the polymerisation under inert conditions is expected to increase the polymerisation speed, experiments are done, both under inert and non-inert conditions. The final membrane, coated under the optimum conditions, is further characterised for their permeability under different conditions like transmembrane pressure (TMP), model foulant experiments and a fixed volume flow (section 5.2.3). Further characterisation is done by contact angle, SEM, AFM (section 5.2.5 to 5.2.7).

The prepared PBM membranes are foreseen to be finally applied for model textile dye wastewater treatment by Membrane BioReactor (MBR) technology. According to the previous results of Deowan et al. (2016) higher permeate quality through increased COD, TOC, dyestuffs removal efficiency and stronger anti-fouling properties are expected. Consequently, lower operation/maintenance costs due to reduced necessary aeration for scouring purposes and reduced membrane cleaning cycles as well as less membrane replacement are of special interest for commercial applications.

In the previous work of Deowan et al. (2016) a lab scaled MBR with a single membrane housing was used. As of the biocenosis of the bacteria inside the reactor tank, a comparison of the membrane performance of the PBM and commercial membrane is difficult to achieve. Therefore an existing MBR system was redesigned to allow the simultaneous run of a commercial and a PBM coated membrane (section 4.1). As the revamp requires also additional sensors, the data acquisition needs to be adapted as well. To assure the proper function of the MBR the system was running for long term with two commercial membranes using a model textile wastewater (see 5.3.2). Finally the PBM coated membrane was compared with a commercial one for their performance in the MBR. Initial experiments for the water permeability are done as preparation for future work (see 5.3.3).

Riassunto

L'obbiettivo principale di questa tesi è consistito nella preparazione di rivestimenti (coatings) basati su microemulsioni bicontinue polimerizzabili (PBM) applicati su membrane commerciali, al fine di migliorarne le proprietà anti-sporcamento (anti-fouling) e le prestazioni in termini di flusso all'acqua e di rimozione di composti inquinanti.

I materiali microstrutturati e nanostrutturati ottenuti dalle PBM sono stati ampiamente investigati nel corso degli ultimi 30 anni. L'interesse nelle microemulsioni risiede principalmente nella possibilità di miscelare tra di loro grandi quantità di olio e di acqua utilizzando tensioattivi polimerizzabili o non-polimerizzabili. Attraverso la polimerizzazione delle microemulsioni bicontinue è possibile produrre materiali solidi polimerici, trasparenti e porosi [Gan et al. (1995), Gan and Chew (1997)].

La presente tesi rappresenta il proseguo del lavoro svolto da Galiano et al. (2015) e Deowan et al. (2016). Galiano et al. (2015) svilupparono la formulazione delle PBM utilizzando tensioattivi non-polimerizzabili (DTAB) e polimerizzabili (AUTAB). In questi lavori le PBM sono state polimerizzate attraverso l'uso di iniziatori redox secondo un processo che è molto difficile da poter effettuare su larga scala per applicazioni commerciali. I punti critici di un possibile up-grade della tecnologia risiedono nel lungo tempo di polimerizzazione (circa 20 minuti) e nella riproducibilità del coating.

Per questo motivo, lo scopo del presente lavoro è stato quello di sviluppare una nuova tecnica di polimerizzazione che aumenti la velocità di polimerizzazione e che permetta facilmente la riproducibilità delle membrane con specifiche proprietà. La polimerizzazione mediante foto-iniziatori effettuata mediante luce UV rappresenta un'alternativa promettente al fine di superare le suddette limitazioni permettendo di diminuire il tempo di polimerizzazione a soli pochi secondi.

Diversi foto-iniziatori sono stati selezionati per la polimerizzazione delle PBM e studiati sulla base del loro grado di polimerizzazione (sezione 5.1.5). Essendo disponibili un'ampia gamma di potenziali sorgenti UV, diverse tecnologie sono state studiate in base alle loro prestazioni (sezione 5.1.3). In seguito, numerosi esperimenti sono stati condotti al fine di identificare il tipo di foto-iniziatore e la sua concentrazione ideale

attraverso polimerizzazione su lastre di vetro. Il coating sulle membrane commerciali è stato studiato in termini di spessore di stesura e temperatura ambiente (sezione 5.2.2).

Poiché la polimerizzazione in condizioni inerti aumenta la velocità di polimerizzazione, gli esperimenti sono stati condotti in condizioni sia inerti che non-inerti. La membrana finale, preparata secondo le condizioni ottimali trovate, è stata in seguito caratterizzata in termini di permeabilità all'acqua a diverse pressioni transmembrana (TMP) e test di sporcamento (sezione 5.2.3). Ulteriori caratterizzazioni sono consistite in misure di angolo di contatto, di microscopia a scansione elettronica (SEM) e di microscopio a forza atomica (AFM) (sezione 5.2.5 e 5.2.7).

Le membrane PBM sono state preparate nell'ottica di essere infine applicate per il trattamento di acque reflue modello tessili utilizzando la tecnologia dei bioreattori a membrana (MBR). Secondo i precedenti risultati ottenuti da Deowan et al. (2016) ci si aspetta un'alta qualità di permeato attraverso l'aumento dei parametri COD, TOC; un'aumentata efficienza nella rimozione dei coloranti e maggiori proprietà anti-sporcamento. Conseguentemente, ciò permetterebbe di abbassare i costi di manutenzione di un MBR grazie alla riduzione dell'aerazione necessaria alla pulizia delle membrane ed alla riduzione dei cicli di pulizia o di sostituzione delle membrane stesse.

Nel precedente lavoro di Deowan et al. (2016) è stato utilizzato un MBR a livello laboratoriale con un unico alloggiamento per le membrane. In seguito al fenomeno di biocenosi all'interno del bio-reattore contenenti i batteri, è difficile, però, ottenere una comparazione diretta tra le prestazioni delle membrane PBM e di quelle commerciali. Per questo motivo, è stato riprogettato un nuovo sistema MBR che consenta il simultaneo test delle membrane PBM e di quelle commerciali (sezione 4.1). Poiché la modifica richiede l'uso di ulteriori sensori, il sistema di acquisizione dei dati è stato anch'esso adattato. Al fine di assicurare il corretto funzionamento del MBR, il sistema è stato tenuto in funzione per un lungo periodo di tempo con due membrane commerciali usando acque reflue modello tessili (vedi 5.3.2). Infine, le prestazioni a livello di MBR delle membrane PBM sono state raffrontate con quelle delle membrane commerciali. Test preliminari di permeabilità all'acqua sono stati condotti come base per un futuro lavoro (vedi 5.3.3).

Contents

List of Figures

List of Tables

Nomenclature

Greek symbols

ν	cm^{-1}	Frequency of light

Special symbols

(1.1)	Equation number, first number is number of chapter

Non-Dimensional numbers

pH	From latin potentia (force) and hydrogenium (hydrogen)

Abbreviations

A	Atomic weight
APS	Ammonium persulfate
ASP	Activated sludge process
AUDMAA	Acryloyloxy-undecyldimethyl -ammonio acetate
AUTMAB	Acryloyloxyundecyltrimethyl ammonium bromide
AUTEAB	Acryloyloxyundecyltriethyl ammonium bromide
BOD	Biochemical oxygen demand
CAD	Computer-aided design
Cl	Chlorine
COD	Chemical oxygen demand
CT	Capillary tube
CTA	Chain transfer agent
DA	Dalton

DI	Deionized
DO	Dissolved oxygen
DR	Drying residue
DMPA	2,2-Dimethoxy-2-phenylacetophenone
DTAB	Dodecyltrimethylammonium bromide
DTBP	Diphenyl(2,4,6-trimethylbenzoyl) phosphine oxide
DTPO	2, 4, 6-Trimethyl benzoyl diphenyl phosphine oxide
DPP	1,3-Diphenyl-2-propanone
EGDMA	Ethylene glycol dimethacrylate
EPS	Extracellular polymetric substances
FC	Filter cartridge
F/M	Food to microorganism ratio
FS	Flat sheet
H	Hydrogen
h	Planck' constant
HA	Humic Acid
HEMA	2-Hydroxylethyl methacrylate
HF	Hollow fibre
HRT	Hydraulic residence time
iMBR	Immersed membrane bioreactor
IPPT	2-Isopropylthioxanthone
Irg. 184	1-Hydroxy-cyclohexyl-phenyl-ketone
Irg. 819DW	Phenyl-Bis(2,4,6-Trimethylbenzoyl)-Phosphinoxid
ITM	Instituto per la Tecnologia delle Membrane (Institute on membrane technology)
IUPAC	International union of pure and applied chemistry
LabVIEW	Laboratory virtual instrument engineering workbench
MBR	Membrane bioreactor
M	Molar mass
Mc	Critical molecular weight
MC	Methylcellulose
MENA	Middle east and north african
MMA	Methyl metacrylate
MLSS	Mixed liquor suspended solids
MT	Multi tubular
MTDW	Model textile dye water
N	Nitrogen
NDIR	Non-dispersive infrared

NF	Nanofiltration
nm	Nanometer
OLR	Organic loading rate
OUR	Oxygen uptake rate
PA	Poly amide
PBM	Polymerisable bicontinuous microemulsion
PE	Polyethylence
PEG	Poly ethylene glycol
PES	Polyethersulfon
PE	Polypropylene
PEO-R-MA-40	ω-methoxy poly (ethylene oxide)40 undecyl-α-methacrylate
PNIPAAm	Poly(N-isopropyl acrylamide)
PVA	Polyvinyl alcohol
PVP	Polyvinylpyrrolidone
PVC	Polyvinyl chloride
PVDF	Polyvinylidenedifluoride
RO	Reverse Osmosis
SDS	Sodium dodecyl sulfate
sMBR	Sidestream membrane bioreactor
SRT	Sludge retention time
SW	Spiral wound
TC	Total carbon
TMEDA	N,N,N'N'-tetramethylethylene
TN	Total nitrogen
TOC	Total organic carbon
TIC	Total inorganic carbon
TMP	Transmembrane pressure
UF	Ultrafiltration
UV	Ultraviolet
VF	Volume flow
WP	Water permeability
VAC	Voltage alternating current

Chemical formulas

NH_4-N	Ammonia nitrogen
NO_3-N	Nitrate as nitrogen

1 Introduction

1.1 Thesis outline

This thesis is structured in six sections, each of them consisting of several subsections.

Section 1 consists of a general introduction to thesis related matters. As this work represents a follow-up work of the pioneering work of Deowan et al. (2016) and Galiano et al. (2015) a subsection is dedicated to a summary of their work in order to capacitate the reader to understand the history of this work. In addition the objectives of this work are described.

Section 2 is giving an overview of the fundamentals in the field of membrane technology, focused on the relevant topics for MBR technology. Different design configurations, materials, fouling characteristics and surface modification techniques are described.

Section 3 summarises the state of the art of MBR´s in the field of textile wastewater treatment as well as for polymerisation by ultraviolet light induced photopolymerisation.

Section 4 describes all relevant techniques, protocols, materials, theoretical calculations and equipment that was used within this thesis. As it is also part of this thesis to investigate a novel design for the lab-scaled MBR that allows the parallel testing of two membranes under the same conditions and time, all related informations are summarized in this section as well.

Section 5 is giving the results for all experiments that were investigated within this work. It consists of four main subsections giving a) the results for photopolymerisation trials under non-inert conditions, b) inert conditions, c) membrane characterisation results and finally d) results for the lab-scaled MBR.

Section 6 gives a conclusion of this work, highlighting the most important outcomes. An outlook is done to summarise further potential options that might lead to faster polymerisation as well as possible improvement of the novel PBM coated membranes.

All references referred to within this thesis are listed in the **bibliography**.

Detailed documentation about experiments and equipment is given in the **affix**.

1.2 General introduction

Water is a vital necessity of life. Lack of clean drinking water and rising water pollution has become critical issues in the 21st century. Therefore, wastewater treatment plays a more and more important role in municipal as well as industrial areas. According to United Nation's report, water scarcity already affects every continent [UN-Water (2006)]. Around 1.2 billion people, in another word almost one-fifth of the world's population, live in areas of water scarcity, and 500 million people are approaching this situation. Another 1.6 billion people, or almost one quarter of the world's population, face economic water shortage (where countries lack the necessary infrastructure to take water from rivers and aquifers) [UN-Water (2006)]. In contrary the water usage has been growing more than twice the rate of population increase in the last century [UN-Water (2006)].

Wastewater treatment has become a significant issue for environmentally friendly processes in the industrial sector. Sustainable development in industry can be effective by highly appreciating water-reuse systems. Increasingly stringent environmental legislation and generally enhanced intensity, efficiency, and diversity of treatment technologies have made the reuse of water more viable in many industrial processes. Partially the textile and laundry industries can be considered as water intensive factories because every day they release a high amount of wastewater [Hoinkis and Panten (2008), Vu et al. (2015)]. As the textile industry is widely spread especially in the Middle East and North African (MENA) countries as well as in Asian countries like China, India etc. the demand for efficient and sustainable wastewater treatment and reuse is very high [Bionexgen (2016)]. In the manufacture of most textile goods, to properly prepare, purify, color, and finish the products, chemical wet processing

operations are necessary [Venceslau et al. (1994)]. Therefore, in each step of processing, the textile industry has a high demand of water and complex chemicals and thus is also a field of producing a high quantity of wastewater, which contains various complex contaminants [Yusuff and Sonibare (2004)].

Different types of dyes, with a very low biodegradability as of high molecular weights and complex structures, typically affect the textile effluent quality [Kim et al. (2004), Gao et al. (2007)]. The direct discharge into sewage networks can influence the biological treatment processes. As high concentrations of inorganic salts, acids and bases in biological reactors are produced by the effluent, increasing costs for the treatment result [Babu et al. (2007), Gholami et al. (2001)]. As of their complex structure and synthetic origin many dyes are difficult to de-colourise. Anionic, non-ionic and cationic dyes are the typical species. The anionic dyes are the acid and reactive dyes that tend to pass through conventional treatment systems unaffected [Mishra and Tripathy (1993), Willmott et al. (1998)]. Municipal biological aerobic systems, were found to be inefficient in their removal [Moran et al. (1997)].

For 12 to 20 tons of textiles produced per day estimated 1.000 to 3.000 m^3 wastewater are produced [Pagga and Brown (1986), Al-kdasi et al. (2004)]. This discharged wastewater contains all the unused materials which tend to have high biochemical oxygen demand (BOD), chemical oxygen demand (COD), pH, temperature, colour, turbidity and toxic chemicals. The wastewater that is discharged can have an extremely detrimental effect on the environment due to its strong colour, high COD, and very low BOD to COD ratio [Kritikos et al. (2007)]. Water bodies like lakes or rivers can be polluted and flora, fauna can be affected by the directly discharged textile. Membrane technology has been recently applied in wastewater treatment together with conventional treatment [Martin (2015)]. Membrane technology can be regarded as a promising technology for wastewater treatment and reuse in the textile and laundry industries [Hoinkis and Panten (2008)]. Membrane BioReactor (MBR) technology is a combination of the conventional biological sludge process, a wastewater treatment process characterized by the suspended growth of biomass, and a micro- or ultrafiltration membrane system [Judd and Judd (2007)]. The advantages of MBRs are its ability to biodegrade the waste compounds and separate the treated water from the mixed liquor due to the small pore diameter of the membrane. The bacteria and suspended solids can be kept out of the effluent with the membrane having a pore diameter from 0.01 to 0.1 µm. The use of MBRs for wastewater recla-

mation and reuse are effective tools for industrial development programs. The reuse of water has become much more viable in a number of industrial processes. This is due to a variety of factors which include the enhanced efficiency, intensity and diversity of treatment technologies, as well as stricter environmental legislation policies. The rejected constituents in the retentate tend to accumulate at the membrane surface, producing various phenomena (e.g. fouling) which lead to a reduction in the flow of water through the membrane (i.e. the flux) at a given transmembrane pressure (TMP), or conversely an increase in the TMP for a given flux (reducing the permeability, which is the ratio of flux to TMP) [Judd and Judd (2007)]. In the application of MBR technology, fouling effect of membranes is a main obstacle to overcome. Once the membrane is being fouled and extensive chemical cleaning can't regain the flux, the membrane needs to be replaced which results in increasing operation costs.

1.3 Previous work

This work represents the follow-up of an EU funded project "Development of the next generation membrane bioreactor system" [Bionexgen (2016)]. Within this project a novel PBM (Polymerisable Bicontinuous Microemulsion) based coating with anti-fouling properties for the application in wastewater treatment has been developed. In the past, the polymerisation process was started by the use of a redox initiator. As this is a time consuming process, it is the aim of this work to develop a fast UV-based polymerisation process that allows a commercial scale-up.

In September 2010 a collaborative research project started with a consortium of eleven partners from eight countries with the objective to develop novel low fouling membranes for MBRs with high rejection of organic pollutants with low molecular weight as well as a high and constant water flux [Bionexgen (2016)]. It aimed at coating a commercially available membrane from the participating company Microdyn called UP150T. After coating with the novel PBM the membrane proofed their anti-fouling properties.

The previous work is described in detail in the PhD Thesis of Deowan [Deowan (2013)] and Galiano [Galiano (2013)] as well as in several publications (see: Galiano et al. (2015), Deowan et al. (2015), Figoli et al. (2015), Deowan et al. (2016), Deowan

et al. (2013), Hoinkis et al. (2014), Jegatheesan et al. (2016)). The work related to the development of the PBM is done by Galiano while the experiments related with the MBR are described by Deowan. In the following a short summary of their work is given:

A commercial Polyethersulfone (PES) membrane was modified by nano-structured novel coating through a PBM process. Two different surfactants have been successfully used for the preparation of the microemulsion (polymerisable surfactant called acryloyloxyundecyltriethylammonium bromide (AUTEAB), and a non-polymerisable surfactant called dodecyltrimethyl ammonium bromide (DTAB)). The pore size of the PBM membrane can be changed by the temperature during the coating from ultrafiltration to nanofiltration and therefore offers a wide range of possible applications. Also nanoparticles have been successfully incorporated in the matrix of the membrane. By this, specific properties can be achieved for the final membrane [Galiano et al. (2015)]. The structure and single development steps are described in detail in the work of Galiano [Galiano (2013)]. The final application of PBM on the commercial membrane resulted in higher anti-fouling and anti-microbial properties as well as in higher textile dye (blue) removal efficiency [Deowan (2013), Deowan et al. (2016)]. After several tests with a model fouling agent (humic acid) the optimum composition has been chosen for the long term trials in a lab scale MBR. During these tests the characteristics of the novel coated membranes have been compared with the commercial membranes under different operation conditions. For this purpose a model textile dye wastewater has been prepared based on a literature review resulting in a composition that is typical for the effluent water of the textile industry. The results were compared in terms of permeate quality, water permeability, textile dye, COD and Total Organic Carbon (TOC) removal efficiency, anti-fouling and anti-microbial properties, fouling resistance, N-balance, oxygen consumption and process robustness. The following list gives the main results of the novel coated membranes [Deowan et al. (2016)]:

- 20 % higher blue dye removal efficiency

- high anti-fouling/anti-microbial properties

- requires less energy in terms of aeration

- economically viable highly robust process

The membranes were modified by applying a nano-structured coating using PBM and polymerised by a redox process. Unlike the classic techniques for preparing membranes such as phase inversion, sintering, etc., in their work the membrane was prepared by an alternative approach. A commercial membrane was coated by PBM technique which consists of two immiscible phases (oil and water) stabilized by a surfactant. The main advantage of this approach is the structural characteristic of bicontinuous microemulsions that can be conserved and transferred into its polymeric matrix [Galiano (2013)]. Different surfactants can be used in the PBM composition whereas the polymerisable surfactants (i.e. AUTEAB) are of higher interest in comparison to non-polymerisable surfactants (i.e. DTAB). Thanks to the covalent anchorage within polymerisable surfactant itself, leaching of surfactants from the surface of the membrane is impossible, which leads to a significant increase of anti-microbial activity and decrease of membrane bio-fouling phenomenon [Galiano et al. (2015)].

The scanning electron microscopy (SEM) surface image of a PBM coated membrane is shown in Figure 1.1. The structure of a polymeric matrix in a PBM coated membrane is a typical bicontinuous structure made up of an interconnected network of polymer channels (white strips) and water channels (dark strips) [Galiano (2013)]. As seen from the SEM picture, the channels are randomly distributed on the surface and both channels have length in the range of 130 to 240 nm and width in the range of 30 to 50 nm [Galiano et al. (2015)].
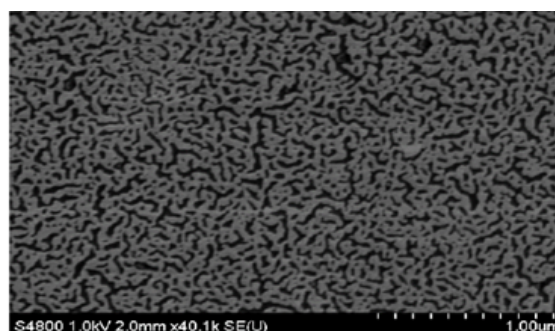
Figure 1.1. SEM surface image of a PBM coated membrane [Galiano et al. (2015)]

1.4 Objectives

A commercially available PES membrane (150 kilodalton (kDa)) from the company Microdyn Nadir was used as supportive membrane for the novel PBM coating both in this work as well as the previous work. In the previous work, a redox based polymerisation of novel PBM was employed. After microemulsion was prepared, the redox initiator was added into a vessel which was inflated already by nitrogen, and the inflation must last for another minute to stop the PBM contacting with oxygen in air. Then the vessel was sealed and kept in a water bath at 20 degree for 4 to 5 minutes. During this time, the vessel should be taken out several times for checking the viscosity of PBM. The casting process should start immediately after having achieved the required viscosity. PBM was poured onto the PES membrane and cast by a casting knife with a thickness of 250 μm. Then, the membrane was left in a nitrogen-inflated sealed chamber overnight till the PBM polymerised completely.

Therefore, regarding a commercial scale-up of the existing process, there are basically two challenges to overcome, viscosity adjustment and polymerisation time reduction. However, in the redox based polymerisation process, as soon as the redox initiators are added into the PBM solution, the polymerisation process starts and drives the viscosity of the solution up. Depending on the ambient conditions of the PBM, for instance room temperature, the polymerisation can be faster or slower. Therefore, the viscosity of the PBM is hard to control at a constant value whereas it is a key factor for the casting process. If the viscosity is too low, which means the PBM is too liquid, after being cast, the resulting membrane is very dense which leads to a low water flux of the membrane. If the viscosity is too high, which means the PBM solution is too sticky, the resulting coating will be inhomogeneous. Besides, after PBM is cast onto the commercial PES membrane, the redox based polymerisation process takes at least 20 minutes. This time factor also limits the process to be scaled-up commercially.

Based on the above mentioned reasons, in order to get the appropriate viscosity prior casting and to reduce the polymerisation time, a new process was investigated and tested in this work. The effect of increasing the viscosity for the DTAB based PBM was studied. In addition, a higher hydrophilicity was expected by adding polymerisable poly ethylene glycol as viscosity enhancer. The effect to the later PBM

membrane was studied for both surfactants. In the new process, the photoinitiator was added into the PBM, subsequently cast onto the PES membrane substrate, and cured by UV light within seconds. Several photoinitiators had to be selected and studied under different conditions for their efficiency (e.g. content, temperature, polymerisation time, UV-intensity, UV-wavelength, coating thickness) under inert and non-inert conditions. By use of infrared spectroscopy the polymerisation rate for the PBM had to be studied. Subsequently, the ideal composition coated under the right conditions had to be defined and characterised by cross-flow and other techniques (SEM, AFM, contact angle and so on). Finally, the PBM membrane was tested in a lab scaled MBR. Therefore, the existing setup had to be redesigned in order to allow the simultaneous run of two membranes. As of the biology within the system otherwise it is very difficult to realistically compare the efficiency of two membranes with each other.

Currently surface modification for polymer membranes are mainly UV initiated graft polymerisation. The surface modification of the commercial PES membranes by coating and photoinitiating the PBM has not been studied. This thesis aims at developing a novel process by applying the proper photoinitiators and the efficient UV light source to make the surface modified PES with anti-fouling property feasible to be reproduced and easy to be scaled up.

2 Fundamentals

In this section the fundamental informations related to this work are summarized and divided into specific topics.

2.1 Fundamentals of membrane technology

A membrane, which is used in wastewater treatment, is actually a selective barrier that separates some physical or chemical components. The wastewater of the feed-stream of the membrane is separated into two flows of liquid. The liquid that passes through the membrane is known as the permeate, and the retained liquid is called the retentate. The rejected constituents in the retentate tend to accumulate at the membrane surface, producing various phenomena (e.g. fouling) which lead to a reduction in the flow of water through the membrane (i.e. the flux) at a given transmembrane pressure (TMP), or conversely an increase in the TMP for a given flux (reducing the permeability, which is the ratio of flux to TMP) [Judd and Judd (2007)].
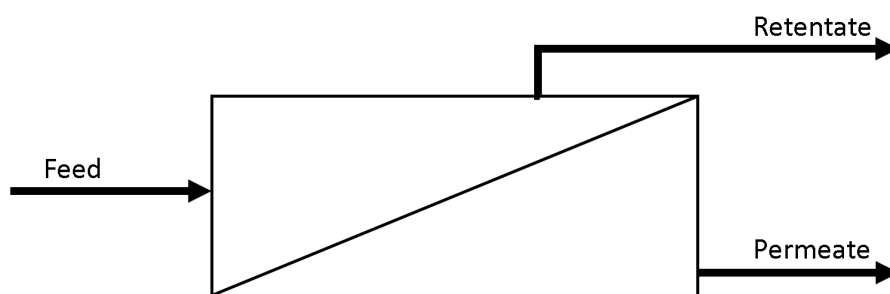
Figure 2.1. Membrane principle

There are four categories of membranes, which are classified as Microfiltration (MF), Ultrafiltration (UF), Nanofiltration (NF), and Reverse Osmosis (RO). The degree of

selectivity of a membrane depends on the pore size. Normally, the pore size can be defined either in the effective equivalent pore diameter in μm or in the equivalent mass of smallest molecule in Daltons (Da) that can be rejected [Judd and Judd (2007)]. As shown in Figure 2.2, microfiltration can separate solids from water which have pore sizes greater than $0.08 - 2$ μm. To filter solids with a pore size of 2 nm to 50 nm, ultrafiltration is an adaptable choice, whereas nanofiltration can achieve separation with less than a 2 nm pore size, and reverse osmosis can reject singly charged ions.
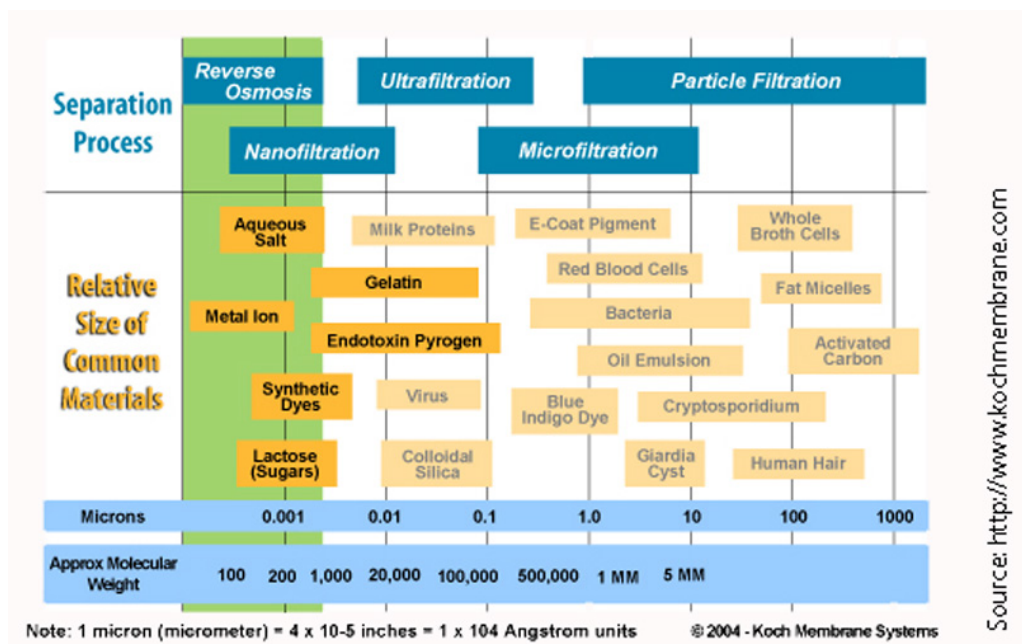
Figure 2.2. Classification of different membrane separation techniques (Koch-Membrane (2010))

A classical MBR comprises a conventional activated sludge process (ASP), characterized by the suspended grow of biomass, coupled with a micro- or ultrafiltration membrane separation process to retain the biomass [Judd and Judd (2007)]. The biomass is degrading harmful substances and the treated water is then separated from the wastewater by membrane filtration. Two configurations, submerged and sidestream are common (see section 2.1.1). Figure 2.3 shows the comparison between ASP and MBR´s. From the wastewater step to the aeration zone, both of the processes are configured exactly the same. However, instead of a settler in the

ASP, this is replaced by the membrane. The biggest advantage of the MBR is the reduction of the reactor volume while the loading rate remains the same. The disadvantage of the MBR is a higher operating cost (mostly because of the necessary aeration). Since the effective pore size can be below 0.1 μm, the MBR effectively produces a clarified and substantially disinfected effluent [Judd and Judd (2007)]. This means that bacteria and solids are kept out of the permeate.
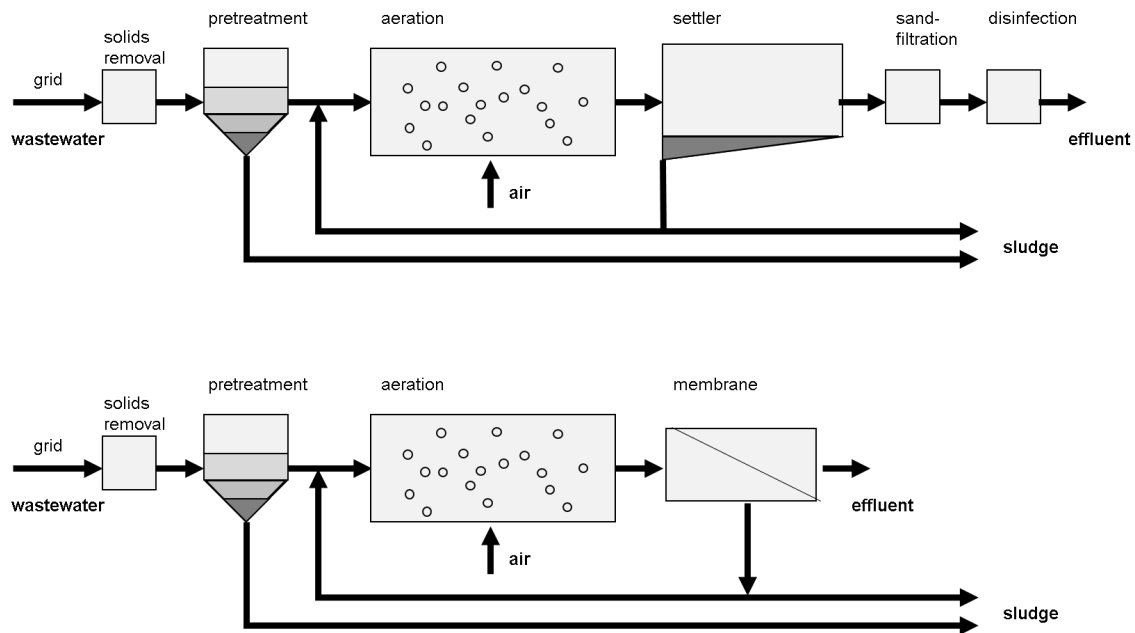
Figure 2.3. Schematic of ASP and sidestream MBR

2.1.1 MBR configurations

Despite the less common setup "external-immersed" (see Clouzot et al. (2010)), there are two main arrangements of membranes in the MBR process: submerged/immersed (iMBR), and sidestream (sMBR) with two hydraulic operations: pumped and airlift (suction). An iMBR is integrated into the biological reactor, whereas the sMBR is separated outside the reactor tank. The pump is usually used with sMBR, whereas with the iMBR an airlift operation is preferred. With the airlift pump, the iMBR can reduce the membrane surface fouling by removing solids from the membrane surface by passing of the air bubbles over the membrane. Another option is a periodic backwash process which pumps the effluent back through the membrane. Regarding

the sMBR, the biomass is pumped directly through the membrane modules and back to the reactor tank. iMBRs are generally less energy-intensive than sMBRs, since employing membrane modules in a pumped sidestream crossflow incurs an energy penalty due to the high pressures and volumetric flows imposed [Judd and Judd (2007)]. sMBR´s allow anaerobic treatment of the sludge and offers the possibility of energy production when biogas is produced during the anaerobic digestion of the sludge.
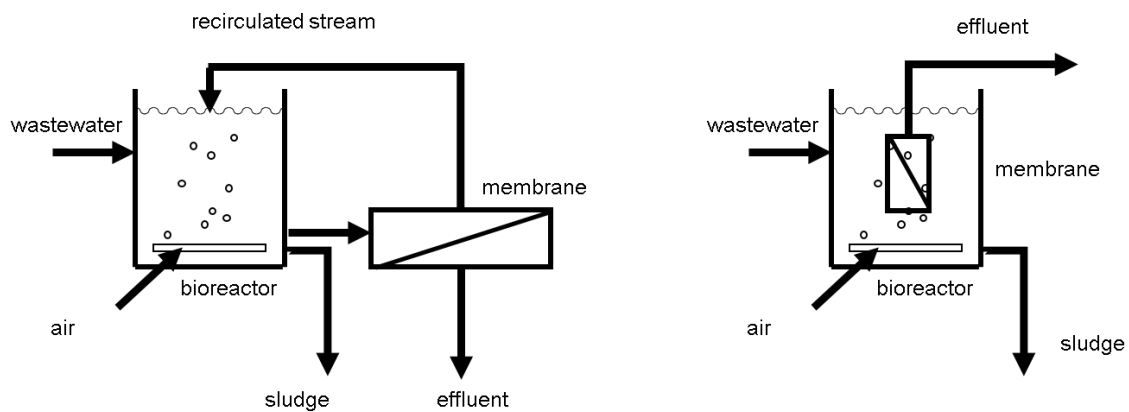
Figure 2.4. Configurations of sidestream (left) and immersed (right) MBR's

2.1.2 Membrane materials

The membrane is the core of any membrane process. Depending on structure, transport properties and separation mechanism, a variety of membranes are available on the market. Polymeric, ceramic, and metallic materials are used to form the membranes [Judd and Judd (2007)]. The characteristics of membranes are generally originated by different raw materials or preparation methods [Drioli et al. (2006)]. With regard to membrane materials, membranes can be generally classified into two categories: inorganic membranes (ceramic, metallic) and organic (polymeric) membranes. Ceramic membranes have not been widely applied yet in either general membrane filtration applications in water industry or specifically for MBR. Metallic membrane filters exist, but have not been applied in MBR technology as well [Hai et al. (2013), Judd and Judd (2011)]. In MBR applications, the selection of membrane materials is governed by the need for a material which has appropriate

mechanical strength and chemical resistance combined with high productivity, narrow pore size distribution, and minor fouling tendency [Li et al. (2011)]. In MBR technology, polymers and ceramics can be used. Although ceramic membranes are excellent in thermal, chemical and fouling resistance, whereas they are far too expensive to be competitive in wastewater treatment applications. Polymeric membranes are cheaper compared to ceramic membranes and versatile with respect to membrane configuration and module types [Li et al. (2011)]. To form membranes, there are many requirements of having a thin surface layer to adapt the perm selectivity, a thicker porous layer to provide mechanical stability, and some resistance to thermal and chemical attack. Due to the intrinsic properties (thermal, mechanical and chemical stability, selectivity and permeability etc.) that can be modulated, polymeric membranes have attracted much more interest [Drioli et al. (2006)]. Therefore, polymeric membranes are mostly used for fabrication [Judd and Judd (2007), Figoli et al. (2015)]. Generally, polyvinylidenedifluoride (PVDF), polyethysulphone (PES), polyethylence (PE), and polypropylene (PP) are suitable materials for forming the membrane.

Table 2.1. Polymer membrane characteristics *

Polymer	Characteristics
Polyethylene (PE)	Chemically resistant
Polyethylsulphone (PES)	Excellent chemical resistance, hydrophobic, reasonable cost
Polypropylene (PP)	Chemically resistant
Polytetrafluoroethylene (PTFE)	Highly hydrophobic, excellent organic and chemical resistance
Polyvinylidene difluoride (PVDF)	Excellent chemical resistance, good chlorine resistance

* [Stephenson et al. (2000)]

2.1.3 Membrane configuration

The configuration of the membrane, that is, its geometry and the way it is mounted and oriented in relation to the flow of feed to be treated, is crucial in determining the

overall process performance [Judd and Judd (2007)]. In commercial manufacturing, there are six principal configurations of membrane. They are plate-and-frame/flat sheet (FS), hollow fiber (HF), (multi)tubular (MT), capillary tube (CT), pleated filter cartridge (FC), and spiral-wound (SW). The configuration depends on the membrane geometry, the relation between the water flow orientation and the membrane mounting. FS, MT and HF are suitable for MBR technology due to their ability of permitting turbulence promotion, cleaning, or both. Turbulence promotion supports the passage of permeate by increasing either feed water or air/water mixture along the membrane surface. Physical cleaning by reversing the flow (back flushing) is a simple step to remove the fouling layer at a rate 2-3 times higher than the forward flow.

2.1.4 Fouling and scaling for membrane applications

Membrane fouling or scaling, is one main obstacle in membrane processes referring to certain constituents in feed which tend to deposit and accumulate on the surface of the membrane or inside the membrane matrix. This results in a flux decline, which can be classified by the type of particulate matter being removed such as inorganic (scaling) fouling, particulate/colloidal fouling, biological/microbial fouling, and organic fouling. Certain fouling compounds can be removed by hydraulic means such as filter backwash, [Liu et al. (2001)]. A brief description of each type of membrane fouling is summarized below.

Inorganic fouling/scaling Inorganic precipitates such as metal hydroxides and carbonates accumulate onto membrane surface or within pore structure which results in pore narrowing [Holman and Ohlinger (2007)].

Particulate/colloid fouling Suspended solids or colloids, here referring to biologically inert particles and colloids that are inorganic in nature and are originated from weathering of rocks cause particulate fouling. Due to their particle size that is smaller than the pore size, the particles can enter and be trapped within the membrane structure matrix and are hard to be backwashed [Liu et al. (2001)].

Biological/microbial fouling Biological/microbial fouling is termed as the fouling caused by a formation of a biofilm and typically leads to a formation of a

cake/gel layer on the membrane surface [Holman and Ohlinger (2007)]. Once the bacteria in wastewater attach onto the membrane surface, they start to multiply and produce extracellular polymetric substances (EPS or exopolymers). They consist of heteropolysaccharides and have a high negative charge density, and form as well a slimy and hydrated gel layer [Liu et al. (2001)].

Organic fouling The fouling that is caused by deposition of the natural organic matter (NOM), which mainly consists of humic substances in feed water to form a gel/cake layer on the membrane surface, is termed as organic fouling [Holman and Ohlinger (2007)].

Fouling in MBR application

The fouling on MBR membranes can occur by inorganic-, organic-, particulate- and bio-fouling. Also a combination of them can take place [Jegatheesan et al. (2016)]. The most common fouling in MBR-application is the biofouling generated over long operation times, where the deposition of organic molecules onto the membrane leads to the forming of a colloidal layer. Inorganic fouling usually occurs on nanofiltration and reverse osmosis membranes that are used at high pressure. One of the factors that contribute to the membrane fouling is the sludge retention time (SRT) as it controls the biomass characteristics [Jegatheesan et al. (2016)]. Higher SRT contributes to higher concentration of MLSS. Xing et al. reported that a high concentration of MLSS is associated with a high viscosity of mixed liquor contributing significantly to membrane fouling [Xing et al. (2000)]. Saddoud et al. found membrane fouling with a SRT more than 140 days [Saddoud et al. (2007)]. In contrary Baeck et al. described that the decrease of SRT from 213 to 40 days reduced the treatment performance of the MBR in regards of membrane fouling [Baek et al. (2010)]. Both cases show that the ideal SRT needs to be adjusted based on the feed water characteristics of different MBR applications. Factors effecting the fouling of membranes in a MBR are MLSS, OLR, SRT, HRT, membrane properties (material, pore size, hydrophilicity), backwash frequency, foulants and scalants (e.g. humic substances, inorganic compounds) and the temperature [Jegatheesan et al. (2016)].

2.2 Microemulsions

According to definition of the International Union of Pure and Applied Chemistry (IUPAC), microemulsion is "an isotropic and thermodynamically stable system which consists of water, oil, and surfactant(s) with dispersed domain diameter varying approximately from 1 to 100 nm, usually 10 to 50 nm" [Slomkowski et al. (2011)]. Microemulsions form spontaneously and thanks to the small droplets, they look optically transparent. Along with the surfactant which is used to stabilize the two immiscible liquids, the presence of co-surfactant lowers the interfacial energy to a very small value. However, with the help of the non-ionic surfactants, some cationic surfactants or double-chain surfactants, the co-surfactant may not be necessary [Galiano (2013)]. Depending on the water (W) / oil (O) ratio, microemulsions are typically divided into three types:

- O/W microemulsions, which are formed at low oil concentration. The oil droplets are dispersed in a water phase

- W/O microemulsions, which are formed at low water concentration. The water droplets are dispersed in a continuous oil phase

- Bicontinuous microemulsions, which are formed at balanced conditions in which the oil droplets and water droplets are randomly dispersed in two phases and form interconnected network giving a sponge-like structure [Galiano (2013)]

At low surfactant concentrations, the so called Winsor systems arise as different multiphase equilibria:

- Winsor I (O/W): surfactant-rich water phase coexisting with surfactant-poor oil phase

- Winsor II (W/O): surfactant-rich oil phase coexisting with surfactant-poor water phase

- Winsor III (bicontinuous): surfactant-rich hybrid phase coexisting with poor phase of water and oil, respectively [Galiano (2013)]

In Figure 2.5, a triangular phase diagram (ternary phase diagram) representing different phases and coexistence regions that occur in a three-component water, oil and surfactant system is shown. Microemulsions can be formed as oil-swollen micelles

dispersed in a continuous water phase (O/W), or water-swollen droplets dispersed in an oil phase (W/O). In the middle region, the sponge-like structure represents the region of bicontinuous microemulsion in which oil and water domains coexist in interconnected domains. The bicontinuous microemulsion is stabilized by adding either non-polymerisable or polymerisable surfactants. The one added with polymerisable surfactant is called polymerisable bicontinuous microemulsion (PBM), in which the polymerisable surfactant acts as a co-monomer in the polymerisation process. The products of PBMs polymerisation process are transparent porous polymeric micro- and nanostructured solid materials [Gan et al. (1995), Gan and Chew (1997), Figoli (2001)], which can be used as the coating for commercial membranes and improve the performance of the commercial membranes [Galiano (2013)].
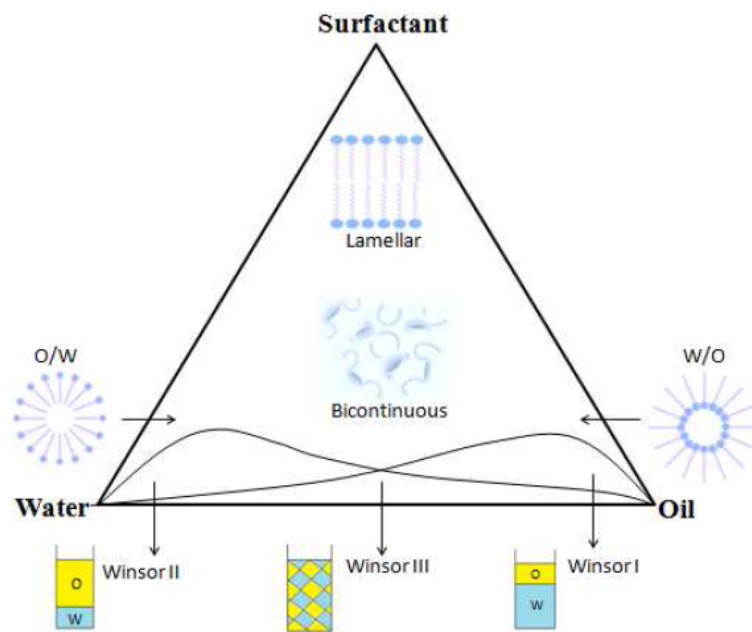
Figure 2.5. Ternary phase diagram of multicomponent systems [Galiano (2013)]

2.3 Radiation cure coatings

Since PBM coating is sensitive to temperature, the radiation cure coatings cross-link by reactions initiated by radiation rather than by heat is a suitable choice [Z.W. Wicks F.N. Jones (1994)]. Two common classes of radiation cure coatings

are known. UV cure coatings initiated by the absorption of photons of UV-visible radiation executed by a photoinitiator [Z.W. Wicks F.N. Jones (1994)]. In addition the electron beam cure coating offers an alternative approach but comes along with some disadvantages for a commercial scale-up of novel membrane coatings as high energy electrons (particle radiation) are needed. Exemplary for a thermal curing are the infrared and microwave radiation procedure [Z.W. Wicks F.N. Jones (1994)]. Those just emit heat which creates the curing.

2.3.1 UV-initiated free radical polymerisation

In 1966 P. Weiss firstly described the UV-initiated free radical polymerisation [Weiss (1966)]. A free radical polymerisation is a chain reaction and involves three fundamental steps: initiation, propagation, termination. The schematic of the reaction is shown as photoinitiator is I, double bond containing monomers are depicted by M and M', and AH is a chain transfer agent (CTA) containing weakly bonded hydrogen atoms. The photoinitiator absorbs UV-energy which equals to h (Planck' constant) multiplied by ν (frequency of light) and generates a carbon based free radical $\bullet$, a molecule containing atom with unpaired electrons in radical formation step. The free radical then initiates the polymer chain through reaction with monomer. Propagation continues until the growing chain radical is deactivated by the chain transfer reaction or termination. In chain transfer reactions a molecule of the CTA is decomposed into a terminating part H and a new radical A which may initiate a new chain [Weiss (1966)].

Radical formation	$I(h\nu) \rightarrow I\bullet$
Initiation	$I \bullet + M \rightarrow IM\bullet$
Ppropagation	$IM \bullet + M' \rightarrow IMM'\bullet$
Chain transfer	$IMM' \bullet + AH \rightarrow IMM'H + A\bullet$
Termination	$IMM' \bullet + IMM'\bullet \rightarrow IMM'M'MI$
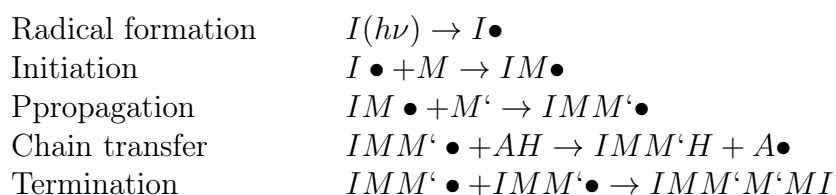
2.3.2 UV classification and hazards

The ISO 21348 defines the classification of UV-light according to its wavelength ranges [SpaceEnvironmentTechnologies (2014)] whereas the ultraviolet light is found

in the range from 100 to 400 nm. Figure 2.6 shows the UV classification with corresponding wavelength ranges. As can be seen the UV-spectrum is divided into several regions, UV visible=400-700nm, UVA = 315 - 400 nm, UVB=280-315 nm, UVC=200-280 nm, VUV=100-200 nm. 98.7 % of the UV irradiation emitted by the sun is blocked by the earth's ozone layer and upper atmosphere. The majority of irradiation reaching the earth's surface is UVA and a very small amount of UVB.
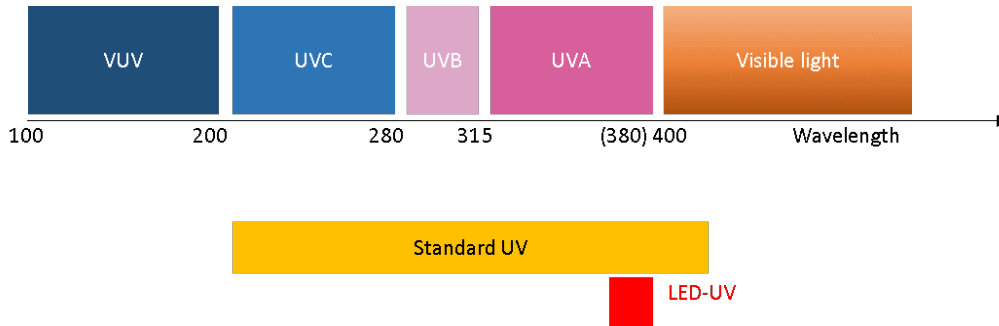
Figure 2.6. UV classification and wavelength ranges

The widely used mercury fluorescent lamps are classified as UV-A/B while the majority of LED lamps rely on UV-A radiation. According to the wavelength region different hazardous effects arise. Because of the hazardous effects of the UV-light to the skin and eyes special rules for handling under UV-light have to be followed. The eyes need to be protected by special UV safety glasses as well as the skin has to be protected with long sleeved clothing and gloves.

2.3.3 Photoinitiator

The suitable photoinitiators can be chosen from available products of several suppliers considering the properties of raw materials and end-application properties. The broad lists of photoinitiators, as well as their structures, absorption spectra and physical properties are available from commercial sources (Sigma-Aldrich, Ciba Specialty Chemicals, BASF).

As described by Koleske (2002), photoinitiators are compounds that, after absorbing radiant energy, are raised to an excited state. From their excited states, photoinitiators photolyse or degrade directly or indirectly to free radicals or ions. The free

radicals and ions become the initiating species and cause very rapid polymerisation of photocurable formulations based on a variety of chemistries. Methacrylate is one of the main chemistries that involves the use of photoinitiators, which cause polymerisation by free radical initiation [Koleske (2002)] (see section 2.3.1).

As the optimum concentration of photoinitiator is depending on the thickness of the film, the ideal concentration must be determined for the selected thickness. The thinner the film the lower the optimum concentration, the thicker the higher the optimum concentration [Z.W. Wicks F.N. Jones (1994)]. Cost-wise the thinner film is preferred as the amount of chemicals used to form the PBM as well as the amount of photoinitiator is lower. The effect of the film-thickness to the latter performance of the membrane needs to be studied more deeply by several characterisation steps.

There are two main types of free-radical generating photoinitiators: Norrish Type I [Bamford and W. (1934)] [Hartley and Guillet (1968)] and Norrish Type II [Trozzolo and Winslow (1968)]. The two main types of photoinitiators are those which form an active species by a fragmentation process or by a hydrogen abstraction process:

Norrish Type I: Photoinitiators photolyse through a homolytic fragmentation or α-cleavage and directly form free radicals capable of initiating polymerisation; the bond break takes place between the carbonyl group and an adjacent carbon [Koleske (2002)].

Norrish Type II: Photoinitiators are activitated by radiation and form free radicals by hydrogen abstraction or electron extraction from a second compound which becomes the actual initiating free radical [Koleske (2002)].

Type 1: Homolytic Fragmentation Type: When the homolytic fragmentation type of photoinitiators photolyse, they will produce two radicals by the means of homolytic fragmentation or α-cleavage mechanism [Koleske (2002)]. As exemplified by the photolyse of a diphenyl (2, 4, 6-trimethylbenzoyl) phosphine oxide (DTBP), the mechanism of homolytic fragmentation is depicted in Figure 2.7.
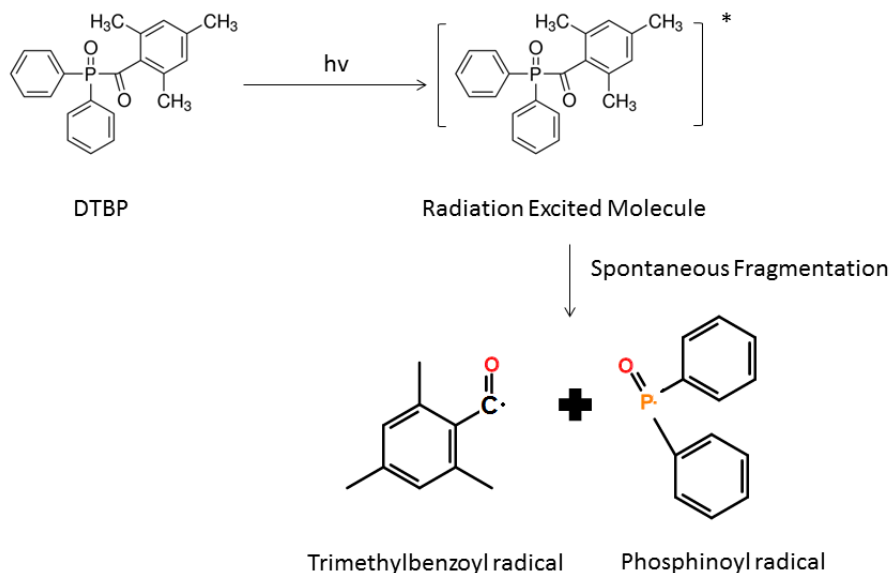
Figure 2.7. Photolysis of DTBP [Koleske (2002)]

After absorbing radiant energy, a DTBP molecule rises to excited state, and spontaneously fragments into two free radicals, a trimethylbenzoyl radical and a phosphinoyl radical. The radicals may or may not have the same capability of initiating polymerisation [Koleske (2002)]. The phosphinoyl radical is very reactive to polymerise ethylenically unsaturated molecules such as acrylates, methacylates etc. [Fouassier (1998)]. However, fragmentation-type photoinitiators are affected by oxygen. Even small concentration of oxygen (10^{-3} molar) can have significant effects and prevent polymerisation [Vesley (1986)]. Therefore, oxygen quenching needs to be considered when fragmentation-type photoinitiators are selected to initiate the polymerisation.

Type 2: Hydrogen abstraction Type: When photoinitiators of hydrogen abstraction type are exposed to UV irradiation, they will be taken from a ground state to an excited state. However, they will not spontaneously fragment or photolyse and generate free radicals capable of initiating polymerisation. These photoinitiators require the presence of a synergist, which is also known as photo-enhancer to interact

with the excited molecules and form free radicals by means of electron transfer and hydrogen abstraction [Koleske (2002)].

In summary an obvious advantage of homolytic fragmentation over hydrogen abstraction is the unnecessarity of a bimolecular reaction taking place in the Norrish Type II reactions [Koleske (2002)]. In this thesis, Norrish Type I photoinitiators were selected in the beginning to be tested for their performance in PBM.

2.3.4 Oxygen inhibition in UV-polymerisation

Especially for the free radical polymerisation the oxygen inhibition of the surface cure is problematic. A peroxy free radical is formed when oxygen reacts with the terminal free radical on a propagating molecule [Z.W. Wicks F.N. Jones (1994)]. This peroxy free radical can not completely add to another monomer molecule leading to the stop in the chain reaction. Therefore the generation of free radicals of some photoinitiators is reduced. In order to coop this issue the curing can be done under inert conditions (e.g. under a nitrogen atmosphere). Another option is to incorporate paraffin wax in the coating shielding the surface of the film against oxygen [Z.W. Wicks F.N. Jones (1994)]. High radiation intensities could also lead to a rapid generation of a high number of free radicals that decimate the oxygen at the surface and allow other radicals to continue the polymerisation before more oxygen diffuses to the surface [Z.W. Wicks F.N. Jones (1994)]. Oxygen inhibition can be reduced by benzophenone/amine systems. Unimolecular photoinitiators can reduce the oxygen inhibition by adding small amount of an appropriate amine [Z.W. Wicks F.N. Jones (1994)].

2.3.5 Curing by UV-light

In curing process, each cure material (ink, coating, adhesive) has specific absorption characteristics that react to a certain UV-wavelength. It is important that the spectral output (the intensity of light at each wavelength over the whole wavelength range emitted by the lamp), matches with the absorption characteristics of the photoinitiator of the cure material. UVC is associated with surface cure; UVB, UVA

improve depth cure; UVV employs visible photoinitiators to absorb light and to provide even greater depth of cure [Excelitas Technologies Corp. (2016)]. In this work, the depth cure of PBM coating by UV-LED with 365 nm in the range of UVA was focused. Figure 2.8 shows the penetration depth of different wavelength.
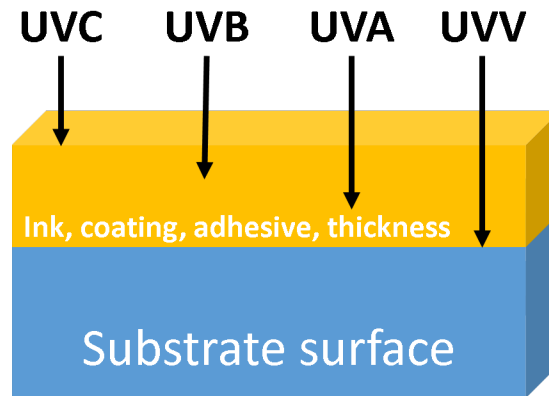
Figure 2.8. Relative penetration of UV-light

The free radical initiated and the acid initiated chain-growth polymerisation reactions are the classes used in UV-curing. The distance between the curing-surface and the UV-lamp needs to be adjusted properly as the intensity of the UV-light drops off with the square of the distance between lamp and surface [Z.W. Wicks F.N. Jones (1994)]. Therefore the distance homogeneity is a challenging factor when three-dimensional surfaces e.g. car-parts have to be cured. Technological solutions are available for this case, anyway the flat-sheet-curing represents the easiest application form. The content of the absorbed radiation I_A/I_0 in the curing is depending on the molar absorptivity ε, the optical path length of the length of the radiation in the coating X and the concentration of the photoinitiator C. A reflecting coating surface below the curing would result in higher intensities as the light gets reflected. Consider the reflection to be zero and there are no other absorber present the fraction of radiation at a given wavelength can be declared by equation 2.1 [Z.W. Wicks F.N. Jones (1994)].

$$\frac{I_A}{I_0} = 1 - 10^{\varepsilon CX} \tag{2.1}$$

The concentration of initiating radicals influences the rate of polymerisation reactions. Therefore an increase in the photoinitiator-concentration should result in a faster polymerisation. But this is only true for the lower concentration area. At a certain concentration the optimum concentration is reached. Above this concentration the curing rate in the lower part of the curing is decreasing. The upper few micrometers of the film get polymerised immediately, so only a negligible intensity reaches the rest of the film [Z.W. Wicks F.N. Jones (1994)]. The optimum concentration is reached when the film is completely polymerised at the lowest photoinitiator concentration resulting in lowest possible costs. For UV-light sources with a wide range of emission bands (like the medium-pressure mercury vapour lamps) a mixture of photoinitiators covering different emission bands can be useful to ensure a proper depth and surface curing. The photoinitiator that is highly absorbed at the surface will act against the oxygen inhibition, while the photoinitiator with the weaker absorption of another emission band will be absorbed more uniformly through the film [Z.W. Wicks F.N. Jones (1994)]. Another factor for the polymerisation speed is the thickness of the film. The optimum concentration of photoinitiator is film thickness dependent: the greater the film thickness, the lower the optimum concentration [Z.W. Wicks F.N. Jones (1994)]. For cost reasons, lower concentration of photoinitiator is also favorable, since it is generally an expensive component. However, the time required to cure a thick film is longer than to cure a thin film. This is due to less radiation absorbed in any volume element with increasing film thickness [Wicks et al. (2007)]

Another factor for the polymerisation efficiency is the type of surface on which the film is cured. Reflecting surfaces mirror the radiation after passing the film resulting in an almost double percolation of the radiation through the film. By using a black surface the radiation passes the film only once.

Medium-pressure mercury vapour lamps

For the UV-curing most common are the medium-pressure mercury vapour lamps as they are comparably cheap in invest and cover a wide range of wavelengths. Common lamps have an output of 80 W/cm but are available up to 240 W/cm [Z.W. Wicks F.N. Jones (1994)]. A significant amount of the emitted infrared radiation causes heating. As the mercury needs to be evaporated in order to emit the UV-light

the lamp is naturally very hot (above 357°C are needed to evaporate the mercury). Therefore this lamp needs to be cooled by water or air to avoid overheating. As this lamps produce the toxic ozone the units must be ventilated to carry the ozone away.

LED-lamps

In the past years, light sources usually used in UV-curing technology were medium pressure mercury lamps, xenon lamps, lasers or electrodeless vapor lamps emitting most between 200 and 500 nm. Whereas the solid-state light emitting diode (LED) arrays applied as novel light sources in curing technology arises market's interest due to its striking difference in comparison to mercury lamps which is its narrow spectral output [Gloeckner (2008)]. Besides emitting a broad multiple line spectrum, mercury lamps are also operate at very high temperatures and the major energy is wasted as heat (and visible light) [Kneissl and Rass (2015)].

A key to successful UV-curing process is the availability of a UV-source being capable of producing a relatively high intensity of UV-irradiation at low cost without generating excessive infrared radiation [Z.W. Wicks F.N. Jones (1994)]. Except above mentioned advantages, in comparison with conventional UV-lamps, UV-LED has more advantages such as:

- Smaller compact body
- No warm-up time needed
- Radiation intensity is adjustable
- No ozone generation thanks to no mercury
- Less energy consumption
- Low heat generation
- Longer full-intensity life time
- Customized size

Since the PBM is coated and cured on a flat sheet membrane, the distance between the lamp and the coating on various parts of the membrane being coated must be fairly uniform [Z.W. Wicks F.N. Jones (1994)].

3 Literature review

In this section a review for publications related to this work is done and summarised under different topics.

3.1 State of the art Membrane BioReactors

Judd et al reported that the first Membrane BioReactors (MBRs) were commercially developed by Dorr-Oliver in the late 1960s [Judd and Judd (2007)], for a ship-board sewage treatment [Bemberis et al. (1971)].

Since then the technology has been constantly improved. As the standards for discharge regulations are perpetually rising and the growing urbanization results in an increasing demand for water recycling the company Microdyn calls MBRs the leading innovation in wastewater treatment through conventional activated sludge [Microdyn-Nadir-GmbH (2014)]. Conventionally activated sludge (CAS) treatment plants depend on a second stage that separates the biomass from the treated wastewater. Therefore CAS run at a low MLSS (mixed liquor suspended solids) and thus require more space and produce a lower quality of the effluent than the MBR [Microdyn-Nadir-GmbH (2014)]. In the current system of Microdyn and other suppliers (see Table 3.1) the second separation stage is replaced by a membrane module in the ultrafiltration (UF) range. By replacing the second stage by an UF membrane the system can be operated at higher MLSS levels and thereby require a smaller overall footprint [Microdyn-Nadir-GmbH (2014)]. The interest in MBRs for the usage in municipal and industrial wastewater treatment has been rising in recent decades [Fenu et al. (2010a)]. Most important factors for a cost effective MBR-system are the quality of the effluent water after the treatment process as well as a durable and energy efficient design of the plant [Fenu et al. (2010a)]. Fenu et al. published the energy costs of different compartments and devices of a MBR in comparison with

a conventional activated sludge treatment followed by ultrafiltration and ultraviolet (UV) light.

Table 3.1
Manufacturer of membranes used in MBRs ∗ modified from Joon (2016)

Manufacturer	Model	Reference
Microdyn Nadir	FS(UP150T)	Microdyn-Nadir-GmbH (2014)
GE Water	HF(ZW500d)	Cote and Liu (2004)
GE Water	HF(ZW500c)	Adham et al. (2004), Brepols (2010)
GE Water	HF(ZW500d)	Brepols (2010)
Koch Puron	-	Herold (2011)
Kubota	FS(SP400), FS(EW400)	Cote and Liu (2004)
Kubota	FS(EK200)	Adham et al. (2004)
Asahi	HF(MUNC-620A)	Cote and Liu (2004)
Econoty	HF(4005CF)	Cote and Liu (2004)
Siemens	HF(B10R)	Adham et al. (2004)
Mitsubishi	HF(SADF)	EUROMBRA (2006)
A3 Water Solutions	HF(SADF)	Grelot et al. (2010)

Both systems should have a similar effluent quality [Fenu et al. (2010b)]. The overall energy consumption of the studied MBR was around 0.64 kWh/m^3 while the energy consumption of the conventional activated sludge treatment is around 0.3 kWh/m^3. In conclusion they showed that the MBR technology is not yet sufficiently competitive. They highlighted the high MLSS as one of the main factors for the high energy demand of the studied MBR. The energy demand is high due to the necessary mixing of the sludge. As well the reduced oxygen transfer leads to a higher energy demand for the increased oxygen supply. This could be covered by usage of anti-fouling membranes described by Deowan et al. (2016) as they require less aeration. It has also been described that in regards to the filtration process the energy demand can be reduced if the coarse aeration is efficiently integrated in the biological process scheme of submerged MBRs. Judd and Judd (2007) described the current market situations for MBR systems. In 1995 the market value has been around $ 10 million. In 2005 the market value already increased to $ 217 million. However, a market study of PR Newswire (engl.) (2015) calculated a global compound annual growth rate of 15 % over the period 2014-2019 that will reach $ 2,927 million by 2019. Stringent government regulations regarding the quality of water is an important factor driving

the growth of the market. These numbers show the significantly increasing market for MBR applications.

3.1.1 Membrane BioReactors in textile wastewater treatment

As the textile industry is widely spread especially in the Middle East and North African (MENA) countries as well as in Asian countries like China, India etc. the demand for an efficient and sustainable wastewater treatment and reuse is very high [Bionexgen (2016)].

More than 100,000 commercial dyes used in the textile industry are available currently, while 700,000 to 1,000,000 tons are produced annually and 280,000 tons are discharged as effluent worldwide [Ali (2010)]. Considering the overall industrial water pollution the World Bank estimates that the textile industry is covering already about 17 to 20 % [Kant (2012)]. Depending on the production process and steps, different waste streams occur. Therefore different technologies could be used for the different requirements. Anyway, in most applications the wastewater of all steps (fillings of padders-dyeing/finishing, printing and dye-baths, washing and rinsing, cooling and floor washing) are just mixed with each other and discharged [Bechtold et al. (2006), Deowan (2013)]. Water and complex chemicals (toxic and persistence) are widely used by textile industries at various stages during textile processing. All the unused materials are discharged in the wastewater. These tend to be high in colour, biochemical oxygen demand (BOD), chemical oxygen demand (COD), very low BOD to COD ratio, pH, temperature, turbidity and toxic chemicals. The flora and fauna are seriously affected by this wastewater discharge, and the water gets badly polluted [Kritikos et al. (2007), Deowan (2013)]. Therefore many countries defined now more stringent standards for the discharge of textile wastewater [Jegatheesan et al. (2016)]. MBRs in wastewater reclamation and reuse are effective tools for sustainable industrial development programs. Based on a cost and benefit study conducted by Dogan et al. (2010), for the end-of-pipe treatment of textile wastewater, MBR is the best available technology. Increasingly stringent environmental legislation and generally enhanced intensity, efficiency, and diversity of treatment technologies have made the reuse of water more viable in many industrial processes.

MBRs are an essential part of advancing such water sustainability, because they encourage water reuse and open up opportunities for decentralized treatment [Deowan (2013)]. An MBR produces high quality recyclable water with several advantages as lower sludge production, low maintenance, higher removal of nutrients, organic and persistent organic pollutants over conventional sludge processes [Chang et al. (2002), Jegatheesan et al. (2016)]. On the other hand the fouling of membranes is its main issue. The control of fouling onto membranes in MBR applications is difficult. A long sludge retention time leads to an increase of the pollutants degradation but on the same time it contributes to membrane fouling [Jegatheesan et al. (2016)] leading to an increase of the transmembrane pressure (TMP) or decrease of permeate flux at constant TMP. This results in higher operation costs for the cleaning of the membranes and eventually in a decrease of life span. Previous research on textile dye wastewater by aerobic MBR showed the following COD and removal efficiencies (see Table 3.2). [Schoeberl et al. (2005)] 89-94 % and 65-91 %; [Brik et al. (2006)] 60-95 % and 46-98.5 %; [Yun et al. (2006)] 94.8 % and 72.9 %. Most of the colour removal was by adsorption of dye molecules onto the biomass, as synthetic azo dyes are not biodegradable and can only be adsorbed to microbial cells followed by sludge withdrawal [Jegatheesan et al. (2016)].

The treatment of industrial textile wastewater by a side-stream MBR with effluent from a polyester finishing company was studied by Schoeberl et al. (2004). They found a COD removal efficiency of 75-91 % with fluctuations in COD of the feed stream between 1380-6035 mg/L. As membrane a PVDF with a filter area of 0.28 m^2 and 15 kDa MWCO was used. The colour removal efficiency found to be between 46-99 %.

A lab-scale MBR equipped with a gravity drain for the treatment of dyeing and printing wastewater from a wool mill was studied by Zheng and Liu (2006). The system was run at a HRT of 6-12 h for 135 days. In the first 35 days the TMP was 0.127 bar at a set flux of 6 L/(h m^2). Keeping the TMP constant the flux increased to 12 L/(h m^2) until the 64th day. Till the 114th day the TMP rose to 0.174 bar at a flux of 15 L/(h m^2). Increasing the TMP after the 114th day from 0.174 to 0.203 bar did not result in a flux increase. The effluent showed average removal rates of COD and colour of 80.3 and 58.7 %.

The performance of a hollow-fibre (PVDF, 0.2 μm) MBR for dye containing wastewa-

ter from a dyeing and printing industry has been studied for a duration of 100 days by Huang et al. (2009). At a pH range from 10-14 different HRTs were tested (6-22.5 h). At the HRT of 6 h the system performed efficiently with a COD removal between 80-90 %. The colour removal was only 60-75 %. The flux of the studied membrane ranged between 2-8 L/(h m^2) at a fluctuating TMP of 0.05-0.1 bar. Another submerged hollow-fibre (0.04 μm) membrane was tested in a MBR (380-1500 L/day) for the treatment efficiency of a jeans textile factory by Yigit et al. (2009). A high TDS (789-4720 mg/L), colour (286-8100 Pt-Co) and conductivity (1578-9440 μS/cm) were characteristic in the influent. Two different stages were operated. Stage 1 where the MBR sludge was not discarded and stage 2 where the SRT was kept at 25 days. The permeate flux was kept constant at 20 L/(h m^2) together with the HRT (14 h) and a MLSS between 13.9-17.0 g/L for both cases. The backwash was done for 15 seconds after 10 minutes of filtration at an intensity of 600 mL/min. In summary the COD and colour removal was very high (>95 %,>97 %) and the stage 2 operation (SRT of 25 days) performed better than stage 1 operation. Despite an unsteady influent quality the MBR showed a stable removal efficiency because of the high MLSS concentration. The effect of different SRT to the COD removal efficiency of a conventional bioreactor and MBR was studied by Huang et al. (2001). They found a decreasing COD removal efficiency for the conventional bioreactor (70 % for 4 days, 80 % for 10 days) but a constant value (90%) at different SRT in the MBR. According to Khor et al. (2006) a long SRT leads to a removal of organic substances above 90 % because of a complete mineralisation and degradation of inert and soluble organic substances. For the removal of red dye-C81, of a synthetic textile wastewater, by an aerobic submerged hollow fibre MBR (PE membrane with 0.4 μm), Konsowa et al. (2013) showed a COD removal of 95 % and a dye removal efficiency of 90 %. You and Teng (2009) studied decolorization bacteria for the treatment of azo dyes (RB5) in a sequential anaerobic and aerobic MBR. For the aerobic MBR a COD influent of 310.6 $\pm$31.7 mg/L corresponding to a COD removal efficiency of 97.5 % are observed. An average colour removal rate of 83.7 % resulted for the aerobic MBR. More than 70 % of the RB5 degraded within 2.5 hours. After 5.5 hours 99 % degraded. The performance of a submerged lab-scale MBR for the treatment of model textile wastewater was studied by Deowan et al. (2016). They found an ammonium removal rate of 90 %. This high result is reasoned by the high sludge age (SRT>30days). As result a COD removal of 90 % and a red and blue colour removal efficiency of 25-70 %

and 20-50 % respectively was found. A removal rate for colour and COD of 100 % and 98 % was shown by Friha et al. (2015) while treating textile wastewater. Also Rondon et al. (2015) obtained a high COD removal rate of 99 % together with a dye removal of 95 % at HRT of 74.4 h. While studying the removal rate of organics and nitrogen in a three-stage textile wastewater treatment plant (Anaerobic, Anoxic and Aerobic MBR) Sun et al. (2015) showed an average removal rate for COD, NH_4-N and TN of 87 %, 96 % and 55 % respectively. Thereby it could be shown a good performance for COD removal meeting the discharge standards of COD<180 mg/L for China.

As a summary of this review it has been shown that MBRs have a good capability for textile wastewater treatment by the aerobic technology. Influent containing COD between 500 to 6000 mg/L, and a generally high colour removal efficiency are reported. A colour removal of more than 70 % and a COD removal of more than 80 % are shown in most cases. The TMP varied between 0.1 and 0.5 bar together with a flux between 5 to 40 L/(h m^2). MLSS values were between 4 and 15 g/L.

For this work, the model textile dye water (MTDW) described in section 4.8 was prepared based on the work done by Deowan (2013). The composition of the MTDW described in section 4.8 has been defined according to different publications [Alaton et al. (2002), Isik and Sponza (2008), Körbahti and Tanyolac (2009)]. One of the key factors for determining the effluent quality of the waste stream was the chemical oxygen demand (COD). Therefore, the composition has been maintained the same of the one used by Deowan (2013) for facilitating the comparison of the results obtained.

Table 3.2. Overview for MBR aerobic textile wastewater treatment ∗ modified from Jegatheesan et al. (2016)

Source	Influent COD [mg/L]	COD removal	Colour removal	MLSS [g/L]	TMP/flux	Reference
Textile wastewater	-	97 %	70 %	5-15	-	Badani et al. (2005)
Industrial, polyester finishing	1380-6035	75-91 %	46-99 %	-	0.4-0.6 bar, 19.5-23 L/h m²	Schoeberl et al. (2004)
Dye house wastewater	1606-2997	89-94 %	65-91 %	4	-	Schoeberl et al. (2005)
Textile wastewater	1380-6033	60-95 %	87 %	5	0.4 bar, 30 L/h m²	Brik et al. (2006)
Dye wastewater	3500±500	94.8 %	-	4.6±0.2	5 L/h m²	Yun et al. (2006)
Industrial dyeing and print wastewater from wool mill	128-321	80.3 %	58.7 %	0.4-3.8	0.174-0.203 bar, 6-15 L/h m²	Zheng and Liu (2006)
Mixed industrial wastewater	-	79 %	54 %	-	-	You et al. (2006)
Synthetic, containing BAA, an intermediate in anthraquinone dyes synthesis	-	50 %	>90 %	~3	0.01-0.03 MPa	Qu et al. (2009)
Textile mill	600-1200	85-92 %	60-75 %	9-11	0.05-0.1 bar, 2-8 L/h m² (stage 1) 0.14-0.56 bar; (stage 2) 0.27-0.34 bar; target constant flux 20 L/h m²	Huang et al. (2009)
Textile mill	1411	>95 %	>97 %	13.9	-	Yigit et al. (2009)
Synthetic	310.6 ± 31.7	97.5 %	83.7 %	2.7	-	You and Teng (2009)
Treatment plant (containing reactive Blue 4)	1100	TOC 88.2 %	91.3	-	<0.35 bar 7.5 L/h m²	Feng et al. (2010)
Synthetic, containing anthraquinone	778±70	~9 3 %	~98 %	4-5.5	4.5 L/h m²	Qin et al. (2012)
From two plants	500-2500	60-94 %/40-80 %/89-90 %	50 %/50-94 %/89-90 %	6-9	0.022-0.03 bar	Thanh et al. (2012)

Source	Influent COD [mg/L]	COD removal	Colour removal	MLSS [g/L]	TMP/flux	Reference
Synthetic, containing red dye CI81	2300	90.9-95.6 %	-	1-3	0.2-1.7 Psi	Konsowa, et al. (2013)
Synthetic textile wastewater	2500	90 %	20-50 %	12	0.5 bar	Deowan et al. (2016)
Textile wastewater	1463-3089	98 %	100 %	-	0.07-0.35 bar	Friha, et al. (2015)
Synthetic textile wastewater	1000	97 %	30-50 %	-	20 L/h m^2	Yurtsever et al. (2015)
Textile auxiliaries wastewater	320	87 %	-	-	-	Sun et al. (2015)
Textile wastewater	-	99 %	95 %	-	-	Rondon et al. (2015)

3.2 Surface modification techniques for membrane fouling reduction

Membrane fouling has been a subject of many studies since the industrial membrane processes emerged in the early 1960s [Kochkodan et al. (2014)]. The attempts to control the membrane fouling by choosing the appropriate membranes, adjusting the operating conditions in a membrane element, such as operating pressure and appropriate pretreatment are not sufficient to cope with the problem [Kochkodan et al. (2014)].

Nowadays, thanks to the good mechanical strength, excellent thermal and pH stabilities, its high flux and reasonable cost compared to the other membrane materials the PES has become the most popular membrane material for ultrafiltration and microfiltration membrane manufacturer [Nady et al. (2011)] [Rahimpour (2011)]. However, due to PESs natural hydrophobic intrinsic property, a relatively low surface energy and high water contact angle, the membranes made of it are vulnerable to adsorptive fouling [Nady et al. (2011)]. Therefore, surface modification for obtaining the desired surface properties which is not processed by the neat unmodified membranes and without changing the bulk (mechanical) properties has attracted extensive attention [Nady et al. (2011)]. The potential surface modification techniques for PES membranes can be divided into six main groups as shown in Figure 3.1.
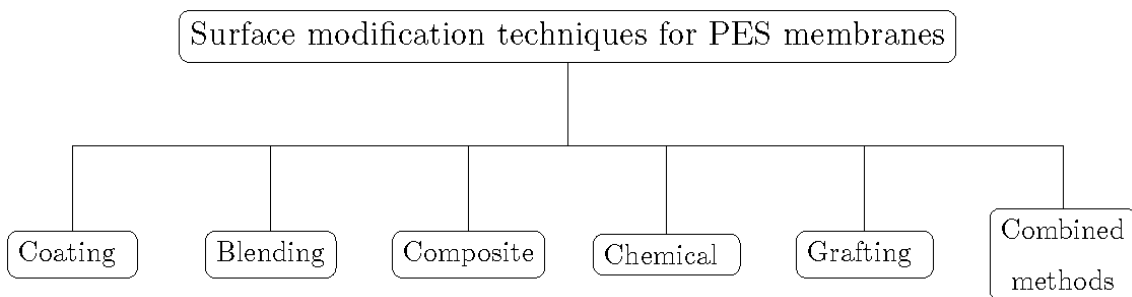
Figure 3.1. Surface modification techniques for PES membranes

Coating is a method where the coating materials form a thin layer that non-covalently adheres to the substrate, and grafting is a method where monomers are covalently bonded onto the membranes [Nady et al. (2011)]. A flexible technique to optimise hydrophilicity, smoothness and surface charge of the membrane surface is coating

a thin layer of water-soluble polymers or surfactants from solution by physical adsorption [Ba et al. (2010), Kim and Fane (1988)]. The findings showed that the fouling of UF membranes with proteins may be reduced by surface adsorption with water soluble polymers such as polyvinyl alcohol (PVA), methylcellulose (MC) and polyvinylpyrrolidone (PVP).

From the present data, over the last few decades, various surface modification methods in reducing membrane fouling with colloids and macromolecules, such as photoinitiated and redox grafting, physical coating with hydrophilic polymers, plasma treatment, chemical reactions on the membrane surface have been more or less successful [Kochkodan et al. (2014)]. In the whole process of membrane surface modification, many factors need to be considered, such as uniformity, reproducibility, stability, controllable process, and low cost [Kochkodan et al. (2014)]. Among the present surface modification techniques, UV/redox initiating graft polymerisation and physical coating of the membranes with hydrophilic polymers layers have the advantages of low cost of operation, mild reaction condition, simplicity to perform, and feasibility to be resembled into the end stages of a membrane manufacturing process [Kochkodan et al. (2014)].

To overcome the membrane fouling problems, many researchers have modified and tested membranes for MBRs. Table 3.3 gives a short review of some surface modification results applied for the MBR application in textile wastewater. Another promising approach to mitigate the fouling is to develop novel low-fouling membrane materials based on the polymerisable bicontinuous microemulsion (PBM) technology [Galiano et al. (2015)]. In general, the research strategy for reducing the fouling should address to low fouling membranes which should have much narrower pore size distributions, stronger hydrophilicity and larger porosity than the currently used membranes. But none of the modified membranes have been applied on a large scale so far due to some significant drawbacks, such as a complicated manufacturing process, increased production costs, complex surface chemistry of modified membranes [Yu et al. (2005a), Yu et al. (2005b), Yu et al. (2007), Yu et al. (2008)], process limitations [Bae and Tak (2005)] and very low permeability [Asatekin et al. (2006)]. The aim of this work was to develop a nano-stuctured low-fouling membrane in the direction of overcoming most of the actual limitations in wastewater treatment by MBR processes.

Table 3.3. Review of surface modification techniques for MBR application

Membrane modification process	Test media	Performance	Reference
Modification of hollow fiber membrane surface via NH3 and CO2 plasma treatment and acrylamide (AAm) and acrylacid (AAc) grafted membranes	Submerged MBR with municipal synthetic wastewater with COD of 700 mg/L	Flux decline: -2 to -14 %; Flux recovery with water cleaning: 6.4 to 15.5 %	Yu et al. (2005a), Yu et al. (2005b), Yu et al. (2007), Yu et al. (2008)
Novel NF membrane via coating commercial PVDF UF membrane with the amphiphilic graft copolymer PVDF-g-POEM	Activated sludge from aerobic MBR with COD of 350 mg/L	Initial WPs [L/h m² bar]: $WP_{um}=270$ $WP_m=3.9$; WP decline [%]: $WP_{um}=84$ $WP_m=$No; WP recovery with water cleaning [%]: $WP_{um}=27$ $WP_m=0$	Asatekin et al. (2006)
TiO_2 entrapped polymeric PVDF membranes prepared via phase inversion	Activated sludge with synthetic wastewater	Initial WPs [L/h m² bar]: $WP_{um}=303$ $WP_m=331$; WP decline [%]: $WP_{um}=98$ $WP_m=96$	Bae and Tak (2005)
Composite microfiltration membrane via blending polyvinylidene fluoride (PVDF) and hydrophilic graphene oxide (GO) nanosheets	Synthetic municipal wastewater	CF [L/h m²]: $CF_{um}=30\text{-}33$ $CF_m=48\text{-}50$; Required cleaning frequency: $C_{um}=3$ times for 60 days of operation $C_m=$No cleaning was required	Zhao et al. (2014)
Functionalized PVDF UF membrane via post-fabrication tethering of surface-tailored silica nanoparticles to poly(methacrylic acid)-grafted PVDF membrane surface	MBR supernatant	Initial flux 100 L/h m²; Flux decline [%]: $F_{um}=15$ $F_m=22$; Flux recovery with water cleaning [%]: $F_{um}=18$ $F_m=70$	Liang et al. (2014)
Quorum quenching (QQ) bacteria entrapped polymeric membranes prepared via phase inversion method	Real wastewater originated from a restaurant	Upper limit of TMP 0.4 bar; Time to reach TMP limit [days]: $t_{um}=3\text{-}10$ $t_m=23$; Deposition of biocakes on used membrane [mg]: $B_{um}=25.8\pm1.2$ $B_m=13.3\pm1.2$	Kim et al. (2014)

One approach of surface modification described by [Galiano et al. (2015)] is a coating of hydrophilic thin PBM layer by physical adsorption followed by redox based initiation techniques (see section 3.3). The UV-irradiation applied in grafting method can lead to severe degradation of the pore structure with loss of membrane function, which needs to be partially compensated by a grafted polymer. This is a drawback of this technique [Nady et al. (2011)]. By applying coating with an appropriate viscosity, the PBM cannot penetrate the PES membrane substrate, thus avoids the PBM from blocking the holes in PES membrane, furthermore it also prevents the possibility of PBM being initiated in the holes of the PES substrate membranes, which means prevent the pore structure of the substrate PES membrane from degradation.

UV curing technique has been widely used in coating industry. In membrane surface modification, UV initiated graft polymerisation has been widely used. This technique has several advantages such as being able to modify the polymer surface to have the distinct properties through choosing different monomers, or bonding the graft chains by covalent bond to have the long-term chemical stability [Kochkodan et al. (2014)]. These advantages enhance the resistance of membranes towards organic and bio-colloidal fouling. Moreover, applying UV curing technique on membrane surface modification requires less polymerisation time which made scale-up of the existing coating process for membrane more feasible.

3.3 Polymerisable bicontinuous microemulsion

In order to utilize the PES membranes in filtration process, many investigations about the surface modification of the PES material to make it more polar and less hydrophobic has been done. Porous membranes produced by microemulsion polymerisation has been first time studied in 1995. Gan et al. (1995) found that bicontinuous microemulsions (PBMs) can be polymerised by using a polymerisable zwitterionic surfactant (acryloyloxy)-undecyldimethyl -ammonio acetate (AUDMAA) to produce transparent solid polymeric materials with open-cell type microstructures. In this study, it was found that transparent solid polymeric materials can be produced by photoinitiated polymerisation of some of these microemulsion compositions containing methyl methacylate (MMA), water, ethylene glycol dimethacrylate (EGDMA).

Based on the combined weight of MMA and AUDMAA, they used 0.2 wt% of photoinitiator 2, 2-dimethoxy-2-phenylacetophenone (DMPA) to initiate the polymerisation of the microemulsion, and then the microemulsion was added into ampules which were later placed in ice-water bath and were purged with nitrogen at 1 atm for 10 min before being sealed. The photoinitiated polymerisation was carried out in a Rayonet photochemical reactor for 1 hour at 35 °C. As this work was focused on the investigation of new bicontinuous microemulsion systems at that time, there was no experiment about PBM cast onto any membranes. Furthermore, considering the polymerisation time of this PBM, this process was quite time consuming.

CHIENG et al. (1996) investigated the morphology, swelling and permeability characteristics of porous polymeric membranes made by PBM, which contained anionic surfactant sodium dodecyl sulfate (SDS) or cationic surfactant dodecyltrimethylammonium bromide (DTAB) along with MMA, HEMA, EGDMA, and redox initiator APS/TMEDA. The redox initiator was chosen because the polymerisation could be carried out at a relatively low temperature, 25 °C, in comparison with the paper of Gan et al. (1995). This system was able to minimise the occurrence of the phase separation as well as the evaporation of monomers. However, the polymerisation time of this process was 6 h, six times longer than in the work of [Gan et al. (1995)]. In this study, it was found that obtaining selective permeable membranes with desired pore size and pore size distribution was difficult, because only slight fluctuations in preparation conditions could lead to a broad pore size distribution. It was also observed in this study that the morphology, swelling and permeability characteristics of the membranes are highly dependent on the concentration of surfactant in both SDS and DTAB systems. With increasing DTAB concentration, the pore size of the DTAB system decreases, while the reverse trend was found in SDS system. The membrane prepared using SDS has larger pore sizes in the range of 100 nm to 3 μm as compared to DTAB that is less than 100 nm.

Gan and Chew (1997) successfully obtained a transparent microporous composite by polymerisation of a PBM containing MMA, HEMA, and a polymerisable nonionic surfactant ω-methoxy poly (ethylene oxide)40 undecyl-α-methacrylate (PEO-R-MA-40). By photoinitiated polymerisation at about 35 °C microemulsions gelled within 30 min. It was found that the pore dimension (<100 nm) of the microstructural composites can be varied by adjusting the aqueous content in microemulsion. Li et al. (1997) coated and polymerised PBM onto the internal surfaces of hollow-fiber

membranes. The coated membranes were studied for their separation efficiency and permeation rate of PEG solutions. The PBM containing MMA, DI water, HEMA, EGDMA, APS/TMEDA and a polymerisable surfactant AUDMAA formed a transparent thin film after being kept in a nitrogen chamber overnight, which was quite a time-consuming process as well. This microemulsion coated membrane showed different performance of PEG separation and permeation that strongly depend on the concentration of HEMA and water in the precursor bicontinuous microemulsion. By increasing the concentration of HEMA to 13 wt% in the precursor bicontinuous microemulsion, the pore size could be moved from 40 to 2 nm and by decreasing the water content from 50 wt% to 30 wt% the pore sizes also decreased from 3.4 to 1.6 nm, which enhances the UF performance due to the small pores on the skin of the membrane. The in-situ polymerisation enables the microstructures of coated membranes to be better controlled. Furthermore, the PBM coated membranes showed higher permeation rates than those membranes solely made by same bicontinuous microemulsion.

Chew et al. (1998) studied PBMs containing MMA, HEMA, EGDMA with the polymerisable ziwitterionic surfactant AUDMAA or a cationic surfactant (acryloyloxy)undecyltrimethylammonium bromide (AUTMAB), by applying 0.2 wt% photoinitiator (DMPA) based on the combined weight of MMA and surfactant. The microemulsion gelled within about 6 min of polymerisation at 45-57 % conversion and then produces a transparent solid polymeric materials. The wavelength of the Rayonet photochemical reactor was set at 253.7 nm. PBMs investigated in this paper were not coated onto membranes.

Kaeselev et al. (2002) published an article about the influence of the surface structure to the filtration performance of UV-modified PES membranes. In his experiments the presence of a monomer during UV-irradiation seemed to retard loss of membrane selectivity compared with membranes irradiated in the absence of any monomers at the same energy density Kaeselev et al. (2002).

The application of transparent nanostructured polymers prepared from PBM sparked interest in recent years. Wang et al. (2004) reported the synthesis and application of a thermosensitive polymer poly(N-isopropyl acrylamide) (PNIPAAm) prepared by bicontinuous microemulsion polymerisation. In their study, nanostructured thermoreversible PNIPAAm was photopolymerised in bicontinuous microemulsion con-

sisting of: MMA, HEMA, NIPAAm, polymerisable macromonomer surfactant C1-PEO-C11-MA-40, and DMPA by applying a UV reactor for 6 hours. This bicontinuous microemulsion was poured onto a glass plate and then spread by levering another glass plate onto it to ensure absence of air. The photoinitiated polymerisation produced transparent and nanostructured polymeric membranes which showed temperature-dependent swelling behaviour with higher water uptake at lower temperature. Thanks to this and their transparent nanostructured property, these membranes have a potential to be used as wound dressing materials and supports for cell grafting.

In 2006 Bosch et al. (2006) published their work about the fluoroscene monitoring of photoinitiated polymerisation reactions. Bis-(2,4,6-trimethylbenzoyl)-phenylphosphine oxide (trademark Irgacure 819 ®) was used as photoinitiator. Also in other publications [Peinado et al. (2006) and Bosch et al. (2006)] they described the successful usage of this initiator. A concentration of 1 % Irgacure 819 as photoinitiator was used for the preparation of various microemulsions using different compositions of MMA, DMAEMA and EGDMA. As UV lamp they used a 400 W Hg medium-pressure lamp and twin quartz optical fiberguides.

In the field of surface modification of flat sheet membranes for the application in the wastewater treatment, Galiano et al. (2015) was the latest that reported a novel PBM prepared by a cationic surfactant acryloyloxyundecyltriethylammonium bromide (AUTEAB). The surfactant has been proved to be anti-microbial, and the PBM its anti-fouling properties. The polymerisation is based on redox initiators APS/TMEDA. The work described by Galiano et al. (2015) represents the basis of this work. In summary all of the PBM based polymerisation processes described in this section have a long polymerisation time in common which is a serious challenge for a commercial application of the coatings.

4 Materials and Methods

4.1 Revamp of lab-scale MBR

In this section the revamp of a lab-scaled MBR is described in detail. In the previous work of Deowan (2013), the MBR setup only allowed the single run of one membrane at a time. It is very difficult to stimulate the biology inside the reactor in such a way that the conditions for the experiment are reproducible when the membranes are tested one after the other. Therefore, a new setup for experiments in parallel was developed.

4.1.1 Previous design of MBR unit

The MBR was previously designed by Koreba (2010). A polyvinyl chloride (PVC) tank was used to build the oxygenated biochemical tank with a total volume around 60 L. The hydraulic volume is 59 L after submerging the MBR module. The system includes membrane module, air compressor, level sensor, differential pressure sensor, feed pump, permeate pump, foam sensor, flow sensor, pH sensor, temperature sensor, conductivity sensor, and air flow meter (see Figure 4.1).

A commercial membrane from Microdyn-Nadir Company (UP 150T) was submerged in the reactor tank [Deowan (2013), Deowan et al. (2016)]. This membrane was composed of hydrophilic polyethersulfone (PES). The dimension is 25x25 cm with pore size of 0.04 μm. The module consists of three flat sheets, which gives a total active membrane surface of 0.34 m^2 (see Table 4.1). The membrane and the reactor tank were equipped with a coarse bubble system connected with an air compressor. The membrane was submerged in the hydraulic volume of the reactor tank underneath the level sensor position. Table 4.1 shows the properties and recommended ranges for the UP 150T used in the MBR.
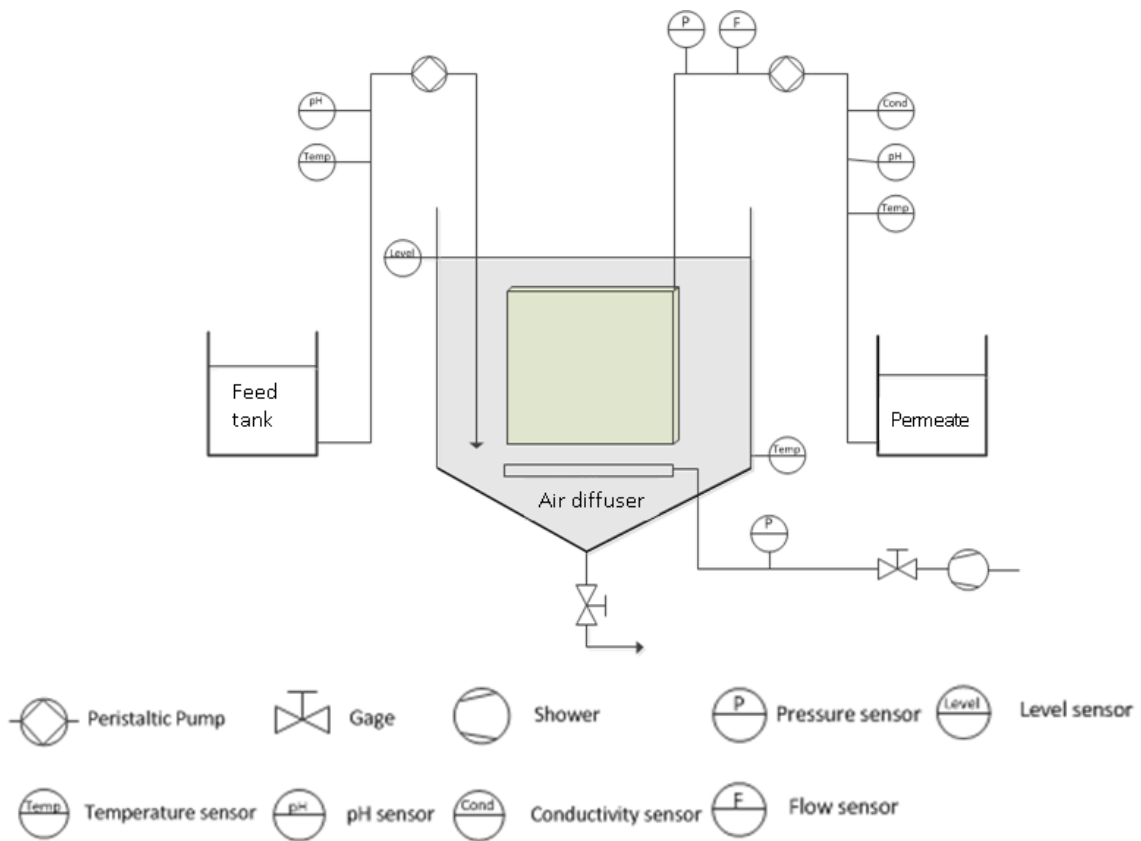
Figure 4.1. Schematic diagram of the previous MBR unit (adapted from Koreba (2010))

Table 4.1. Membrane material and operation data

Polymer	Polyethersulfone
MWCO	150 kDa
Pore Size	0.04 μm
Drainage	Polyester
Membrane Surface	0.34 m^2
Operating pressure	-30 to -400 mbar
Max. Backwash pressure	150 mbar
Max. Operating temperature	40 °C
pH-range	2-11
Max. air flow rate	6 m^3/h
Recommended content suspended solids	12 g/L
Water permeability (DI)	>250 L/h m^2 bar

4.1.2 New design MBR unit

As a variety of influences like temperature, sludge age, oxygen-supply and pH of the feed solution are influencing the biocenosis in the reactor [Buck and Buck (1987)], it is difficult to compare the efficiency of two different membranes as long as they are not tested under the same conditions.

Therefore, the current setup needed to be redesigned to allow the testing of two membranes at the same time. The following list gives an overview of the necessary steps for the new design of the MBR-unit and Figure 4.2 shows the revamped schematic.
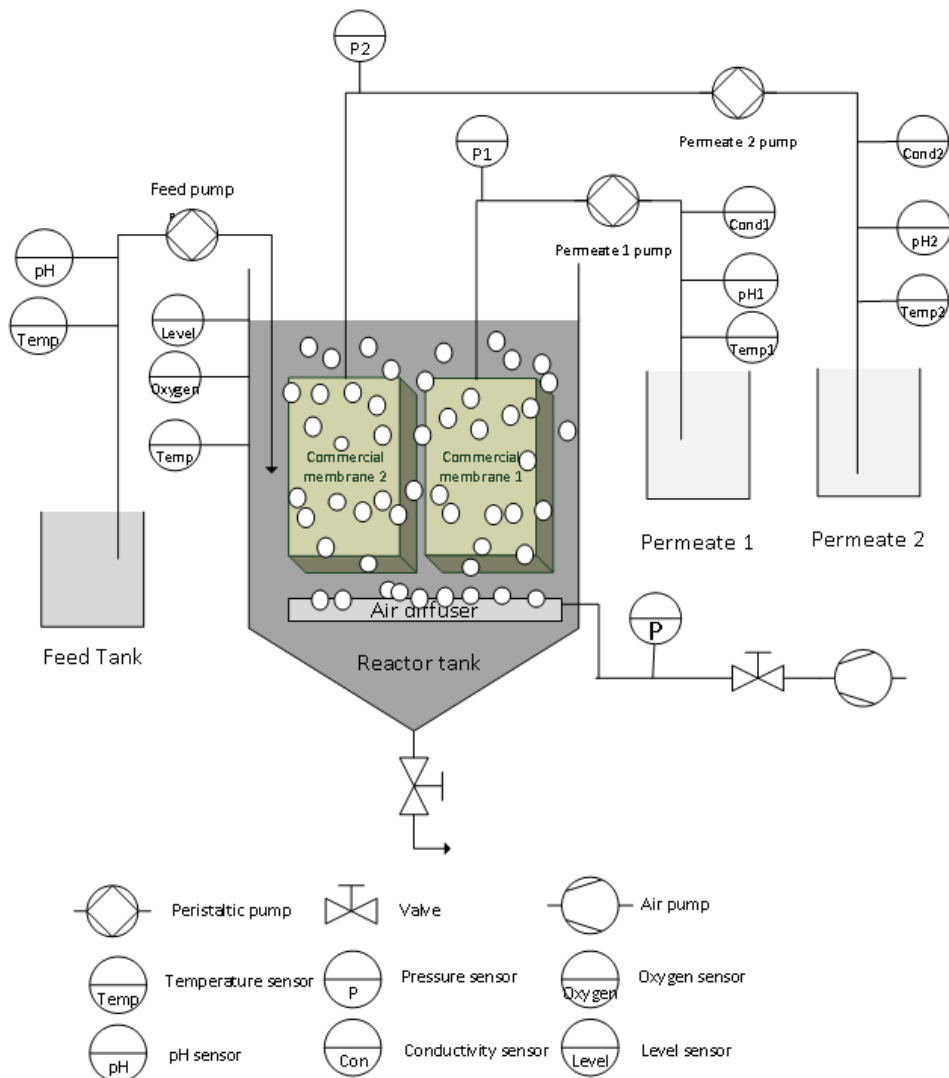
Figure 4.2. Schematic diagram of the revamped MBR unit

- design of the new setup using a CAD-Software (computer aided design) to create technical drawings of the new parts and to highlight dimensions to adjust new parts and sensors

- create a second permeate line for the additional membrane including sensors and a flexible-tube pump

- development of an alternative to the previous anti-foaming system that is using a special anti-foaming liquid that could have some effect to the bacteria activity

- reprogramming of the data acquisition system for the connection of the new sensors

- creation of new circuit boards needed for the data transfer from the sensors to the data acquisition system

- optimizing the oxygen supply of the bacteria to stimulate their activity

Membrane housing

This section describes the new design of the membrane housing and highlights the differences to the previous design. Figure 4.3 compares the old and the new design of the membrane housing.
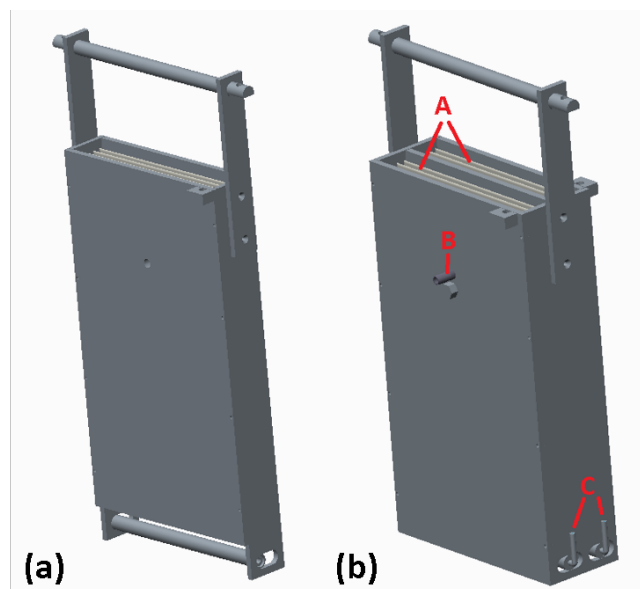
Figure 4.3. Single (a) and double (b) membrane housing

As shown, the new design allows two membrane modules (A) to be adjusted to the housing. Therefore it enables two membranes to be tested in long term and in parallel. As a result of that, an additional connection for the second permeate line (B) and aeration pipe (C) for the cross flow of air bubbles on the membrane surface had to be designed and the single parts adjusted to the new dimensions. The technical drawings of the new membrane housing can be find in the Affix.

Second permeate line

The second permeate line requires an additional tube pump in order to create the mandatory suction pressure. The same parameters as those in the first permeate line had to be considered in order to characterize the efficiency of both membranes tested. Therefore, sensors for pH, temperature, conductivity, volume flow and suction pressure had to be selected, ordered and installed. To connect the sensors to the permeate line it was necessary to create different options to connect them to the frame of the MBR. Figure 4.4 and 4.5 show the custom-made connection parts for the pH, conductivity and volume flow sensors.
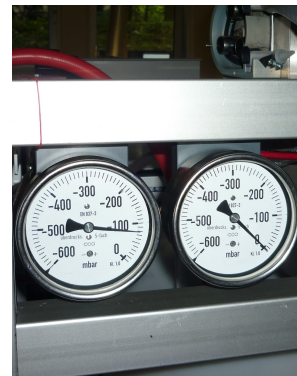
Figure 4.4. Connection of the sensor holders

Figure 4.5. Piping of the sensor holders

Figure 4.6. Analogue pressure sensors

All sensors have to be calibrated periodically to assure proper values. Additional analogue manometers (Figure 4.6) were installed in both permeate-lines which can be used to check the digital value for the suction pressure easily and also for calibration purposes.

Oxygen Sensor

Previously a hand measurement tool for the dissolved oxygen in the reactor was used. By hand measurement a non-homogeneous distribution of the oxygen inside of the reactor was found. Therefore, it was difficult to get comparable results as the values could not be taken from the exact same spot due to the handling procedure. So in order to get online values, for convenience and to enable the measurement of the oxygen distribution in different heights the reactor was equipped with a sensor that is continuously measuring. For that purpose a sensor holder had to be designed that is water proof and allows the sensor to be mounted at different heights of the reactor. This flexibility allows the monitoring of the oxygen at a fixed spot inside the reactor as well as the homogeneity of the oxygen by comparing the results of different heights. Figure 4.7 shows how the depth of the sensor can be adjusted by the use of two screws (Figure 4.8).

Figure 4.7. Oxygen sensor with customized holder
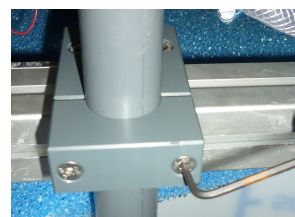
Figure 4.8. Adjusting screws of oxygen sensor

Anti-foaming system

The previous setup used an anti-foaming oil in order to prevent the foaming of the reactor liquid. Based on discussions with the production company of the membranes it has been decided to search for alternative options for the anti-foaming, as the oil itself may have an impact on the membrane characteristics. After considering different ideas for a solution one idea got further developed. Figure 4.9 shows where the initial inspiration for the novel anti-foaming system came from. The basic idea is to circulate the reactor liquid and create a shower on top of the reactor. As soon as foam gets in contact with the rinsing water the surface tension of the foam should collapse. In order to test this idea a simple pump was brought together with some piping and a sprinkling device that is usually used for gardening. Due to the fact

that the built up creation of foam is a process that takes several hours it has been decided to run the pump just for 5 minutes every 2 hours. After a long term test over 4 weeks this system turned out to be feasible.

Figure 4.9. Initial idea for the novel anti-foaming system

Figure 4.10 shows the test setup of the anti-foaming system and Figure 4.11 shows the final setup of the system in the reactor. The holding unit for the sprinkling device is designed in such a way that it can be adjusted 3-dimensional. Figure 4.12 shows how the sprinkling device can be adjusted in three axes. Therefore it is possible to exactly install this unit in the centre of the reactor and in the ideal height. A valve (Figure 4.14) allows to control the intensity of the rinsing. Figure 4.13 shows how the unit was installed in the reactor tank.
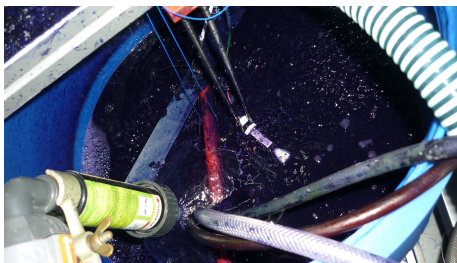
Figure 4.10. Test setup of the anti-foaming system
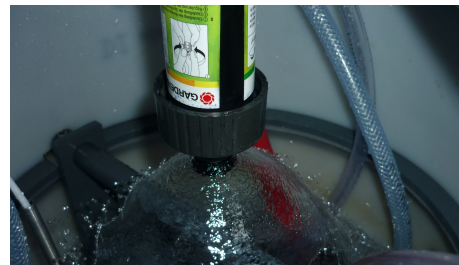
Figure 4.11. Final setup of the anti-foaming system

As another sanction against the foam the distance from the reactor liquid to the top part of the reactor was increased. This allows the installation of the sprinkler to a height above the previous highest position. First of all a channel had to be milled into the top reactor holder in order to assure a proper connection of the top part (Figure 4.15 to 4.16). Afterwards the top part had to be cut in addition to the necessary geometry (Figure 4.17). Finally a cover was installed at the top of the reactor in order to protect the surrounding against small drops in case the regulation valve for

the sprinkler is set too strong. The material that was chosen is ultra porous and therefore allows the air to easily pass but retains any drops. Figure 4.18 to Figure 4.20 show the production of the cover and its final placement in the system.

Figure 4.12. Anti-foaming holder
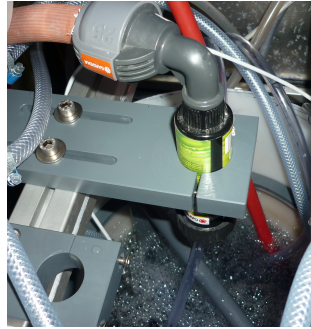
Figure 4.13. Anti-foaming holder in reactor

Figure 4.14. Drossel valve
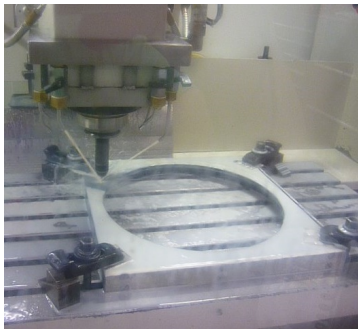
Figure 4.15. Milling of channel

Figure 4.16. Test if top part fits

Figure 4.17. Cut of the top part
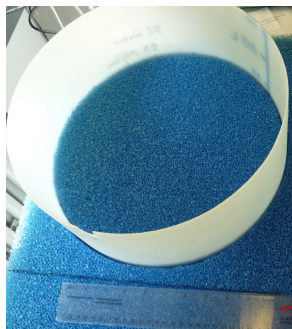
Figure 4.18. Cover material with top part

Figure 4.19. Cut of the channel for the top part
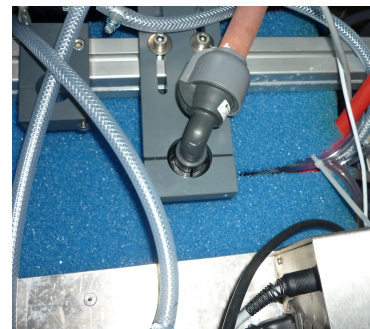
Figure 4.20. Final cover installed in MBR

Sample taking valve

For the purpose of measuring different parameters like MLSS and oxygen consumption of the reactor liquid it is necessary to frequently take samples from the reactor. Therefore a valve has been installed in the middle of the reactor. Using this valve it can be assured that the samples are taken from the same spot every time and additionally the handling is much easier. Figure 4.22 shows the 3-way-valve that is connected to the reactor using a tank connector.
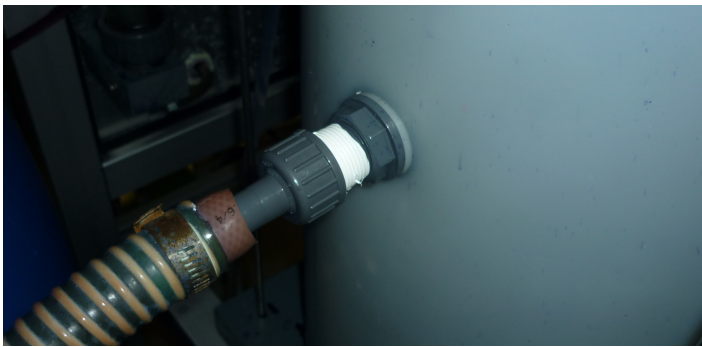
Figure 4.21. Connector at the reactor tank
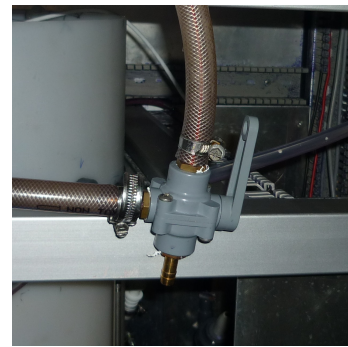
Figure 4.22. Sample taking valve

4.1.3 Data acquisition hardware

The existing sensor system had to be revamped in order to realise the data transfer to the new sensor setup. The data acquisition system, includes sensors, transmitters and a controller. The sensors were connected with transmitters through the IP67 jack connector on the front board. The output signals of the connector went to the terminal blocks and were defined clearly by the name of each sensor. The terminal block was also connected with the power supply for the sensors. From the terminal, only the signal wires were plugged with transmitters. In this part, only the transmitter for the flow sensors was self made, the other transmitters were used from Meinsberg Electrodes Company. Industrial standard signals (0 to 5 V) were connected with Meilhausbox (ME-REDLAB PDM-1208FS). This application used eight A/D ports to convert analog to digital, eight digital inputs, eight digital outputs and two analogue outputs. Finally, a computer with the program LabVIEW

was set up with a communication interface of Meilhausbox. Figure 4.23 shows the general arrangement of the data acquisition system.
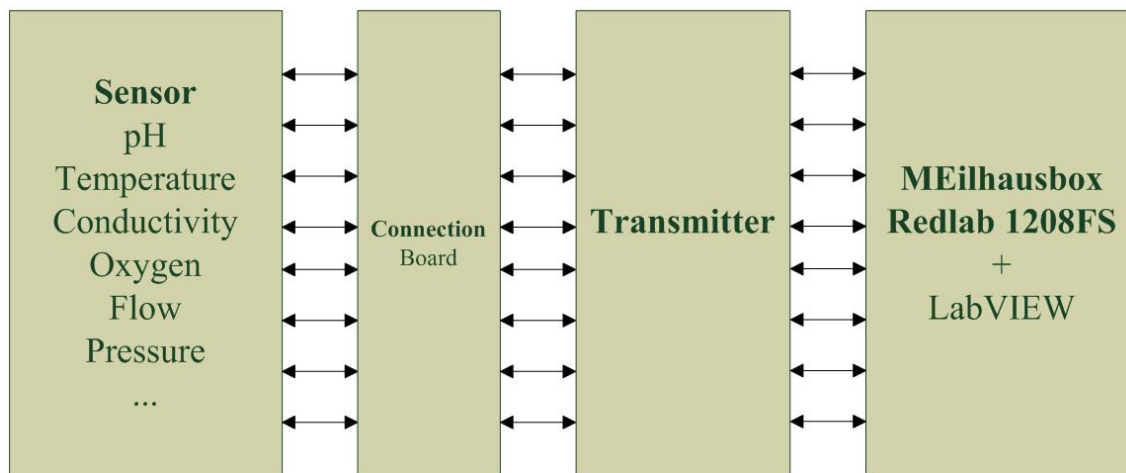
Figure 4.23. Wiring of the data acquisition

Oxygen/temperature sensor

The Oxygen sensor was chosen from Meinsberg Electrodes Company with an integrated temperature compensation. The sensor was also used to measure the temperature in the reactor tank. The range of the sensor is from 0 to 60 mg/L in water or 0 to 200 % for air saturation. The operating condition is from -5 to 45°C.

Figure 4.24. Oxygen Sensor MF 39 [Meinsberg (2014b)]

The sensor was plugged with transmitter MV3030 (Figure 4.25) which needed a power supply of 24 V. The output voltage is from 0 to 5 V. There are two output signals, which are oxygen and temperature.
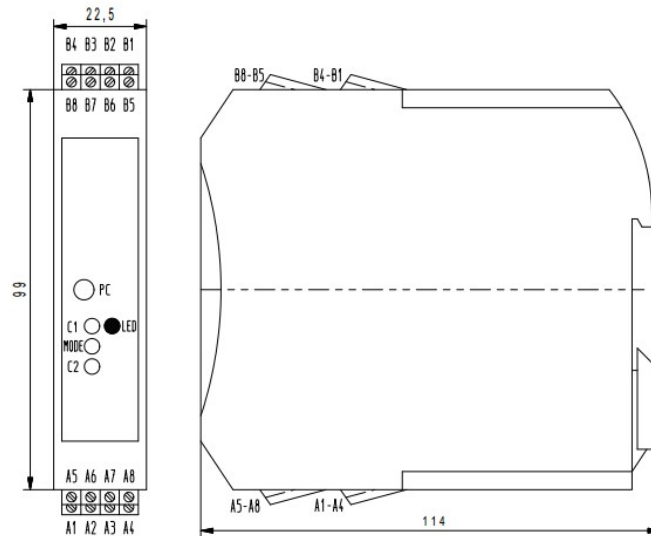
Figure 4.25. Transmitter MV3030 [Meinsberg (2014c)]

pH / temperature sensor

The pH sensor EGA143 from Meinsberg Electrodes has a pH range from 0 to 14 with a combined temperature sensor PT1000. The operating temperature is from -5 to 80 °C.

Figure 4.26. pH sensor EGA 143 [Meinsberg (2014d)]

The pH sensor is connected with the Meinsberg MV3010 transmitter described in section 4.1.3.

Conductivity sensor

The conductivity sensor called LTC 0,35/23 from Meinsberg Company has the range of 5 μS/cm to 500 μS/cm with an operating temperature range of -5 to 80 °C.

Figure 4.27. Conductivity sensor LTC 0,35/23 [Meinsberg (2014a)]

The conductivity sensor is connected with the Meinsberg MV3010 transmitter described in section 4.1.3.

4.1.4 Data acquisition software

For data acquisition the software LabVIEW (Laboratory Virtual Instrument Engineering Workbench) is used. It was supplied by National Instruments and the graphical language is called "G". LabVIEW uses symbols to make a circuit diagram. Moreover, LabVIEW offers wide communication to all devices that have the interface to control or transmit data. It can be used with an included library. Figure 4.28 shows the program structure made for the MBR. It consists of programs, which are executed sequentially. At the beginning, the software calls the main while loop that keeps the whole LabVIEW program running and allows it to call individual programs. Each part of the program (calibrations, configuration, etc.) can be executed when an appropriate event (button) occurs. The buttons were located outside the event structure and had the same name. Therefore, it is possible to start an event structure independently of the other structures. When an event was called, only the program inside this event structure could be run. Normally, the program, which is arranged in stacked structure, is processed sequentially. Figure 4.29 shows the front panel of the previous main program with a control and display element. All of the register cards are associated with event structures. The main program will be started with measurement and supervision of MBR system. In the program structure, all of the structures in sequence were put in a time loop, which was executed after a certain time interval. This means whenever the sub-program for data measurement and storing data was finished, it must wait until the period ending time.
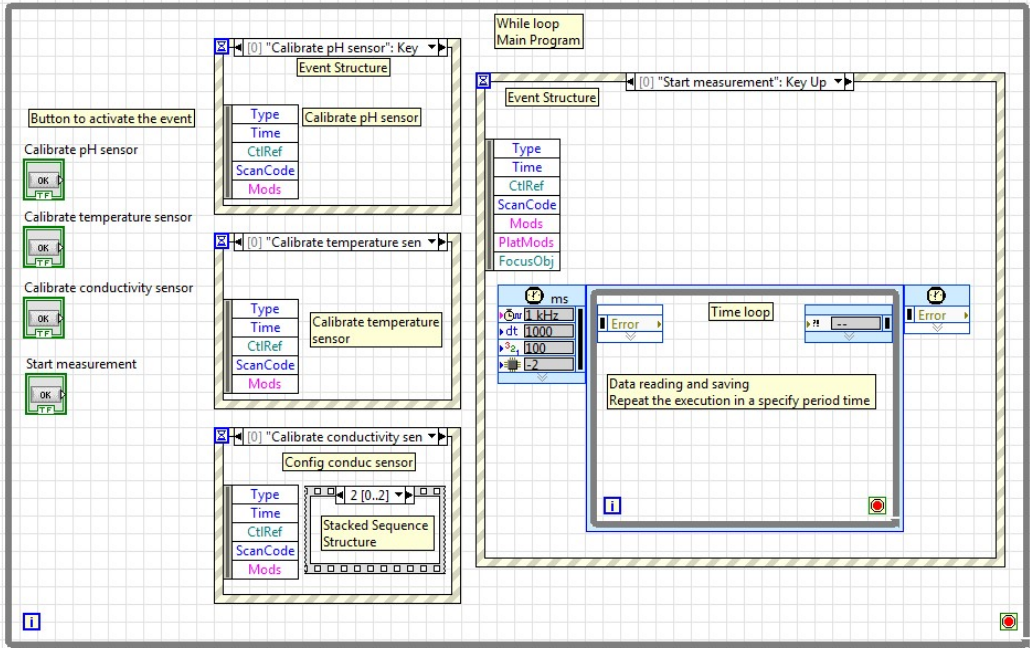
Figure 4.28. Program structure of LabVIEW
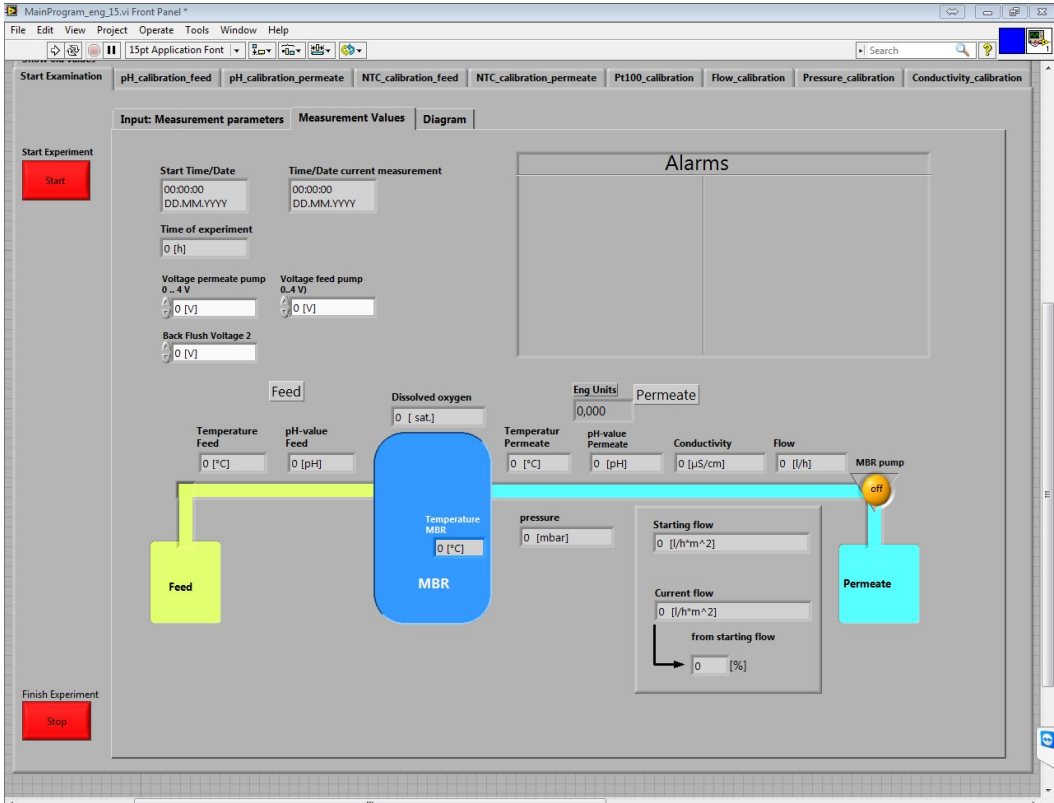
Figure 4.29. Registercard of main program interface

Redesigned data acquisition software

Figure 4.30 shows the redesigned front panel. The pH, temperature, conductivity and flow sensors were programmed for the data acquisition of the second effluent together with the oxygen sensor for the reactor.
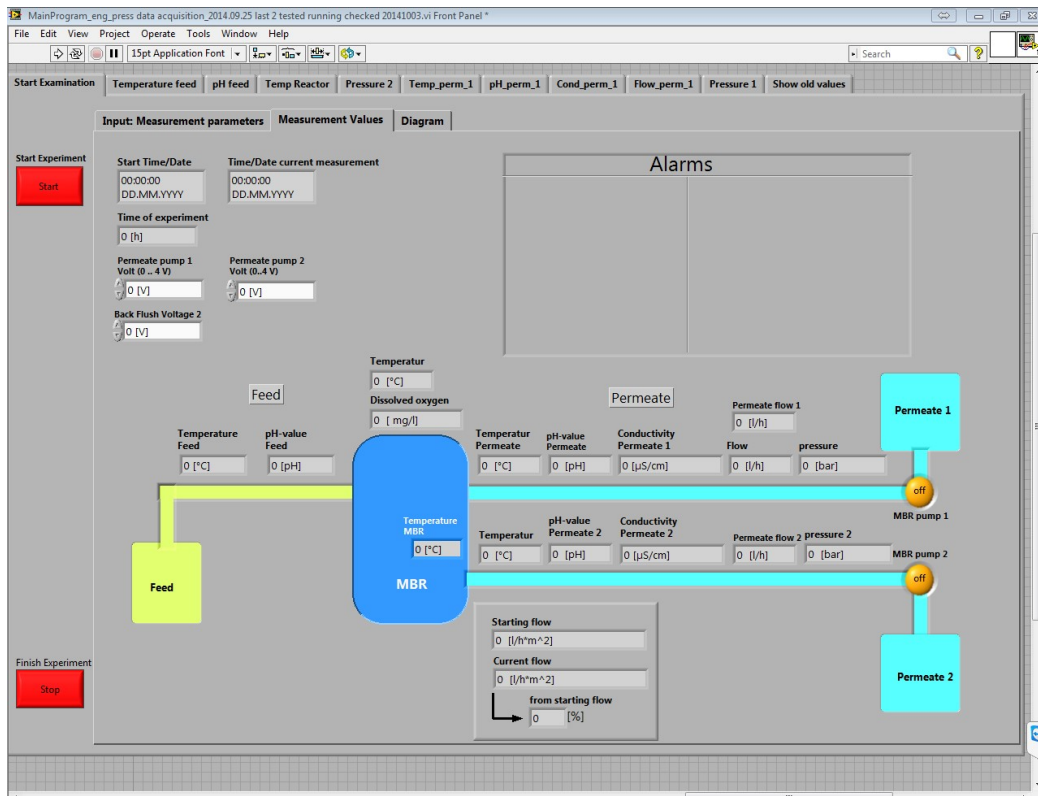
Figure 4.30. Revamped front panel of LabVIEW

4.1.5 Wire connection

The following transmitters use a plug for the connection with the front panel of the control board. Figure 4.31 shows their connection.
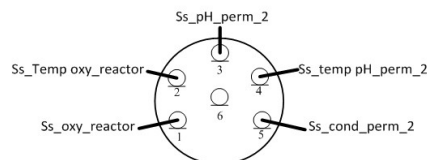
Figure 4.31. Plug for front panel connection

A cable supplied by the manufacturer of the sensor called K-VP was used to connect the sensors to the transmitters. As the wiring is the same for the oxygen/temperature, pH/temperature and conductivity sensor, the wires connection is shown just exemplary in Figure 4.32.
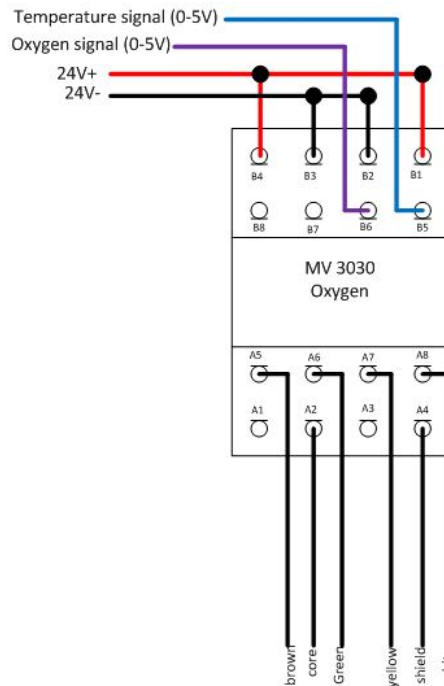
Figure 4.32. Wiring of Oxygen sensor

For the pH/temperature sensor the cable K19 given by the sensor company is used to connect the sensor with the transmitter called MV3010. Cable K17 is connected to the terminal of transmitter MV 3025 for the conductivity sensor.

Meilhausbox

A Meilhausbox is used to convert the analogue to digital signals supplied by the sensors. The Meilhausbox offers four different analogue inputs or eight single ends analogue input with the ground reference. Table 4.2 and 4.3 show the signal and control wiring of the Meinhausbox.

Table 4.2. Signal wiring of Meilhausbox

Data acquisition	Relay pin 1 Digital A2 = 0	Relay pin 14 Digital A2 = 1
CH0	Conductivity of permeate 2	pH of permeate 2
CH1	Spare part	Temperature of permeate 2
CH2	Pressure membrane 2	Voltage in conductivity of permeate 1
CH3	Temperature of oxygen in	Current in conductivity
CH3	reactor tank	of permeate 1
CH4	Oxygen in reactor tank	pH of permeate 1
CH5	Temperature in reactor tank	Temperature of permeate 1
CH6	Temperature of feed water	Spare part
CH7	pH of feed water	Pressure membrane 1

Table 4.3. Control wiring of Meilhausbox

Control pin		Name
Digital	A0 output	On/off conductivity 1
	A2 output	Multiplexer
	A3output	Multiplexer relay of flow sensor
	A4 output	Air pump
	A5 output	Start/stop of counter for flow sensor
	A6 output	Start/stop pump 1 + 2
	A7 output	Direction pump 1 + 2
	B7 input	NOT AUS (emergency signal)
Analog output	D/A A0	Analog pump 1
	D/A A1	Analog pump 2

4.2 Polymerisable bicontinuous microemulsion

Within this work two kind of polymerisation techniques are studied. In the initial phase the redox based polymerisation described by Galiano et al. (2015) was reproduced in order to justify the results. Afterwards the photoinitiator based polymerisation has been studied as novel technique for the polymerisation of the PBM. The compositions for both techniques are described in the following sections 4.2.1 and 4.2.2.

4.2.1 Redox based PBM
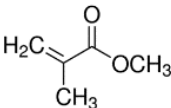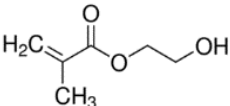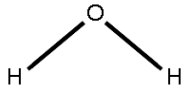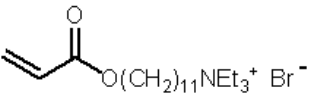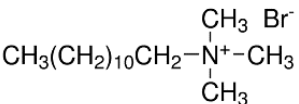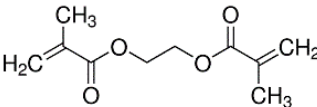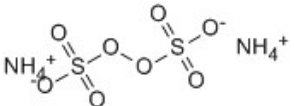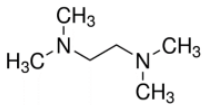
The chemicals used for preparing the PBM were supplied by Sigma Aldrich, BASF and Esstech, Inc. Compositions of PBM were developed by Galiano (2013), Galiano et al. (2015). In the following the composition used for preparing the PBM initiated by redox initiator is given. Each chemical and their function in PBM are described detailed in Figure 4.33.
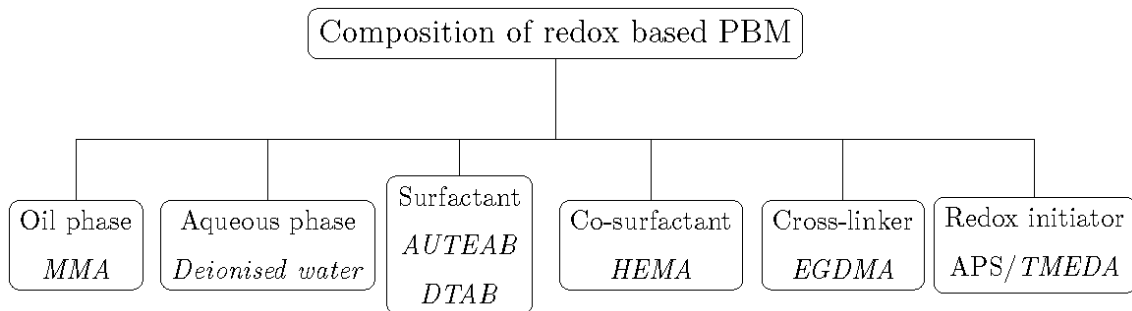
Figure 4.33. Composition of redox based PBM

Table 4.4 shows details about the chemicals that were applied for the redox based PBM.

Table 4.4. Constituents of redox based PBM

Chemicals	Supplier	Purity	Molecular weight [g/mol]	Molecular structure
Methyl Methacrylate (MMA)	Sigma Aldrich	99 %	100.12	
2-Hydroxylethyl methacrylate (HEMA)	Sigma Aldrich	>99 %	130.14	
Deionised water (DI water)	Lab produced	conductivity < 10 μS/cm	18	
Acryloyloxy-undecyltriethyl ammonium bromide (AUTEAB)	University of Calabria	>95 %	374.44	
Dodecyltrimethyl ammonium bromide (DTAB)	Sigma Aldrich	98 %	308.34	
Ethylene glycol dimethacrylate (EGDMA)	Sigma Aldrich	98 %	198.22	
Ammonium persulfate (APS)	AppliChem GmbH	>98 %	228.20	
N,N,N'N'-tetramethylethylene (TMEDA)	Sigma Aldrich	99 %	116.20	

Methyl methacrylate (MMA) which was used in this PBM is a monomer for constituting the oil phase of the microemulsion. Short chain alcohols can be added to microemulsions to lower the surface tension of the interfacial film [Leung and Shah (1987)]. Therefore, the short chain alcohol 2-Hydroxylethyl methacrylate (HEMA)

was added as a co-surfactant in order to facilitate the dispersion of the oil phase and the aqueous phase in the microemulsion [Galiano (2013)]. Deionised water was added to constitute the aqueous phase of the microemulsion. Acryloyloxyundecyltriethyl ammonium bromide (AUTEAB) is a polymerisable cationic surfactant which was produced at Laboratory of Industrial and Synthetic Organic Chemistry (LISOC), Department of Chemistry and Chemical Technologies of the University of Calabria. AUTEAB contains a quaternary ammonium group and an acrylate group. The quaternary ammonium salts have an important anti-microbial activity which is especially effective against gram-positive bacteria and fungi [Galiano (2013), Galiano et al. (2015), Gregan et al. (1998)]. The double bond in acrylate group is very reactive and polymerisable. Therefore, AUTEAB is a reactive and polymerisable surfactant which can be attached by chemical bonds to the polymeric network [Galiano (2013)]. The cationic surfactant Dodecyltrimethyl ammonium bromide (DTAB) contains also a quaternary ammonium group. Whereas due to the absence of the acrylate group, it is not polymerisable. DTAB was chosen to be applied in first trials for its commercial availability and low price [Galiano (2013)]. Ethylene glycol dimethacrylate (EGDMA) was added as a cross-linker. Ammonium persulfate (APS) and N,N,N'N'-tetramethylethylene (TMEDA) were added as redox initiators. APS and TMEDA start the polymerisation reaction at relatively low temperature, therefore the occurrence of phase separation and evaporation of monomers can be minimised [Deowan (2013)]. In Table 4.5, the optimal compositions of PBMs which contained commercial available surfactant DTAB and lab-made surfactant AUTEAB are listed respectively.

Table 4.5. Composition of redox based PBM

Chemicals	10 w% DTAB	25 w % AUTEAB
Methyl Methacrylate (MMA)	10 w%	21 w%
2-Hydroxylethyl methacrylate (HEMA)	40 w%	10 w%
Distilled Water (DI water)	40 w%	41 w%
Ethylene glycol dimethacrylate (EGDMA)	4 w%	3 w%
Ammonium persulfate (APS)	0.3 w%	0.3 w%
N,N,N'N'-tetramethylethylene (TMEDA)	40.5 μL	28 μL

4.2.2 Photoinitiator based PBM

The chemicals used for preparing the PBM initiated by photoinitiator are shown in Figure 4.34.
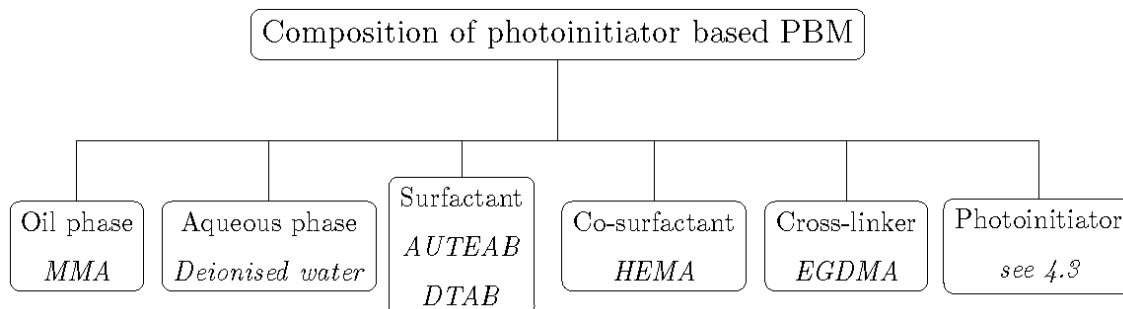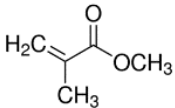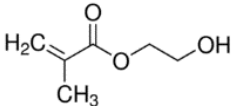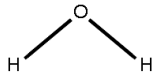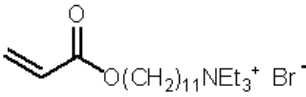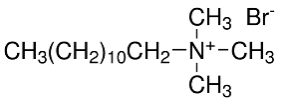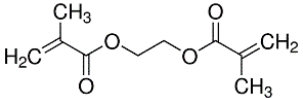
Figure 4.34. Composition of photoinitiator based PBM

The surfactant called AUTEAB is synthesized at Laboratory of Industrial and Synthetic Organic Chemistry (LISOC), Department of Chemistry and Chemical Technologies of the University of Calabria, Italy consisting of a double bond which could be chemically fixed and therefore keeping its anti-microbial properties after washing the membrane [Galiano et al. (2015), Galiano (2013), Deowan (2013), Figoli et al. (2015)]. For the synthesis chemicals with a purity higher than 98 % were purchased from Sigma-Aldrich [Galiano et al. (2015)]. Starting from the commercially available 11-bromoundecanol a esterification and quaternization step lead to the production of AUTEAB [Galiano et al. (2015)]. All other components of the PBM, given in Table 4.6, are purchased commercially (Sigma-Aldrich). Further information about the studied photoinitiators is given in section 4.3.

As shown, in contrary to the redox based PBM, photoinitiators are used to form the radicals needed for the polymerisation of the PBM. In order to get the optimal composition, both surfactants DTAB and AUTEAB were tested with different photoinitiators respectively. The composition of PBM containing photoinitiators is shown in Table 4.7.

Table 4.6. Constituents of photoinitiator based PBM

Chemicals	Supplier	Purity	Molecular weight [g/mol]	Molecular structure
Methyl Methacrylate (MMA)	Sigma Aldrich	99 %	100.12	
2-Hydroxylethyl methacrylate (HEMA)	Sigma Aldrich	>99 %	130.14	
Deionised water (DI water)	Lab produced	conductivity < 10 μS/cm	18	
Acryloyloxy-undecyltriethyl ammonium bromide (AUTEAB)	University of Calabria	>95 %	374.44	
Dodecyltrimethyl ammonium bromide (DTAB)	Sigma Aldrich	98 %	308.34	
Ethylene glycol dimethacrylate (EGDMA)	Sigma Aldrich	98 %	198.22	

Table 4.7. Composition of photoinitiator based PBM

Chemicals	10 w% DTAB	25 w%AUTEAB
Methyl Methacrylate (MMA)	10 w%	21 w%
2-Hydroxylethyl methacrylate (HEMA)	40 w%	10 w%
Deionised Water (DI water)	40 w%	41 w%
Ethylene glycol dimethacrylate (EGDMA)	4 w%	3 w%
Photoinitiator	0.6 w%	0.6-2.2 w%

Storage properties

In order to study the storage behaviour of the photoinitiator based PBM (final composition described in section 5.2.3), the PBM was kept without access to light at room temperature in order to study its stability in time. This is especially interesting for a potential commercial application as the PBM can be prepared together with the photoinitiators and kept in a storage tank before the coating onto the membranes. Even after one month the PBM did not polymerise and kept the microemulsion. The application onto a membrane resulted in a successful coating. Further experiments should be done to check for chemical decompositions after time.

4.2.3 Preparation of PBM

In order to prepare the PBM, first of all the monomer MMA and water are mixed in a flask (see Figure 4.35). By adding the surfactant AUTEAB, a homogeneous and transparent microemulsion was formed. The co-surfactant HEMA is added and after that the cross-linker EGDMA. The next steps depend on the polymerisation procedure described in section 4.4.1 and 4.4.2.
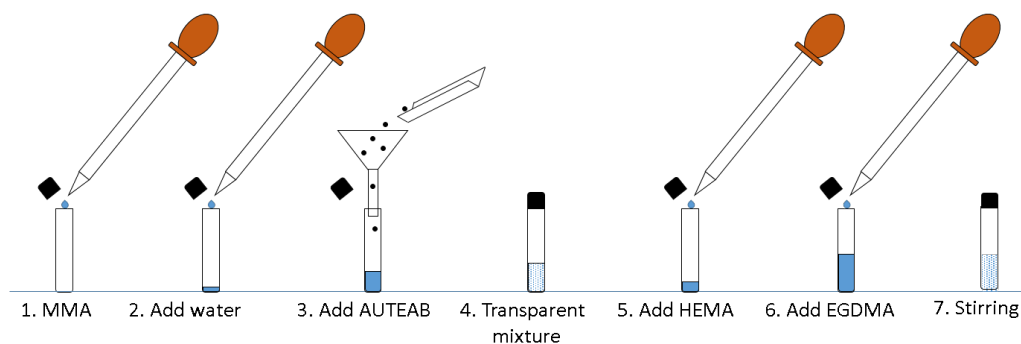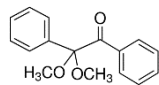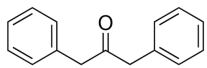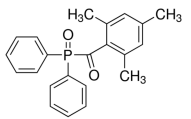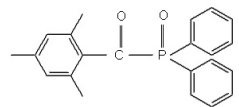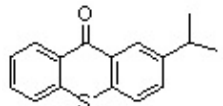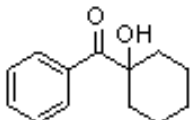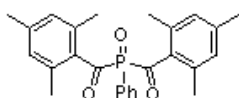
Figure 4.35. PBM preparation

4.3 Photoinitiators

Based on several criteria different photoinitiators where selected to be tested for their performance. The initiators showed no absorption in the wavelength-range of the used PBM chemicals. Another factor was the solubility in monomers. In addition

a promising efficiency for polymerisation in similar applications where described in the company product sheets.

Table 4.8. Overview of photoinitiators

Photoinitiators	Supplier	Purity	Molecular weight [g/mol]	Molecular structure
2,2-Dimethoxy-2-phenylacetophenone (DMPA)	Sigma Aldrich	99 %	256.3	
1,3-Diphenyl-2-propanone (DPP)	Sigma Aldrich	99 %	210.27	
Diphenyl(2,4,6-trimethylbenzoyl) phosphine oxide (DTBP)	Sigma Aldrich	97 %	348.37	
2, 4, 6-Trimethyl benzoyl diphenyl phosphine oxide (DTPO)	ESSTECH, INC.	99 %	348.4	
2-Isopropylthioxanthone (IPPT)	ESSTECH, INC.	99 %	254.3	
1-Hydroxy-cyclohexyl-phenyl-ketone (Irg. 184)	BASF	99 %	204.3	
Phenyl-Bis(2,4,6-Trimethylbenzoyl)-Phosphinoxid (Irg. 819DW)	BASF	98 %	418.46	

Among these initiators only the Irgacure 184 is reported to be less prone to oxygen inhibition. Irgacure 184 is a highly efficient non-yellowing photoinitiator which is used to initiate the photopolymerisation of chemically unsaturated prepolymers for instance acrylates in combination with mono- or multifunctional vinyl monomers

[BASF (2012)]. In Table 4.8 the studied photoinitiators are given. Irgacure 819 DW is a dispersion of Irgacure 819 in water with dispersants, where the content of Irgacure 819 is 44 - 46 %, that itself has a purity of minimum 98.0 %. DMPA is a widely used photoinitiator for photocuring and polymerisation (Konkin et al., 2003). Therefore, it has been studied in many publications (Jaegerman et al., 1987), (Jent et al., 1988), (Forbes, 1992) (Savitsky et al., 2001), (Fouassier and Merlin, 1980), (Merlin and Fouassier, 1980), (H. Fischer R. Baer, 1990), (Groenenboom et al., 1982). Based on the literature review of (Konkin et al., 2003), the radical kinetics and the polarisation development are intensively linked with the properties of the solvents, temperature and irradiation intensity. Studies showed that the photoindused polymerisation of DMPA in ethylene glycol produces two radicals, benzoyl and 7,7-dimethoxy-benzyl (Konkin et al., 2003).

4.4 Casting procedure

Figure 4.36 compares both techniques for photoinitiator (A) and redox (B) based
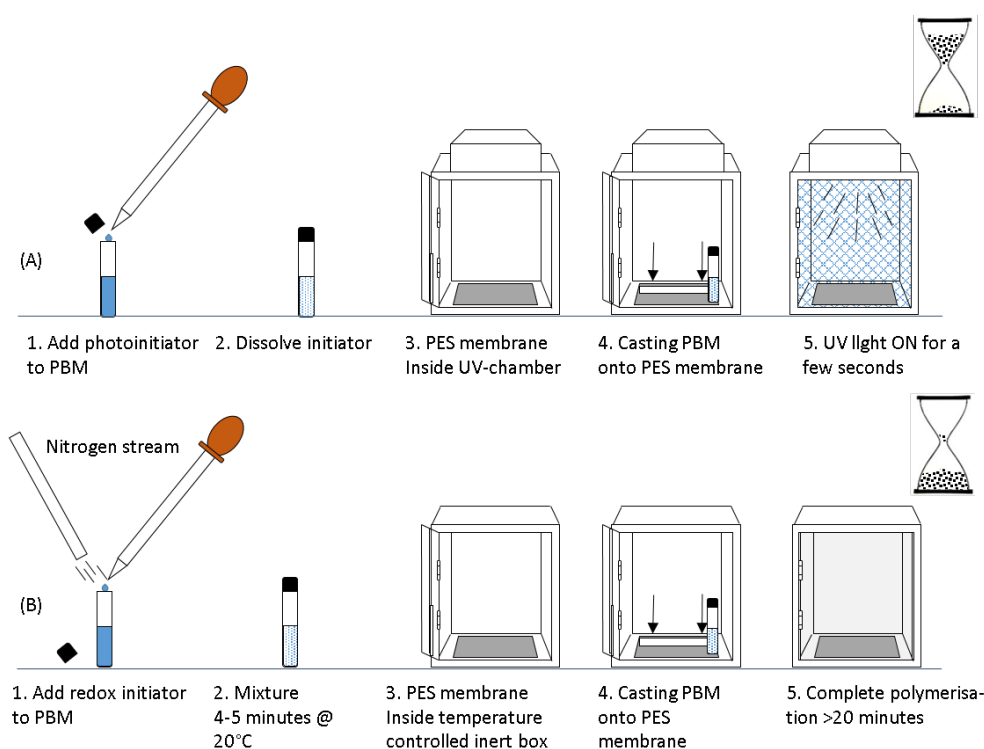
Figure 4.36. Photoinitiator (A) vs. redox (B) based coating procedure

coatings. The photoinitiator based casting requires less preparation steps and is polymerised in a few seconds while the redox based casting requires several minutes to be fully polymerised. In the following the redox and photoinitiator based casting procedure is explained in detail. For the membrane coating (see: Bionexgen (2016), Galiano (2013), Deowan (2013), Galiano et al. (2015), Figoli et al. (2015)), a commercially available UF membrane (UP150T, 150 kDa, with a thickness of 0.225 millimetre supplied by the company Microdyn-Nadir) for MBR application has been modified by applying a nano-structured coating on top with a PBM structure.

4.4.1 Redox based casting

In a previous work, the redox based polymerisation of novel PBM was developed [Galiano et al. (2015)]. As shown in Figure 4.36 (B), after microemulsion was prepared, the redox initiators are added into the vessel which gets inflated already by nitrogen, and the inflation must last for another minute to stop the PBM exposure to oxygen in the air. Then, the vessel is sealed and kept in a water bath at 20 °C for four to five minutes. During this time, the vessel has to be taken out several times for checking the viscosity of PBM. In the redox based polymerisation process, as soon as the redox initiators are added into the PBM, the polymerisation process starts. Depending on the ambient conditions of the PBM, for instance room temperature, the polymerisation can be faster or slower. Therefore, the viscosity of the PBM is hard to control at a constant value whereas it is a key factor for the casting process. If the viscosity is too low, which means the PBM is too liquid, after being casted, the membrane is very dense which leads to a low water flux of the membrane; and if the viscosity is too high, which means the PBM is too sticky, the PES membrane will be casted inhomogeneously. As the viscosity cannot be measured continuously during the redox polymerisation, it is obvious that the proper and reproducible adjustment of the "right" viscosity is very much related to personal experience and a bit of luck. Anyway, the casting process starts immediately as soon as the PBM reaches the right viscosity. PBM is poured onto the PES membrane and casted by a casting knife. Then the membrane stayed in a nitrogen-inflated sealed chamber for at least 20 minutes until the PBM polymerised completely. This time consuming factor limits the process to be scaled-up commercially.

The redox based PBM was casted in a plastic chamber (3) which is connected via

tubes to a nitrogen bottle as shown in Figure 4.37. This chamber was placed in a thermostat chamber from Sartorius (CERTOMAT H) (4). Outside of the thermostat chamber, an air conditioner (1) was placed next to the thermostat. The aim of using a thermostat and air conditioner was to keep the air temperature constant. In order to control the temperature of the nitrogen entering the plastic chamber, a temperature controlled water bath (2) equipped with a heat exchanger is used.

1. Air conditioner   3. Casting chamber
2. Water bath thermostat   4. Thermostat

Figure 4.37. Casting chamber for redox based experiments

4.4.2 Photoinitiator based casting

Regarding the commercial scale-up for the existing process, the main challenge is a significant polymerisation time reduction. For the commercial scale-up one option is to move from a redox based process to a photoinitiated polymerisation that is expected to last just a few seconds in comparison to about 20 minutes of the redox based polymerisation. As soon as the photoinitiator gets dissolved in the PBM, the casting liquid needs to be kept dark to avoid the immediate formation of radicals, and therefore polymerisation of the PBM inside the flask. If needed, the sample can be kept for several days before coating a membrane (see section 4.2.2). As shown in Figure 4.38, depending on the requirements the casting chamber can be flooded by nitrogen. Detailed information about the setup for the photoinitiator based casting is also given. As support for the preparation of membranes for the final application in

a MBR a commercial ultrafiltration membrane is used from Microdyn Nadir GmbH, Germany (UP 150T, 150 kDa). In order to study the performance onto another substrate type (PA), a reverse osmosis membrane from DOW Chemicals (BW XLE) has been investigated as well. The PBM gets homogeneously distributed onto the commercial membrane by use of a casting knife with a defined thickness (supplier TQC: (4, 10, 20 μm), self made: (40, 80, 100, 150, 250 μm)). After irradiation by UV-light the PBM is polymerised and ready to use.

4.5 UV-Lamps

In this section, all the UV lamps applied in the experiments are described respectively. Initial trials are made under non-inert conditions by the use of several different UV-light sources. Table 4.9 shows a selection of these trials. As shown, different sources with changing intensities where tested for their performance on polymerising PBM membranes.

The Solidcure 2 UV LED system (IST METZ GmbH) with power of 12 W/cm^2 and the low pressure Hg Lamp (IST METZ GmbH) were mounted on top of a moving belt. The low power mercury lamp consists of four parallel fluorescent tubes each with power of 200 W. The working distance of the low pressure Hg Lamp was fixed at 2 cm and the speed of the moving belt adjustable. The working distance of the Solidcure 2 UV LED system was adjustable, as well as the speed of the moving belt. The power of the UV-LED light guide is the strongest studied intensity with 50 W/cm^2. The distance from the light source to illuminated surface was adjustable. UV light was emitted from a tubular light guide of UV LED light guide (IST METZ GmbH). The working distance of the handheld M-Zero UV LED system (IST METZ GmbH) was fixed at 2 cm with a power of 4 W/cm^2. The Mercury Lamp (IST METZ GmbH) with a power of 200 W/cm worked at a fixed distance with an adjustable speed of the moving belt. The air cooled UV-LED series L (Opsytec Dr. Gröbel GmbH) provided UV light with a wavelength of 365 nm. The distance from the substrate to the light source was adjustable, so that the irradiation varied along with it.

Table 4.9. Summary of studied UV-lamps
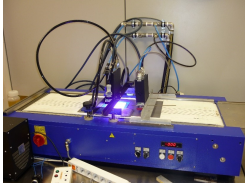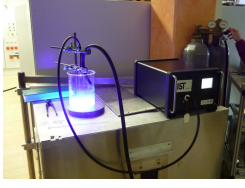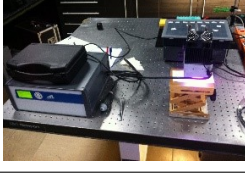
UV-lamps	Company	Wavelength	Irradiation @ exit of lamps	Picture
Solidcure 2 UV LED system	IST METZ GmbH	385 nm	12 W/cm²	
UV LED light guide	IST METZ GmbH	385, 405 nm	50 W/cm²	
The M-Zero UV LED system	IST METZ GmbH	395 nm	4 W/cm²	
Low pressure Hg Lamp	IST METZ GmbH	main Hg emission peaks at 185, 254, 365 nm	800 W	
Mercury Lamp	IST METZ GmbH	Wide range with an especially high emission in the UV-C range	200 W/cm	
UV-LED SERIES L	Opsytec Dr. Gröbel GmbH	365, 450 nm	4 W/cm²	

Figure 4.38 shows the setup that represents the outcome of the pre-selection trials done with the UV-light sources described before. A taylor made UV-lamp was ordered and installed in a glove box. This setup allows polymerisation trials, both

under inert and non-inert conditions as the UV-LED is installed within a special UV-light resistant glove box. In order to assure inert conditions, an oxygen sensor is used.

Figure 4.38. Final UV-LED setup for inert and non-inert experiments

To achieve an oxygen level less than 1 % the glove box needs to be flushed about one and a half hour with 20 L/min, consuming about 50 bar of nitrogen. The ambient temperature within the glove box is measured by a sensor, while the temperature underneath the UV-LED-lamp is shown at the display of its control device.

To achieve a homogeneous UV-light distribution over the substrate an area of 250x510 mm is the limit. The distance between LED's and substrate can be adjusted manually as shown in Figure 4.38. The membrane coating is done by usage of casting knifes with different thickness's. The wavelength is fixed at 365 nm, with adjustable intensities. The intensities can be regulated in a range from 0 to 100 % by the control device shown in Figure 4.38. For ongoing studies the samples were irradiated with an intensity of 300 mW/cm².

Rather than that, the intensity changes also by the distance between substrate and the LEDs. Figure 4.39 shows the intensities over distance distributed by the UV-LED manufacturer at a 100 % setting. To achieve a homogeneous distribution of UV-light over the substrate the distance should be adjusted within the given range. The selected distance for the ideal coating conditions is given in Table 5.5 of section 5.2.3.
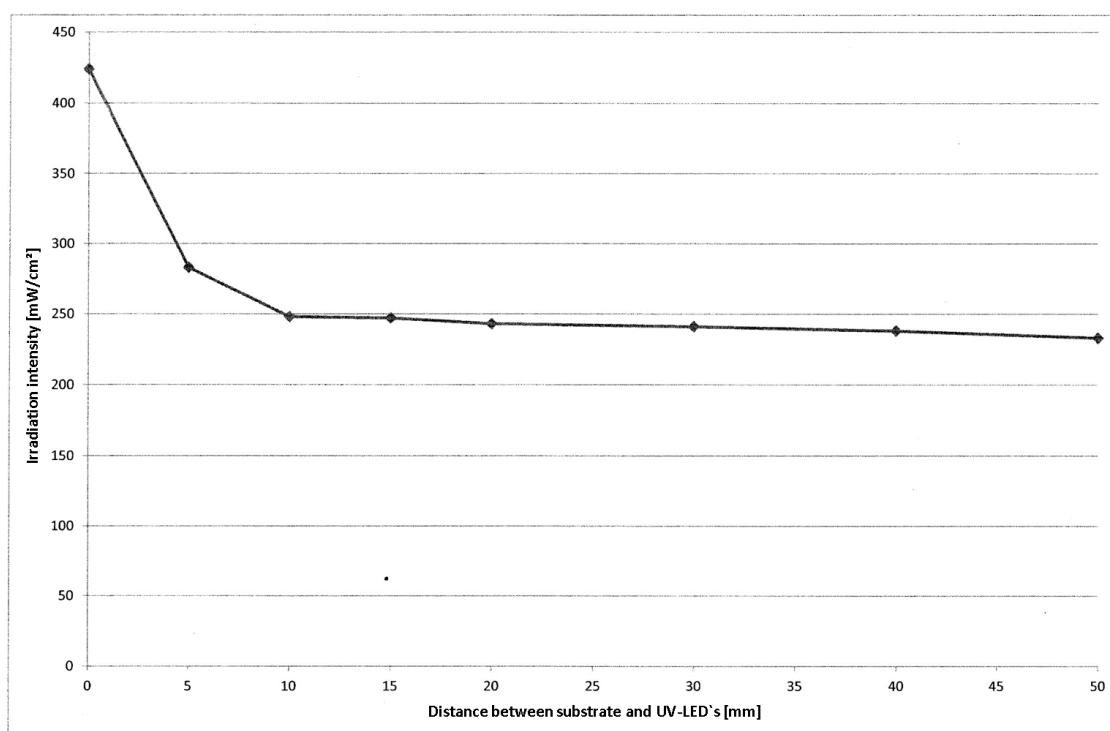
Figure 4.39. UV-LED intensity over distance

Figure 4.40 shows the temperature increase over time for the UV-LED when it is installed inside the glove box. As the glove box is a closed system the ventilation of the UV-LED cannot transport the heat away from the unit. However, as the polymerisation is foreseen to be done within a few seconds (30 seconds for the final membrane, see section 5.2.3), the temperature increase is only about 0.5 K and therefore negligible. However, in view of possible scale-up of the process a proper cooling concept for the UV-LED and also a controllable ambient temperature inside the box should be considered.
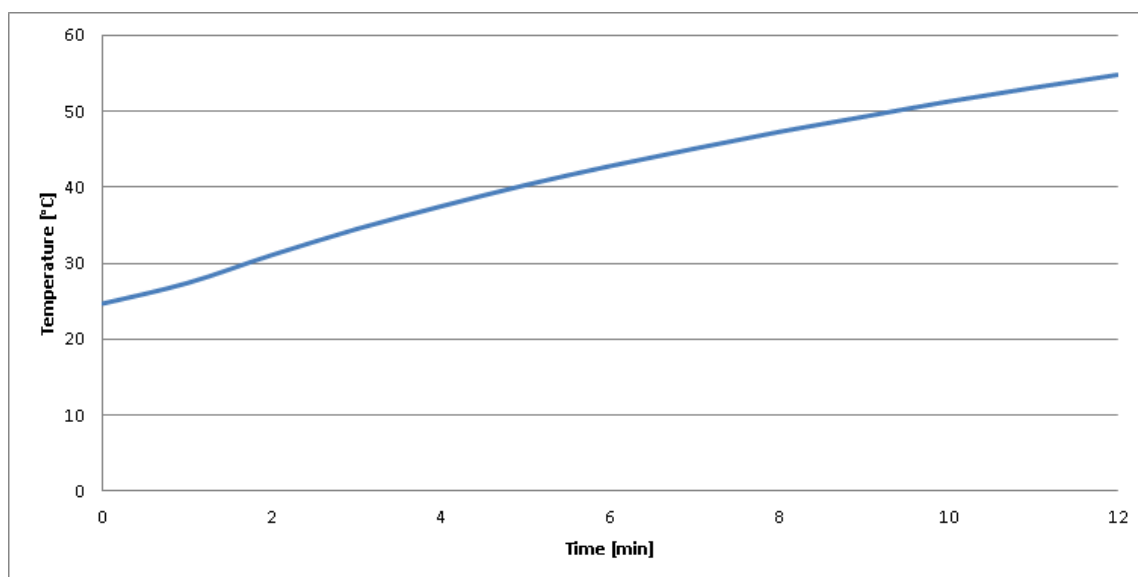
Figure 4.40. Temperature increase for UV-LED inside glove box

4.6 Viscosity enhancer

Normally, the viscosity of a polymer in solution is related to its molecular weight [Holding (1995)] but also to temperature. As Flory (1953) reported in Principles of Polymer Chemistry, "high polymer molecules possess the unique capacity to greatly increase the viscosity of the liquid in which they are dissolved, even when present at concentrations which are quit low". Therefore, a polymer with high molecular weight was considered to be added into the PBM for getting an appropriate viscosity of the PBM solution.

In the membrane formation process, poly ethylene glycol (PEG) is usually employed as a pore-forming agent enhancing permeation properties [Kim and Fane (1988)]. Due to its hydrophilic property, by adding PEG of different molecular weights, the membrane permeability is improved [Shieh et al. (2001), Idris et al. (2007)]. Therefore, PEG with different molecular weights was considered to be added into PBM solution to increase the hydrophilicity of the PBM casted membrane as well as the viscosity of PBM solution. Moreover PEG is a non-toxic low-cost chemical which has no adverse effect on the environment and can be degraded in common sewage treatment plants.

As Chanda and Roy (2006) reported in "Plastics Technology Handbook", the critical molecular weight (Mc) of a polymer is a key factor determining the viscosity of the solution in which it is dissolved. Below the Mc, the molecules move independently as in low-molecular-weight liquids. Above the Mc, movement of the mutual entangled long-chain molecules are remarkably hindered due to one molecule's movement involves dragging others along with it. For most polymers, Mc is between 5,000 and 15,000 g/mole [Chanda and Roy (2006)].

Thus, viscosities of typical PEGs with molecular weight, 2,000 (PEG-2,000) and 20,000 (PEG-20,000), and viscosity of polymerisable PEG are investigated in section 5.1.4 at different concentrations.

Different types of PEG have been used to tune the casting viscosity of the PBM. To find the proper viscosity, tests have been performed using the commercial surfactant DTAB in the PBM composition and different amount of PEGs. DTAB was used to avoid the use of a big amount of the polymerisable surfactant AUTEAB which is synthesised at lab scale, as already reported in section 4.2.2. The following types of PEGs were used in order to increase the viscosity of the microemulsion.

- PEG 20.000 (Polyethylenglycol 20.000, Merck-Schuchardt, 20.000 g/mol)

- PEG 2.000 (Polyethylenglycol 2.000, Merck-Schuchardt, 1800-2200 g/mol)

- PEG Polymerisable (Poly (ethylene glycol) methyl ether methacrylate, Sigma Aldrich, 1.05 g/cm^3 at 25°C)

After preparing the single probes their viscosity was measured by an Ubbelohde-Viscosimeter (see section 4.7.1) with an accuracy of ± 0.8 % and then directly cast onto the commercial PES membranes.

4.7 Bicontinuous microemulsion and PBM membrane characterisation equipment

In this section all instruments used for the characterisation of the bicontinuous microemulsion as well as the PBM coated and pure commercial membranes are reported.

4.7.1 Ubbelohde-viscosimeter

As shown in Figure 4.41, Ubbelohde viscosimeters (Micro Ubbelohde DIN 51562-2) from LAUDA inc. with an accuracy of ± 0.8 % were used to measure the viscosity of samples at 20 °C. The capillary constants of the two used viscosity meters were 0.03 mm^2/s^2 and 0.3 mm^2/s^2.

The PBM sample with a known volume was forced by gravity to flow through the capillary of the viscosimeter. By measuring the time t the sample passes the two volume marking lines and multiplying with the instrument's constant K the kinematic viscosity υ is calculated. By measuring density ρ and multiplying with the kinematic viscosity the dynamic viscosity η is calculated.

$$\upsilon = K \cdot t \tag{4.1}$$

$$\eta = \upsilon \cdot \rho \tag{4.2}$$
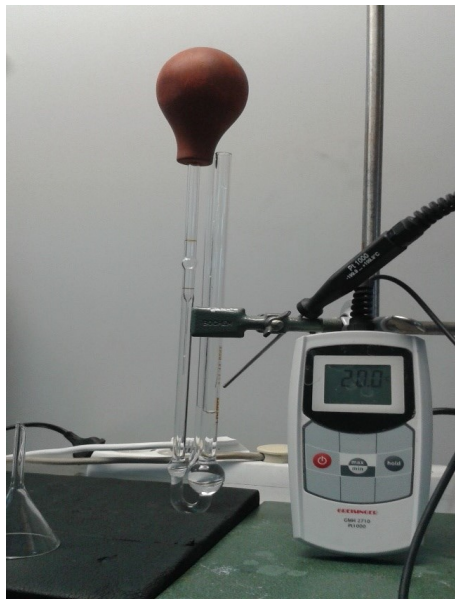
Figure 4.41. Ubbelohde-viscosimeter

4.7.2 FT-IR

In order to study the performance of the polymerisation process the ALPHA FT-IR-spectrometer from the company BRUKER was used. All PBM solutions were first applied onto a glass plate for checking their individual conversion rate without the membrane substrate. Compositions with high conversion rate and short irradiation time were pre-selected as coating for the PES membranes. To investigate the conversion rate of the respective PBM solutions, the transparent polymerised PBM were peeled off the glass and then placed in the centre of the lens of spectrometer. Spectrum and conversion rate of each PBM was automatically recorded by PC. The spectral range of the FT-IR spectrometer is 375-7.500 cm^{-1}. As the PBM mainly consists of acrylates, the transformation of their C=C double into single bonds where measured in order to evaluate the performance of the photoinitiators. Significant peaks in the FTIR spectrum are:

- 813 cm^{-1}: - It corresponds to the unreacted $CH = CH_2$ double bonds. So the lower the peak the better it is because it means better polymerisation

- 2900 cm^{-1}:- It corresponds to $-CH_3$. After polymerisation, the $CH = CH_2$ is converted into the $-CH_3$ group. So there is an increase in peak height around 2900 cm^{-1}. The higher the peak the better it is because it means better polymerisation.

- 1726 cm^{-1}: - For the characterisation of PBM coated membranes, only this peak is suitable owing to overlapping peaks of the membrane substrate. It corresponds to the carbonyl group (C=O), present in the chemical structure of MMA, HEMA, EGDMA and AUTEAB (components of the PBM coating) and absent in the PES membrane. Therefore, the presence of this peak can be also used as evidence of the presence of the PBM coating on the PES commercial membrane.

Figure 4.42 shows an exemplary IR spectrum highlighting the peaks of interest for the interpretation of the conversion rate.

In order to calculate the polymerisation rate of the single probes (y) a protocol was developed based on the integration of the peak height (at 813 cm^{-1}) of the single probes (x) using glass plates as substrate. Considering the peak height of a fully

polymerised probe (defined by the absence of the C=C peak after polymerisation) as 100 % polymerisation (A) (see Figure 4.44) and a wet probe before polymerisation (B) as 0 % (see Figure 4.43), the polymerisation rate (y) of all single probes is easily calculated by the height of the samples peak.

$$\frac{x - A}{y - 100} = \frac{B - A}{0 - 100} \tag{4.3}$$
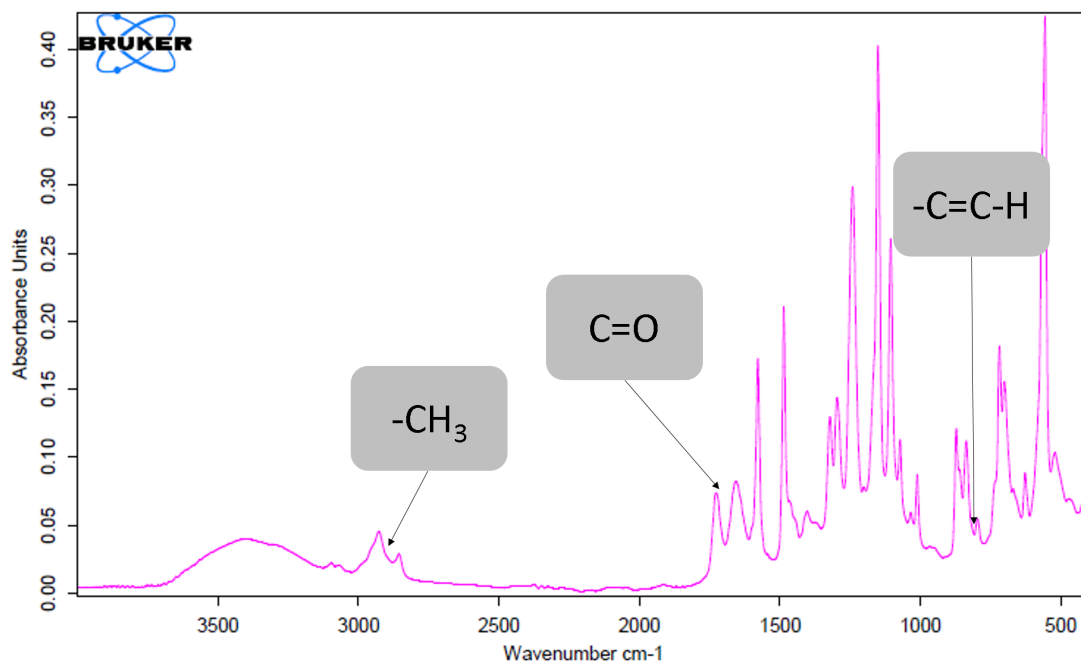
Figure 4.42. Exemplary graph showing interesting peaks for conversion rate
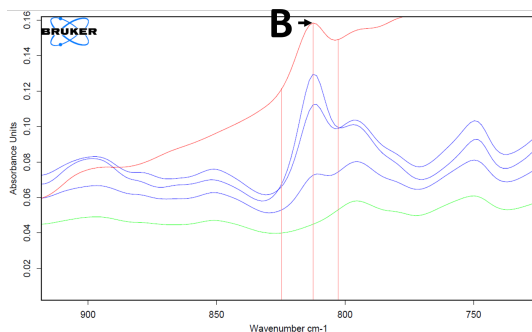
Figure 4.43. Integration for wet probe
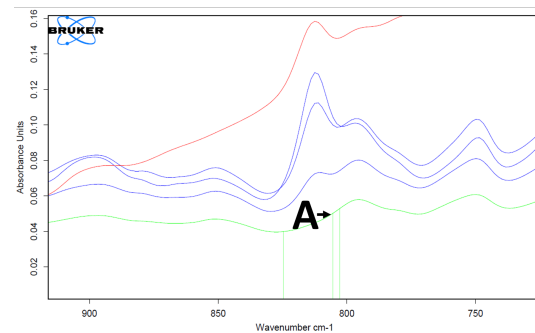
Figure 4.44. Integration for full conversion

Different integration possibilities are given by the software of the FT-IR instrument. While comparing them with each other, only the integration by peak hight given in Figure 4.44 and 4.43 resulted in conversion rates corresponding to the physical appearance of the polymerised PBM. For example, the integration of the area underneath the peak was not possible in all cases as the necessary form of a Gaussian curve is not given. Anyway, considering that this method is just used as a pre-selection tool for further experiments, it was found to be a reliable technique.

4.7.3 UV/visible spectrophotometer

UV/visible spectrophotometer is a useful tool for qualitative and quantitative analysis. In this thesis, the spectrophotometer (Model: UV-1800) from Shimadzu (Japan) was used to analyse the spectrum of applied chemicals. The spectral range of the spectrophotometer was 200 nm to 1100 nm. Visible, near infrared and near UV-irradiation interact with valence electrons in sample molecules as they absorb photons of wavelengths equal to the energy gap between their discrete energy levels and undergo electronic transitions. The spectrometer sends light through the sample while measuring the intensity versus wavelength using a detector device. Reference cuvettes are placed in a standard cuvette holder. In order to get a reference line, deionised water is measured and used. After having the reference measured, the single emulsions are measured for their absorbent properties. The energy E of light can be expressed as:

$$\text{E} = \frac{ch}{\Lambda} \tag{4.4}$$

c is the velocity of light, h is the Planck's constant, and Λ is wavelength. When light is irradiated on a substance, the light of certain wavelength is absorbed according to the molecule structure of that substance. This is due to the electrons at ground state of that substance transiting to an excitation state after absorbing light energy. The absorption differs depending on wavelength, therefore the absorption spectrum becomes unique to that substance. To assure that the absorption rate of all used components are not in the same range of the desired photoinitiators all components are analysed in the range from 200 to 500 nm. The liquid chemicals MMA, HEMA

and EDGMA are measured non-diluted in order to get the highest possible intensity. The solid chemicals of the PBM were dissolved in DI water. All the photoinitiators except DPP were dissolved at 0.6 % in MMA. DPP was dissolved in MMA at 6 %, as it showed no absorption effect at 0.6 %. All studied PEGs were dissolved in DI water at 10 %.

4.7.4 Scanning electron microscopy (SEM)

The SEM (EVO/MA10) from ZEISS was applied to obtain the cross-section and surface image at micrometer scale. As preparation for the cross-section-pictures the membrane had to be dipped in liquid nitrogen for several seconds before braking the membranes in the centre part.

Both, membrane pieces for surface and cross-section had to be coated by an approximately 15 nm thick layer of gold making the membrane structure visible in the SEM. The gold film onto the membrane probes is done by Instrument from company Quorum Technologies LTD (Model: Q150R).

4.7.5 Atomic force microscopy (AFM)

A Multimode AFM with a nanoscope Illa controller (Veeco, USA) using manufacturer-supplied software is used to perform AFM measurements of the membrane. Ambient laboratory conditions are used to conduct the analyses using tapping mode. TESP (nominal spring constant 20-80 Nm) and cantilevers (Bruker AXS) were used throughout. The resolution of the images is 512 * 512 pixels. The roughness values are root mean squared (RMS) calculated by the instrument software.

4.7.6 Contact angle

The contact angle measurement allows the characterisation of membranes in regards of their hydrophilicity. In order to measure the contact angle the membrane probes have to be prepared in the following way. First small probes are cut out of the membrane sample (about 5 x 1 cm). These samples are than either washed or kept untreated. For the washing procedure the samples are washed with deionised water

three times for one hour each in order to release the glycerine that is used for preservation of the commercial PES membrane. Keeping the membranes in an oven over night at 40 °C for drying. Having the probes ready the contact angle is measured by an optical contact angle meter from the company KSV INSTRUMENTS LTD, Finland (Product: CAM 200 Optical Contact Angle Meter). The resolution of the meter is 800 * 600 pixel. A ultrapure water droplet of defined volume of 5 mL is produced and immediately after getting in contact with the membrane surface a picture is taken and the contact angle automatically calculated. To increase the accuracy of the measurements and check the homogeneity of the coating this procedure is repeated at least 10 times at different locations of the probe. The contact angle is then calculated by the average value together with the standard deviation of the measurements. The specific standard deviation for each measurement is depending on the homogeneity of the coating and given in the specific sections (see section 5.2.5).

4.7.7 Cross flow test unit

Two cross flow test devices from the company SIMATEC were employed to characterise flat sheet samples (84 cm^2) for their water permeability under laboratory conditions. The advantage of the double stage versus the single stage unit is that two membranes can be tested at the same time and similar operating conditions.

The single stage unit (SIMATEC LSta80/10) allows the test of membrane sheets under different operating conditions like temperature (2) and operating pressure (1) (see Figure 4.45). This unit was used for water permeability and model foulant tests. By using the connected PC a data acquisition programme is used for monitoring real time values from the SIMATEC unit and for later interpretation of the logged values. The accuracy for the pressure sensor is given at ± 2 % and for the temperature sensor ± 1 %. The error for the flux is depending on the applied pressure but has its maximum at ± 2 %. The maximum flow for the feed is given at 100 L/h, and for the permeate at 8 L/h.

In addition another double stage cross flow test system (LSta05-2SPS) from SIMATEC was used to test membrane sheets under different parameters such as temperature, pressure and flow (see Figure 4.46). This unit can test water permeability

with e.g. pure water and model foulants. Transmembrane pressure can be set by the control panel. After the starting of the test, the modelling solution will flow through the gear pump, passing by the first membrane cell.

1. Pressure control	2. Temperature control	3. Feed tank
4. Membrane module	5. Permeate sample valve	6. Concentrate sample valve
7. Feed sample valve	8. Drain valve	9. Pressure damper
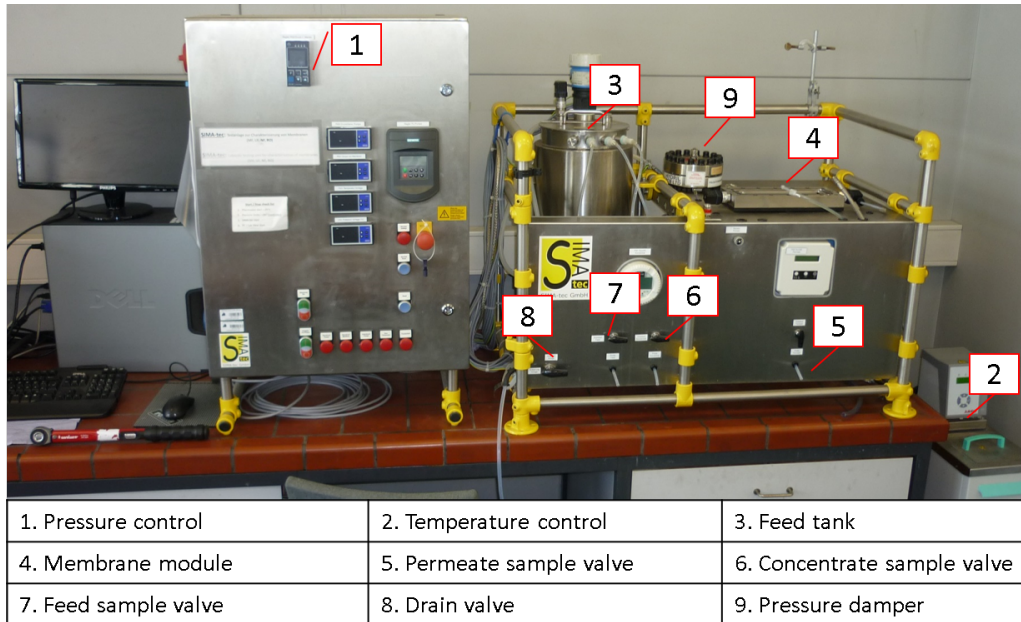
Figure 4.45. SIMATEC single stage cross-flow testing unit

1. Control panel	2. 1st membrane module	3. 2nd membrane module
4. Data acquisition	5. Permeate sample valve	6. Concentrate sample valve
7. Feed sample valves	8. Drain valve	9. Flow sensors
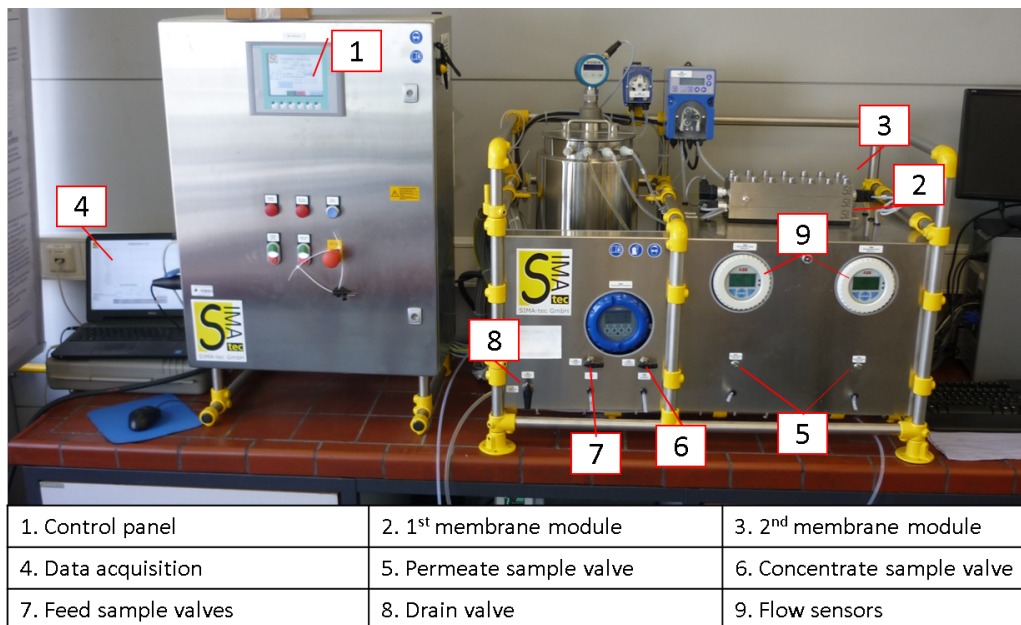
Figure 4.46. SIMATEC double stage cross-flow testing unit

The permeate will flow back to the collection tank and the retentate will flow to the next membrane as feed. Permeate and retentate from the second membrane will also flow back to the collection tank. With the help of the two flow sensors, the flux of two membranes is monitored. The maximum flow for the feed is given at 100 L/h, and for the permeates at 8 L/h.

This device allows the test of two membranes at the same time and under same conditions. The novel coated membrane as well as the pristine commercial membrane were prepared and tested in parallel in order to get comparable values. To improve the wetability, the membranes are prepared before testing. The preparation consists of three times treatment with pure deionised water for one hour in order to remove the preserving glycerin of the membrane. Afterwards the membranes are tested first for 24 hours with water at 20 °C and a conductivity of 60 µS (the minimum conductivity is required for the measuring principle of the sensors from the setup). In the next step a 24 hours run with a model foulant (100 mg/L humic acid (Alfa Aesar CAS:1415-93-6)) is done (details see Table 4.13). After 24 hours the humic acid gets replaced by deionised water and the membranes washed three times for one hour while replacing the water after every hour.

As the membranes are installed in series there might be an influence to the performance of two tested membranes due to a low drop in cross flow resulting of the difference from feed to first permeate production. As shown in Figure 4.47 the feed of the second membrane is the result of the feed from the first membrane minus the permeate of the first membrane.
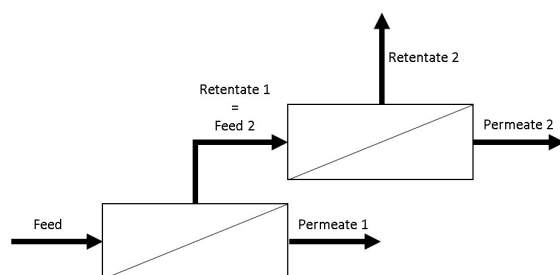
Figure 4.47. Flow chart of double membrane SIMATEC unit

In order to study a potential influence to the tested membranes the commercial UP 150T has been tested as shown in Figure 4.48.
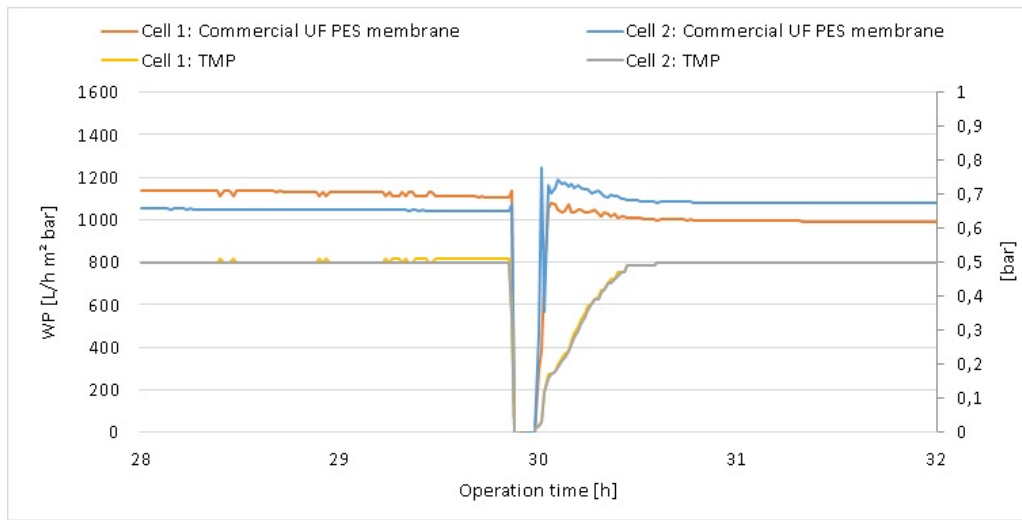
Figure 4.48. Cross flow test of impact on installation in series

As the UP 150T is a very hydrophilic membrane resulting in a high permeate flow the influence of the installation of the second stage in series is obviously decreasing by testing less permeable membranes. Therefore the result of this test can be seen as upper limit in effecting the performance of the second stage membrane for the work described in this thesis. As shown it has been waited 29 hours to achieve stable conditions at a TMP of 0.5 bar. Afterwards the membranes have been changed, meaning the membrane of the first stage has been replaced with the second stage membrane and reverse. Table 4.10 shows the average values for the delta in volume flow before and after they have been replaced.

Table 4.10. Influence of installation in series

	Average WP before change	Delta WP before change	Average WP after change	Delta WP after change
Cell 1:	1111.17	68.64	988.21	89.24
Cell 2:	1042.54		1077.45	
Result +/-				**20.60**

Considering this values the resulting influence to the final permeability caused by

the installation in series is calculated by:

$$\mathrm{R}esult = \frac{100 \ \%}{1111.17 \ [L/h \ m^2 \ bar]} \cdot 20.60 \ [L/h \ m^2 \ bar] = 1.85 \ \% \tag{4.5}$$

Salt rejection experiment

For the salt rejection experiment the model salt $MgSO_4$ has been chosen according to the work of Deowan (2013). The test conditions are given in table 4.11.

Table 4.11. Test conditions for salt rejection experiment

Applied Salt	$MgSO_4$
Concentration of Salt	2,000 ppm
Temperature	25 ±1 °C
TMP	0.5 ± 0.02 bar
Operation time	1 h
Active surface area of the used membrane	84 cm²

Water permeability experiment

The conditions for the water permeability experiment (see Table 4.12) where applied based on the previous testing procedure described by Deowan (2013).

Table 4.12. Test conditions for water permeability test experiment

Test media	DI water
Conductivity of feed solution	60 μS/cm
pH	6.5-7
Temperature	20 ±1 °C
TMP	0.5 ± 0.02 bar
Operation time	24 h
Active surface area of the used membrane	84 cm²

The water permeability is calculated by:

$$WP = \frac{p_{Feed}}{Flux_{Perm.}} \tag{4.6}$$

$$WP = \frac{p_{Feed} \cdot A_{Membrane}}{Volumeflow_{Perm.}} \tag{4.7}$$

After 24 hours the membrane has been kept in the test device and continued with the model foulant experiment.

Model foulant experiment

For the model foulant experiment, humic acid (Alfa Aesar, stock numer: 41747, A.28) is used. The testing conditions where adopted from the previous work of Deowan (2013). Table 4.13 gives an overview of the test conditions.

Table 4.13. Test conditions for model foulant experiment

Test media	Humic acid dissolved in DI water
Concentration	100 mg/L
Conductivity of feed solution	60 μS/cm
pH	6.5-7
Temperature	20 $\pm$1 °C
TMP	0.5-2.2 $\pm$0.02 bar
Operation time	24-72 h
Active surface area of the used membrane	84 cm^2

Two protocols are followed within this work. Initial experiments where done at 0.5 bar for 24 hours. Afterwards the feed solution was three times replaced by DI water and run for one hour each. As the improved performance of the PBM coated membranes could not be shown at 0.5 bar, another protocol was developed. In the first phase of it, the TMP was set to 0.5 bar until stable permeabilities of the membranes are achieved. Subsequently, the TMP was set to 2.2 bar to force the membrane fouling. The TMP of 2.2 bar represents the maximum for the test device.

Again, stable permeabilities had to be reached. At this point samples where taken for measuring the TOC content, and to calculate the rejection rate. The TMP was set to 0.5 bar again and run for one hour. Afterwards the cleaning by DI water (three times for one hour) was done.

The value for the rejection of humic acid (HA) is calculated by measuring the TOC of the feed and a permeate samples. By knowing both values the rejection rate can be calculated by:

$$Rejection_{HA} = \frac{TOC_{Feed} - TOC_{Permeate}}{TOC_{Feed}} \cdot 100 \ \% \tag{4.8}$$

4.8 Composition of model textile feed aqueous solution

The composition of wastewater is an important factor in the biological degradation process. To keep the composition constant and as the wastewater is hard to transport from the textile dye company to the laboratory a model textile dye wastewater (MTDW) was prepared. Table 4.14 shows the composition of the model textile feed aqueous solution. Only the Albatex DBC formula is unknown because the supplying company keeps this confidential. This composition has beed developed based on literature review and optimized during long term trials. Details are given in the work of Deowan (2013). The error for the weighting balance is given at ± 0.12 %.

The MTDW consists of two different dyes called Acid Red 4 and Ramazol Brilliant Blue R. Their molecular weights are 380.4 g/mol and 626.5 g/mol. The acid red represents an reactive azo dye that typically hydrolyses within the dye bath, while the blue dye is an anthraquinone dye [Deowan (2013)]. Azo dyes are the species that are mainly used in the textile industry, e.g. for colouring of textiles and leather products [Deowan (2013)]. The anthraquinone dyes represent the second largest group, used in the textile industry, due to their simple application and variety of colour shades [Deowan (2013)].

Table 4.14. Model textile dye water composition

No.	Dyestuff/chemicals	Formula	Concentration [mg/L]
1	Remazol Brilliant Blue R	$C_{22}H_{16}N_2Na_2O_{11}S_3$	50
2	Acid Red 4	$C_{17}H_{13}N_2NaO_5S$	50
3	Sodium chloride	NaCl	2500
4	Sodium Hydrogen Carbonate	$NaHCO_3$	1000
5	Glucose	$C_6H_{12}O_6$	2000
6	Albatex DBC (Detergent)	unknown	50
7	Ammonium chloride	NH_4Cl	300

To prepare 100 L of MTDW, the process includes some steps that must be followed. Firstly, five gram of Acid Red 4 was added to 4 L of DI water. The mixture must be heated up to 80 °C and stirred at 200 rotation/minutes in 30 minutes in order to dissolve the red dye. Then the mixture was cooled down for 10 minutes before adding the rest of the composition. The chemical solution continued to stir until the chemicals were fully dissolved. Finally, 96 L of DI water was added to the solution to create a total volume of 100 L of MTDW.

4.9 Analytical methods of MBR process

In the MBR system, the online and offline measurements were carried out simultaneously. The online measurement includes the pH, temperature, conductivity, dissolved oxygen and suction pressure. All of these parameters were collected by sensors and stored on the computer. However, other parameters have to be analysed in the lab with the proper equipment as described below.

4.9.1 COD analysis

For the analyses of the COD a fast test spectrophotometer from the company Merck KGaA was used (Model type Merck Spectroquant Nova 60). A variety of different

cell tests can be applied but for the COD the Method 1.14541 is taken. The measuring range is between 25 and 1500 mg/L with a standard deviation of ± 0.68 % [Deowan (2013)]. The COD determines indirectly the amount of organic compounds in the solution. The samples were analysed with cell tests, serial number 08311069, supplied by the company Merck, Darmstadt, Germany. The range of this test was 25 – 1500 mg/L with the coefficient of variation from the manual ± 0.68 %. However, the experimental test was ± 1.02 % [Deowan (2013)]. The NH_4-N analyses were also carried out by cell tests from Merck (method 1.14558). The measuring range of these cell tests is 0.2-8 mg/l. The manual shows the accuracy as ± 1.0 % whereas the experimental test was ± 6.85 % [Deowan (2013)]. The NO_3-N analyses were also conducted by the cell tests from Merck (method 1.14542). The measuring range of these cell tests is 0.5-18 mg/l and the accuracy stated in the brochure is ± 1.5 %. However, the experiment was ± 7.9 % which might have occurred due to low concentrations of the samples [Deowan (2013)].

4.9.2 TOC/N analyser

The TOC values were analysed by total organic carbon analyser, supplied by Shimadzu (Model Number TOC-L CPH/CPN). The applied measuring range is between 5 and 100 mg/L. To achieve accurate measurements the device needs to be calibrated periodically. Therefore the accuracy of the measurement is varying and given for the specific measurements in the experimental part.
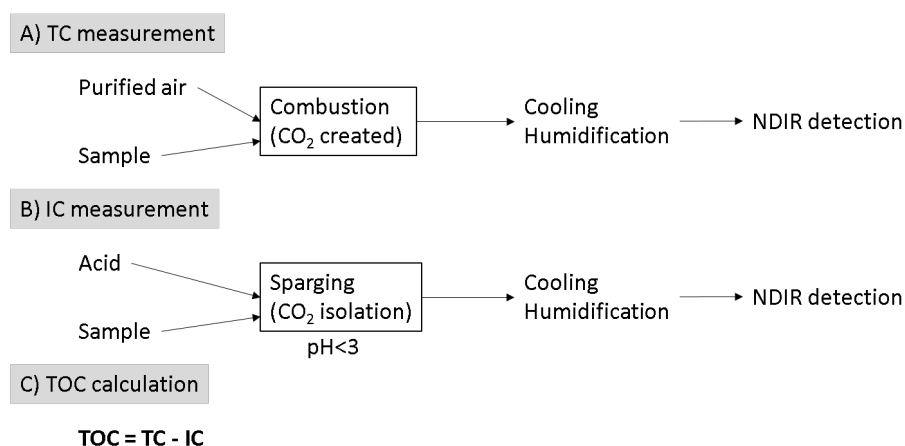
Figure 4.49. TOC analysing principle

The combustion catalytic oxidation method achieves total combustion samples by heating them to 680 °C in an oxygen-rich environment inside total carbon combustion tubes filled with a platinum catalyst. The schematic of this method is shown below in Figure 4.49.

The sample gets delivered to the combustion furnace, which is supplied with purified air. In the furnace it is heated up to 680 °C with a platinum catalyst. By combustion, it converts to CO_2. The CO_2 generated was cooled and dehumidified, and then detected by the Non-Dispersive Infrared (NDIR) detector. The concentration of TC (total carbon) in the sample is obtained through comparison with a calibration curve formula. Furthermore, by subjecting the oxidised sample to the sparging process, the IC (inorganic carbon) in the sample is converted to CO_2, and the IC concentration is obtained by detection with the NDIR. The TOC concentration is then obtained by subtracting the IC concentration from the obtained TC concentration.

4.9.3 Biochemical oxygen demand (BOD)

The BOD is the amount of dissolved oxygen needed by bacteria to break down organic material in water. The BOD was tested by the manometric BOD5 measuring device OxiTop®IS6 from WTW GmbH (Germany). The coefficient of variation was ±13 % [Deowan (2013)].

4.9.4 Red and blue dyes concentration determination

The concentrations of red and blue dyes were determined by the spectrophotometer, Model: UV-1800, from Shimadzu, Japan (see section 4.7.3). The accuracy of the red and blue dye results were ±4,08 % and ±1,8 %, respectively [Deowan (2013)].

4.9.5 MBR COD and dyes

To analyse the COD and dyes of the sample from the reactor, about 100 ml of the sample were taken and sonicated for 10 minutes, then filtered through the micro-filter (PS MF membrane 150 kDa from Microdyn-Nadir, Germany). The filtrate was then taken for the measurement of the COD and dyes. The accuracies of the reactor

COD, reactor red dye, and reactor blue dye were ± 1.02 %, ± 4.08 %, and ± 1.8 %, respectively [Deowan (2013)].

4.9.6 Mixed liquor suspended solids (MLSS)

Mixed liquor suspended solid (MLSS), is the concentration of suspended solids in the MBR. It consists primarily of the biomass and non-biodegradable suspended substances. The MBR and permeate samples were taken for the MLSS measurement. The sample volume was 40 ml, this was poured into a ceramic crucible and put in the oven at around 103-105 °C for 24 hours. After being dried in the oven for 24 hours, the samples were cooled down in the desiccator to room temperature and weighed for MLSS. The MLSS was determined with the following formula:

$$\mathrm{M}LSS = \left\{ \left(\frac{C_1 - D_1}{40} \right) - \left(\frac{C_2 - D_2}{40} \right) \right\} \cdot 1000 \; \frac{g}{L} \tag{4.9}$$

Where,

- C1: weight of ceramic crucible and dried residue of reactor sample, g

- D1: weight of empty ceramic crucible used for reactor sample, g

- C2: weight of ceramic crucible and dried residue of permeate sample, g

- D2: weight of empty ceramic crucible used for permeate sample, g

The accuracy was around ± 3.4 % [Deowan (2013)].

4.9.7 Dissolved oxygen (DO) and oxygen uptake rate (OUR)

The dissolved oxygen concentration was analysed with an oxygen sensor from WTW GmbH, model Oxi 340i meter and CellOX® 325 O_2 electrode. The accuracy in the brochure was ± 0.5 %, while it was ± 3.2 % based on 10 of our samples [Deowan (2013)]. The OUR was determined by the following procedure: 100 mL reactor

sample was taken for the first DO measurement (DO_1). The rest of this sample portion was stirred for 10 minutes at the ambient temperature. The samples after stirring were measured for the DO (DO_2). The calculation of OUR is shown in equation 4.10.

$$OUR = \frac{DO_2 - DO_1}{10} = (\frac{mg}{L \cdot min}) \tag{4.10}$$

4.9.8 Drying residue (DR) of permeate

The sample volume for the DR determination is 20 ml. The samples were dried in an oven at 105 °C for 24 hours. The DR values are defined by the following formula:

$$OUR = \frac{C - D}{20} \cdot 1000 \ \frac{g}{L} \tag{4.11}$$

Where,

- C: weight of ceramic crucible + dried residue, g

- D = weight of empty ceramic crucible, g

The accuracy of the analysis was ±3.0 % due to the weighting samples [Deowan (2013)].

4.9.9 pH and temperature

pH and temperature of the samples were determined by the pH meter and temperature sensor from WTW GmbH, model pH 323 meter and Sentix® 41-3 electrode. The accuracies are given at ±0.01 pH (-10 °C to 35 °C) and ±0.1 K (15 °C to 35 °C).

4.9.10 Electrical conductivity

The electrical conductivity of the samples were measured by the conductivity meter from WTW GmbH, model: Cond 315i meter. The meter has a range up to 19.99 mS/cm with an accuracy of ± 0.5 %.

4.9.11 Hydraulic residence time (HRT)

HRT indicates the length of time that the MTDW was kept in the reactor tank before it passes through the membrane as effluent. The total hydraulic volume of reactor tank is 47 L. The HRT is calculated by dividing the hydraulic volume (L) of the MBR by the Influent flow (L/h).

4.9.12 Food to microorganism (F/M) ratio

F/M ratio indicates the relation between the quantities of food (BOD_5, COD, or TOC) with the microorganism in the aeration tank. With a high F/M ratio, this means that there is plenty of food for the bacteria to consume. The F/M ration is calculated in equation 4.12.

$$\text{F/M} = \frac{COD(\frac{mg}{L}) \cdot Q(\frac{L}{d})}{MLSS(\frac{mg}{L}) \cdot TankVolume(L)} (\frac{kgCOD}{kgMLSS \cdot d}) \qquad (4.12)$$

4.9.13 Organic loading rate (OLR)

OLR shows the weight inflow of organic matter, such as COD applied to a reactor tank per day. This is shown in equation 4.13.

$$OLR = \frac{COD(\frac{mg}{L}) \cdot Q(\frac{L}{d})}{TankVolume(m^3)} (\frac{kgCOD}{m^3 \cdot d}) \qquad (4.13)$$

4.10 Calculation of theoretical values for MTDW

In order to proof that the experimental procedure described in section 4.9.1 and 4.9.2 results in realistic values, the theoretical values are calculated as well for COD and TOC.

4.10.1 Total organic carbon (TOC)

The total organic carbon (TOC) gives the sum of total carbon in organic compounds. Organic carbon is in the chemical structure of red dye, blue dye, Albatex and Glucose. The molecular weight of red dye and blue dye is calculated in equation 4.18 and 4.23.

$$M_{blue} = M_{C_{22}H_{16}N_2Na_2O_{11}S_3} \tag{4.14}$$

$$M_{blue} = 22 \cdot A_C + 16 \cdot A_H + 2 \cdot A_N + 2 \cdot A_{Na} + 11 \cdot A_O + 3 \cdot A_S \tag{4.15}$$

$$M_{blue} = 22 \cdot 12,011 \frac{g}{mol} + 16 \cdot 1,0079 \frac{g}{mol} + 2 \cdot 14,007 \frac{g}{mol} + \tag{4.16}$$

$$2 \cdot 22,99 \frac{g}{mol} + 11 \cdot 15,999 \frac{g}{mol} + 3 \cdot 32,065 \frac{g}{mol} \tag{4.17}$$

$$M_{blue} = 626,55 \frac{g}{mol} \tag{4.18}$$

$$M_{red} = M_{C_{17}H_{13}N_2NaO_5S} \tag{4.19}$$

$$M_{red} = 17 \cdot A_C + 13 \cdot A_H + 2 \cdot A_N + A_{Na} + 5 \cdot A_O + A_S \tag{4.20}$$

$$M_{red} = 17 \cdot 12,011 \frac{g}{mol} + 13 \cdot 1,0079 \frac{g}{mol} + 2 \cdot 14,007 \frac{g}{mol} + 22,99 \frac{g}{mol} \tag{4.21}$$

$$+ 5 \cdot 15,999 \frac{g}{mol} + 32,065 \frac{g}{mol} \tag{4.22}$$

$$M_{red} = 380,18 \frac{g}{mol} \tag{4.23}$$

The molecular weight of Glucose is calculated by:

$$M_{Glucose} = M_{C_6H_{12}O_6} \tag{4.24}$$

$$M_{Glucose} = 6 \cdot A_C + 12 \cdot A_H + 6 \cdot A_O \tag{4.25}$$

$$M_{Glucose} = 6 \cdot 12,011\frac{g}{mol} + 12 \cdot 1,0079\frac{g}{mol} + 6 \cdot 15,999\frac{g}{mol} \tag{4.26}$$

$$M_{Glucose} = 180,15\frac{g}{mol} \tag{4.27}$$

The TOC of red dye, blue dye and Glucose is calculated by:

$$180,15\frac{g}{mol} \; M_{Glucose} = 6 \cdot 12,011\frac{g}{mol} \tag{4.28}$$

$$180,15\frac{g}{mol} \; M_{Glucose} = 72,07\frac{g}{mol \, TOC} \tag{4.29}$$

$$2000\frac{mg}{L} \; M_{Glucose} = X_{TOC_{Glucose}} \tag{4.30}$$

$$X_{TOC_{Glucose}} = \frac{72,07\frac{g}{mol \, TOC}}{180,15\frac{g}{mol} M_{Glucose}} \cdot 2000\frac{mg}{L} M_{Glucose} = 800,11\frac{mg}{L} \tag{4.31}$$

$$380,18\frac{g}{mol} \; M_{red} = 17 \cdot 12,011\frac{g}{mol} \tag{4.32}$$

$$380,18\frac{g}{mol} \; M_{red} = 204,02\frac{g}{mol \, TOC} \tag{4.33}$$

$$50\frac{mg}{L} \; M_{red} = X_{TOC_{red}} \tag{4.34}$$

$$X_{TOC_{red}} = \frac{204,02\frac{g}{mol \, TOC}}{380,18\frac{g}{mol} M_{red}} \cdot 50\frac{mg}{L} M_{red} = 26,83\frac{mg}{L} \tag{4.35}$$

$$626,55\frac{g}{mol} \; M_{blue} = 22 \cdot 12,011\frac{g}{mol} \tag{4.36}$$

$$626,55\frac{g}{mol} \; M_{blue} = 264,02\frac{g}{mol}_{TOC} \tag{4.37}$$

$$50\frac{mg}{L} \; M_{blue} = X_{TOC_{blue}} \tag{4.38}$$

$$X_{TOC_{blue}} = \frac{264,02\frac{g}{mol}_{TOC}}{626,55\frac{g}{mol}M_{blue}} \cdot 50\frac{mg}{L}M_{blue} = 21,08\frac{mg}{L} \tag{4.39}$$

The TOC for Albatex is calculated based on its data sheet (see A.32). Considering the theoretical value of 7.5 % the TOC is calculated by:

$$50\frac{mg}{L}Albatex \rightarrow 100\% \tag{4.40}$$

$$X_{TOC_{Albatex}} \rightarrow 7.5\% \tag{4.41}$$

$$X_{TOC_{Albatex}} = \frac{50\frac{mg}{L}Albatex}{100\%} \cdot 7.5\% \tag{4.42}$$

$$X_{TOC_{Albatex}} = 3.75\frac{mg}{L} \tag{4.43}$$

The sum of red dye, blue dye, Glucose and Albatex is giving the theoretical value for TOC of the feed water.

$$TOC_{total} = X_{TOC_{Glucose}} + X_{TOC_{red}} + X_{TOC_{blue}} + X_{TOC_{Albatex}} \tag{4.44}$$

$$TOC_{total} = 800,11\frac{mg}{L} + 26,83\frac{mg}{L} + 21,08\frac{mg}{L} + 3.75\frac{mg}{L} \tag{4.45}$$

$$TOC_{total} = 851.77\frac{mg}{L} \tag{4.46}$$

4.10.2 Chemical oxygen demand (COD)

The chemical oxygen demand (COD) is the value that gives the concentration of organic material. The COD is calculated based on the oxygen demand necessary for the oxidation [van Haandel and van der Lubbe (2012)]. The COD of glucose is

calculated by considering the oxidation reaction of $C_6H_{12}O_6$. For one mol glucose six mol oxygen are needed:

$$C_6H_{12}O_6 + 6O_2 \rightarrow 6CO_2 + 6H_2O \tag{4.47}$$

$$M_{Glucose} \rightarrow 6O_2 \tag{4.48}$$

$$180,15\frac{g}{mol}\ M_{Glucose} \rightarrow 6 \cdot 32\frac{g}{mol}O_2 = 192\frac{g}{mol}O_2 \tag{4.49}$$

$$2000\frac{mg}{L}\ M_{Glucose} = X_{COD_{Glucose}} \tag{4.50}$$

$$X_{COD_{Glucose}} = \frac{192\frac{g}{mol}\ O_2}{180,15\frac{g}{mol}\ M_{Glucose}} \cdot 2000\frac{mg}{L}\ M_{Glucose} = 2133,33\frac{mg}{L} \tag{4.51}$$

In the data sheet of Albatex (see A.32) a COD of 205 mg O_2/g is given. That means that 205 mg O_2 is needed to oxidise 1000 mg of Albatex. Therefore the COD for 50 mg/L Albatex can be calculated by:

$$205\ mgO_2 \rightarrow 1000\ mg\ Albatex \tag{4.52}$$

$$50\frac{mg}{L}\ M_{Albatex} = X_{COD_{Albatex}} \tag{4.53}$$

$$X_{COD_{Albatex}} = \frac{50\ \frac{mg}{L}M_{Albatex}}{1000\ mg\ Albatex} \cdot 205\ mg\ O_2 = 10,25\ \frac{mg}{L} \tag{4.54}$$

As the oxidation reactions of the dyes are unknown and the significant amount for COD is covered by glucose it has been decided to take into account the experimental results (see section 4.11).

Considering the COD values for the dyes as a variable X the total COD is calculated by the sum of glucose and Albatex:

$$COD_{total} = X_{COD_{Glucose}} + X_{COD_{Albatex}} + X \tag{4.55}$$

$$COD_{total} = 2133,33\frac{mg}{L} + 10,25\frac{mg}{L} + X \tag{4.56}$$

$$COD_{total} = 2143,58 + X \tag{4.57}$$

4.11 Verification of theoretically calculated values in model textile dye water

In order to verify the theoretical values for COD, TOC and Total Nitrogen (TN) each and every component of the model textile dye water has been measured and compared with the theoretical values.

4.11.1 Experimental setup

Based on the composition given in section 4.14 model solutions with the given concentration were measured. To increase the accuracy of the measurement while minimising the weighting-error a high volume of 1.5 litres has been prepared. Figure 4.50 shows the setup for the different samples. For the preparation of red dye the solution had to be heated above 80 °C in order to dissolve the red dye (Figure 4.51).

Figure 4.50. Setup for check-up of theoretical values
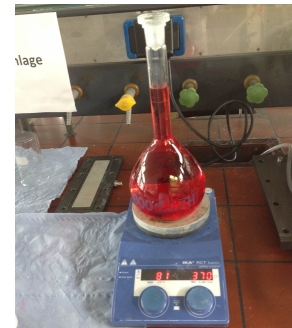
Figure 4.51. Red dye preparation

4.11.2 TOC

The TOC device is described in section 4.9.2. Table 4.15 gives the results for the TOC analyses including dilution factors. The result for the standard solution is expected to be around 50 mg/L, a deviation of +/- 5 mg/L is considered as normal. Glucose had to be diluted with the factor 9 in order to stay within the ideal measuring range.

Table 4.15. Final experimental values for TOC for MTDW

Dyestuff/chemicals	Average value [mg/L]
Standard	55.10
Remazol Brilliant Blue R	16.34
Acid Red 4	18.73
Glucose	767.70
Albatex DBC (Detergent)	2.58
Total	**805.35**

4.11.3 COD

The final results are given in Table 4.16.

Table 4.16. Final experimental values for COD for MTDW

Dyestuff/chemicals	Average value [mg/L]
Remazol Brilliant Blue R	63
Acid Red 4	64
Glucose	2105
Albatex DBC (Detergent)	6.78
Total	**2238.78**

For the measurement of COD a spectrometer from the company Merck was used. The device is described in section 4.9.1.

As the theoretical value of COD for Glucose is above the measuring range of the spectrometer it had to be diluted. A dilution factor of five was applied. The value for Albatex was below the measuring range. Therefore a new solution with a concentration of 300 mg/L was prepared and measured for COD. For this concentration a COD of 41, 40, 40 [mg/L] was measured.

4.12 Discussion of calculated and experimental results

Table 4.17 gives the complete overview of all calculated and measured values.

Table 4.17. Overview of calculated and measured values

Parameter	Dyestuff/chemicals	Theoretical value [mg/L]	Measured value [mg/L]
TOC	Acid Red 4	26.84	18.73
	Remazol Brilliant Blue R	21.08	16.34
	Glucose	800	767.70
	Albatex DBC (Detergent)	3.75	2.58
Total		**851.77**	**805.35**
COD	Acid Red 4	-	64
	Remazol Brilliant Blue R	-	63
	Glucose	2133.33	2120
	Albatex DBC (Detergent)	10.25	6.83
Total		**2143.58 + x**	**2238.78**

It is shown that the experimentally achieved results are close to the calculated ones. The slight differences might be due to measuring errors of the applied instruments.

5 Experimental part

The structure of this chapter is shown in Figure 5.1. In the initial phase it was necessary to perform the experiments with the target of replicate the results obtained using the PBM membranes made by redox polymerisation. In addition, a proper UV-light source and intensity had to be chosen. The effect of PEG to the PBM viscosity was studied. Finally, a PBM composition including the ideal photoinitiator type and concentration was defined.
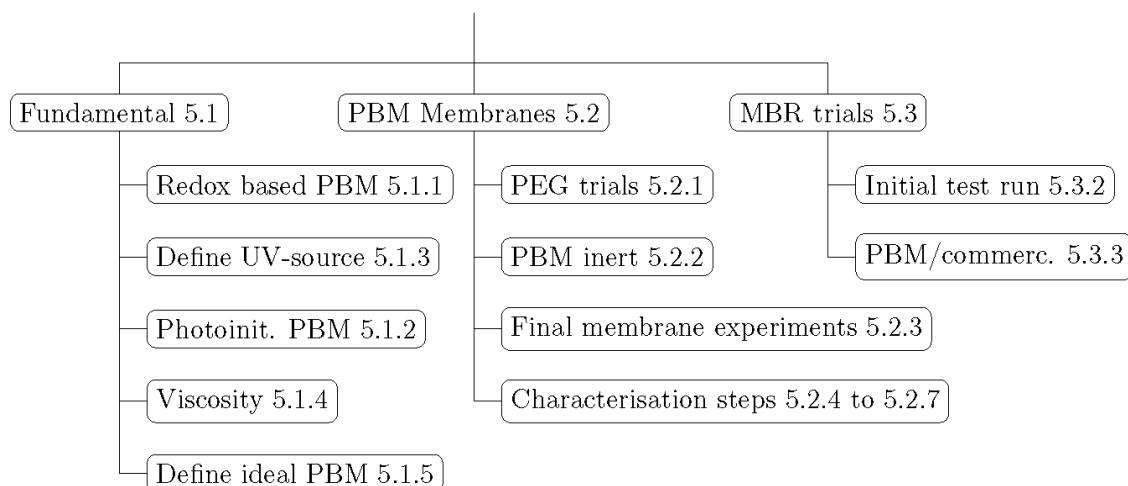
Figure 5.1. Structure of experimental part

The ongoing studies focused then on the coating onto a commercial ultrafiltration (UF) membrane substrate (UP 150T Microdyn Nadir) under different irradiation properties. Trials under inert and non-inert conditions for the pure PBM as well as for PBM containing different PEG´s were studied. The membranes were characterised by SEM, AFM, contact angle and water permeability set-up.

The final aim it is to test the PBM membranes in a lab scale MBR. Therefore, the existing MBR was redesigned in order to allow parallel experiments of PBM coated and commercial membranes. The setup proofed its durability within a long term

run of two commercial membranes. Afterwards, initial experiments with the PBM coated membrane where done in comparison with the commercial membrane.

In order to study the effect on another membrane support, a commercial RO membrane (PA) was coated and characterised as an outlook to future research.

5.1 Foundation for further studies

5.1.1 Replication of coating process with redox based PBM technique

The redox based coating in this thesis followed the approach of Galiano et al. (2015). However, some modifications of the casting chamber were conducted like an air conditioner and a thermostat were added to control the ambient temperature. In order to confirm previous findings, the redox based PBM coating was replicated. The redox based coating process is described in section 4.4.1.

The performance of the produced membranes was carried out by applying the SI-MATEC cross-flow testing unit (4.7.7) and the TOC analysis instrument (section 4.9.2). For the characterisation with the SIMATEC-unit, two kinds of tests were done, water permeability (WP) test and model foulant (MF) test. Protocols of both tests were described in section 4.7.7.

In the work done by [Deowan (2013)] the WP of PES and PBM coated membranes usually was around 630 and 200 L/h m² bar, respectively. This shows that the novel coating of PBM on top of PES membrane reduces WP due to the presence of the additional layer compared to PES membrane. A result in the same range was obtained in this work.

In Figure 5.2, the WP of PES and PBM membrane are 633 L/h m² bar and 215 L/h m² bar respectively. This PBM membrane was casted at 22 °C, with double amount of TMEDA comparing to the original PBM composition. TMEDA as one factor was doubled because it was expected that the quality of it decreased during the storage.
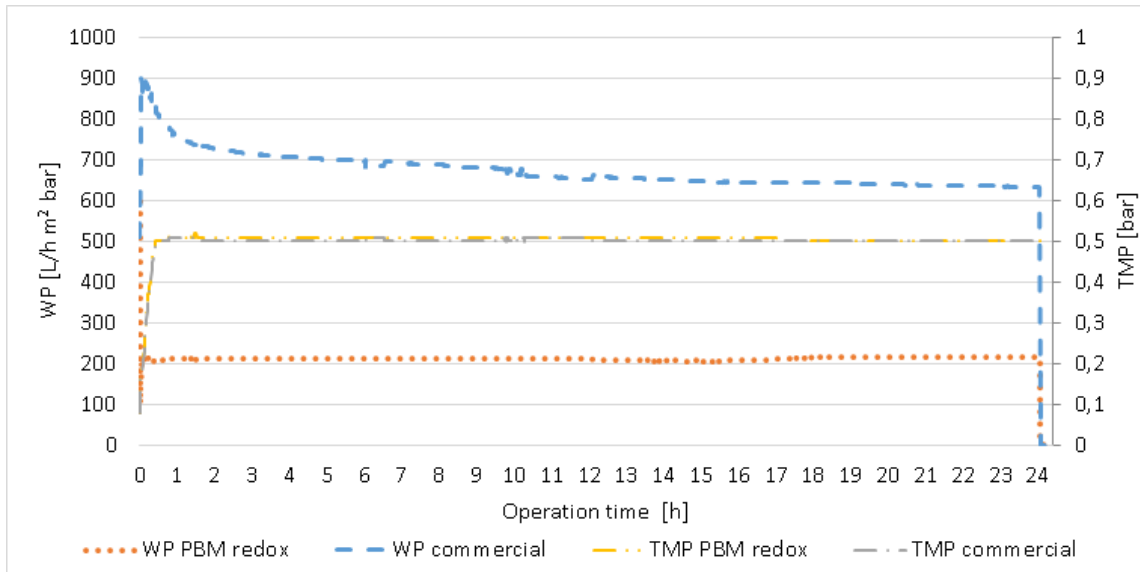
Figure 5.2. Final water permeability test of redox PBM coated membrane

Figure 5.3 shows the result of the model foulant test of PES and redox (DTAB) PBM membranes.
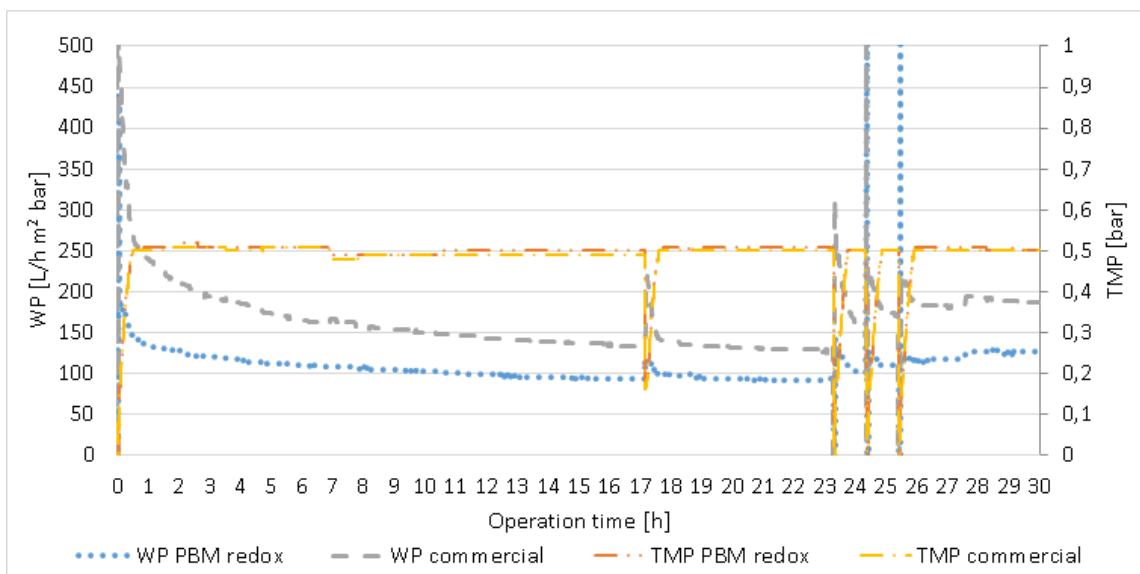
Figure 5.3. Final foulant test of redox PBM coated membrane

The comparison of water permeability (WP) between WP test and model foulant test showed that the WP with PES membrane showed 76 % reduction (reduced from 633 L/h m² bar to 154 L/h m² bar) whereas the reduction of WP for the PBM

membrane is only 54 % (reduced from 215 L/h m² bar to 100 L/h m² bar). The results are in line with [Deowan (2013), Galiano (2013), Galiano et al. (2015)] and indicate that the PES membrane without PBM coating is more prone to fouling by humic acid.

The WP increase for the PBM membrane after 3rd. cleaning was about 26 % while the PES membrane showed about 21 % only. Hence there is a slightly higher WP regain for the PBM membrane and this can be interpreted by greater fouling reversibility which means ability to remove HA with DI water from the surface of the membrane. Consequently, for the commercial PES membrane the greater part of the total fouling (76 % WP reduction) is due to irreversible fouling and only a smaller part can be reversed (21 %). For the PBM membrane the initial WP loss is smaller (54 %) and the regain is comparatively greater (26 %). This result confirms that the PBM coated membrane has a slightly better anti-fouling effect than the pure PES membrane.

5.1.2 Influence of photoinitiators to formation of microemulsion

To verify formation of microemulsion by adding the seven chosen photoinitiators described in section 4.3, the PBM compositions for DTAB and AUTEAB (see 4.2.2) were prepared. By adding the initiators at concentrations between 0.6 and 2.2 w% to the PBM the transparent appearance of the PBM was observed. Despite Irgacure 819DW, all studied initiators had no visible influence to the formation of PBM. For Irgacure 819DW a change in colour to a yellowish appearance of the PBM was observed. Anyway, as the PBM remained transparent the microemulsion was formed in all cases.

5.1.3 Study of UV-irradiation sources

The data of UV-lamps used in this thesis are described in section 4.5. During the experiments with the mercury lamps it was shown a temperature increase on the membrane surface up to 200 °C. This high temperature might destroy the structure of the PES membranes, therefore the mercury lamp will not be considered as the

light source in the following trials. The photoinitiator applied in the light sources test was Irgacure 819DW. The experiments are done with DTAB as surfactant and under non-inert conditions (except for UV-LED light guide).

Table 5.1 shows an overview of the experiments done in order to select the suitable UV-source. At this point the polymerisation rate of the PBM was not measured by FT-IR. As the access to the UV-lamps was limited, only the physical appearance after irradiation is given in the following Table 5.1. As it is shown, except the Solicure 2 UV-LED system, all UV-lamps were not able to polymerise the PBM. The bottom cured PBM was irradiated by the Solidcure 2 UV-LED system with an irradiation of UVA at 302 mW/cm². The M-Zero UV-LED system and UV-LED light guide were not the appropriate light source for the flat sheet membrane curing since the flat sheet membrane has a surface of 26 x 8 cm, which is far beyond the possible coating area.

In order to get an uniform irradiation at the membrane surface, and avoiding light loss at the same time, the UV-LED SERIES L (see section 4.5), with an irradiation of 300 mW/cm² at the substrate surface, was chosen as the ultimate light source. As of the high content of informations, the detailed description of its experiments is not given in Table 5.1 but summarised in section 5.1.5.

Table 5.1. Experiments for selection of UV-light source

Source	PEG	Working distance [cm]	Irradiation @ substrate [mW/cm^2]	Irradiation time [min]	Photoinitiator [%]	Result
Solidcure 2 UV LED system	15% PEG 20.000	5	UVA: 391 UVA2: 490 UVV: 774	1 / 2	0.6	Sticky
Solidcure 2 UV LED system	15 % PEG 20.000	8	UVA: 302 UVA2: 627 UVV: 734	3 / 3.5	0.6 / 1.2	Sticky / bottom polymerised, surface sticky
UV LED light guide (CO_2 inflated onto the membrane surface)	No PEG / 15% PEG 20.000	14	UVA: 0 UVA2: 43 UVV: 119	2 / 2	0.6 / 1.2	Sticky
UV LED light guide (CO_2 inflated onto the membrane surface)	No PEG	2	UVA: 583 UVA2: 2569 UVV: 5288	1	0.6	Sticky
UV LED light guide (CO_2 inflated onto the membrane surface)	15 % PEG 20.000	4	UVA: 183 UVA2: 36 UVV: 10	2	2.4	Sticky
Low pressure mercury lamp	No PEG	2	Total: 100 Vis.: 8 UVA: 1 UVB: 2 UVC: 89	3	2.4	Sticky
M-Zero UV LED system	No PEG / 15% PEG 20.000	0.5	UVA: 209 UVA2: 2102 Vis: 4749	2 / 3	2.4	Sticky

5.1.4 Viscosity adjustment by PEG

Despite the chemicals used for polymerisation of the PBM, it has been tried to increase the viscosity in order to ensure a proper casting onto the commercial membrane by using DTAB as surfactant. In addition, the use of polymerisable PEG should increase the hydrophilicity of the coated membrane. In all cases described in this section a transparent formation of PBM was observed.

As the novel developed surfactant AUTEAB is not yet commercially available and the production is very time and cost intense it has been decided to perform the viscosity experiments using the surfactant DTAB.

For the DTAB based PBM (see section 4.2.2) an immediate permeation of the emulsion in the pores of the membrane was observed. For this purpose different types of Poly Ethylene Glycol (PEG) are used in different concentrations in order to find the most suitable one. The overview of the different types of PEGs is given in section 4.6. Several different compositions were tested for their performance. They all have in common the same basic PBM composition for DTAB that is given in section 4.2.2. The photoinitiators as well as the different PEGs act only as additives. Table 5.2 shows the additives as well as the ranges they were studied for their casting properties.

Table 5.2. Additives to PBM for viscosity trials

Photoinitiator Irgacure 819DW <u>or</u> Irgacure 184	0.6 w%
PEG 2.000	15 w%
PEG 20.000	1 - 15 w%
PEG polymerisable	15 - 45 w%

As PEG 20,000 has the highest molecular weight, first trials were made with this viscosity enhancer in order to find a proper casting-viscosity which still forms a stable microemulsion. This part of the experiment is only based on visual observations of the resulting membrane coating. Table 5.3 shows the result of this trials.

Table 5.3. Testing PEG 20.000 as viscosity enhancer

Irg. 819DW	Irg. 184	PEG 20.000	Visual observation
-	0.6 w%	1 w%	transparent, very good dissolved, dissolved, permeating through membrane
0.6 w%	-	5 w%	transparent, very good dissolved, dissolved, permeating through membrane
0.6 w%	-	10 w%	transparent, very good dissolved, dissolved, permeating through membrane
0.6 w%	-	20 w%	became very viscous no homogenious thickness, became to viscous
0.6 w%	-	15 w%	transparent, very good dissolved, viscosity increased, homogenious coating, no visible permeation into membrane, homogenious coating
-	0.6 w%	15 w%	transparent, very good dissolved, viscosity increased, homogenious coating, no visible permeation into membrane

By use of the Ubbelohde-viscosimeter, as described in section 4.7.1, the viscosity of several compositions was measured. Figure 5.4 shows the results of the viscosity adjustment experiment. The highlighted target viscosity was defined by the probe
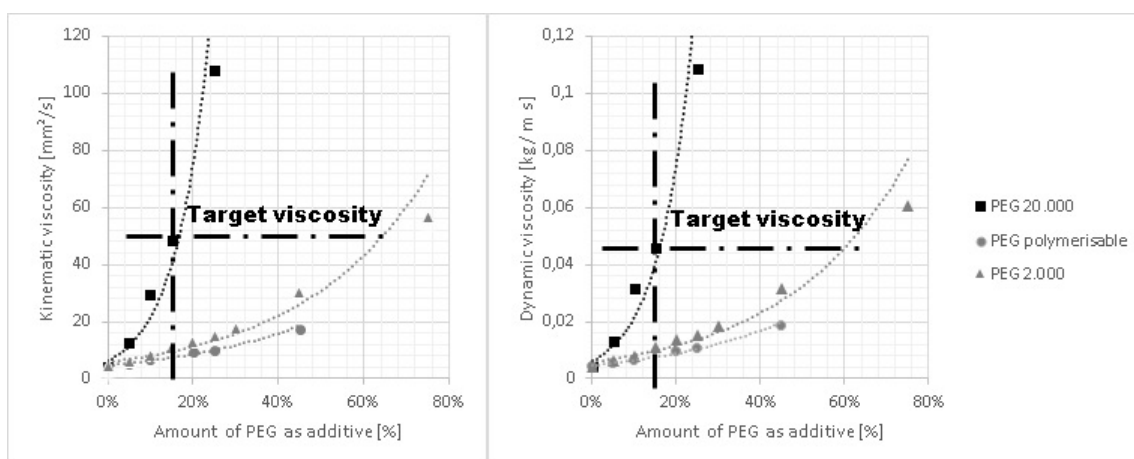
Figure 5.4. Results for viscosity adjustment trials

that consisted of a PBM that did not permeate into the membrane pores and remained onto the membrane surface (see Table 5.3). By achieving a similar target-viscosity by using PEG 2,000 an amount above 45 w% is needed. In order to keep the influence to the formation of the microemulsion of the PBM as low as possible 15 w% of PEG 20,000 is used for further trials. Anyway, it has to be mentioned that the PEG will be washed off later and also influences the costs for the PBM.

5.1.5 UV process characterisation

In order to scale up the conventional redox based polymerisation process developed by Deowan (2013) and Galiano (2013) the polymerisation time needs to be fastened significantly. Therefore it is the approach of this thesis to realise the polymerisation by the use of photoinitiators activated by UV-light which is expected to increase the polymerisation speed intensively.

Spectral analysis

A variety of influences may effect the progress and quality of the polymerisation. Therefore the first step was to characterise all involved chemicals regarding their UV cure readiness.

By the use of the UV/VIS Spetrophotometer described in section 4.7.3, the single components of the composition given in section 4.2.2 for UV polymerised microemulsion were analysed regarding their absorption properties.

All values in Figure 5.5 were measured three times and in different concentrations in order to avoid measuring errors.

As described in section 5.1.4 different qualities of poly ethylene glycol (PEG) were analysed. Details about the PEG types are given in section 4.6. Therefore they have been analysed for their spectral properties as well. It is shown that non of the chemicals show an absorption in the target range of the UV-LED (365 nm).
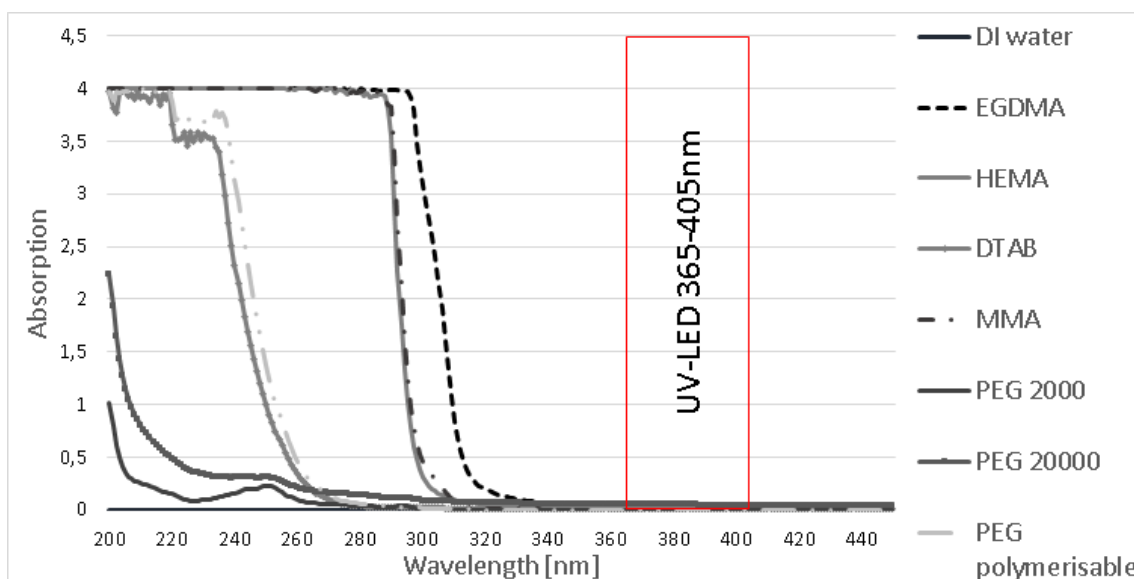
Figure 5.5. Spectral analyses of chemicals used for microemulsion preparation

Figure 5.6 shows the results for the studied photoinitiators. As shown, despite DPP, all of them show significant absorption properties in the wavelength of 365 nm. In the next step the photoinitiators were studied for their influence to the conversion rate of the PBM (see section 5.1.5) in order to define the ideal one.
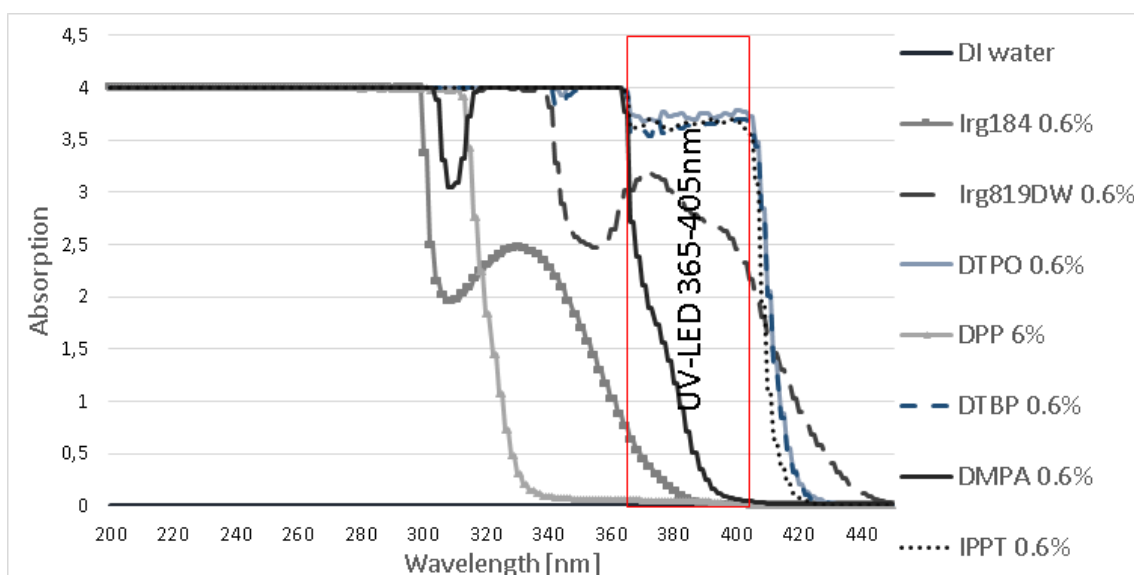
Figure 5.6. Spectral analyses of studied photoinitiators

Conversion rate experiments

A protocol was developed for obtaining the optimal composition for the photo induced polymerisation process. The method is explained in section 4.7.2.

The following factors influence the polymerisation process of coatings using a UV-lamp:

- Substrate type
- Photoinitiator concentration
- Exposure time

- Temperature
- Photoinitiator species
- Wavelength

- Oxygen inhibition
- Coating thickness
- UV-intensity

As described in section 4.7.2 a FT-IR instrument is used for the calculation of the conversion rates. In order to avoid the influence of the supporting membrane to the measurement (by overlapping peaks in the interesting wavelength region), the trials with the PBM were made on glass plates. Then, the optimum compositions were coated onto membranes and their performance was studied (see section 5.2).

The following experiments were all done at 20 °C under non-inert conditions. A small drop was applied onto glass plates (see Figure 5.7) and polymerised at 300 mW/cm² at the wavelength of 365 nm using a UV-LED lamp. All other factors were varied and are shown in Figure 5.8 to Figure 5.14.
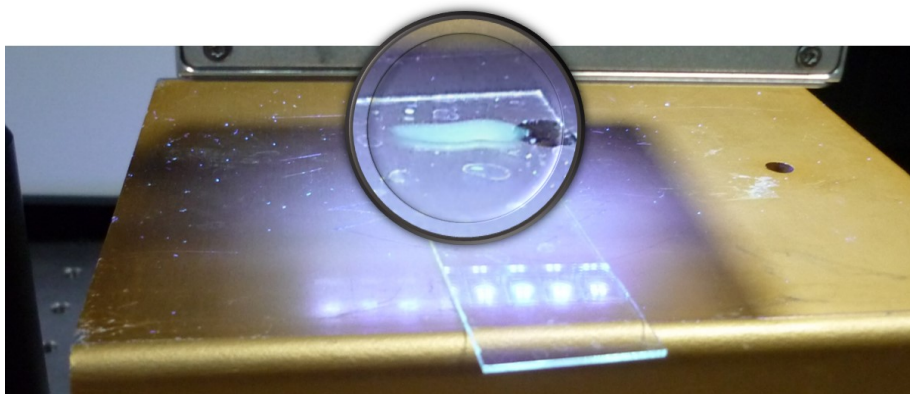
Figure 5.7. PBM drop onto glass plate for conversion rate experiments

Initial trials are done in order to study the effect of the surfactant type on the conversion rate of the PBM. Figure 5.8 highlights the results for the photoinitiator

Irgacure 184. For all other photoinitiators a complete conversion never occurred by using the DTAB surfactant. The effect on the polymerisation rate is clearly shown. To achieve a full conversion, the DTAB based PBM required more than double irradiation time.
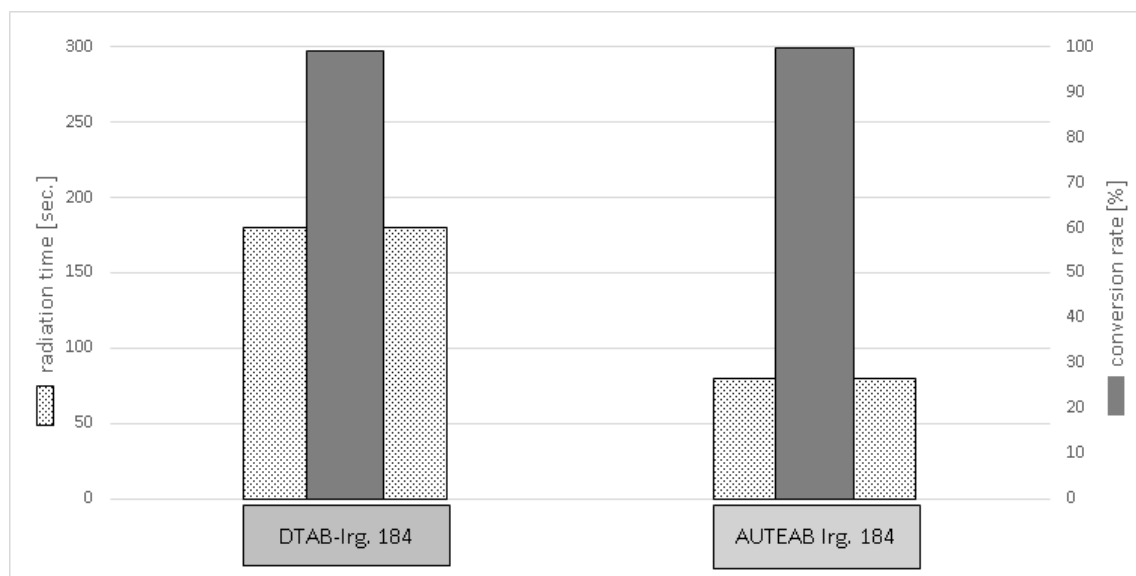
Figure 5.8. Conversion rate DTAB vs. AUTEAB

Therefore, as it is the target of this work to lower the polymerisation time, all experiments described in the following part are based on the use of AUTEAB for making the PBM as described in section 4.2.2.

Initially all photoinitiators described in section 4.3 were tested for their polymerisation efficiency of the basic PBM described in section 4.2. Additive concentrations ranging from 0.6 to 2.6 w% were examined. Only DMPA and Irgacure 184 were able to polymerise the PBM under non-inert conditions, and therefore they are used in the ongoing experiments.

The conversion rate experiment for DMPA at different concentrations and irradiation time is summarised in Figure 5.9.
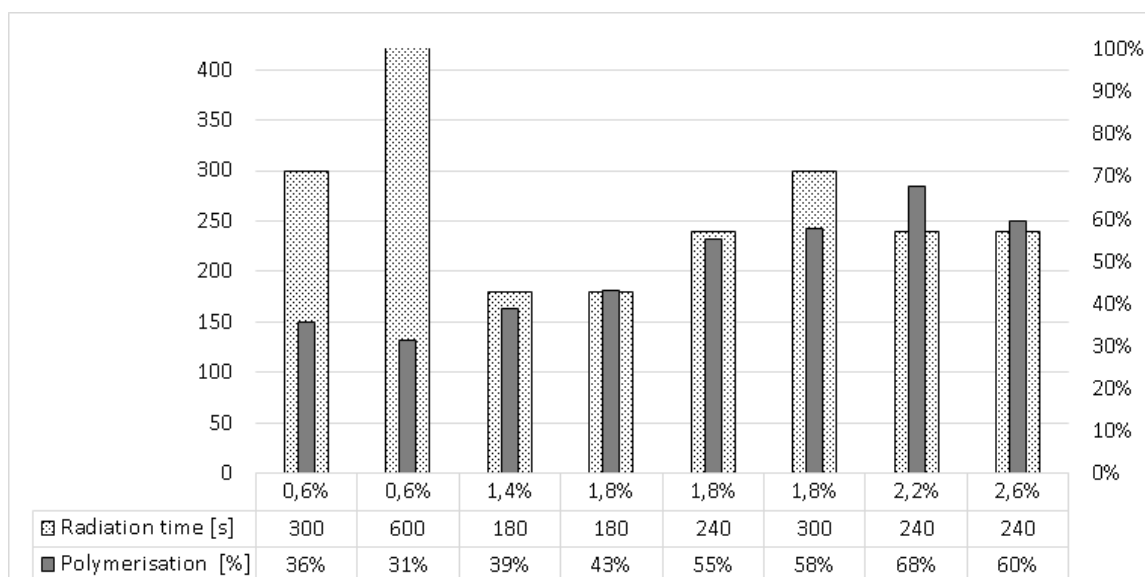
Figure 5.9. Conversion rates for DMPA

The highest conversion rate is found for 2.2 w% of DMPA with a radiation time of 240 seconds. However, the PBM did not completely polymerise.

To study the influence of 15 w% PEG 20.000 as additive, a high number of trials were done with DMPA as photoinitiator. The results are given in Figure 5.10.
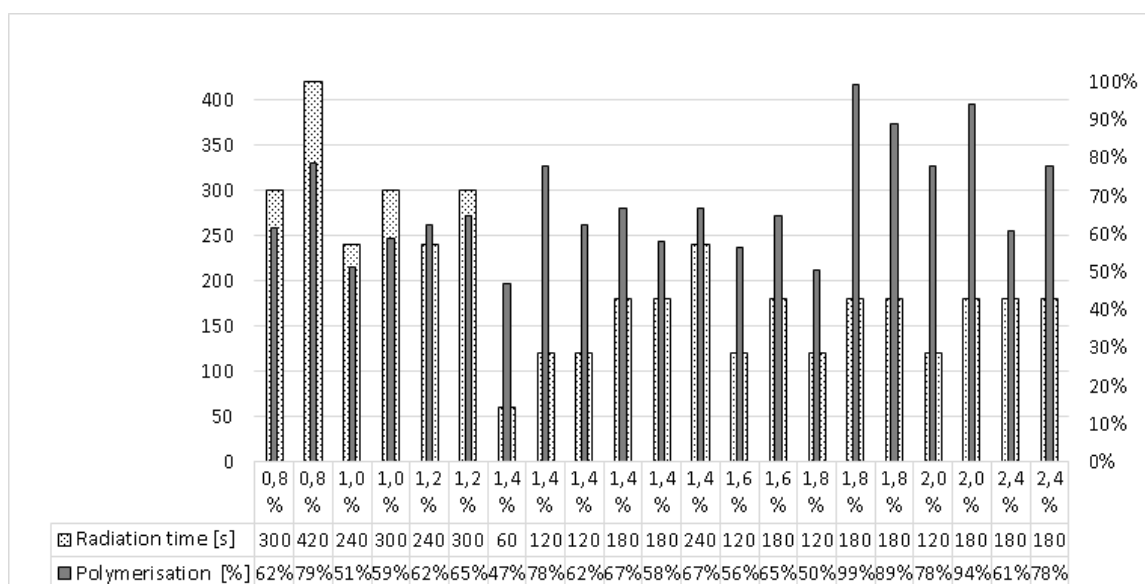
Figure 5.10. Conversion rates for DMPA with PEG 20.000

Comparing these results with the ones without PEG the first remarkable fact is that the addition of PEG seems to improve the conversion properties of the PBM. This is linked to the fact that the trials were done under non-inert conditions. The PEG acts as oxygen inhibitor to the PBM which lowers the oxygen inhibition effect described in section 2.3.4. The highest conversion rate was found at a photoinitiator concentration of 1.8 w% after 180 seconds of irradiation. However, another trial with 1.8 w% irradiated for the same time resulted in a 10 % lower conversion rate. The same trend is shown for 1.4 w% after 120 and 180 sec. This might be linked with different drop heights of the applied PBM.

The results for Irgacure 184 are given in Figure 5.11. In comparison to the results for DMPA (Figure 5.9) higher conversion rates were achieved. This is most probably because this photoinitiator is less prone to oxygen inhibition than the DMPA (see section 4.3.

	0,6%	1,0%	1,4%	1,4%	1,8%	1,8%	1,8%	2,2%	2,2%	2,2%	2,2%
Radiation time [s]	300	240	180	240	120	180	240	60	90	120	180
Polymerisation [%]	59%	60%	58%	78%	73%	94%	88%	55%	74%	91%	85%
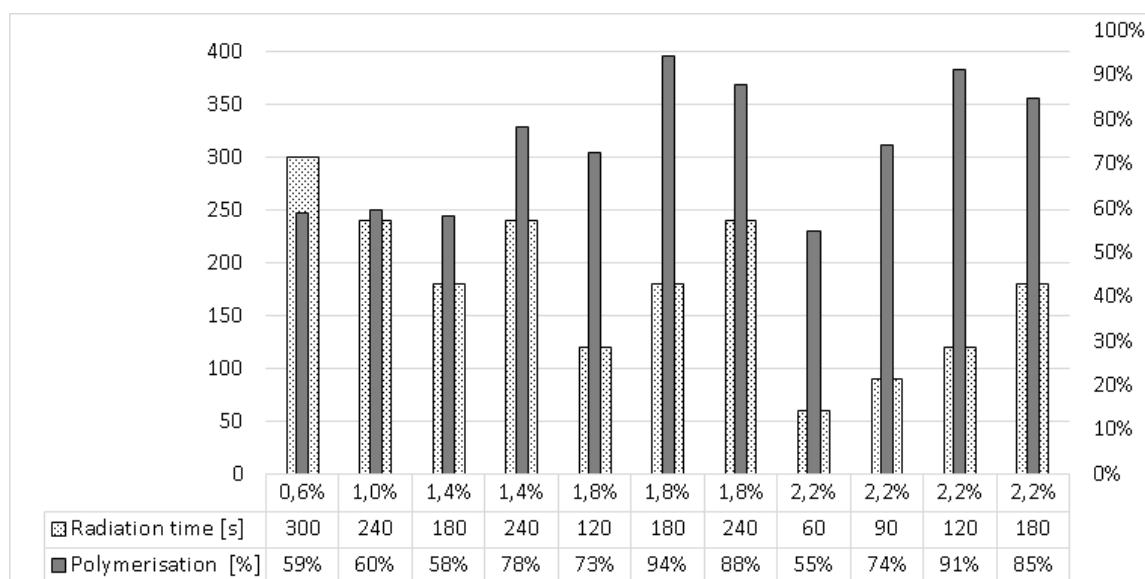
Figure 5.11. Conversion rates for Irgacure 184

The highest conversion rate was found at a photoinitiator concentration of 1.8 w% after irradiation of 180 seconds. Another observation is that a longer irradiation time does not necessarily contribute to the conversion rate. In two cases with 1.8 w% and 2.2 w% photoinitiator the increase in time seemed to even lower the conversion rate. This might happened due to a heat effect which decomposed the coating.

By adding 15 w% of PEG 20,000 to the PBM the trend described for Figure 5.10 was not kept for all concentrations. In contrary to DMPA, for some of the concentrations with Irgacure 184 the PEG lowered the conversion rate. Nevertheless, for others it improved it (see Figure 5.12). However, as the coating onto the membranes resulted in very dense membranes a water permeability of about zero was determined (see section 5.2.1). Therefore, this effect was not studied further.
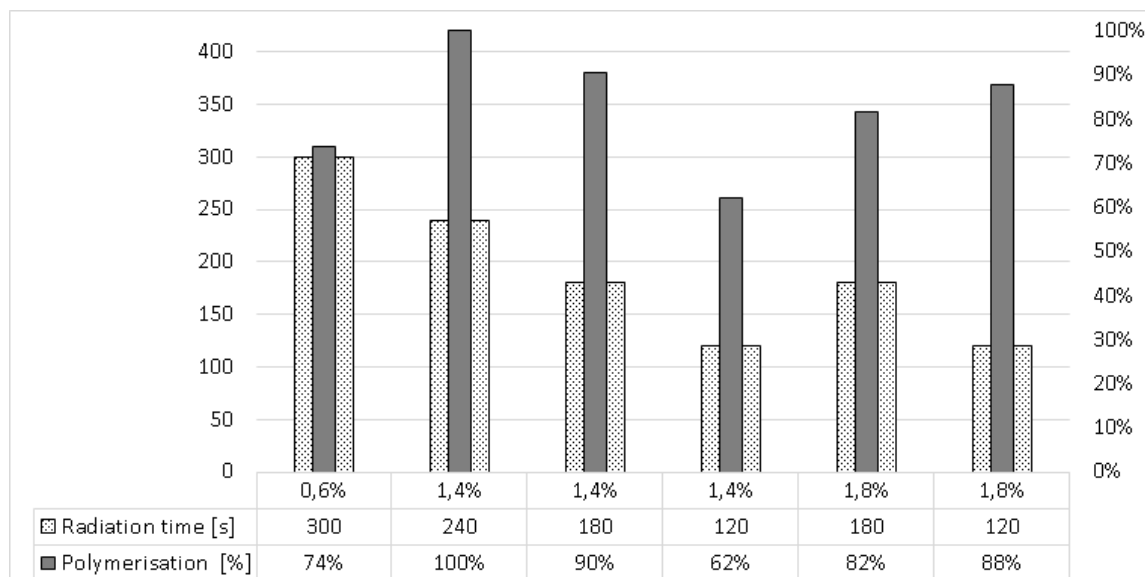
Figure 5.12. Conversion rates for Irgacure 184 with PEG 20.000

As the oxygen inhibition effect is hindering the polymerisation process, a coating under inert conditions should affect the polymerisation positively. Therefore, this effect has been studied more deeply. The following Figures 5.13 and 5.14 compare the conversion rates for DMPA and Irgacure 184 under inert and non-inert conditions. Both are polymerised as single drop onto a glass plate.

Figure 5.13 compares the results for DMPA. It is clearly shown, that the inert conditions improve the conversion rate as well as the polymerisation speed. As the concentration of 2.2 w% resulted to be most efficient under non-inert conditions, the effect to this concentration was further studied. For the comparison of the Irgacure 184 results under inert and non-inert conditions, again the best concentration from the non-inert trial (1.8 w%) was selected (see Figure 5.14). The conversion rate as well as the polymerisation time improved under inert conditions. A full conversion
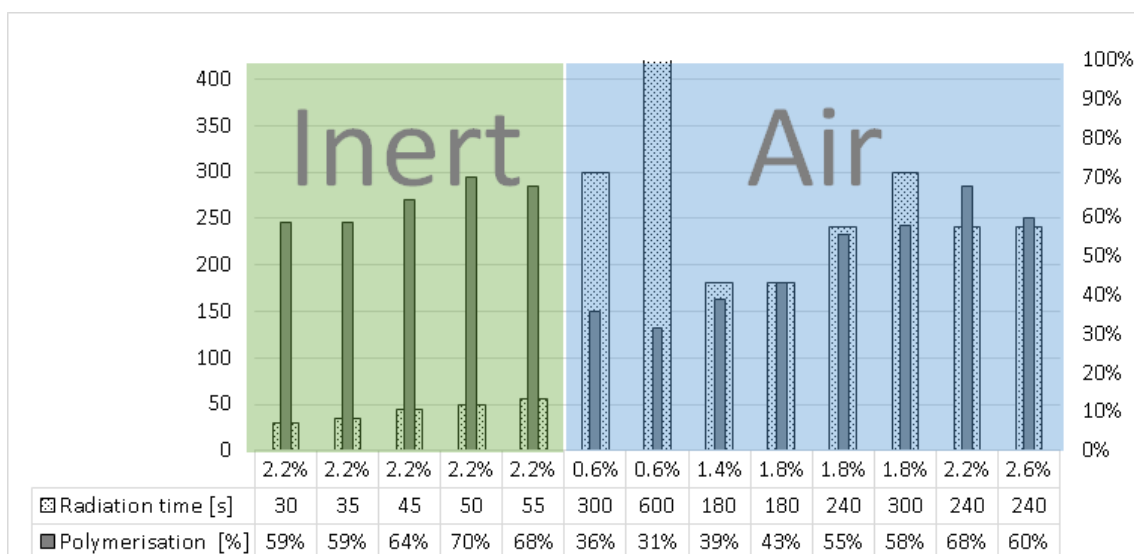
Figure 5.13. Conversion rates for DMPA inert and in air

was achieved already after 30 seconds under inert conditions. By contrast, under non-inert conditions the highest conversion was found at 94 % after 180 seconds. It is also shown that an increase of photoinitiator concentration (air, 1.8-2.2 w%) leads to lower polymerisation rate at the same radiation time. Based on these results further experiments were done with Irgacure 184 at a concentration of 1.8 w% with an irradiation time of 30 seconds (results see section 5.2.3).
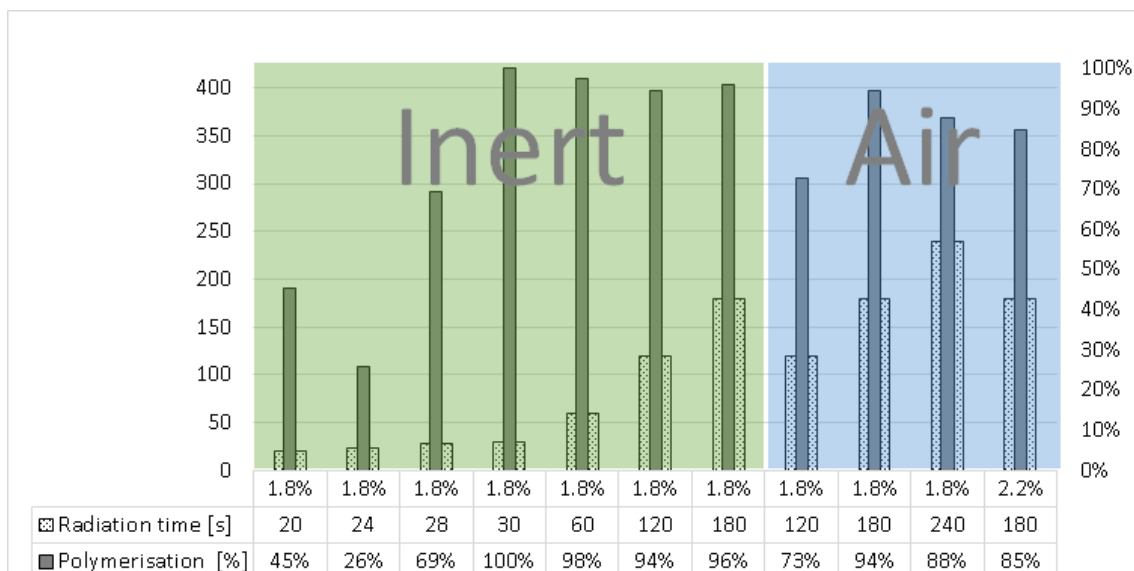
Figure 5.14. Conversion rates for Irgacure 184 inert and in air

5.2 Membrane characterisation

This section summarises the results for the PBM coated membranes. The influence of the addition of PEG (polymerisable and non-polymerisable) as well as the influences of coating conditions (e.g. temperature, coating thickness) on PBM formation are reported. The WP of the commercial membrane is highly fluctuating according to the membrane supplier for the pure water test (see Table 4.1 and [Microdyn-Nadir-GmbH (2014)]). However, stable WPs are shown for the model foulant experiments.

5.2.1 Water permeability for PEG trials under non-inert conditions

As described in section 5.1.4 the addition of different types of PEG is studied to evaluate their effect on the viscosity of the PBM solution. In the following, the influence of PEG 20,000 and polymerisable PEG on membrane formation is reported.

Water permeability of PBM+PEG 20.000 coated membrane

Based on the experiments described in section 5.1.5 (PBM applied onto glass plate) two PBM compositions with additional 15 w% PEG 20,000 were chosen to be further studied. The performance of the novel PBM and commercial PES membrane is shown in Figure 5.15. The water permeability represents the results for the pure water test using the set-up described in section 4.7.7. In total three different PBM coatings and the referencing UF commercial membrane are plotted. Two of the PBM membranes are done by using the photoinitiator called Irgacure 184. In order to replicate the results, the same conditions were chosen for the PBM and coating conditions. Both membranes show a permeability around zero. Another photoinitiator (DMPA) was studied as well. A decreasing coating thickness is expected to increase the permeability of the membrane. Therefore membranes coated with 100 and 250 μm are compared with each other. However, no remarkable increase is noticed. In addition to that, the membrane surface resulted to be glueish after polymerisation, most probably caused by a non-complete polymerisation. The glueish

surface appeared as well in experiments with a glass support that showed low conversion rates (see section 5.1.5). For this reason, the choice of having the PEG in the PBM solution has not been further studied.
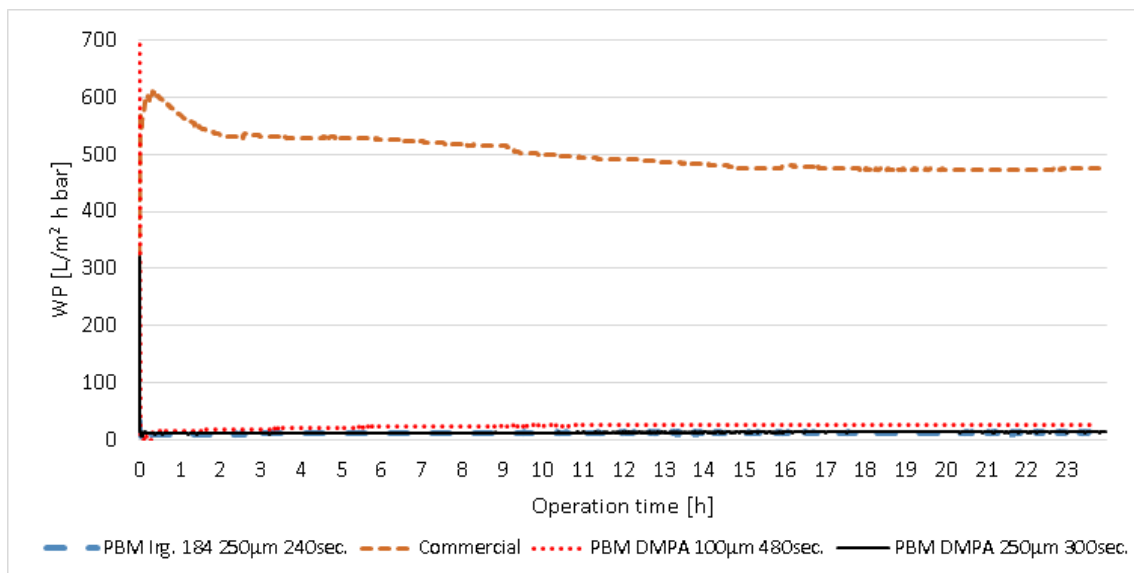
Figure 5.15. Water permeability of PBM with PEG 20.000 vs. commercial membrane

Water permeability of PBM+polymerisable PEG coated membrane

In this section the influence of the addition of polymerisable PEG to the PBM coating and the resulting water permeability of the membrane is studied. The conditions of the PBM coating on the UF commercial PES membrane are reported in Table 5.4.

Table 5.4. Coating conditons of PBM with polymerisable PEG

Photoinitiator for UV-LED	Temperature	Casting knife	Polymerisation time
1-Hydroxy-cyclohexyl-phenyl-ketone (Irgacure 184) 1.8 w%	20 °C	250 μm	240 sec.

Figure 5.16 highlights the water permeability of the coated vs. the commercial

membrane. The PBM coated membrane did not show any water permeability, at a TMP of 0.5 bar, probably due to a dense layer formed by the PBM membrane.
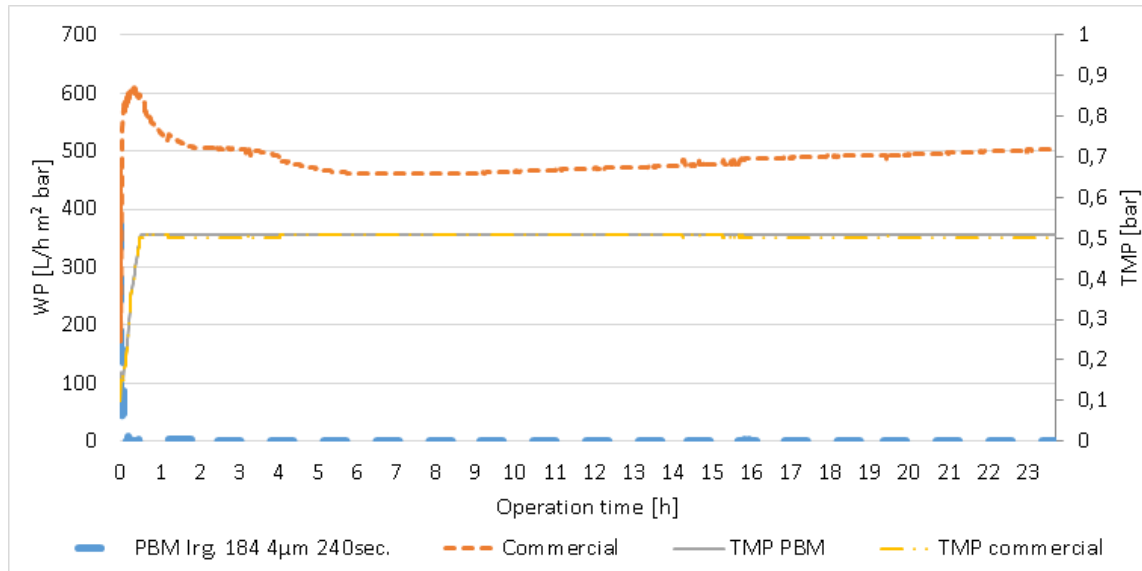
Figure 5.16. Water permeability of PBM with polymerisable PEG

Tests have been performed as well with a model foulant. Even by increasing the TMP up to 3.25 bar the water permeability did not increase (see Figure 5.17).
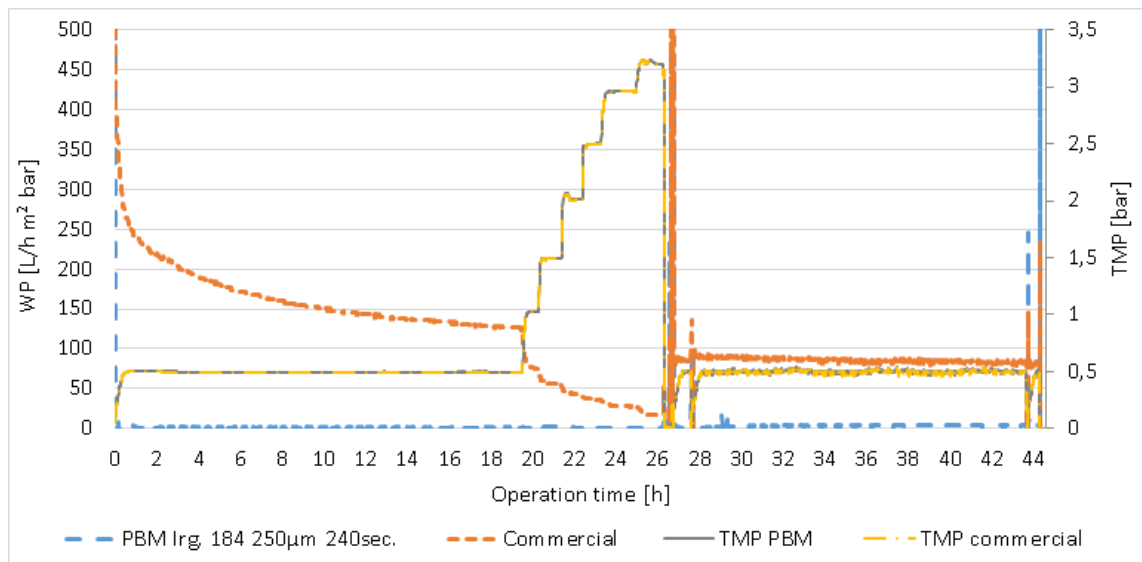
Figure 5.17. Fouling permeability of PBM with polymerisable PEG

Both results indicate that the addition of polymerisable PEG leads to a very dense

membrane coating. For this reason, the PBM coating is prepared further without the addition of PEG additive. Moreover, also in this case the membrane coating remains glueish, meaning that the full polymerisation did not occur.

5.2.2 Water permeability of PBM coated membrane under inert conditions

This section describes the water permeability experiments performed using the PBM coating with the AUTEAB surfactant, under inert conditions (Nitrogen atmosphere) and photoinitiator Irgacure 184 at a conc. of 1.8 w%, as resulted of section 5.1.5.

Influence of the coating thickness

Figure 5.18 shows the water permeability of the PBM coated membrane made with the composition reported above. In particular the effect of the thickness of different PBM membranes is reported. All coatings were done at 24 °C and polymerised for 30 seconds. The PBM coating was cast on the commercial UF PES membrane at different casting knife heights from 4 to 150 μm, while the thickness of 4 μm represents the thinnest commercially available casting knife height.
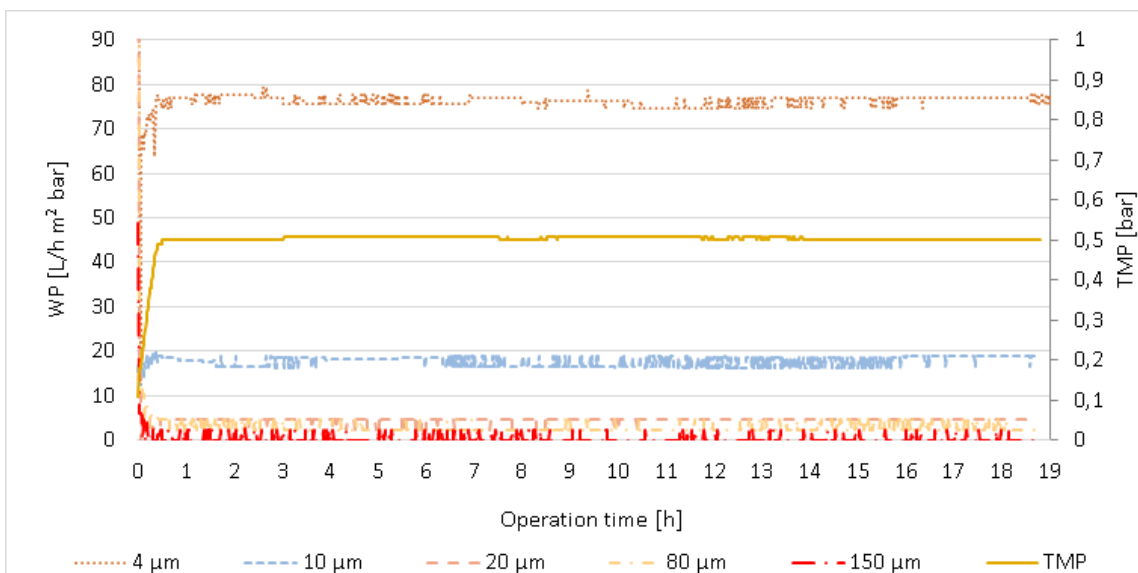
Figure 5.18. Influence of coating thickness to the water permeability

In order to show the correlation between coating thickness and water permeability Figure 5.19 is given in addition.
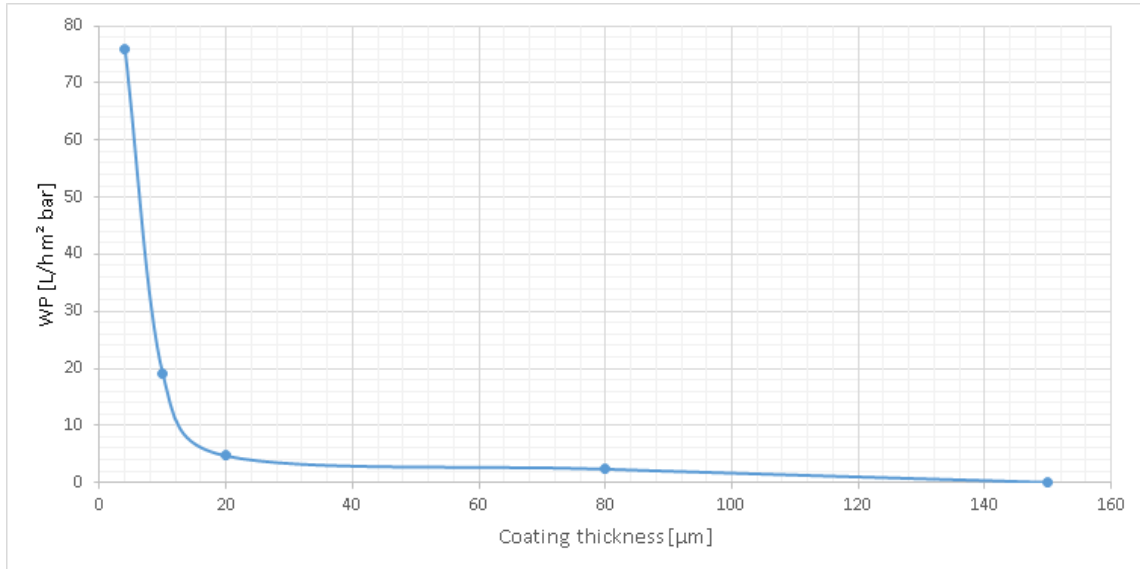
Figure 5.19. Correlation between coating thickness and water permeability

It is clearly shown that the coating thickness influences the water permeability of the final membrane. The thicker the coating, the lower the permeability. The highest permeability was found with the lowest casting knife thickness used (for SEM cross section picture see section 5.2.7). At 20 μm and above the permeability gets too low for the purpose of an application in the MBR, but might be interesting for different applications.

The decreasing permeability with increasing coating thickness is due to the extra layer on the membrane which increases the resistance and therefore reduces the water permeation across the membrane. This effect might be linked with the micro-channels that are formed by the PBM on top of the membrane (see section 5.2.7). If we imagine these channels as single mesh as shown in Figure 5.20, and add another 3 layers of mesh on top of it (Figure 5.21), the free area between the mesh decreases already. If we then increase to ten mesh (Figure 5.22) it becomes even more visible that the open area gets very less. Considering that the micro-channels behave similar to stacked mesh it could explain the decrease of permeability as simply more resistance is created.
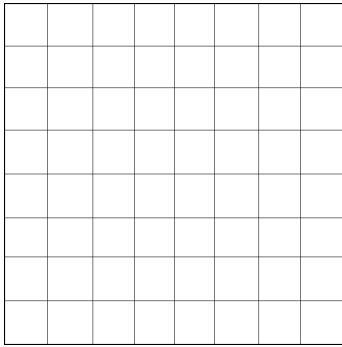
Figure 5.20. Single mesh
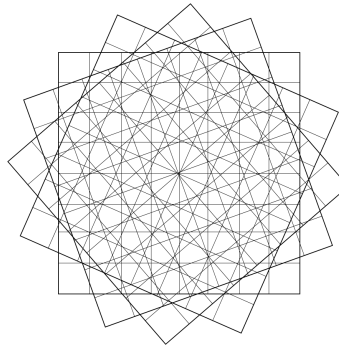
Figure 5.21. Four stacked mesh
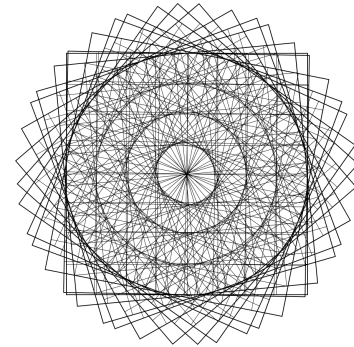
Figure 5.22. Ten stacked mesh

Figure 5.23 shows the result for the model foulant permeability of the 10 μm (up to 46 h) and the 4 μm (up to 73 h) coated membrane, together with their referencing commercial membranes (Reference 4 μm, Reference 10 μm). All other coating thickness are not given as they resulted in a permeability value near to zero.
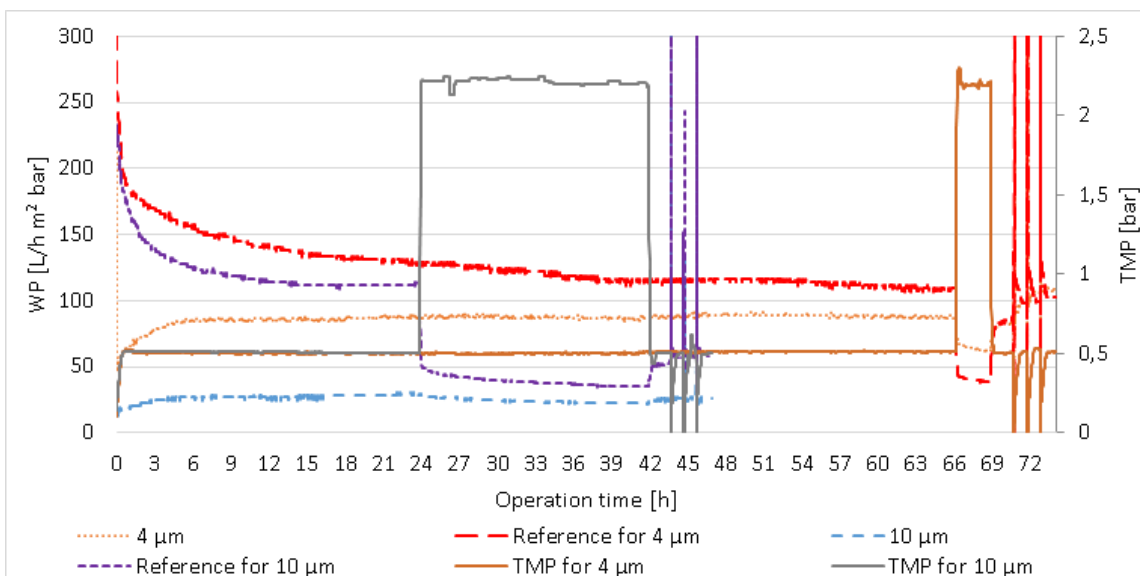
Figure 5.23. Influence of coating thickness to the model foulant permeability

For the coating with 10 μm the permeability remains very stable around 25 L/h m^2 bar even by increasing the TMP up to 2.2 bar. The subsequent cleaning procedure (TMP back to 0.5 bar and three times purging with DI water for one hour) resulted in an increase of permeability for the reference commercial membrane but the coated membrane kept its permeability. In contrary, the 4 μm coated membrane had a

very stable permeability around 87 L/h m² bar before the TMP was set to 2.2 bar. At that point (66 h) the permeability of the reference commercial membrane drops below the coated membrane. Even after the cleaning protocol, the coated membrane kept a permeability above the referencing commercial one.

The results for the 4 μm coated membrane will be discussed more deeply in section 5.2.3. The TOC rejection for the 4 μm is 86.47 $\pm$2.22 % while the reference membrane showed 94.51 $\pm$2.22 %. For the 10 μm a TOC rejection of 89.51 $\pm$1.40 % was measured and for the commercial 91.59 $\pm$1.40 %. Both PBM´s show a slight decline in TOC rejection in comparison to the commercial membrane. However, this might be due to normal fluctuations of the supporting commercial membrane properties as their values are also not constant.

Figure 5.24 shows the membranes with and without PBM after the model foulant tests and it can be noticed that the membranes with the PBM show a less dark colour index of a less fouling when the PBM layer is present than the commercial one.
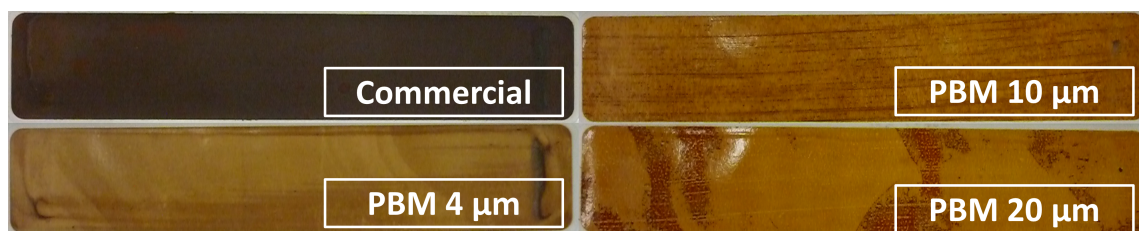
Figure 5.24. Commercial and PBM coated membranes after study of coating thickness

Influence of the polymerisation temperature

A higher temperature should increase the polymerisation rate of the PBM. However, as described in section 2.3.5 if the polymerisation reaction is to fast the upper few micrometers of the film get polymerised immediately, so only a negligible intensity of UV-light reaches the rest of the film leading to an uncompleted polymerisation [Z.W. Wicks F.N. Jones (1994)].

Figure 5.25 shows the WP (DI water with 60 μS/cm) of PBM coated membranes that were irradiated at temperatures of 20, 25 and 30 °C. The highest WP results

for the coating at 25 °C (98 L/h m² bar), while the temperatures of 20 and 30 °C result in lower permeabilities of 70 and 88 L/h m² bar.
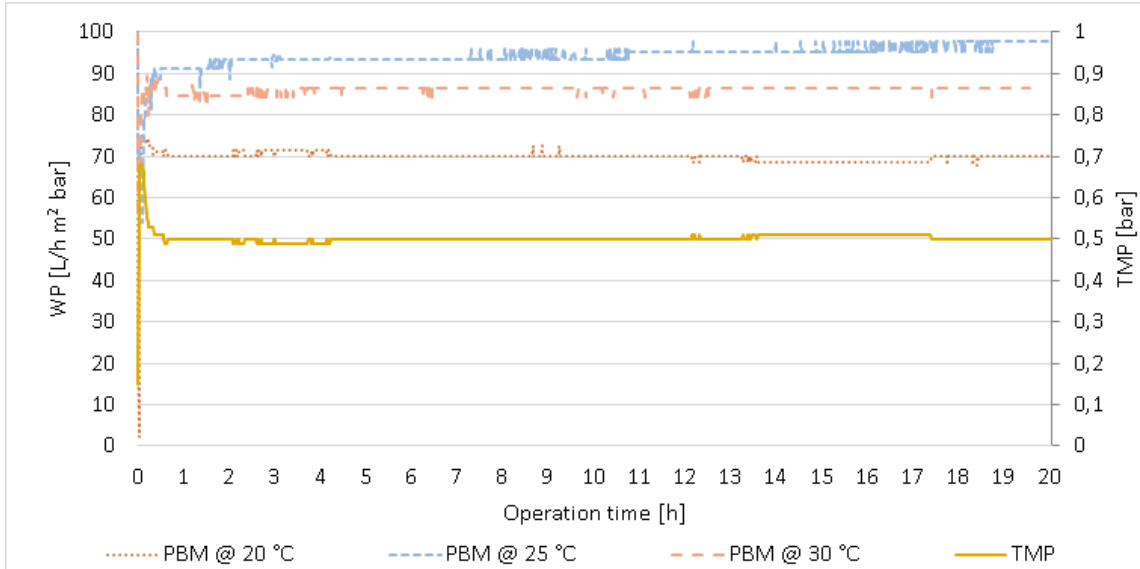
Figure 5.25. Influence of coating temperature to the water permeability

Figure 5.26 to 5.28 show the results for the model foulant experiment. The PBM membranes where always treated in parallel to a commercial membrane (highlighted as Reference).
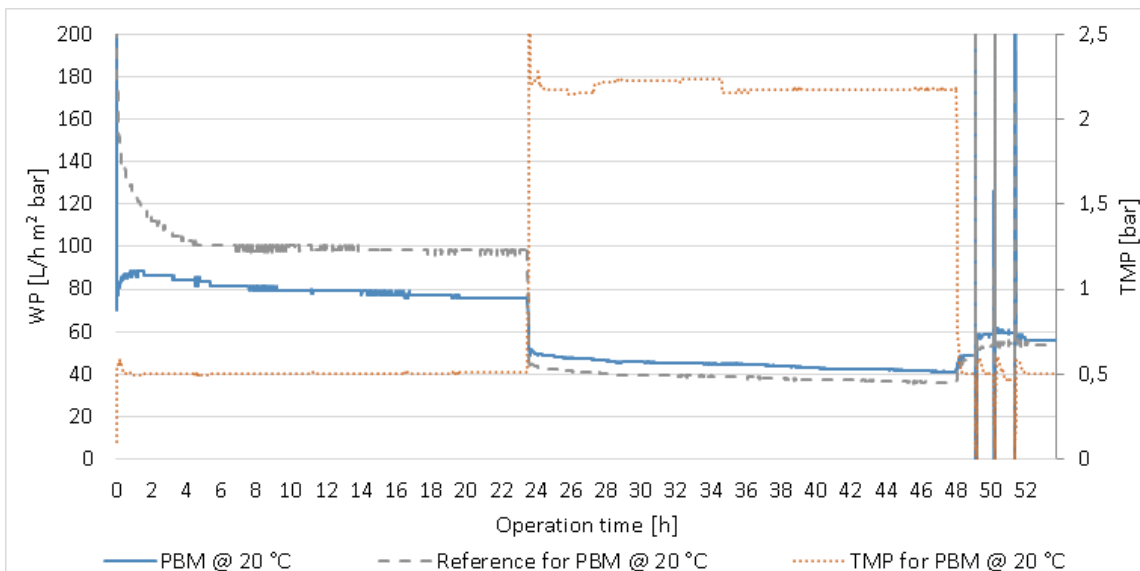
Figure 5.26. Model foulant permeability of PBM coated at 20 °C
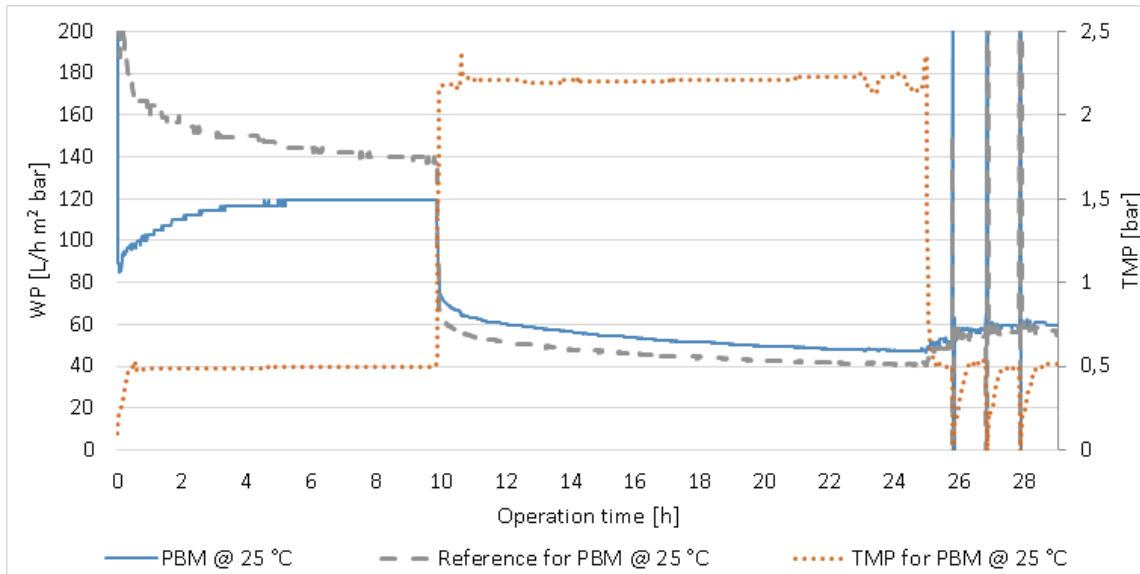
Figure 5.27. Model foulant permeability of PBM coated at 25 °C
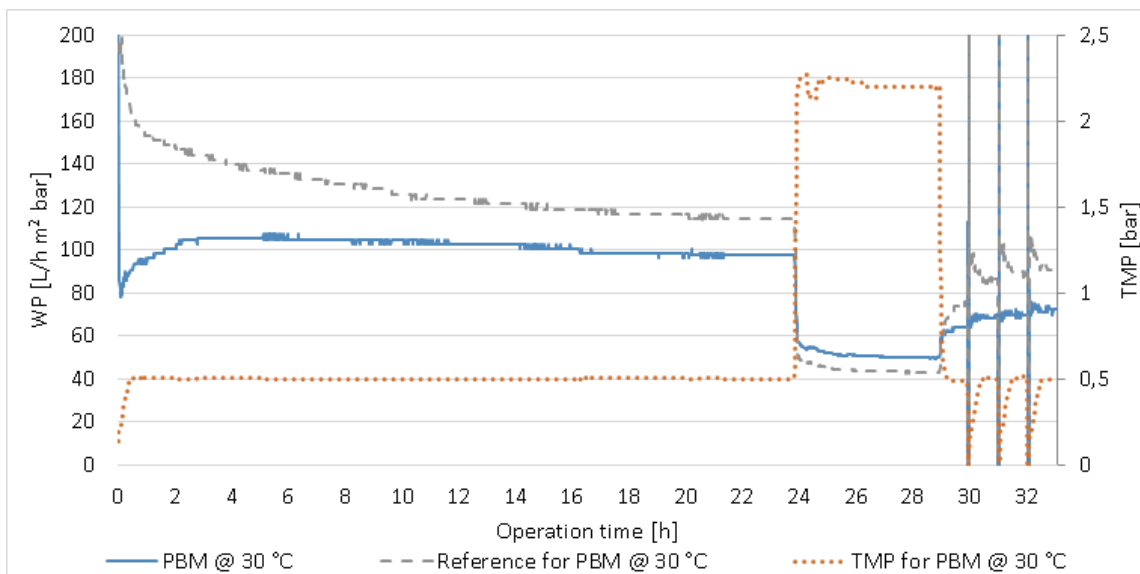
Figure 5.28. Model foulant permeability of PBM coated at 30 °C

For the model foulant experiment, as soon as stable conditions are reached at 0.5 bar, the TMP was set to 2.2 bar in order to further force the fouling of the membranes. At that point, all PBMs exceeded the permeabilities of their referencing commercial membrane around 14-17 %. Subsequently, the TMP was set back to 0.5 bar and the reduction compared to the WP before the increase to 2.2 bar was calculated

(20 °C = 25 %, 25 °C = 49 %, 30 °C = 28 %). The highest reduction is found for the 25 °C PBM at 49 % as of the high WP before the TMP increase. However, the highest WP at 2.2 bar occurred for the PBM coating of 4 μm prepared at 25 °C (53 L/h m² bar). Another interesting effect is shown while comparing the WPs of the pure water with the model foulant experiment. The WP results to be higher at the initial TMP setting of 0.5 bar, by running the setup with the model foulant humic acid. This effect was shown for all experiments within this work, and might be linked to higher hydrophilic properties of the humic acid itself. However, this fact needs to be further studied by follow up experiments.

5.2.3 Optimum PBM membrane

Based on the experimental tests to define the optimal conditions for the preparation of the PBM coating (as reported in the section 5.2.2) a PBM coating with the composition and preparation conditions reported in Table 5.5 has been selected.

Table 5.5. Characteristics of optimum PBM coating

PBM Chemicals	
AUTEAB	25 w%
Methyl methacrylate (MMA)	21 w%
2-Hydroxylethyl methacrylate (HEMA)	10 w%
Deionised water (DI water)	41 w%
Ethylene glycol dimethacrylate (EGDMA)	3 w%
Photoinitiator Irgacure 184 for UV-LED	1.8 w%
Coating conditions	
Coating thickness	4 μm
Irradiation time	30 sec.
Irradiation intensity (UV-LED)	300 mW/cm²
Room temperature	24 °C
Ambient conditions	Inert (Nitrogen, oxygen <1 %)

Reproducibility experiments

Figure 5.29 shows the WP of the selected PBM membrane produced (PBM final). As shown, the experiments were performed in total three times in order to assure the reproducibility of the coating. It is clearly shown the reproducibility of the produced membrane as the permeability is in the same range of 60-80 L/h m² bar in every case.
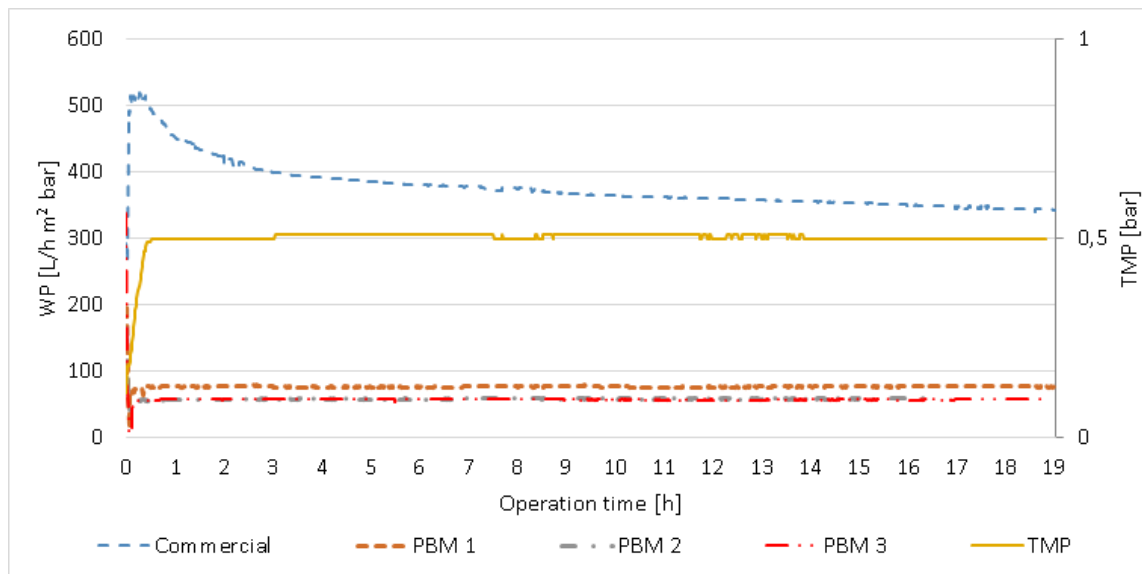
Figure 5.29. Water permeability of the selected PBM coated membrane (final membrane)

Influence of fixed volume flow adjustments to the water permeability

In order to study the influence of different fixed volume flow adjustments to the pure water permeability, the PBM and commercial membrane were run for a simple water test as shown in Figure 5.30 and 5.31.

The purpose of this experiment was to simulate the conditions in realistic applications where the volume flow of the produced water has to be kept constant and the TMP is regulated according to the fixed volume flow setting. Both results are given in separate graphs for a better visualization of the obtained results.

As shown in Figure 5.30, even by increasing the volume flow (VF) from 0.25 to 1.25 L/h for the PBM membrane the WP keeps a relatively constant value at 60 L/h m² bar. In contrary to the low WP of the PBM membrane, the commercial

membrane shows a higher WP around 250 L/h m^2 bar (see Figure 5.31. This result was expected since the PBM layer increases the water flux resistance.
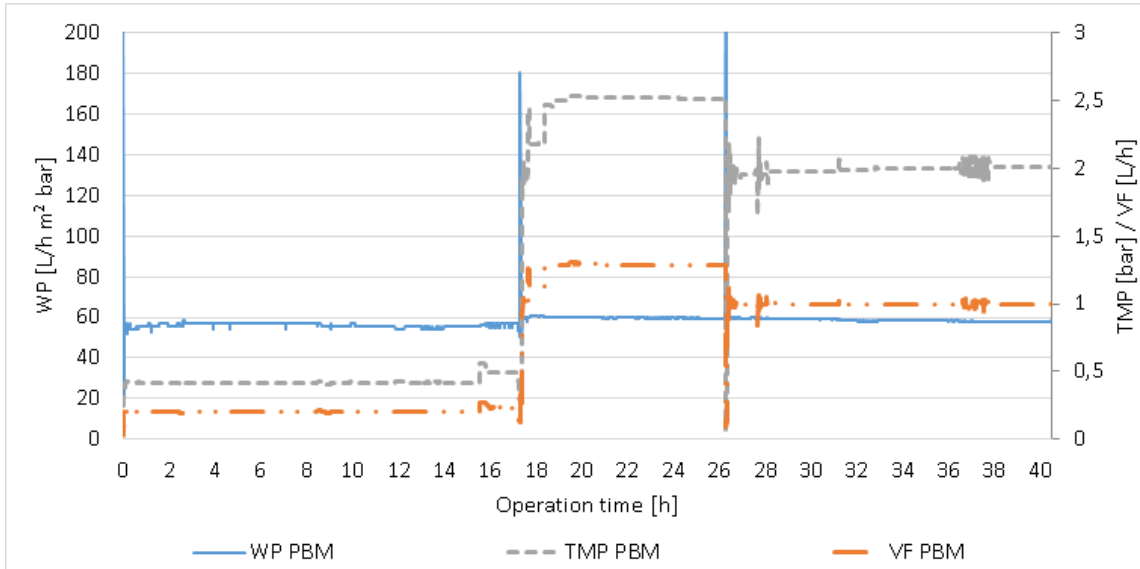
Figure 5.30. Influence of fixed permeate flow to the water permeability for PBM coated membrane
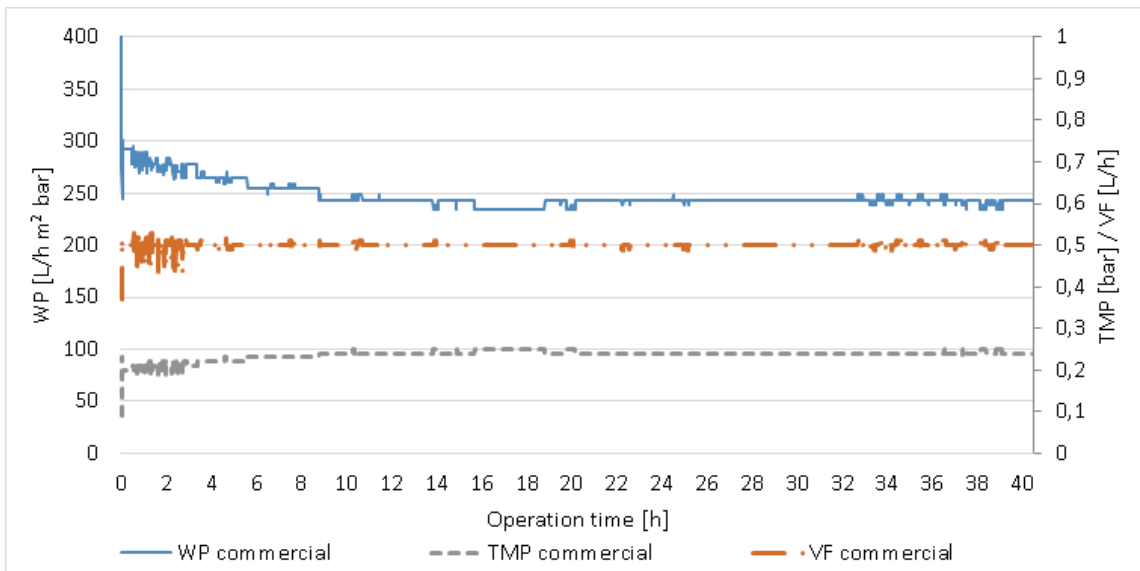
Figure 5.31. Influence of fixed permeate flow to the water permeability for commercial UF membrane

Influence of fixed volume flow adjustments to the model foulant permeability

The effect of a constant VF for the produced permeate to the TMP and WP is studied for both, PBM and commercial membrane, by using humic acid as model foulant (details are reported in section 4.7.7).

As shown in Figure 5.32, while keeping the VF constant at 0.5 L/h the TMP of the PBM coated membrane increases until a stable value of about 3.5 bar. The WP also reaches a stable value around 17 L/h m² bar. At this point (48 h) the cleaning protocol (described in section 4.7.7) leads to a slight increase for the WP to 20 L/h m² bar and a drop in TMP to 2.8 bar.
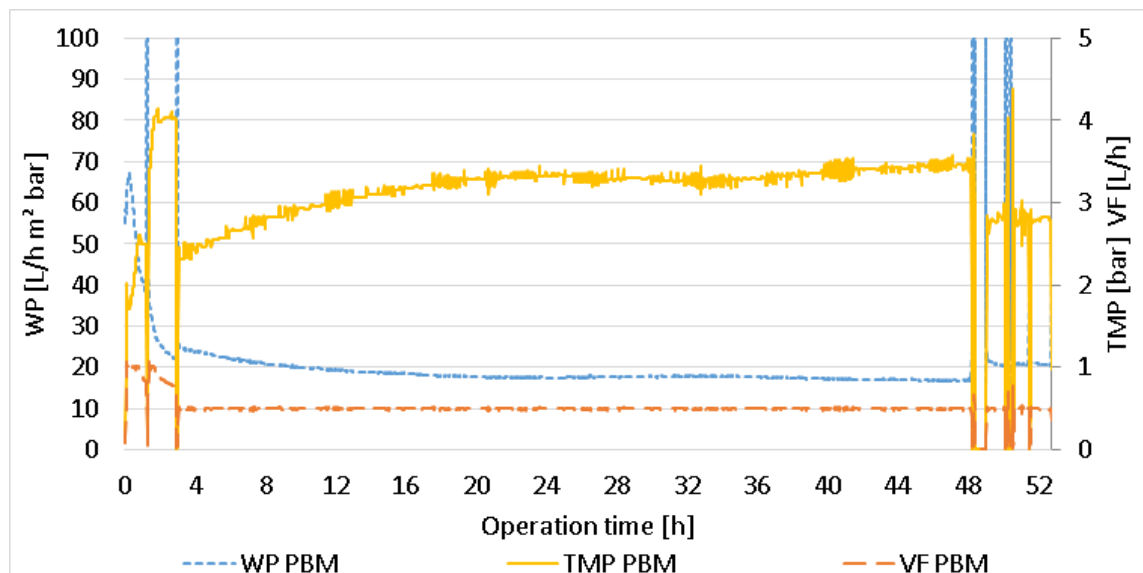
Figure 5.32. Influence of fixed permeate flow (0.5 L/h) to the model foulant (HA 100 mg/L) permeability of PBM membrane

The same experiment is done for the commercial membrane (see Figure 5.33 and Figure 5.34). For comparison, the same operation time is given in Figure 5.32 and 5.33. Since stable conditions could not be reached for the commercial membrane, the experiment was extended to 172 hours (Figure 5.34).
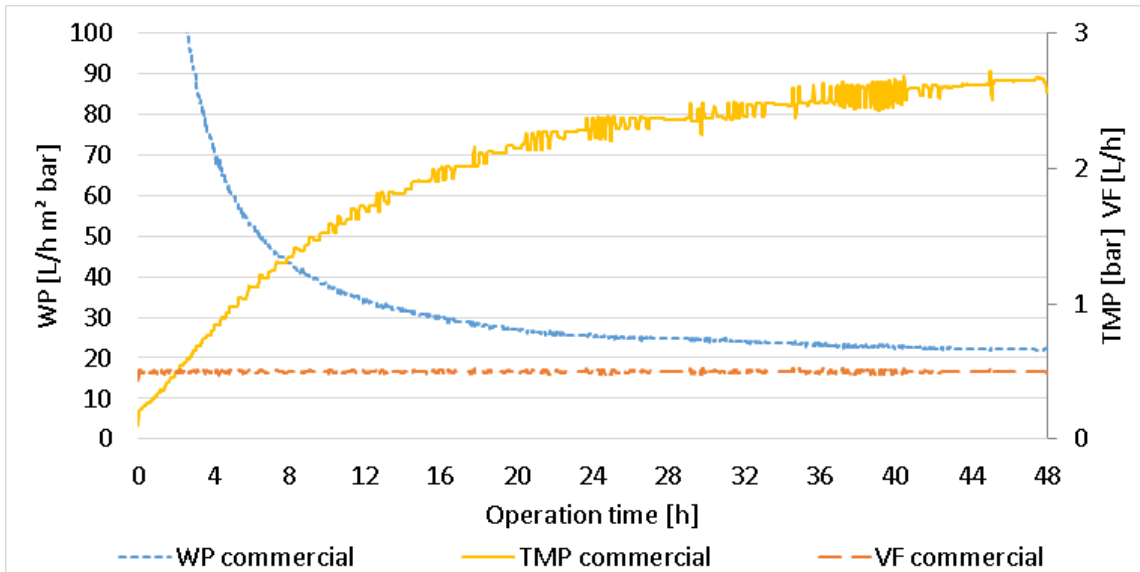
Figure 5.33. Influence of fixed permeate flow (0.5 L/h) to the model foulant (HA 100 mg/L) permeability of commercial UF membrane after 48 hours
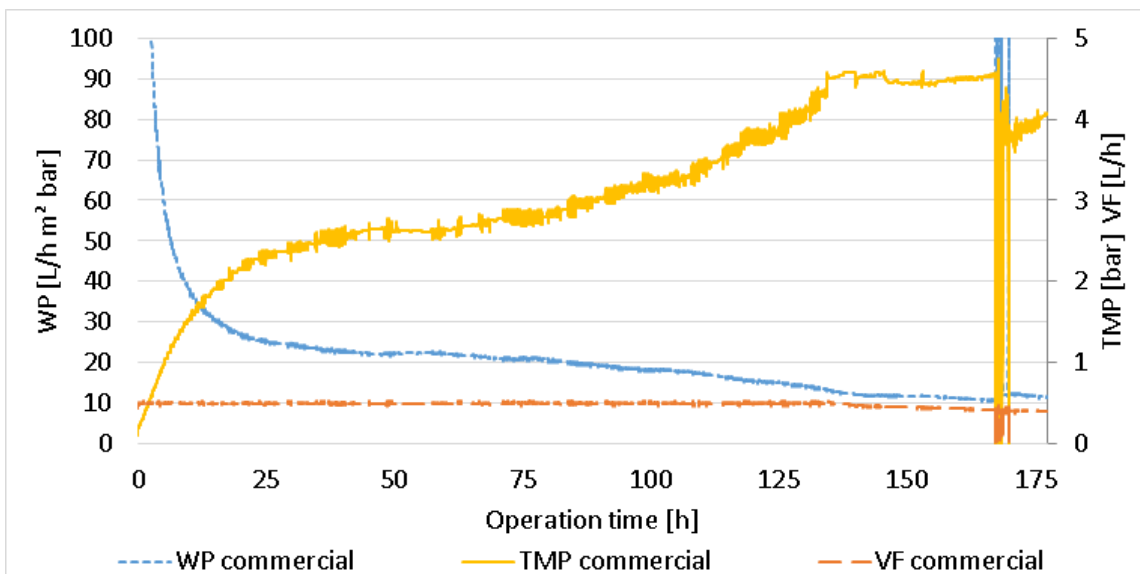
Figure 5.34. Influence of fixed permeate flow (0.5 L/h) to the model foulant (HA 100 mg/L) permeability of commercial UF membrane

After 134 hours the maximum TMP of the cross-flow test unit (see section 4.7.7) was reached at 4.5 bar. Therefore, the VF shows a small drop at that time as the system could not increase the TMP further. However, the WP drops continuously until 10 L/h m² bar and would decrease probably further if the TMP increased.

After 169 hours the cleaning protocol leads to a decrease of TMP down to 4 bar, but the WP remains around 10 L/h m² bar.

Comparing both results for the PBM and commercial membrane, the advantages of the PBM coated membrane become visible. Especially for the application in real wastewater treatment plants, where the TMP is regulated in order to get a constant water production. At the adjusted VF of 0.5 L/h stable conditions were found at a TMP of about 3.5 bar for the PBM membrane, while the commercial membrane did not reach a stable TMP and found its maximum at 4.5 bar only because of the system boundaries. In real applications a cleaning cycle, most probably with chemicals, would be required for the commercial membrane. Regarding the WP, the PBM produces around 17 L/h m² bar, having the stable TMP reached, while the WP for the commercial membrane ends up around 10 L/h m² bar. Running the membranes without a cleaning cycle therefore results in an about 70 % higher WP for the PBM coated membrane. The TOC rejection for the PBM is 91.73 ±8.38 % and for the commercial 88.99 ±8.38 %. Considering the measuring error, no negative or positive influence to the TOC rejection is measured. While cleaning the membranes with deionised water three times for one hour the TMP for the PBM membrane reaches almost its initial value of 2.5 bar. For the commercial membrane the TMP after cleaning is around 4 bar. Keeping in mind that a higher TMP is leading to a higher energy demand (e.g.for the suction pump in an MBR), the PBM could also safe running costs in terms of energy consume. Figure 5.35 shows the PBM and commercial membrane after this experiment.
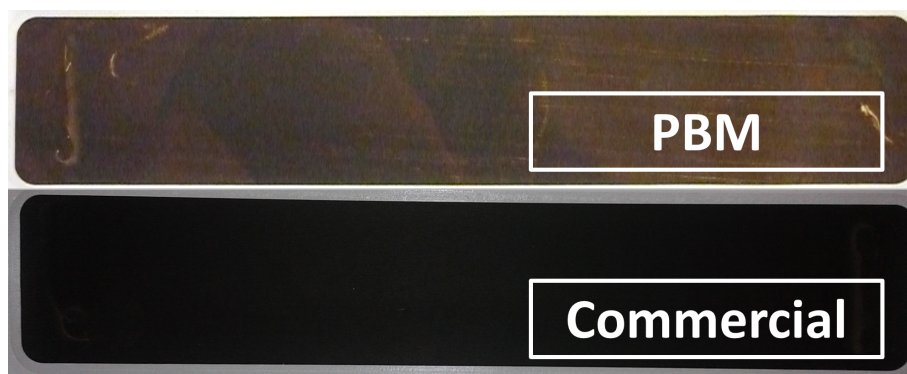
Figure 5.35. PBM and commercial membrane after fixed permeate flow experiment

The PBM is covered with a brownish layer created by the model foulant, while the

commercial membrane is covered with a darker fouling layer. The Figure shows clearly that the PBM coated membrane is less prone to fouling than the commercial membrane.

5.2.4 Chemical cleaning resistance of PBM membrane

It is one of the targets of the surface modification by PBM to finally avoid or minimise the chemical cleaning necessity of the membranes. However, the possibility of chemical cleaning has been studied in this section.

In order to do so, the optimal PBM coated membrane with the properties/polymerisation conditions given in Table 5.6 for the AUTEAB based PBM described in section 4.2.2 has been examined.

Table 5.6. Polymerisation conditions of PBM used in the chemical cleaning experiments

Photoinitiator for UV-LED	Temperature	Casting knife	Polymerisation time
1-Hydroxy-cyclohexyl-phenyl-ketone (Irgacure 184) 1.8 w%	24 °C	4 μm	30 sec.

A standard water test (see section 4.7.7) was done for both, the commercial and the PBM coated membranes. After an acclimation phase of 70 hours, the membranes were cleaned for 30 minutes each at pH 13 (KOH>50 %, MEMPUR SX 040 ZIMMERMANN), DI and pH 1 (HNO3 15<30 % H3PO4 15<30 %, RMK-FLB 001, ZIMMERMANN). Afterwards the chemically cleaned membranes were analysed by FT-IR. Figure 5.36 shows the range that is corresponding to the unique acrylate components of the PBM.

In total three spots of the PBM membrane surface were measured (indicated as blue, red, purple in Figure 5.36). For comparison the commercial membrane is also given (green). It is clearly shown that the PBM coating is still present on the membrane support even after strong cleaning at pH 1 and pH 13. Figure 5.37 shows the PBM

coated membrane after the chemical cleaning. The red circles show the spots used for FT-IR.
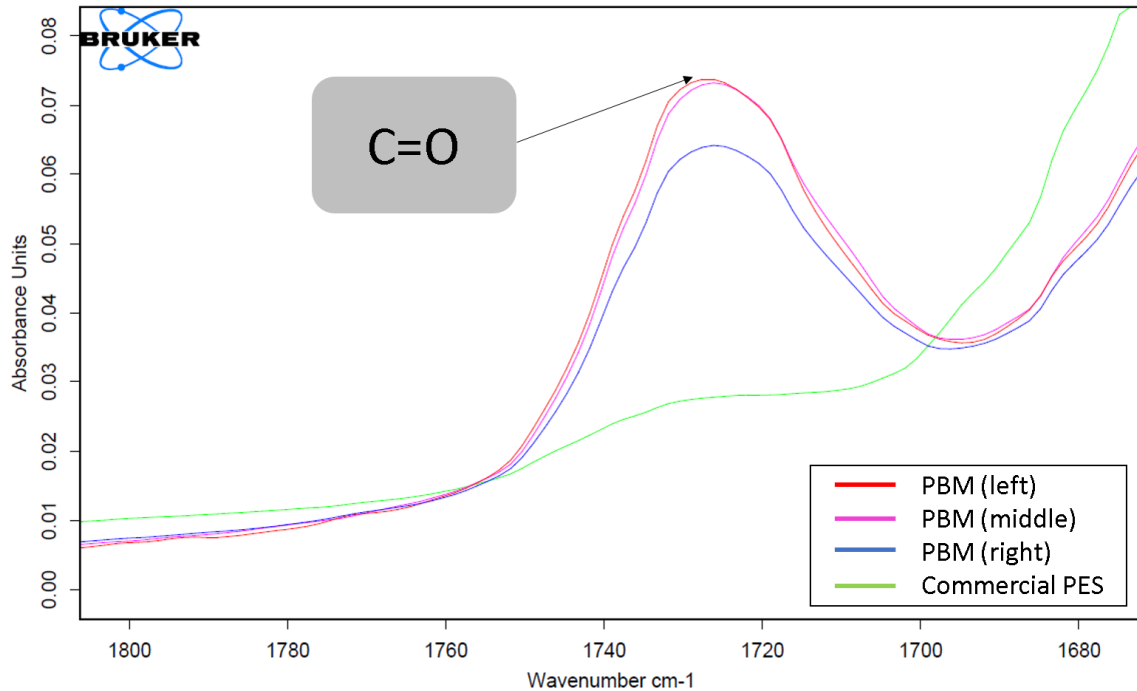
Figure 5.36. FTIR of PBM and commercial membrane after chemical cleaning

Figure 5.37. PBM membrane after chemical cleaning

5.2.5 Contact angle

In this section, the comparison of the contact angle of PBM coated membranes and commercial PES UF membranes are discussed. For the measurement of the contact angle deionised water is applied onto the membrane surface. Figure 5.38 shows the result for the contact angle measurement of the commercial PES UF membrane.

CA (left)	CA (right)	CA (mean value)
58.90°	57.84°	58.37°
59.11°	57.38°	58.25°
54.78°	55.18°	54.98°
55.86°	56.74°	56.30°
61.27°	58.36°	59.82°
Average		57.54°
St. Dev.		+/-1.90°
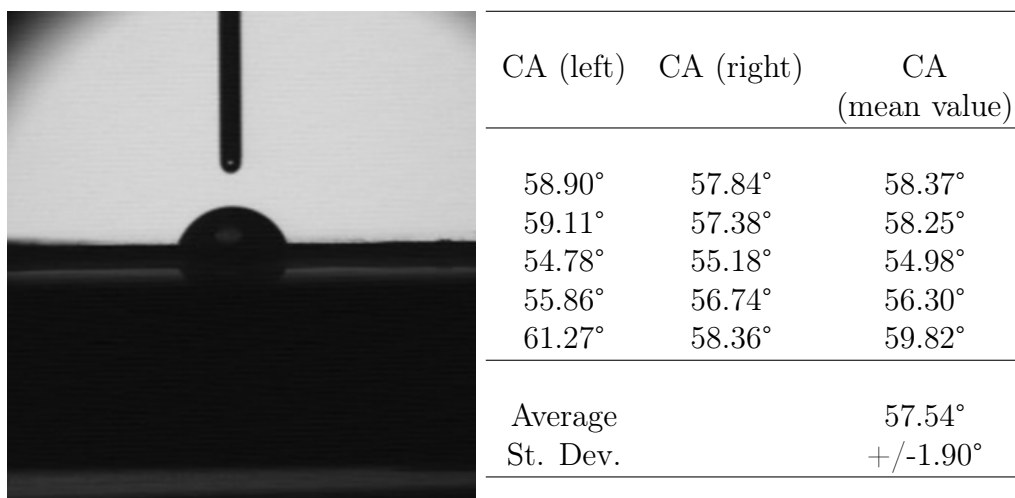
Figure 5.38 & Table 5.7. Contact angle of commercial PES UF membrane

Figure 5.39 gives the contact angle result for the optimal PBM composition of the coating having a final thickness of 4 μm by polymerisation at 26 °C for 30 seconds. It is shown a contact angle reduction of about 32 % in comparison to the commercial membrane. Therefore the PBM coating leads to a more hydrophilic membrane.

CA (left)	CA (right)	CA (mean value)
38.06°	37.67°	37.87°
38.34°	37.43°	37.89°
39.87°	39.08°	39.48°
40.13°	41.31°	40.72°
39.55°	40.20°	39.88°
Average		39.16°
St. Dev.		+/-1.26°
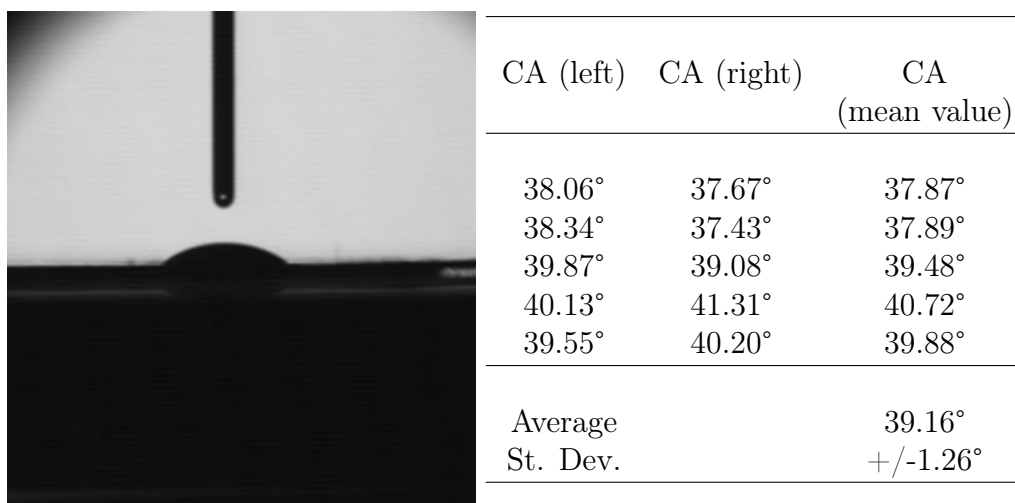
Figure 5.39 & Table 5.8. Contact angle for PBM (4 um, 30 seconds, 26 °C)

Figure 5.40 shows the contact angle of another coated PBM with lower temperature during polymerisation (24 °C). For this contact angle the polymerisation time remained at 30 seconds with a casting thickness of 4 μm and a temperature of 24 °C. For this coating a contact angle reduction of 62 % occurred.

CA (left)	CA (right)	CA (mean value)
22.72°	21.23°	21.98°
23.82°	20.11°	21.97°
21.35°	23.23°	22.29°
20.22°	18.31°	19.27°
22.51°	23.53°	23.02°
Average		21.70°
St. Dev.		+/-1.43°
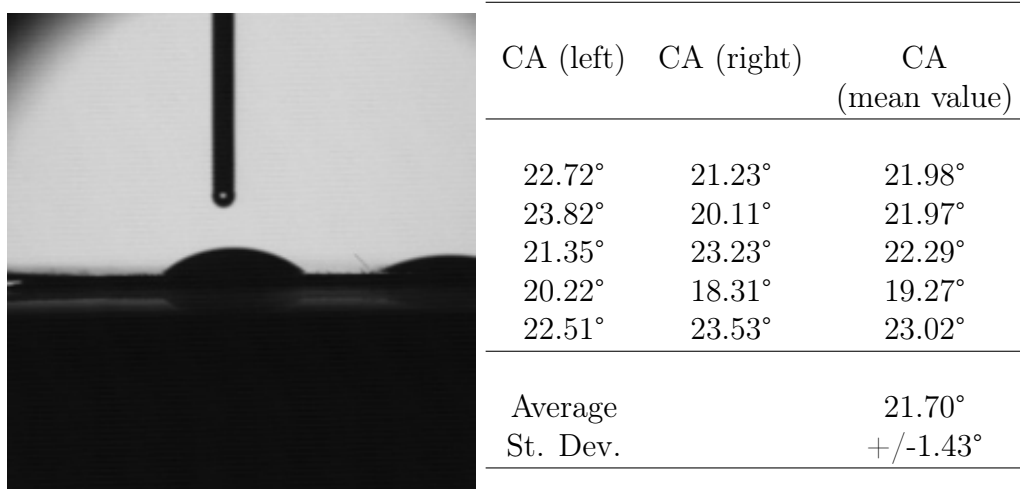
Figure 5.40 & Table 5.9. Contact angle for PBM (4 um, 30 seconds, 24 °C)

To highlight the complexity of conditions influencing the polymerisation, the effect of less polymerisation time and temperature is additionally shown in Figure 5.41. Under the given conditions (20 seconds, 22 °C) the contact angle reduced around 48 %.

CA (left)	CA (right)	CA (mean value)
30.55°	30.38°	30.47°
29.77°	27.68°	28.73°
29.94°	30.30°	30.12°
32.94°	27.65°	30.30°
29.71°	30.72°	30.22°
Average		29.96°
St. Dev.		+/-0.70°
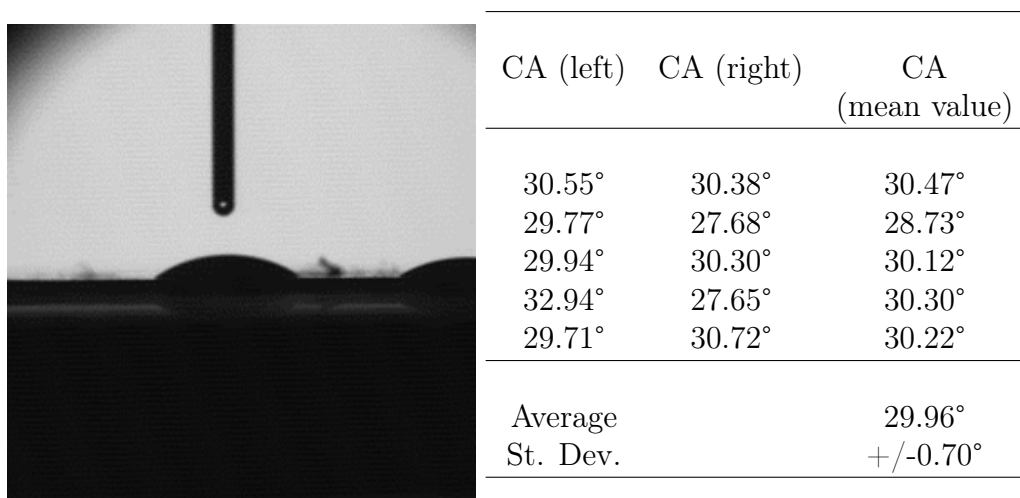
Figure 5.41 & Table 5.10. Contact angle for PBM (4 um, 20 seconds, 22 °C)

The results for contact angle of the PBM coated membranes indicate the coating results in higher hydrophilic membranes in all studied cases, and that the effect of temperature has a strong impact to the hydrohilicity. These results are generally in agreement with the previous work of Galiano et al. (2015).

5.2.6 AFM

The AFM result for the commercial and the PBM coated membranes is discussed in this section. Figure 5.42 gives an average roughness of 51.73 nm for the commercial membrane. By comparing this value with the roughness results for the PBM coated membranes it becomes clear that the coating results in a much smoother membrane surface.

This contributes to the anti-fouling characteristics as particles are hindered to attach to the membrane surface. In comparison to the commercial membrane a roughness reduction for the PBM coated membrane of about 18.52 % (30 sec., 26 °C, Figure 5.43), 86.76 % (30 sec., 24 °C, Figure 5.44) and 92.90 % (20 sec., 22 °C, Figure 5.45) results.
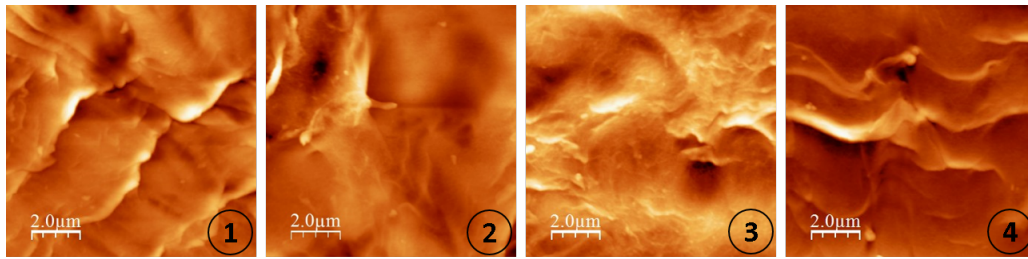
Sample	Roughness average S_a (nm)	RMS S_q (nm)	Peak to peak S_z (nm)
1	58.65	77.30	730.85
2	50.72	68.83	609.41
3	45.50	65.04	609.39
4	52.03	64.85	482.87
Average	51.73	69.01	608.13
Standard deviation	5.41	5.83	101.25

Figure 5.42 & Table 5.11. AFM of commercial membrane
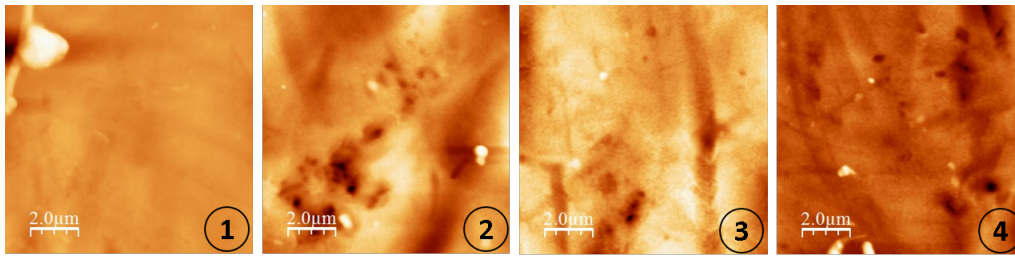
Sample	Roughness average S_a (nm)	RMS S_q (nm)	Peak to peak S_z (nm)
1	40.00	90.52	685.55
2	67.73	86.71	634.57
3	38.04	47.79	388.73
4	22.84	31.06	360.39
Average	42.15	64.02	517.31
Standard deviation	18.70	29.25	166.54

Figure 5.43 & Table 5.12. AFM for PBM (4 um, 30 seconds, 26 °C)
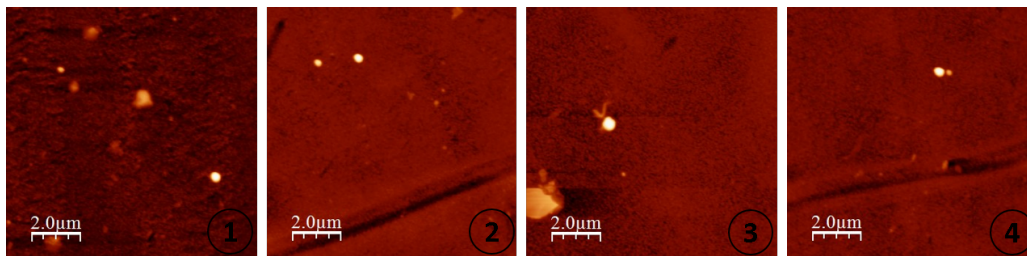
Sample	Roughness average S_a (nm)	RMS S_q (nm)	Peak to peak S_z (nm)
1	7.05	15.96	379.11
2	6.94	12.53	348.59
3	7.37	17.33	281.95
4	6.05	12.94	407.49
Average	6.85	14.69	354.29
Standard deviation	0.57	2.33	53.89

Figure 5.44 & Table 5.13. AFM for PBM (4 um, 30 seconds, 24 °C)
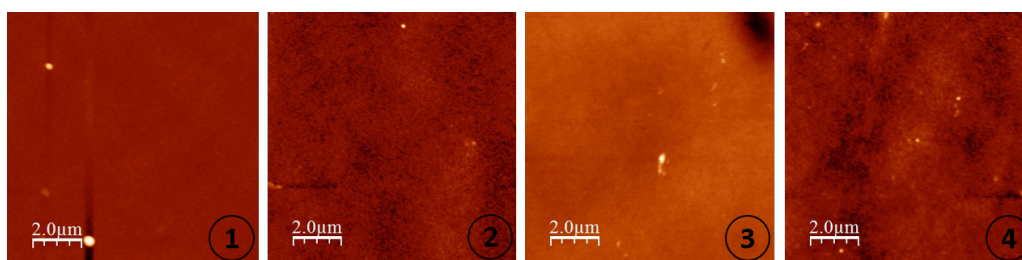
Sample	Roughness average S_a (nm)	RMS S_q (nm)	Peak to peak S_z (nm)
1	3.68	10.68	379.42
2	3.44	4.47	123.39
3	2.55	3.39	78.22
4	5.02	7.90	171.20
Average	3.67	6.61	188.06
Standard deviation	1.02	3.33	133.10

Figure 5.45 & Table 5.14. AFM for PBM (4 um, 20 seconds, 22 °C)

5.2.7 SEM

This section gives the results for the SEM pictures. The given results are limited to the resulting composition of the optimal PBM (see section 5.5).

Membrane surface analysis

Figure 5.46 shows the surface of one exemplary PBM coated membrane. The same structure was found for all characterised PBM membranes. The micro-channels that are characteristic for a bicontinuous microemulsion are clearly visible, even if they look slightly different to those described in the previous work of Galiano et al. (2015). However, other publications show a structure that corresponds with the ones achieved for the PBM coating that result within this work [Yan and Texter (2006), Gan et al. (2005)].
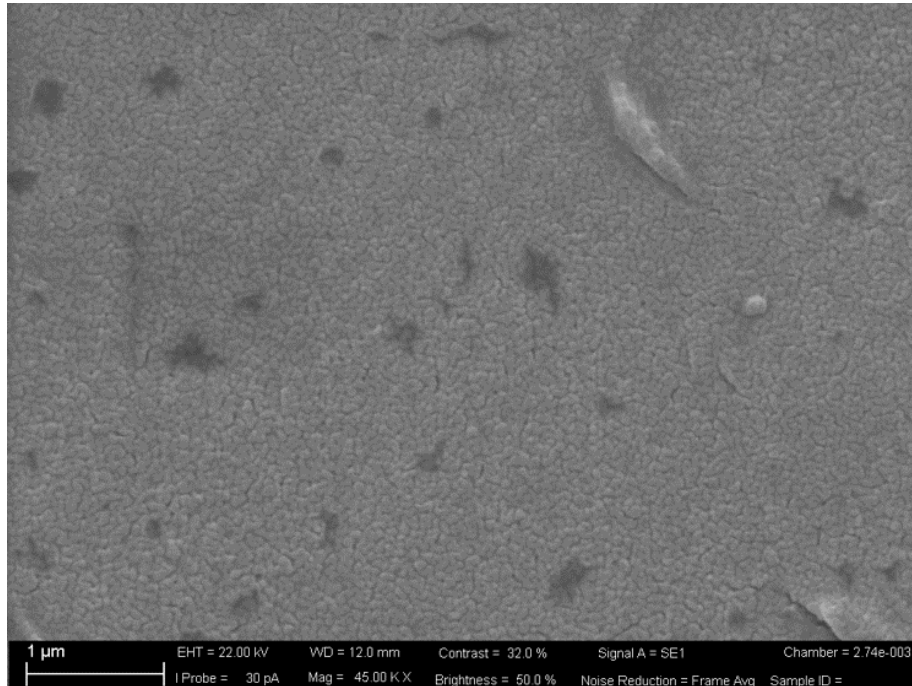
Figure 5.46. SEM surface of PBM coated membrane

In order to compare the structure with other bicontinuous microemulsion structures described in the literature, Figure 5.47 and 5.48 are given. Figure 5.49 to 5.52 report the surface pictures taken of the commercial as well as the PBM coated membranes, before and after the treatment with model foulant. The typical bicontinuous structure is shown for all PBM coated membranes before the model foulant experiments.
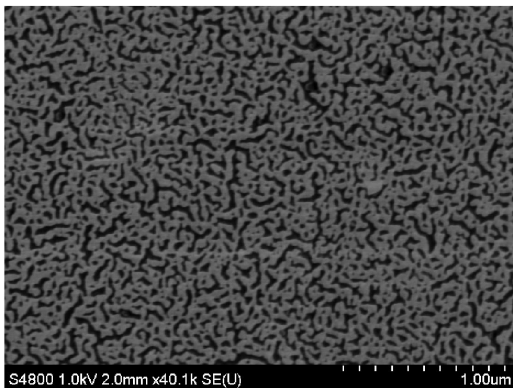
Figure 5.47. SEM surface of PBM coated membrane by Galiano et al. (2015)
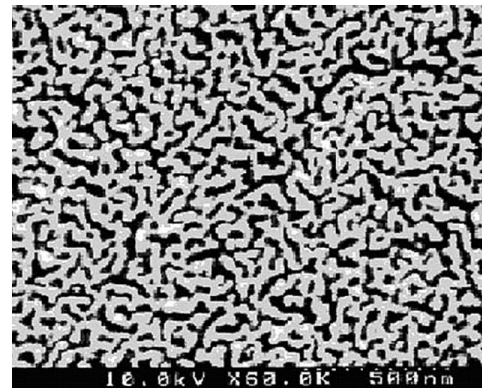
Figure 5.48. SEM surface of PBM coated membrane by Yan and Texter (2006)

The treatment by model foulant (as described in section 4.7.7) consists of a long

term run at 2.2 bar and the subsequent cleaning protocol with DI water at 0.5 bar. Afterwards, the fouling layer is shown for all treated membranes.
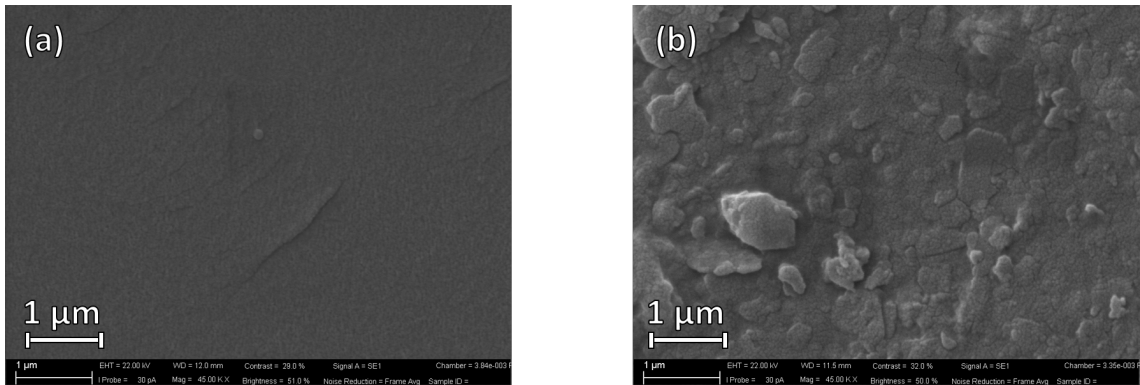
Figure 5.49. SEM surface before (a) and after (b) fouling of commercial PES UF membrane
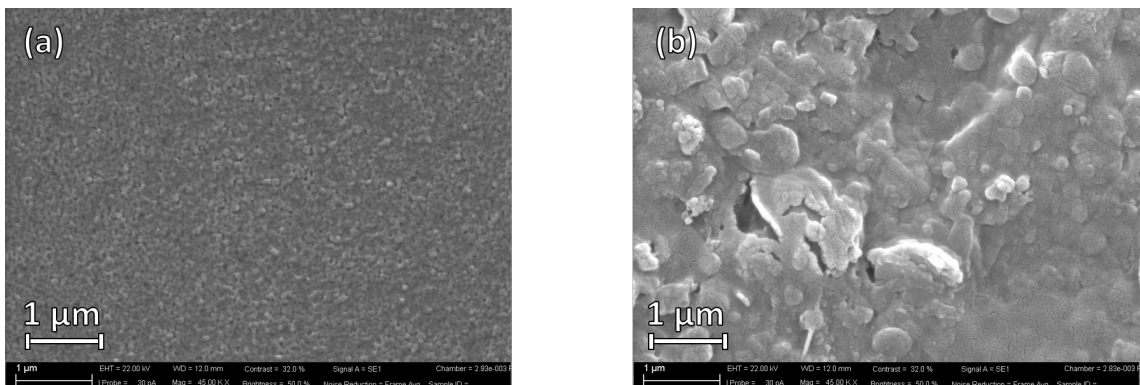
Figure 5.50. SEM surface before (a) and after (b) fouling of PBM membrane (4 μm, 30 sec., 26 °C)
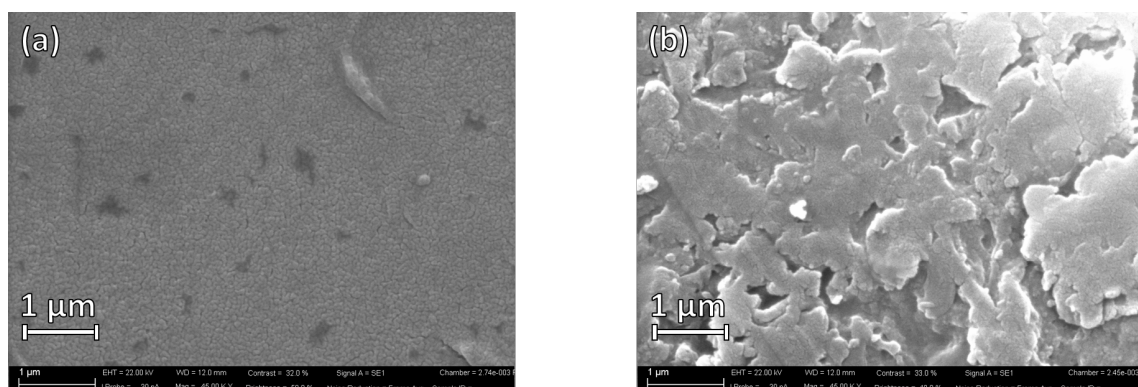
Figure 5.51. SEM surface before (a) and after (b) fouling of PBM membrane (4 μm, 30 sec., 24 °C)
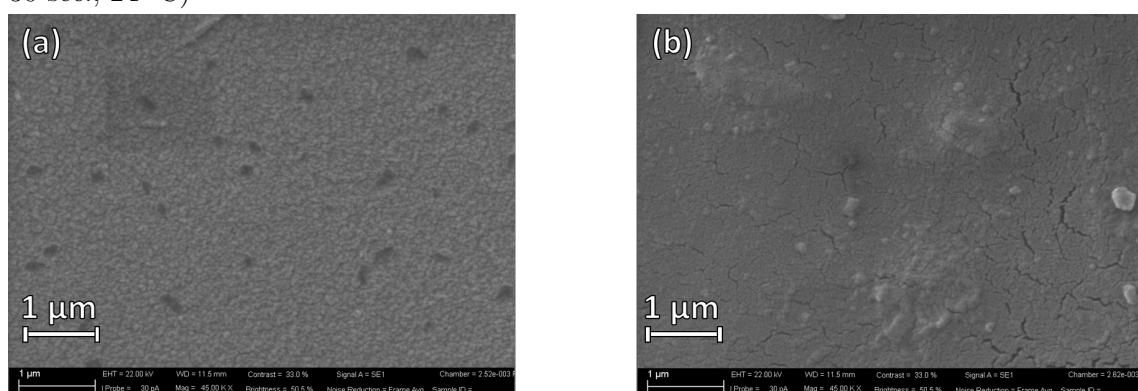
Figure 5.52. SEM surface before (a) and after (b) fouling of PBM membrane (4 μm, 20 sec., 22 °C)

Cross section

The optimal PBM coated membrane was achieved using the lowest coating thickness of the casting knife of 4 μm (see section 5.2.3). In Figure 5.53, it is reported as example a cross-section picture showing the PBM coating on the PES UF commercial porous membrane after polymerisation. A thickness of about 2.4 μm was measured. As the AUTEAB based PBM (see Table 4.7) consists of 41 w% water, this result is in line with the expected value (59 % = 2.4 μm) as the water evaporates in the polymerised coating. Figure 5.54 and 5.55 show the cross section after the model foulant test run, described in section 4.7.7, including the resulting fouling layer on top of the membranes. For the model foulant test all membranes were treated under
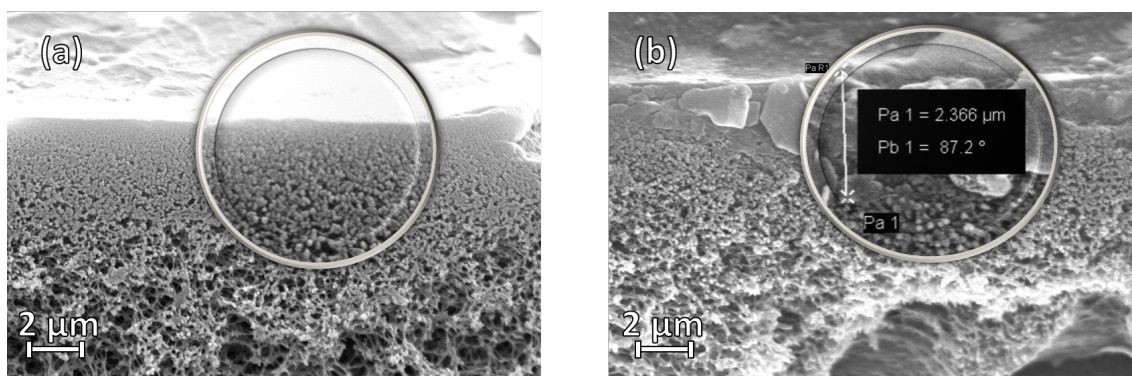
Figure 5.53. SEM cross section of commercial (a) and PBM coated membrane (b); applied with a casting knife of 4 μm thickness
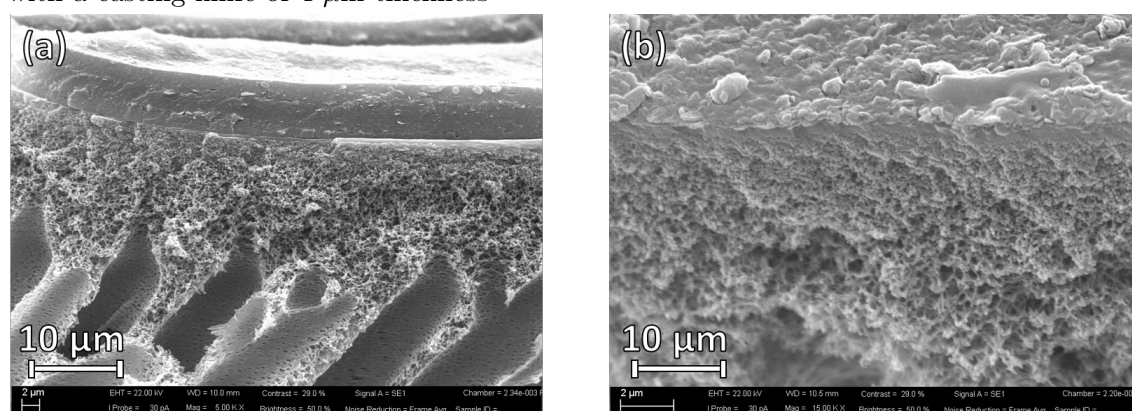
Figure 5.54. SEM cross section after model foulant experiment of commercial (a) and PBM membrane (4 μm, 30 sec., 26 °C) (b)
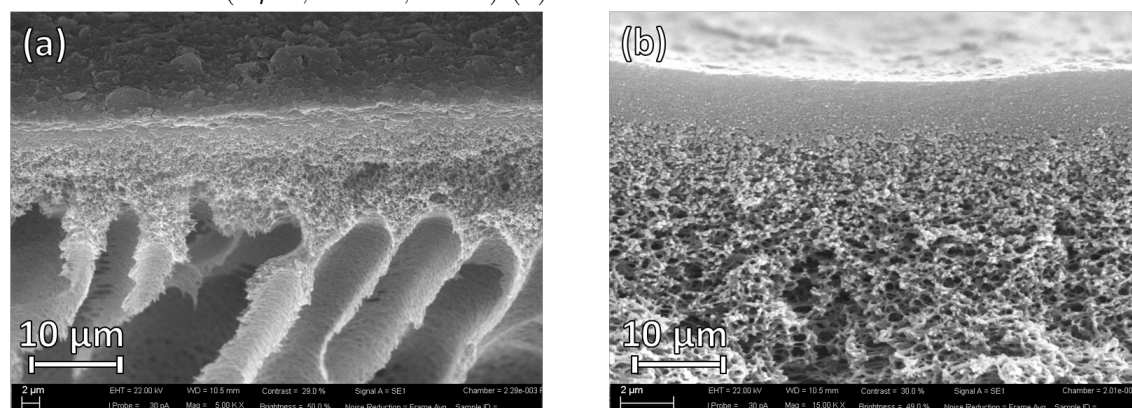
Figure 5.55. SEM cross section after model foulant experiment of PBM membrane (4 μm, 30 sec., 24 °C) (a) and PBM membrane (4 μm, 20 sec., 22 °C) (b)

the same conditions (forced fouling at 2.2 bar and three times cleaning with deionised water for one hour each).

In order to determine the thickness of the remaining fouling layer after the model foulant experiment Figure 5.56 is given. The highlighted thickness in Figure 5.56 (b) represents the fouling layer only. It is clearly shown that the remaining fouling layer onto the commercial membrane is about 9.5 times thicker than the PBM coated membrane.
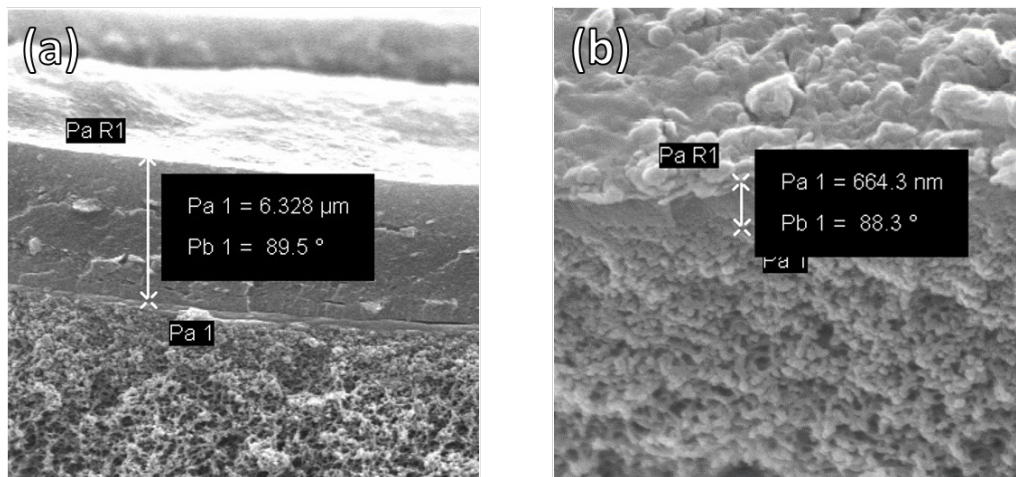
Figure 5.56. Foulant layer after model foulant experiment of commercial (a) and PBM membrane (4 μm, 30 sec., 26 °C) (b)
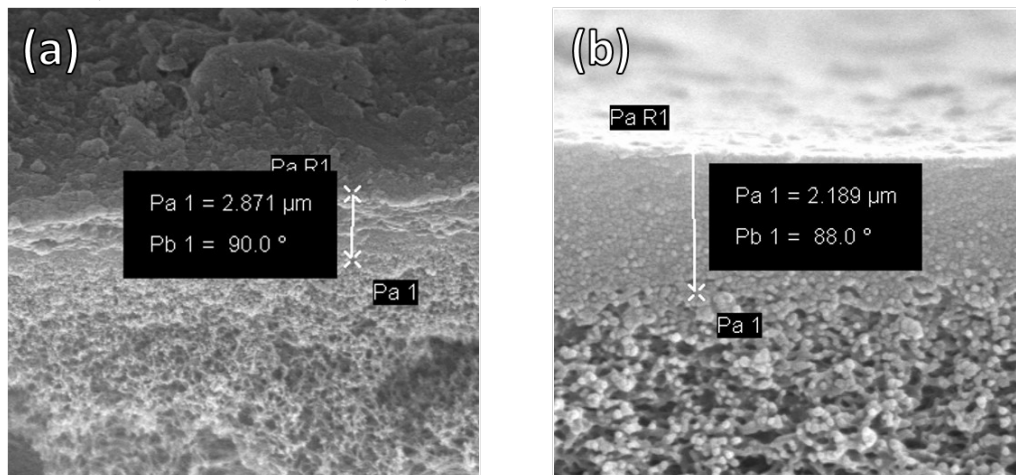
Figure 5.57. PBM and foulant layer after model foulant experiment of PBM membrane (4 μm, 30 sec., 24 °C) (a) and PBM membrane (4 μm, 20 sec., 22 °C) (b)

In addition Figure 5.57 shows the thickness of the layer onto the support after the model foulant experiment. In those cases the highlighted thickness consists of the PBM layer and the fouling layer. Considering the coating thickness of the PBM it becomes also clear that the fouling layer is very thin as well. In any case a thinner

fouling layer in comparison to the commercial membrane results for all studied PBM coatings.

5.3 MBR trials

In this section the experiments done with the lab scaled MBR unit, described in section 4.1.2, are summarised. First of all the proper function of the revamped MBR had to be proven within a simultaneous long term run of two commercial membranes (section 5.3.2). Afterwards, first experiments were done for the PBM coated membrane in comparison to the commercial membrane (see section 5.3.3).

5.3.1 Dissolved oxygen distribution inside the bioreactor

To assure a homogeneous distribution of the dissolved oxygen in the MBR, an air diffuser was installed. Another air source is given by the coarse air supply placed underneath the membranes, which is used to support the removing of organic particles that otherwise stick more easily to the membrane surface. The dissolved oxygen distribution over different depths of the MBR is measured with water in the beginning phase of the MBR trials. The locations of the measurements are given in Figure 5.58.
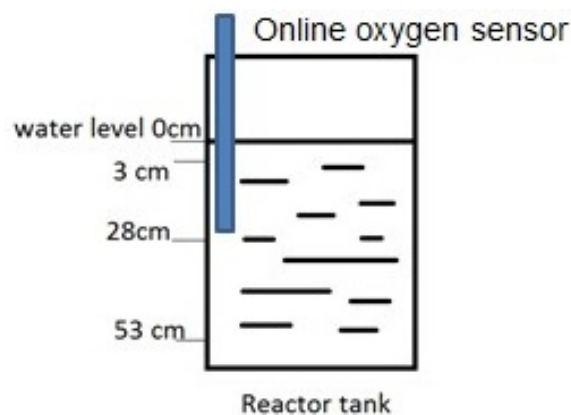
Figure 5.58. Oxygen distribution measurement of the MBR

Table 5.15 shows the dissolved oxygen distribution over different depths of the MBR. A very homogeneous distribution results at different settings of both air sources. The setting of 0.1 m³/h represents the lowest possible adjustment possibility of the current setup.

Table 5.15. Dissolved oxygen distribution at different depths of the MBR

Depth	Diffuser: 1.10 m³/h Coarse air: 0.40 m³/h	Diffuser: 0.20 m³/h Coarse air: 0.15 m³/h	Diffuser: 0.10 m³/h Coarse air: 0.10 m³/h
3 cm	8.60 mg/L	8.60 mg/L	8.62 mg/L
28 cm	8.72 mg/L	8.63 mg/L	8.63 mg/L
53 cm	8.75 mg/L	8.66 mg/L	8.63 mg/L

5.3.2 Initial test run of two commercial UF PES membranes in parallel

The redesigned MBR system was operated continuously for 117 days. Two commercial UF PES (UP150T) membrane modules (denoted Com1 and Com2) were tested in this period. Each module included three flat sheet membranes, which had the total area of 0.34 m². Different parameters for the aerobic treatment of textile wastewater by the lab scaled MBR are analysed in this part. They are presented in two phases. As shown in Table 5.16, Phase 1 covers the acclimation phase of the MBR.

Table 5.16. Phases of MBR test run

Phase	Operation	Period
Phase 1	Acclimation phase	Day 1 to day 68
Phase 2	Reduced speed of permeate pump	Day 68 to day 117

This phase is required as the system including the bacteria needs a certain time

to achieve stable conditions. For the Phase 2 the flux was reduced to study the condition of reduced flux and higher HRT.

Start-up of the system

Before running the MBR with MTDW, the WP of the system was measured with DI water. In addition, all of the equipment and sensors were checked for functionality. The DI water had a conductivity of 130 μS/cm at 21 °C. The results (see Figure 5.59 and Figure 5.60) were compared with the cross-flow test unit (SIMATEC unit) results of the commercial membrane (single UP150T flat sheet with membrane area of 0.0084 m^2) shown in Figure 5.61.

As shown in Figure 5.59, the intention of the start-up experiment was to increase the TMP by adjusting the same pump speed for both membrane modules in order to achieve the highest flux. As can be clearly seen, there was a difference in the initial TMP for Com1 (55 mbar) and Com2 (95 mbar). This might be linked with the lamination process of the membrane modules, which were hand-made by the company Microdyn-Nadir. By the step by step increase of the pump speed, the flux was proportional with the TMP. The maximum TMP was achieved at 210 mbar and 225 mbar for Com1 and Com2, respectively. At the maximum TMP, the average flux of Com1 was around 90 L/ h m^2, whereas Com2 was slightly lower at 86 L/ h m^2.
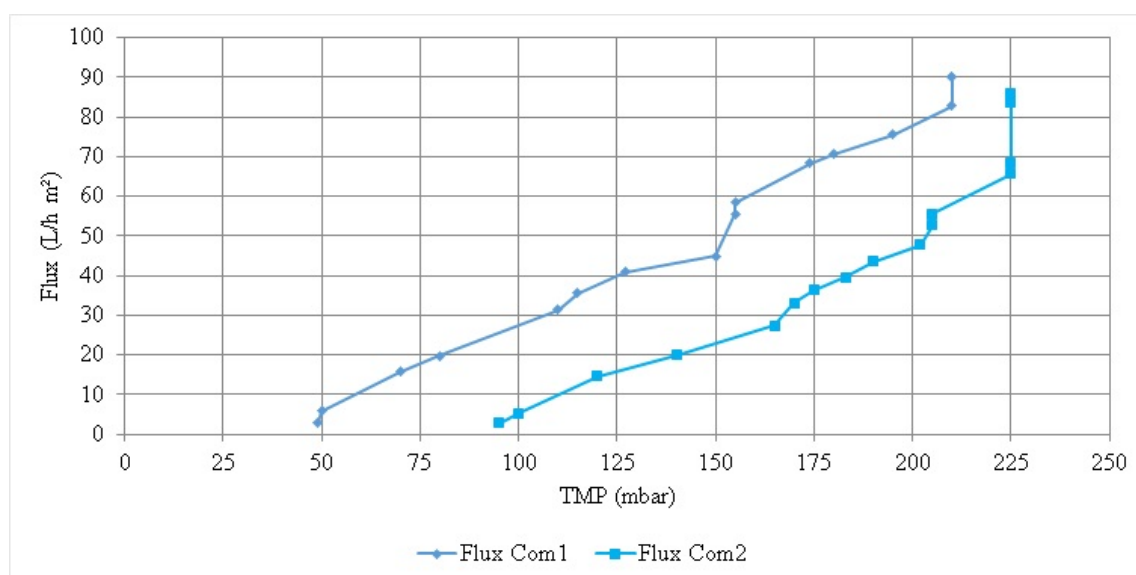
Figure 5.59. Initial water flux of two commercial membranes

The WP (Figure 5.60) of Com1 and Com2 at the highest TMP were 430 and 380 L/h m² bar, respectively. It should be shown that the WP was independent of the TMP, whereas Figure 5.60 indicates the contrary.

This could be explained by an unfinished adaptation time, to balance the membrane compaction of the membranes in the MBR when the speed of the suction pump was increased every half an hour. In fact, later experiments comparing the WP of PBM and commercial membranes in the MBR are in line with this theory (see Figure 5.75).
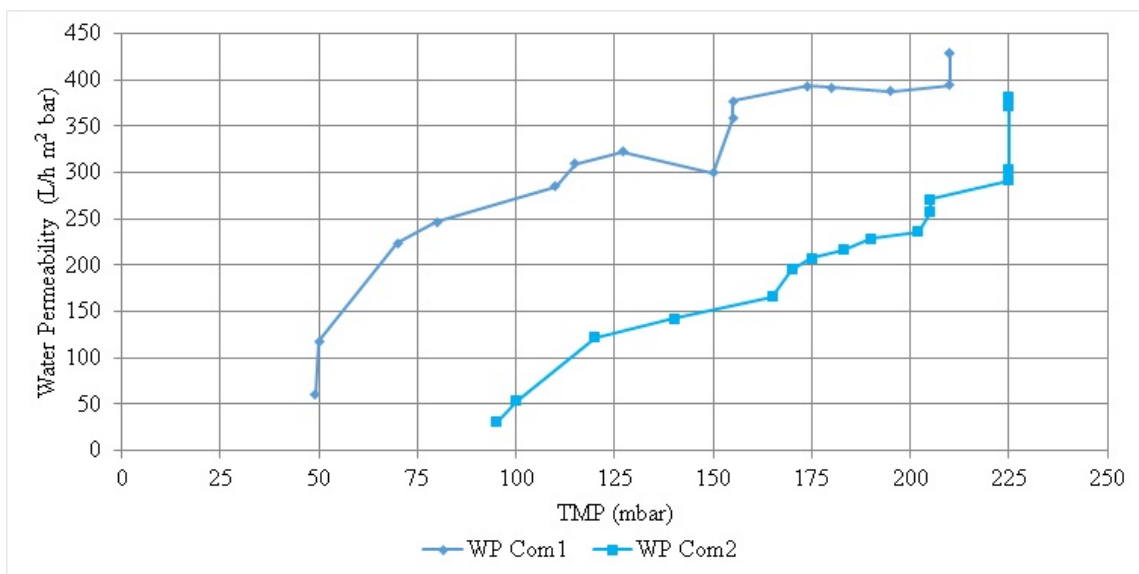
Figure 5.60. Initial water permeability of two commercial membranes

For a better understanding Figure 5.61 shows a standard cross flow test of the commercial UF PES membrane. As it is shown, a constant permeability is achieved only after a certain time. While running the cross-flow test unit with DI water, the stable WP was usually found after more than ten hours at a value between 200 and 250 L/h m² bar.

In contrary to that, the results for the MBR given in Figure 5.60 find their maximum around 400 L/h m² bar. As shown in Figure 5.61 the WP is usually very high in the initial phase of the cross-flow experiment, which could explain the high WP results of the MBR in contrary to the cross-flow test unit, as the TMP was increased to fast resulting in unstable and to high permeabilities at the single TMP settings.
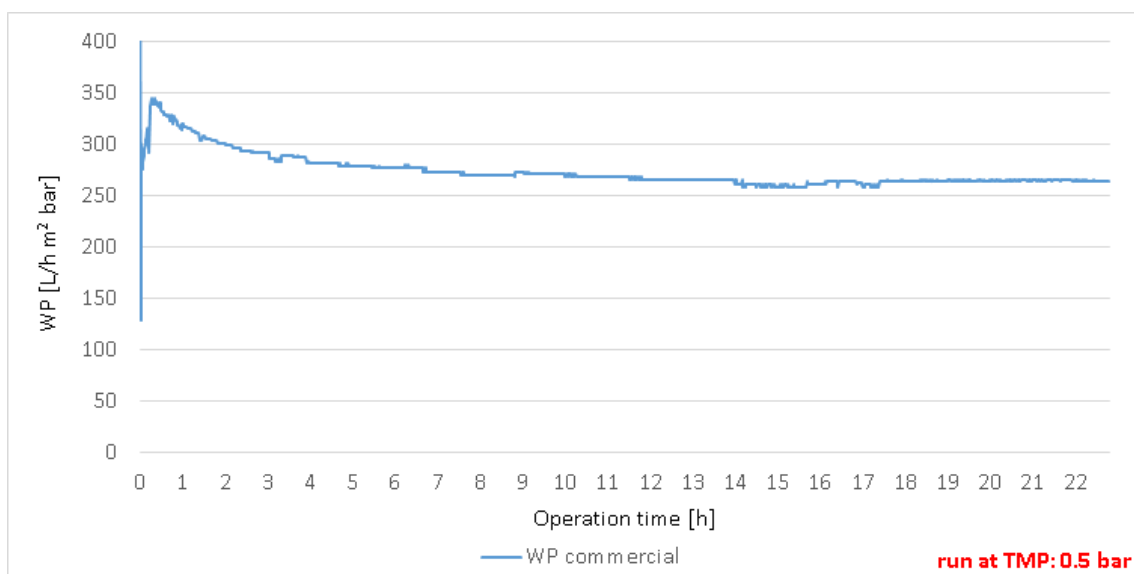
Figure 5.61. Water permeability for commercial membrane using cross-flow setup

Based on this results the start-up procedure was changed for the later study of the PBM coated membrane. As described in section 5.3.3 the adoption time between the different TMP settings had to be extended to at least 24 hours.

Flux with model textile dye water

Figure 5.62 indicates the flux and TMP of the experiment after replacing the DI-water by model textile dye water (MTDW). In the acclimation phase, the flux of both membranes was between 1.0 L/h m² and 3.0 L/h m². The flux in phase two was more stable around 1.5 L/h m². The reason for the fluctuations of fluxes on day 27 might be linked with the calibration of the pressure sensor of line one (blue). In order to achieve that, the TMP was changed lot of times in short period from 0 mbar to 250 mbar by adjusting the pump speed. The higher reading of line one was measured right after the calibration at a slightly higher TMP than for line two. On day 90 both pressure sensors were calibrated. These changes assumed to cause the blocking of both membrane modules and result in the drop of fluxes on day 90. In this case the readings are measured some hours after the calibration. The fluxes went back to stable values on day 95 because of the reduction of blocking thanks to aeration and back flush. The graph indicates a correlation between fluxes and transmembrane pressure in contrast to the water test. By increasing the TMP

from day 20 to day 50 the fluxes increased as well. The experiment shows the TMP stabilised around 50 mbar.
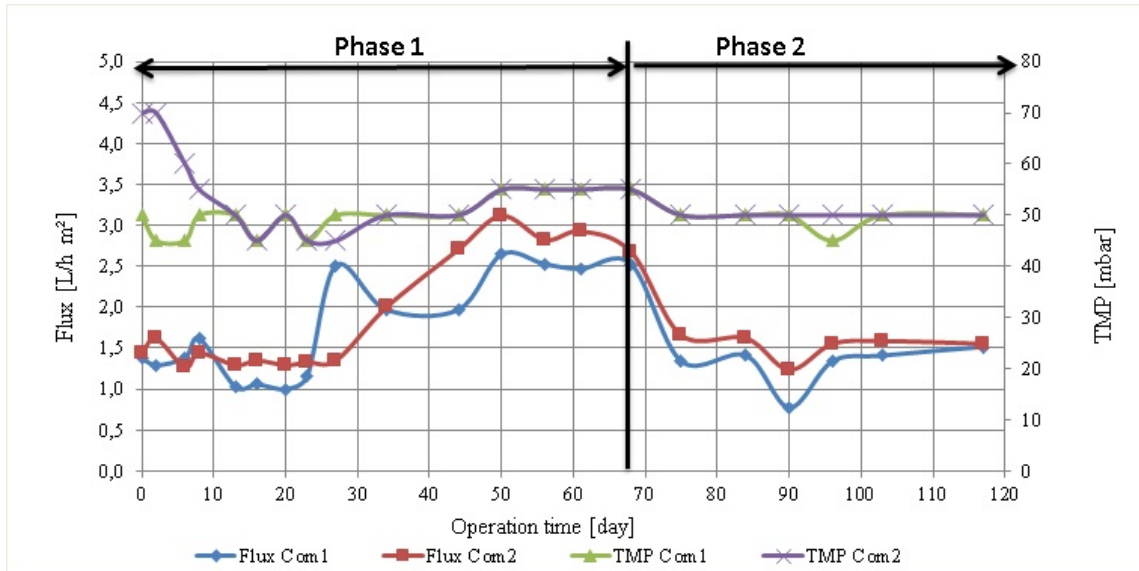
Figure 5.62. Initial MTDW test of two commercial UF PES membranes in MBR-flux

The WP of the commercial membranes is shown in Figure 5.63. Overall, the WP of Com1 and Com2 fluctuated in the range from 20 to 35 L/h m² bar in the first 26 days. After increasing the TMP from day 27 to day 68, both membrane modules showed a WP around 47 and 53 L/h m² bar for Com1 and Com2 at day 56.
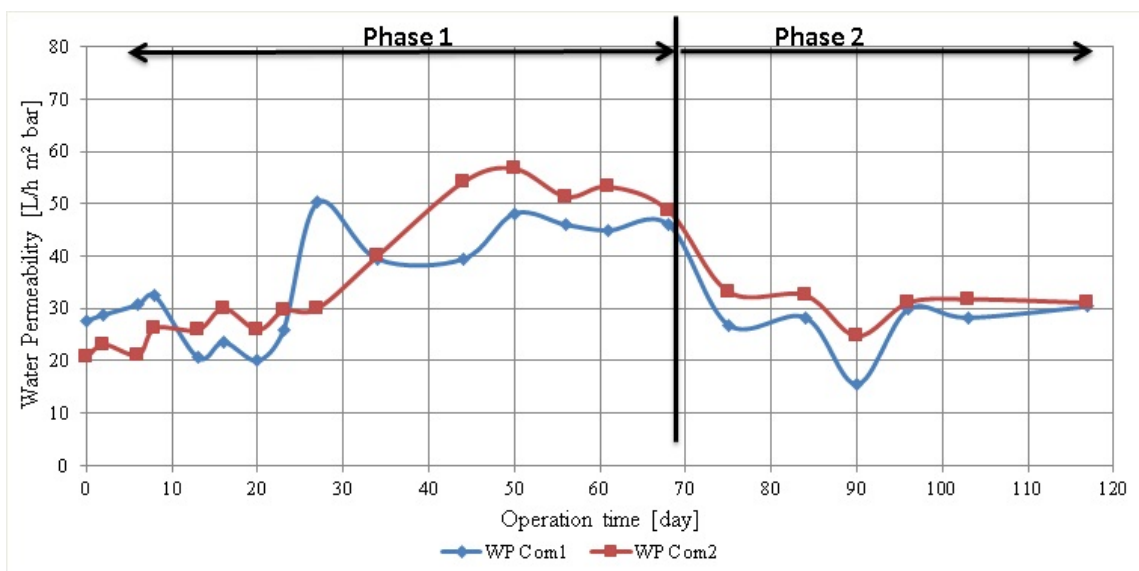
Figure 5.63. Initial MTDW test of two commercial UF PES membranes in MBR-WP

In the previous work of Deowan (2013) the WP fluctuated in a higher range from 75 to 85 L/h m^2 bar. This could be due to several factors like different hydraulic retention time (HRT) or less membrane fouling as of different activity of the bacteria. In phase two, they were generally stable at around 30 L/h m^2 bar.

Mixed liquid suspended solids (MLSS) and food to microorganism (F/M) ratio

The relation of mixed liquid suspended solids (MLSS) and food to microorganism (F/M) ratio is shown in Figure 5.64. The MLSS was increasing from day 50 from 8 g/L to more than 14 g/L in the beginning of phase two. Then it went down to approximately 11.5 g/L because of the decreasing F/M ratio from day 68 and the increasing HRT. The MLSS is expected to stay in this range from 10 g/L to 12 g/L later on.
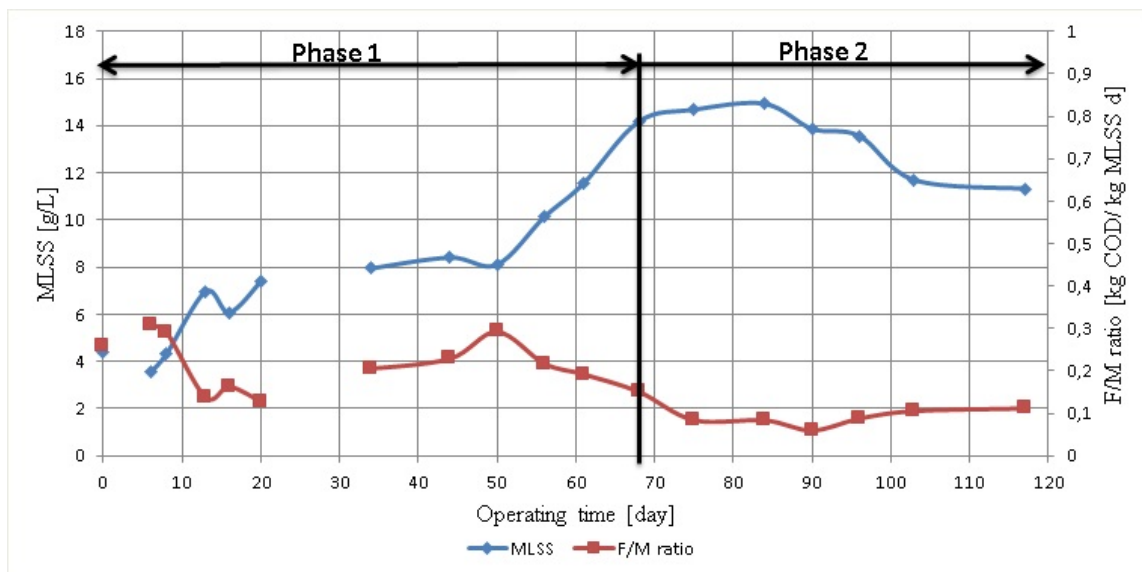
Figure 5.64. Initial MTDW test of two commercial UF PES membranes in MBR-MLSS + F/M ratio

Dye removal efficiency

Figure 5.65 shows the dye removal efficiency of the two commercial membrane modules and their relation to the dissolved oxygen concentration. The blue dye removal

efficiency was higher than the red one most of the time which is in line with the results obtained by Deowan (2013).

The efficiencies have been relatively stable until day 96. Then it went down on day 117. The reason is probably the reduction of dissolved oxygen concentration which happened on day 105. The bacteria did not have enough oxygen to be able to break down the dye molecules. The dye removal efficiency was expected to stabilise again after the increase of aeration.
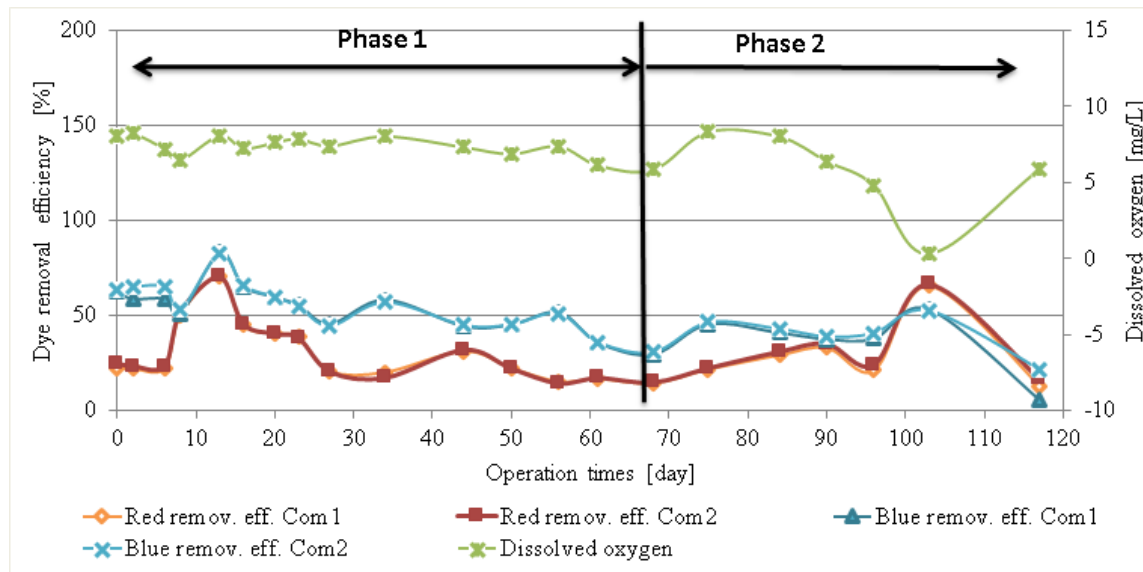
Figure 5.65. Initial MTDW test of two commercial UF PES membranes in MBR-Dye removal + dissolved oxygen

Dissolved oxygen (DO) concentration and consumption

Figure 5.66 shows the dissolved oxygen (DO) concentration and oxygen uptake rate (OUR) inside the reactor tank. At day 103 the dissolved oxygen went down to 0.3 mg/L. The reason of this might be the increase of MLSS and the consequent activity of the bacteria. This happened when the permeate pump speeds were decreased to put the system into standby mode which led to the surge of HRT. An important observation is that from day 61 to 91 the OUR remained stable from 0.5 to 0.7 mg/L min despite the fluctuation in DO concentration. After the incidence on day 103 the OUR went back to the previous value on day 117 at about 0.6 mg/L min. This suggests a stable oxygen consumption and regular activity of the bacteria.
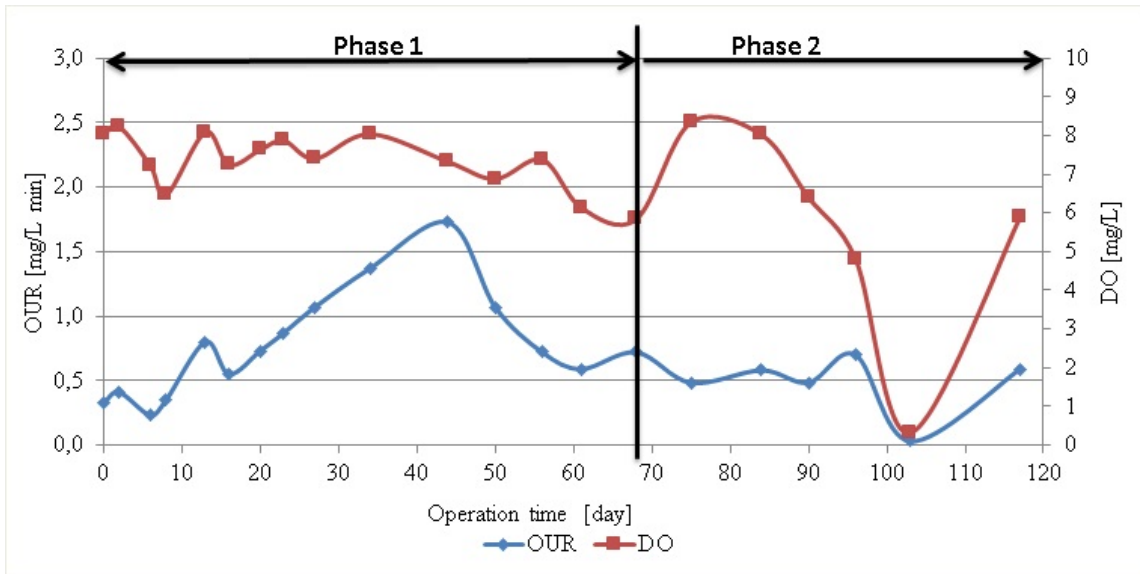
Figure 5.66. Initial MTDW test of two commercial UF PES membranes in MBR-dissolved oxygen + oxygen uptake rate

Hydraulic retention time (HRT)

Figure 5.67 shows the fluctuation of the HRT from 45 h to 60 h until day 27. After this day, the HRT dropped down to 25 h due to the increase of flux, it was then stable at around 25 h from day 50. In comparison with Deowan (2013) the HRT
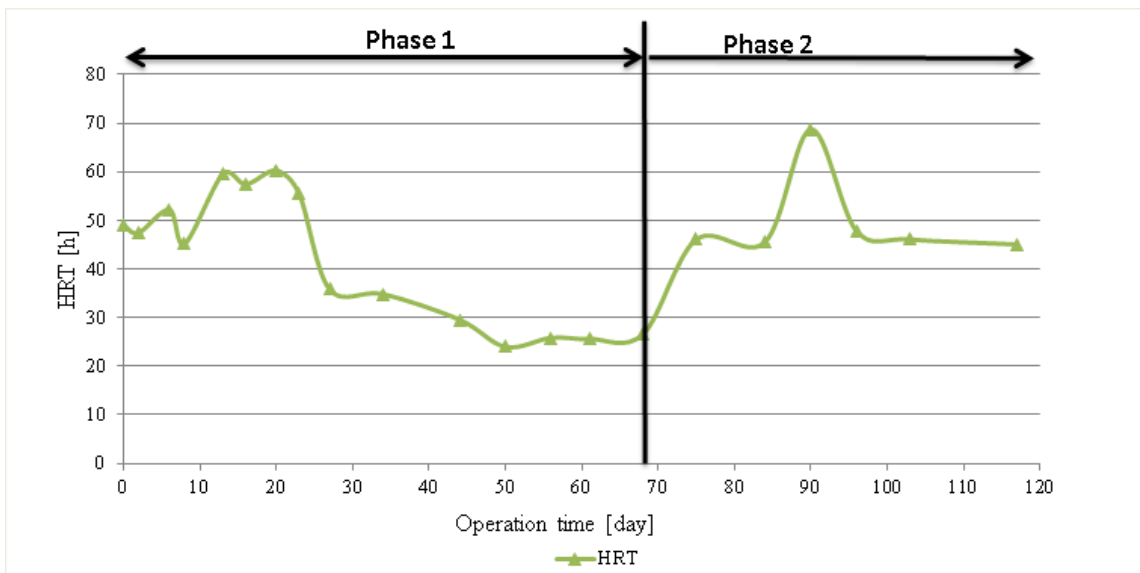
Figure 5.67. Initial MTDW test of two commercial UF PES membranes in MBR-HRT

was low also due to the double capacity of the membranes. HRT increased to approximately 45 h due to the decrease of flow in phase two. A rise in HRT was observed on day 90 because the membranes module was temporarily blocked due to the calibration of the pressure sensors.

COD and COD removal efficiency

Figure 5.68 presents the COD removal efficiency for the entire duration of the experiment. The result demonstrates the same COD removal ability of both membranes. The average COD for the feed was 2235 mg/L. Typically, COD removal efficiency indicates good performance around 95 %.
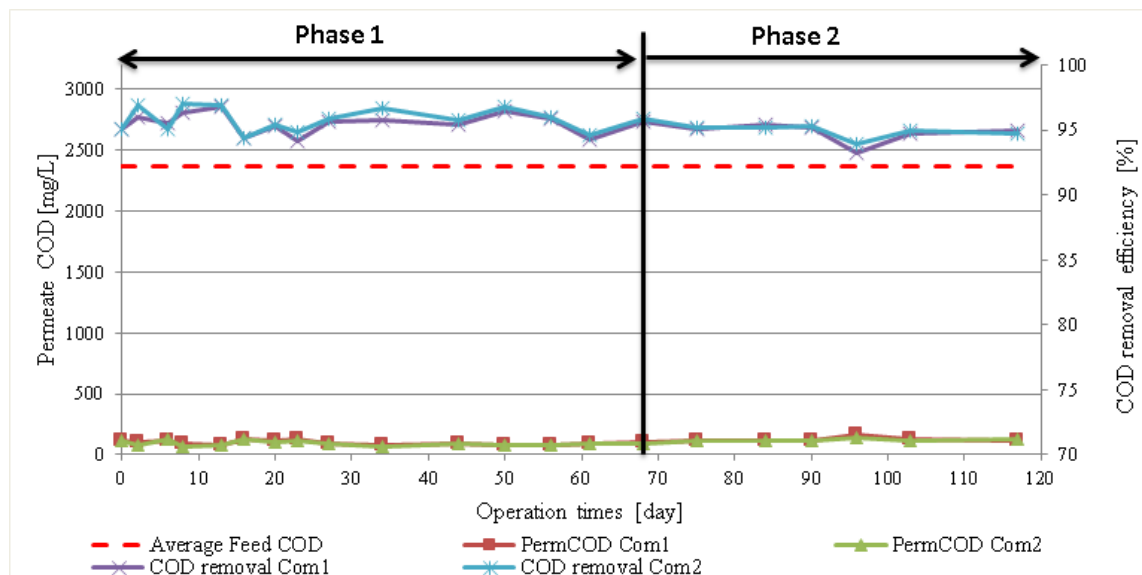
Figure 5.68. Initial MTDW test of two commercial UF PES membranes in MBR-COD

Permeate COD and reactor COD

Due to the biological process, degradation or adsorption mainly affected the COD removal efficiency [Deowan (2013)]. The degradation converts organic substances to inorganic substances or smaller sized organics. Moreover, the organic or inorganic substances were adsorbed by the bacteria in the reactor [Deowan (2013)]. Figure 5.69 shows the reactor COD was always higher than the permeate COD which is in-line with the work by Deowan (2013).
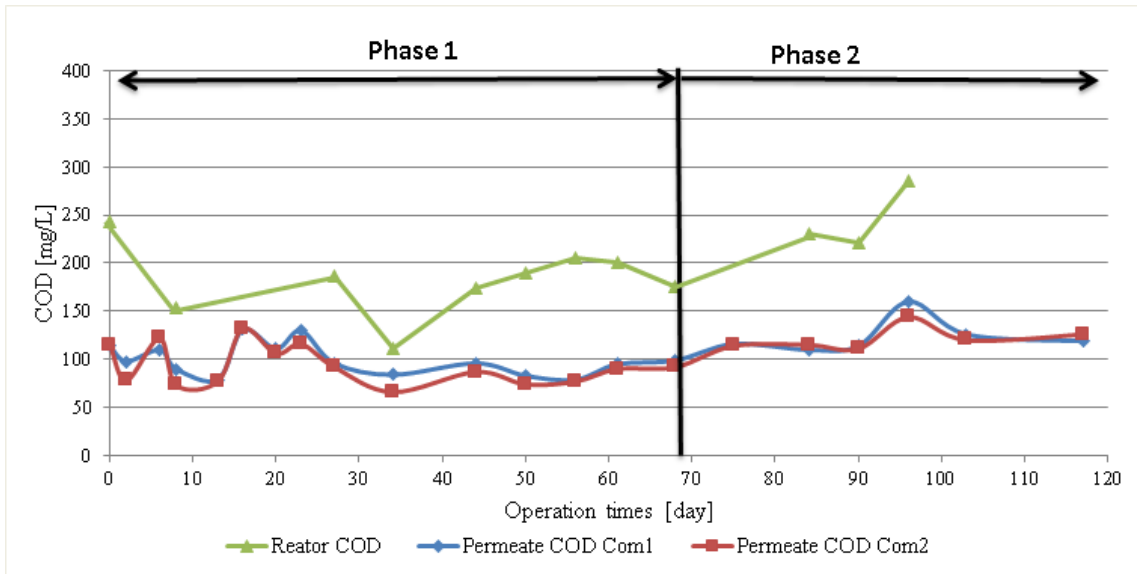
Figure 5.69. Initial MTDW test of two commercial UF PES membranes in MBR-COD in reactor and Permeate

Effect of HRT on COD removal efficiency

Figure 5.70 indicates that the COD rejection was generally independent of the HRT. The COD removal efficiency was stable at around 95 % even when the HRT
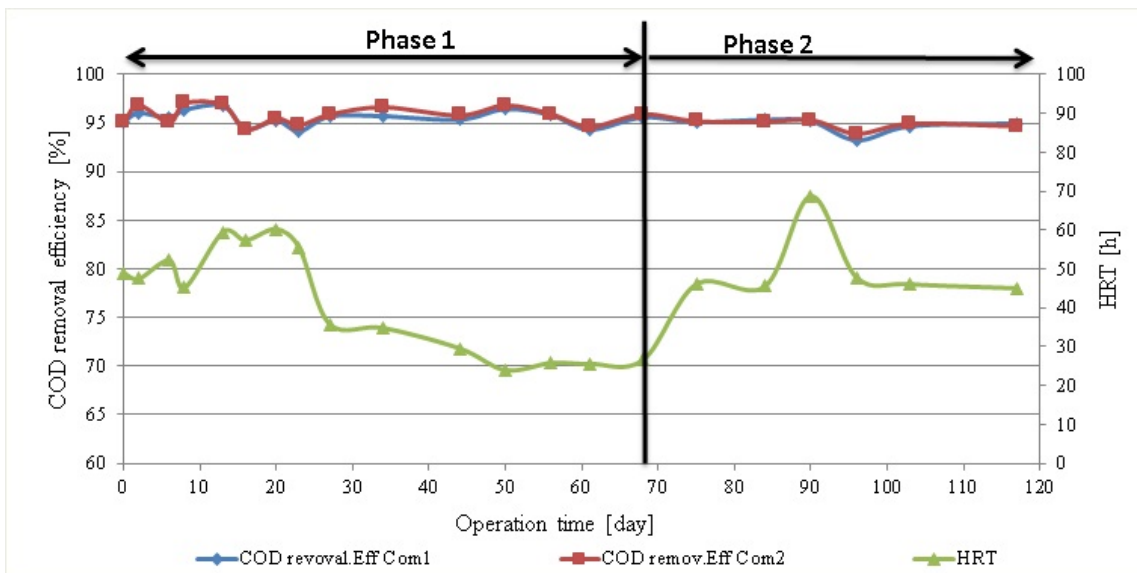
Figure 5.70. Initial MTDW Test of two commercial UF PES membranes in MBR-COD+HRT

dropped down from 60 h to 25 h within phase one. The HRT increased from 25 h to approximately 45 h due to the decrease of flow in phase two. A rise in HRT was observed on day 90 because of the calibration of the pressure sensors. However, this had no effect on the COD removal efficiency of both modules. This experiment was in-line with Deowan (2013), who concluded that there was no relation between HRT and COD removal.

COD and TOC relation

Figure 5.71 shows the relation between COD and TOC in the permeate. Both membranes show similar trends. The permeate TOC values were always lower than the permeate COD. The reduction in dissolved oxygen concentration on day 103 to nearly 0.5 mg/L (see Figure 5.66) had no effect on COD and TOC of the permeates. Regarding the amounts of COD and TOC, permeates 1 and 2 show the same trend but less fluctuation is observed in TOC than for the COD values.
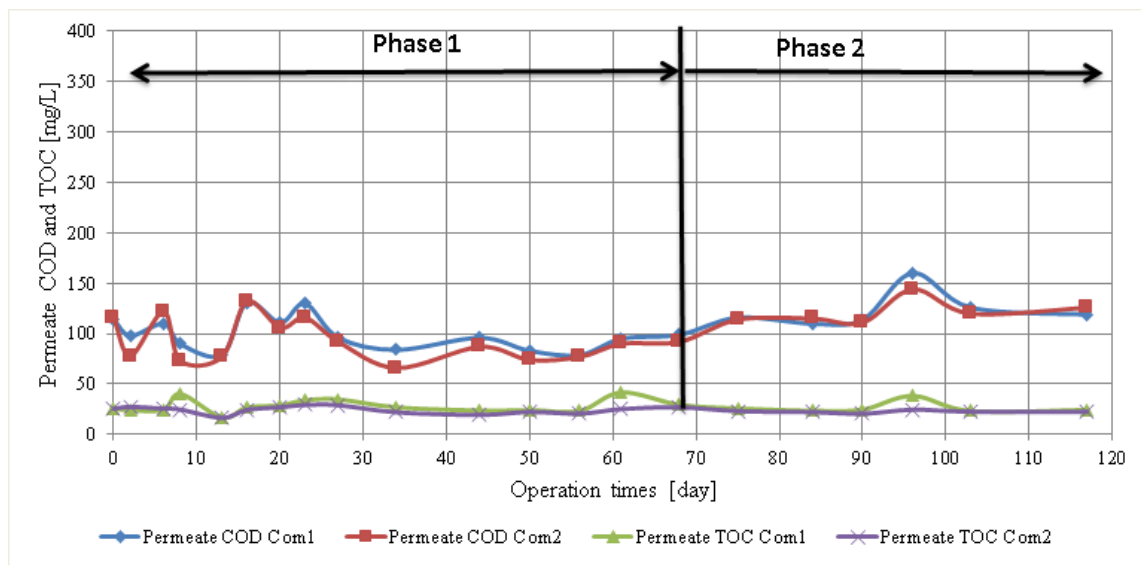
Figure 5.71. Initial MTDW test of two commercial UF PES membranes in MBR-COD+TOC

Figure 5.72 (a+b) shows similar rejection rates for both membranes with regards of TOC and COD. The TOC removal efficiency of Com1 and Com2 were both around 97 %, which was slightly higher than COD removal efficiency of about 95 %. For the TOC removal, both membranes performed at a slightly higher efficiency in

comparison to the work of Deowan (2013), while the COD removal is in the same range (92 % and 96 % in TOC and COD rejection, respectively).
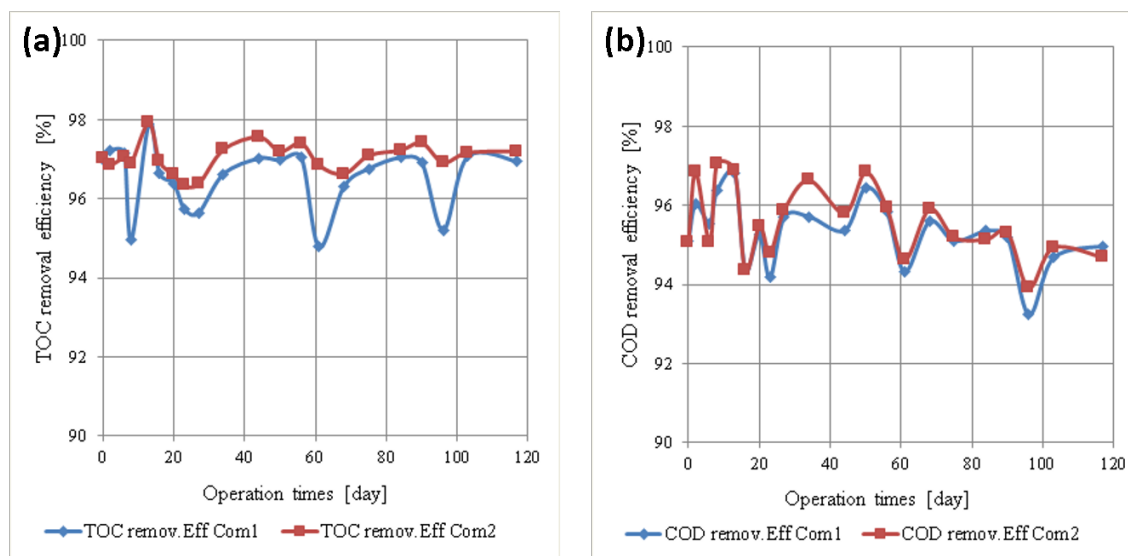
Figure 5.72. Initial MTDW test of two commercial UF PES membranes in a) MBR TOC and b) COD removal efficiency

Conclusion

On the basis of these results, some preliminary conclusions are reported:

- As the dissolved oxygen concentration (DOC) in the reactor tank decreased, the dye removal efficiency (red and blue) was also reduced.

- The acclimation phase for the water test took more than half an hour for each setting of the TMP. Future experiments (section 5.3.3) should consider acclimation phases of at least 24 hours.

- The TOC and COD removal efficiency was in line with the previous results of Deowan (2013).

- Different HRTs showed no significant influence to the COD and TOC removal.

5.3.3 PBM vs. commercial membrane

For the coating of the envelop membrane sheets used for the MBR tests, the following conditions were chosen based on the results given in section 5.2.3.

Table 5.17. Coating conditons of PBM for MBR envelop sheets

PBM Chemicals	
AUTEAB	25 w%
Methyl methacrylate (MMA)	21 w%
2-Hydroxylethyl methacrylate (HEMA)	10 w%
Deionised water (DI water)	41 w%
Ethylene glycol dimethacrylate (EGDMA)	3 w%
Photoinitiator Irgacure 184 for UV-LED	1.8 w%

Coating conditions	
Coating thickness	4 μm
Irradiation time	30 sec.
Irradiation intensity (UV-LED)	300 mW/cm^2
Room temperature	24 °C
Ambient conditions	Inert (Nitrogen, oxygen <1 %)

As the envelop sheets are laminated (see Figure 5.73), the surface might have other

Figure 5.73. Envelop sheets used for MBR application

characteristics than the pure membrane sheets used for the previous experiments discussed in section 5.2. The polymerisation efficiency is partially depending on the substrate type. This might lead to different characteristics of the PBM coated envelop membranes. The following experiments are done in order to study this influence.

FT-IR of PBM coated envelop membrane

The PBM coated envelop membrane was kept in DI-water for three times one hour while refreshing the DI-water every time. Afterwards the membrane was dried at 40 °C over night, and measured by FTIR for the range (1726 cm^{-1}) corresponding to the unique acrylate groups of the PBM (see section 4.7.2). As shown in Figure 5.74, the acrylate group is still present meaning that the PBM coating has not been removed. Therefore it was decided to prepare the envelop membrane sheets under the conditions given in Table 5.17 and run them in the MBR.
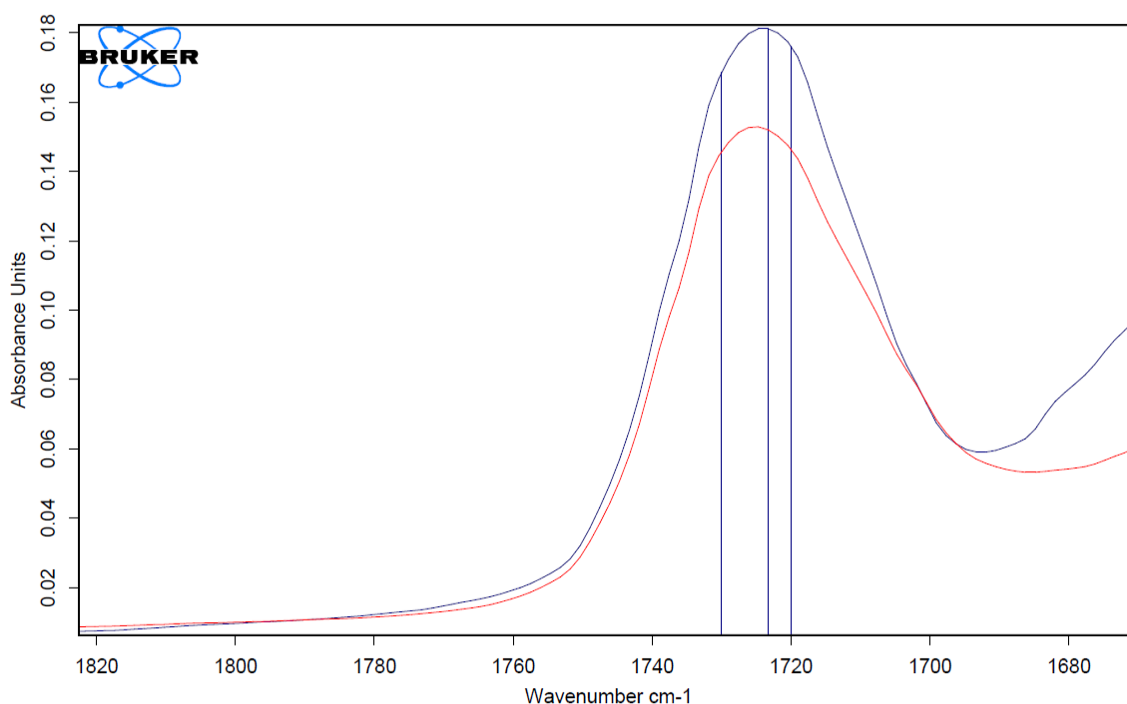
Figure 5.74. FTIR of PBM coated membrane before and after washing

Start-up of the MBR using the PBM coated envelop membranes

The WP of the PBM coated and a new commercial envelop membrane was studied by increasing step by step the speed of the pumps in both permeate lines resulting in an TMP increase. Figure 5.75 shows the WP for the salt rejection experiment as described in section 4.7.7. In contrary to the result described in section 5.3.2 the WP is stable by increasing TMP. The reason for that is a much longer acclimation phase for each TMP. For each TMP at least two days of acclimation time where given. It is also shown that the PBM coated membrane had a permeability that is about five times lower than the commercial one. This is in line with the results of the cross flow experiments described in section 5.2.3. The only discrepancy resulted for the permeability values itself. For the cross flow experiments, the permeability is usually around six times higher than for the results in the MBR. One reason might be due to scaling onto the membrane surface when it is installed in the MBR. The better fluid dynamic in the cross-flow test unit (cross flow of 28 L/h), than in the MBR, reduces the scaling affinity of the membrane, increasing the WP. However, the factor for the permeability difference between commercial and PBM membrane remains the same around five.
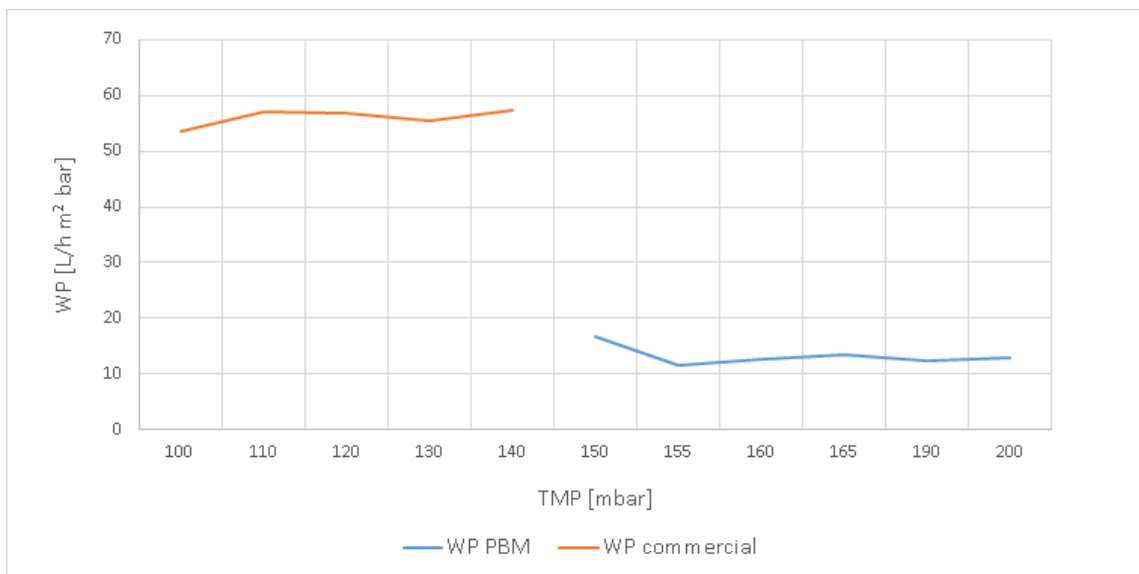
Figure 5.75. MBR water permeability vs. TMP for PBM and commercial membrane

In order to study this effect further, the commercial membrane was run for another salt rejection experiment with the cross-flow test unit. The conditions for salt rejec-

tion described in section 4.7.7 were applied. As the installation in the MBR results in no cross flow, the lowest possible setting of the cross-flow test unit was chosen. A cross flow of 14.4 L/h at a TMP of 0.07 bar was run for several days (see Figure 5.76).

A WP of about 250 L/h m² bar resulted under these conditions. Comparing this result with other results for the WP of the commercial membrane (see Figures 5.29, 5.15, 5.16), a decrease of at least 100 L/h m² bar is observed. As the limitations of the cross-flow test unit do not allow lower adjustments of the cross flow, the effect of further decreased settings could not be studied. However, this results supports the theory of membrane scaling.
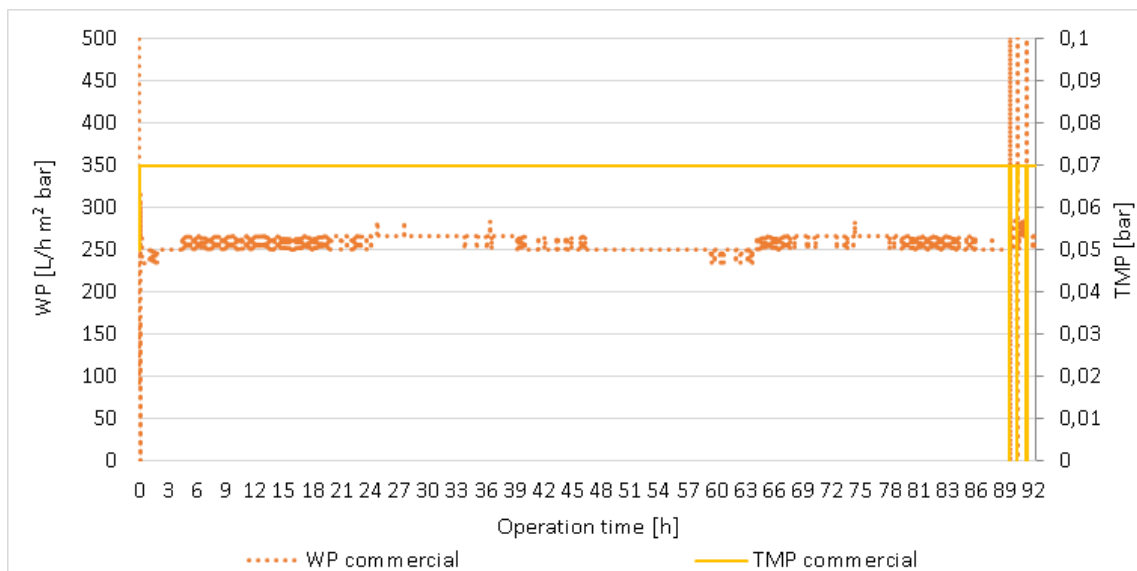
Figure 5.76. Water permeability for commercial PES UF membrane with 2.000 ppm $MgSO_4$

Salt rejection of PBM coated envelop membrane

As the experiment in section 5.4 showed a slightly higher salt rejection rate for the PBM coated RO membrane the influence to the envelop membranes was studied as well. Figure 5.77 shows the salt rejection rate of the commercial and PBM coated envelop membrane over TMP. As it is shown, no salt rejection was observed by both the PBM and commercial membrane.
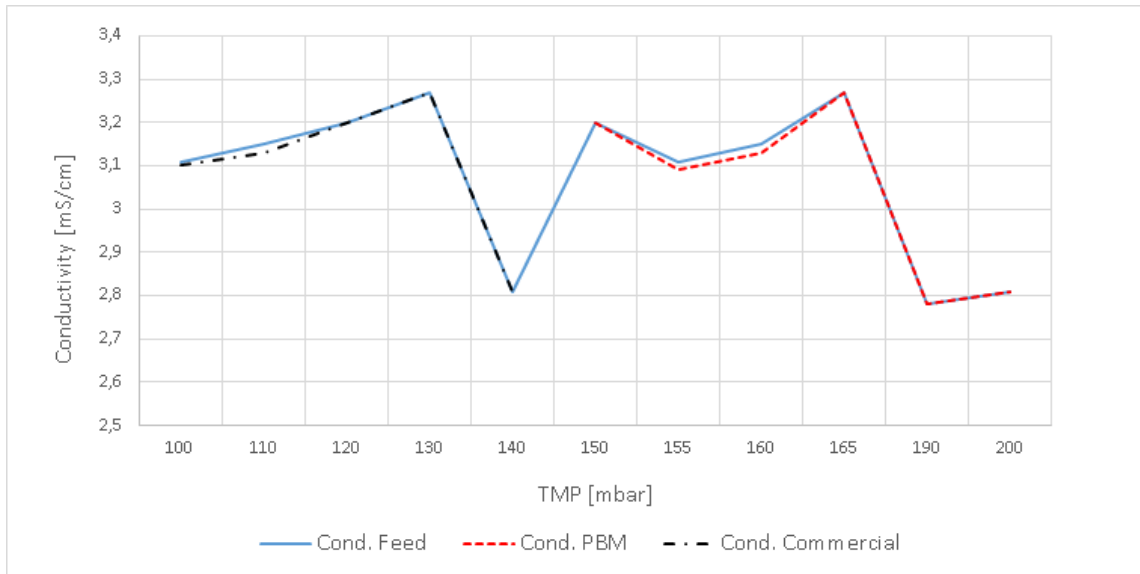
Figure 5.77. MBR conductivity vs. TMP for PBM and commercial membrane

5.4 Potentiality of PBM coating onto RO (PA) membranes

In this section preliminary results on the use of PBM coating on commercial RO membranes are discussed. Therefore, a commercial reverse osmosis RO membrane from DOW Chemicals (BW XLE), consisting of a poly amide (PA) layer is used [DOW (2015)]. In order to proof the chemical cleaning resistance of the PBM coated RO, a standard salt rejection test (protocol supplied by DOW Chemials, see Table 5.18) was done before and after an alkaline (pH 13) and acid (pH 1) cleaning step

Table 5.18. Salt rejection conditions for RO

Conductivity (NaCl)	3.13 mS/cm
Temperature	25 °C
Cross flow	28 L/h
TMP	7.8 bar [1]

---

[1]maximum of current sensor setup

of each one hour using the single stage cross-flow setup described in section 4.7.7. The optimum PBM composition using ATEAB surfactant has been employed, as discussed in section 5.2.3. The following coating conditions are chosen (Table 5.19).

Table 5.19. Coating conditons of PBM for commercial RO membrane

PBM Chemicals	
AUTEAB	25 w%
Methyl methacrylate (MMA)	21 w%
2-Hydroxylethyl methacrylate (HEMA)	10 w%
Deionised water (DI water)	41 w%
Ethylene glycol dimethacrylate (EGDMA)	3 w%
Photoinitiator Irgacure 184 for UV-LED	1.8 w%
Coating conditions	
Coating thickness	4 μm
Irradiation time	30 sec.
Irradiation intensity (UV-LED)	300 mW/cm²
Room temperature	24 °C
Ambient conditions	Inert (Nitrogen, oxygen <1 %)

Table 5.20 summarises the results for both, PBM coated and commercial RO. For both cleaning cycles, first at pH 13 and second at pH 1, the TMP was reduced to 4 bar for the one hour of cleaning. In between the cleaning cycles the system was flushed with DI water in order to remove all chemicals.

The salt rejection decreased slightly having both cleaning cycles done for the PBM coated RO, while the commercial RO decreased dramatically from 96.20 to 83.50 %. This results leads to the impression that the PBM coated membrane increases the cleaning resistance under the discussed conditions, while the commercial membrane may have started to decompose.

In contrary, a reduction in permeate flow of factor ten results for the PBM coated membrane visa the original RO membrane (0.03 vs. 0.31 L/h). However, this results need to be verified by repeating the experiment for future research.

Table 5.20. PBM RO vs. standard RO

PBM before cleaning	**BW XLE before cleaning**
Permeate flow: 0.03 L/h	Permeate flow: 0.31 L/h
Conductivity Permeate: 34.6 μS/cm	Conductivity Permeate: 120.9 μS/cm
Conductivity Feed: 3.06 mS/cm	Conductivity Feed: 3.18 mS/cm
Salt rejection: 98.87 %	Salt rejection: 96.20 %
PBM after cleaning	**BW XLE after cleaning**
Permeate flow: 0.03 L/h	Permeate flow: 0.31 L/h
Conductivity Permeate: 100 μS/cm	Conductivity Permeate: 510 μS/cm
Conductivity Feed: 3.10 mS/cm	Conductivity Feed: 3.09 mS/cm
Salt rejection: 96.77 %	Salt rejection: 83.50 %

In order to proof that the PBM remains bonded onto the membrane surface after the chemical cleaning steps, the FT-IR described in section 4.7.2 was used. Figure 5.78 shows the pure RO membrane (red), PBM coated RO before treatment (purple)
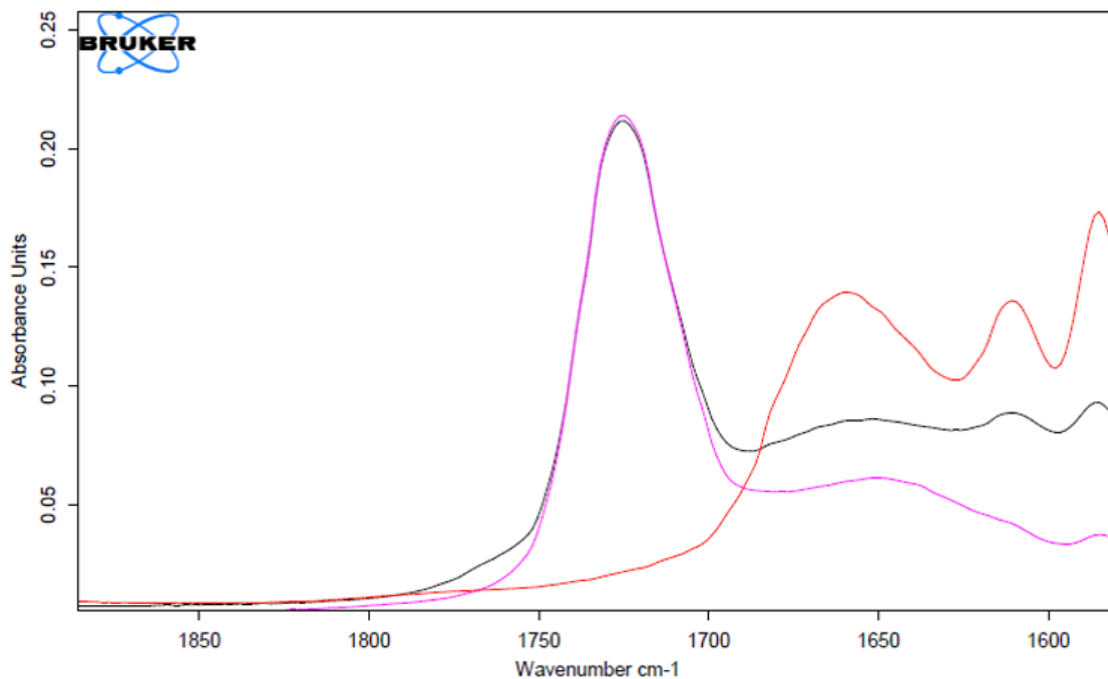
Figure 5.78. FT-IR spectrum of pure RO and PBM RO

and after chemical cleaning (black). The characteristic peak at 1726 represents the C=O group existing in the PBM components.

As shown, the PBM seems to be permanently attached to the membrane surface even after intense chemical cleaning at pH 13 and pH 1. However, this result should be verified by SEM analyses in future research. This result highlights the flexibility of the PBM coating process even with different substrates. Further studies with PBM coated RO membranes can be done, seeing their rejection of different components e.g. trivalent and pentavalent Arsenic. The coating thickness needs to be further decreased in order to increase the permeability of the membrane. Therefore different casting technologies should be studied.

6 Conclusion and outlook

The main aim of this research was to improve the polymerisation step of the novel coating based on polymerisable bicontinuous microemulsion (PBM) in view of a potential scale-up and its membrane application at larger scale. Therefore, UV-irradiation techniques have been employed for the polymerisation of the PBM coated membranes. This allows to improve the polymerisation rate (few seconds) in comparison of previous work by Galiano et al. (2015) where the polymerisation rate was of about 20 minutes using redox polymerisation. Moreover, the other main limitation of the polymerisation by redox is related to the optimal viscosity of the microemulsion to be used for the coating which is difficult to be controlled particularly in view of the up-scaling.

As preparation for the coating onto the commercial UF PES membrane (UP 150T Microdyn-Nadir-GmbH (2014)) several experiments had to be done. First of all the redox based coatings have been reproduced (see 5.1.1). To initiate the polymerisation by UV-light, in total seven different photoinitiators were selected (see 4.3). Their influence to the formation of a microemulsion was studied. Out of them only Irgacure 819DW showed a yellowing effect to the PBM (see 5.1.2).

As there is a wide field of different UV sources available, different types where studied for their application in this work (see 5.1.3). Out of them only the UV-LED showed a very low temperature increase to the membrane surface. First polymerisation trials onto glass plates where done for all selected photoinitiators under different conditions. For non-inert conditions only DMPA and Irg. 184 showed promising conversion rates, and where therefore focused on for subsequent experiments. In addition, the effect of the surfactant type was studied. Two surfactants, the commercially available non-polymerisable DTAB, and polymerisable AUTEAB that was synthesised by the Department of Chemistry of the UNICAL, where selected. Considering a full conversion of the PBM the AUTEAB surfactant could increase the polymerisation

time about the factor of two (see section 5.1.5). Therefore ongoing experiments focused on the AUTEAB surfactant. As the oxygen inhibition effect is hindering the polymerisation speed of the PBM, conversion rate experiments are also done under inert conditions leading to another significant reduction of polymerisation time. For both photoinitiators DMPA and Irg. 184, the inert conditions resulted in a faster polymerisation. However, a full conversion was only achieved for Irg. 184 (see Figure 5.14). The ideal concentration of Irg. 184 was found at 1.8 w% irradiated for 30 seconds.

As for the DTAB based PBM the coating onto membranes resulted always in an immediate permeation into the pores, the influence of adding different kinds of PEG to the PBM where studied in order to increase the viscosity. The target viscosity, representing the value the PBM did not enter the pores anymore, was defined with the usage of non-polymerisable PEG 2,000, PEG 20,000 and another polymerisable PEG. PEG 20,000 with a concentration of 15 w% was defined as target concentration. However, even if the coating onto membranes was successful, the permeability of the coated membrane resulted to be very low, both for PEG 20,000 and the polymerisable PEG. In addition the surface of the membrane was very sticky after coating, even after a storage time of several months (see section 5.2.1), indicating an unfinished polymerisation.

The influence of the coating thickness to the permeability of the PBM coated membranes was studied. The highest permeability was found at 4 μm. At 20 μm and above the permeability gets too low for the purpose of an application in the MBR, but might be interesting for future research of other applications (see section 5.2.2).

Another influence that has been studied to the formation of the PBM membrane is the temperature during the coating (see section 5.2.2). The highest WP results for the coating at 25 °C (98 L/h m^2 bar), while the temperatures of 20 and 30 °C result in lower permeability of 70 and 88 L/h m^2 bar. For the WP with model foulant at high TMP of 2.2 bar all PBMs exceeded the permeabilities of their referencing membrane around 14-17 %.

It has been shown the dependency of the polymerisation process of the parameters such as temperature, inert/non inert conditions and coating thickness. The detailed study of coupled effects remain for future research.

The target membrane was defined for a PBM coated under 24 °C, with a coating thickness of 4 μm and a photoinitiator content of 1.8 w% under inert conditions. The reproducibility of the coating was proven (see section 5.2.3), and a pure water permeability in the range of 60-77 L/h m² bar resulted at a TMP setting of 0.5 bar.

Regarding the storage properties of the photoinitiator included PBM it was shown that the PBM keeps its micro-emulsion for at least one month (see 4.2.2). A successful coating proved the stability. Never the less further studies should be done in this field as soon as the PBM needs to be stored in big scale for a commercial scale-up.

As in real applications the permeate flux is of interest and the TMP regulated in order to achieve a constant flux, the effect of a constant permeate flow was studied (see section 5.2.3). Running the membranes with pure water the PBM permeability remains below the commercial one (WP PBM: 60 L/h m² bar, WP commercial: 250 L/h m² bar). However, running the membranes with humic acid as model foulant, the advantages of the PBM became visible. At the adjusted VF of 0.5 L/h stable conditions were found at a TMP of about 3.5 bar for the PBM membrane, while the commercial membrane did not reach a stable TMP and found its maximum at 4.5 bar only because of the system boundaries. In real applications a cleaning cycle, most probably with chemicals, would be required for the commercial membrane. Regarding the WP, the PBM produces around 17 L/h m² bar, having the stable TMP reached, while the WP for the commercial membrane ends up around 10 L/h m² bar. Running the membranes without a cleaning cycle therefore results in an about 70 % higher WP for the PBM coated membrane. While cleaning the membranes with deionised water three times for one hour the TMP for the PBM membrane reaches almost its initial value of 2.5 bar. For the commercial membrane the TMP after cleaning is around 4 bar. Keeping in mind that a higher TMP is leading to a higher energy demand (e.g.for the suction pump in an MBR), the PBM could also safe running costs in terms of electricity.

A chemical cleaning experiment of the PBM coating indicated the stability of the coating even by cleaning the membranes at pH 1 and pH 13 for one hour each (see section 5.2.4). The typical C=O group of the PBM was shown after the treatment by FTIR. However, this result should be reproduced for future research. SEM cross section images could confirm the FTIR result.

Further characterisation of the PBM coated membrane was done by contact angle (see section 5.2.5), AFM (see section 5.2.6) and SEM (see section 5.2.7). In comparison to the commercial membrane, the target membrane showed a contact angle reduction of 62 % indicating a higher hydrophilic membrane. The surface roughness reduction decreased about 87 % indicating a very smooth surface for the PBM membrane. This contributes to the anti-fouling characteristics as particles are hindered to attach to the membrane surface. The typical bicontinuous structure on the membrane surface described by Galiano et al. (2015) was not visible by the SEM picture of the membrane surface. However, another bicontinuous structure is shown that matches with pictures in other publications [Yan and Texter (2006), Gan et al. (2005)]. The cross section pictures showed the coating thickness of the PBM of 2.4 μm. As the AUTEAB based PBM (see Table 4.7) consists of 41 w% water this result is in line with the expected value (59 % = 2.4 μm) as the water content evaporated in the polymerised coating. The thickness of fouling layers after the model foulant experiment was measured as well and indicates a 9.5 times ticker layer for the commercial membrane in comparison to the PBM membrane.

In order to create qualified and significant results it was indispensable to update the existing MBR system in such a way that two membranes can be tested in parallel (see section 4.1.2). One main reason for that is the biocenosis of the activated sludge that is permanently changing. For the redesign, among other things, a new membrane housing had to be designed and equipped with a second permeate line including all sensors and a suction pump. In addition, it was necessary to change the software programming. The signals from some new sensors had to be converted in digital signals and all signals had to be processed by LabView, displayed on the programme surface and finally stored in an Excel-file.

Consequently to the MBR redesign the system had to proof its reliability within an initial run comparing two commercial membranes simultaneously. The proper function of all sensors, as well as the signal conversion, visualisation in LabView and storage in an Excel-file had to be assured as preparation for later experiments that will compare the PBM and commercial membrane. While equipping the MBR with an air diffuser (see section 4.1.2), the homogeneous distribution of oxygen in the reactor was proofed (see section 5.3.1). During a long term run of 117 days several factors were studied (see section 5.3.2). It was shown a decrease of dye removal efficiency with decreased oxygen concentration in the reactor. As result of

an initial water test it was shown that the acclimation phase for different TMPs is time consuming. Stable permeabilities are expected after about 20 hours of run for the commercial membrane. However, for the PBM coated membrane stable permeabilities occurred almost immediately for the trials with the SIMATEC cross flow unit (see section 5.2.3). As the PBM membrane will be studied in the MBR in parallel with the commercial membrane an appropriate time should be foreseen. Periodic inspection of the sensor readings with subsequent calibrations are necessary to assure realistic readings of the MBR sensor setup.

In addition to the coating onto PES membranes used for MBR application, that was focused on within this work, the coating on another substrate was studied as an outlook to future research in section 5.4. The PBM was successfully coated onto a PA based RO membrane from DOW. A salt rejection test was done showing a decrease in permeability for the PBM membrane about factor ten but also an increase in salt rejection of about 2.6 %. A strong chemical cleaning at pH 1 and pH 13 for one hour each decreased the salt rejection of the PBM membrane about 2 %, while the commercial membrane decreased 12.7 %. Therefore, the cleaning resistance seemed to be improved for the PBM membrane. Both membranes kept their permeability after the chemical cleaning. A subsequent FTIR measurement of the PBM membrane showed the characteristic C=O group of the PBM. Both the constant permeability and FTIR result indicate that the PBM remained on the membrane after the chemical cleaning. However, this experiment represents only a potential field of research for the future. The results need to be reproduced and the membranes should be characterised e.g. by SEM. As the permeability resulted to be very low for the PBM membrane alternative coating techniques than the casting knife should be studied as the applied 4 μm represent the thinnest possibility for this technique.

As an outlook to future experiments, the process developed within this work can be potentially further optimised for several membrane types, in regards of the polymerisation time, by the following tasks:

- Combination of different photoinitiators with specific properties (combine deep cure and surface cure photoinitiators). This might even lead to a successful full non-inert polymerisation.

- Study of higher and lower irradiation intensities combined with the influence to the polymerisation by coating thickness and photoinitiator type, blend and amount.

- Use of a mirror as membrane substrate. The irradiation will be reflected and penetrate the PBM a second time.

- Create coating thickness below 4 μm by other coating techniques than the casting knife.

Bibliography

Adham, S., DeCarolis, J., and Pearce, W. (2004). Optimization of Various MBR Systems for Water Reclamation — Phase III, Desalination and Water Purification Research and Development Report No. 103. Technical report, US Department of Interior.

Al-kdasi, A., Idris, A., Saed, K., and Guan, C. T. (2004). Treatment of Textile Wastewater By Advanced Oxidation Processes – a Review. *Global Nest: the International Journal*, 6(3):222–230.

Alaton, I. A., Balcioglu, I. A., and Bahnemann, D. W. (2002). Advanced oxidation of a reactive dyebath effluent:comparison of O3, H2O2/UV-A processes. *Water Research*, 36:1143–1154.

Ali, H. (2010). Biodegredation of synthetic dyes-a review. *Water Air Soil Pollution*, 213(1-4):251–273. DOI 10.1007/s11270–010–0382–4.

Asatekin, A., Menniti, A., Kang, S., Elimelech, M., Morgenroth, E., and Mayes, A. M. (2006). Antifouling nanofiltration membranes for membrane bioreactors from self-assembling graft copolymers. *Journal of Membrane Science*, 285(1-2):81–89. DOI 10.1016/j.memsci.2006.07.042.

Ba, C., Ladner, D. A., and Economy, J. (2010). Using polyelectrolyte coatings to improve fouling resistance of a positively charged nanofiltration membrane. *Journal of Membrane Science*, 347:250–259. DOI 10.1016/j.memsci.2009.10.031.

Babu, B. R., Parande, A., Raghu, S., and Kumar, T. P. (2007). Cotton Textile Processing: Waste Generation and Effluent Treatment. *The journal of cotton science*, 153(11):141–153. ISSN 15243303.

Bae, T. H. and Tak, T. M. (2005). Preparation of TiO2 self-assembled polymeric nanocomposite membranes and examination of their fouling mitigation effects in

a membrane bioreactor system. *Journal of Membrane Science*, 266(1-2):1–5. DOI 10.1016/j.memsci.2005.08.014.

Baek, S. H., Pagilla, K. R., and Kim, H.-J. (2010). Lab-scale study of an anaerobic membrane bioreactor (AnMBR) for dilute municipal wastewater treatment. *Biotechnology and Bioprocess Engineering*, 15(4):704–708. DOI 10.1007/s12257–009–0194–9.

Bamford, C. and W., N. R. G. (1934). Primary Photochemical Reactions. Part VII. Photochemical Decomposition of. *Journal Chemical Society*, (1504):1504–1511. DOI 10.1039/JR9350001504.

BASF (2012). Technical Information Irgacure 184. https://www.basf.com (accessed August 15, 2016).

Bechtold, T., Burtscher, E., and Hung, Y. (2006). Treatment of textile wastes. *Waste Treatment in the Process Industries*, pages 363–392. ISBN 0–8493–7233–X.

Bemberis, I., Hubbard, P., and Leonard, F. B. (1971). Membrane sewage treatment systems-potential for complete wastewater treatment. *American Society of Agricultural Engineers Winter Meeting*, pages 1–28,71–878.

Bionexgen (2016). Bionexgen. http://www.bionexgen.eu/ (accessed June 9, 2016).

Bosch, P., Peinado, C., Martín, V., Catalina, F., and Corrales, T. (2006). Fluorescence monitoring of photoinitiated polymerization reactions: Synthesis, photochemical study and behaviour as fluorescent probes of new derivatives of 4-dimethylaminostyryldiazines. *Journal of Photochemistry and Photobiology A: Chemistry*, 180(1):118–129. DOI 10.1016/j.jphotochem.2005.10.002.

Brepols, C. (2010). *Operating Large Scale Membrane Bioreactors for Municipal Wastewater Treatment*. IWA Publishing. ISBN 9781843393054, London, 1st edition.

Brik, M., Schoeberl, P., Chamam, B., Braun, R., and Fuchs, W. (2006). Advanced treatment of textile wastewater towards reuse using a membrane bioreactor. *Process Biochemistry*, 41(8):1751–1757. DOI 10.1016/j.procbio.2006.03.019.

Buck, H. and Buck, S. (1987). *Mikroorganismen in der Abwasserreinigung. ISBN 3-921288-58-4*. 1st edition.

Chanda, M. and Roy, S. K. (2006). *Plastics Technology Handbook.* CRC Press. ISBN 9780849370397. Boca Raton, 4th edition.

Chang, I., Le Clech, P., Jefferson, B., and Judd, S. (2002). Membrane Fouling in Membrane Bioreactors for Wastewater Treatment. *Journal of Environmental Engineering*, 128(11):1018–1029. DOI 10.1061/(ASCE)0733–9372(2002)128:11.

Chew, C. H., Li, T. D., Gan, L. H., Quek, C. H., and Gan, L. M. (1998). Bicontinuous-nanostructured polymeric materials from microemulsion polymerization. *Langmuir*, 14:6068–6076. DOI 10.1021/la970990a.

CHIENG, T. H., GAN, L. M., TEO, W. K., and PEY, K. L. (1996). Porous polymeric membranes by bicontinuous microemulsion polymerization : effect of anionic and cationic surfactants. *Polymer*, 37(26):5917–5925. ISBN 0032–3861.

Clouzot, L., Doumenq, P., Vanloot, P., Roche, N., and Marrot, B. (2010). Membrane bioreactors for 17a-ethinylestradiol removal. *Journal of Membrane Science*, 362(1-2):81–85. 10.1016/j.memsci.2010.06.020.

Cote, P. and Liu, M. (2004). MBR beats tertiary filtration for indirect water use. *Internation desalination and water reuse quarterly*, 13:32–37. ISBN 1022–5404.

Deowan, S. A. (2013). *Development of Membrane Bioreactor (MBR) process applying novel low fouling membranes.* Phd thesis, ITM at UNICAL, Italy.

Deowan, S. A., Galiano, F., Hoinkis, J., Figoli, A., and Drioli, E. (2013). Submerged Membrane Bioreactor (SMBR) for Treatment of Textile Dye Wastewater towards Developing Novel MBR Process. *APCBEE Procedia*, 5:259–264. 10.1016/j.apcbee.2013.05.045.

Deowan, S. A., Galiano, F., Hoinkis, J., Johnson, D., Altinkaya, S. A., Gabriele, B., Hilal, N., Drioli, E., and Figoli, A. (2016). Novel low-fouling membrane bioreactor (MBR) for industrial wastewater treatment. *Journal of Membrane Science*, 510:524–532. DOI 10.1016/j.memsci.2016.03.002.

Deowan, S. A., Islam, R., Buccheri, S., Galiano, F., Mueller, K., Schmidt, S., Bouhadjar, S., Hoinkis, J., Gabriele, B., and Figoli, A. (2015). Preparation and application of Novel Antifouling Membranes for Forward Osmosis (FO) Process in Concentrating of Textile Dye Wastewater. In *Euromembrane 2015*, page 174, Aachen. DOI 10.1117/12.844453.

Dogan, B., Kerestecioglu, M., and Yetis, U. (2010). Assessment of the best available wastewater management techniques for a textile mill: cost and benefit analysis. *Water Science & Technology*, 61(4):963. DOI 10.2166/wst.2010.006.

DOW (2015). DOW Chemical Company, DOW Filmtec SW http://www.dow.com/en-us/markets-and-solutions/products (accessed December 30, 2015).

Drioli, E., Criscuoli, A., and Curcio, E. (2006). Membrane Contactors: Fundamentals, Applications and Potentialities. *Elsevier Membrane Science and Technology*, 11:40. ISBN 0–444–52203–4.

EUROMBRA (2006). Membrane bioreactor technology (MBR) with an EU perspective for advanced municipal wastewater treatment strategies for the 21st century. D1-Data acquisition and compilation. Project No. 018480. Technical report, http://www.wise-rtd.info/en/info/membrane-bioreactortechnology- mbr-eu-perspective-advanced-municipal-wastewater-treatment. (accessed September 20, 2016).

Excelitas Technologies Corp. (2016). Excelitas Technologies. http://www.excelitas.com (accessed June 13, 2016).

Fenu, A., Guglielmi, G., Jimenez, J., Sperandio, M., Saroj, D., Lesjean, B., Brepols, C., Thoeye, C., and Nopens, I. (2010a). Activated sludge model (ASM) based modelling of membrane bioreactor (MBR) processes: A critical review with special regard to MBR specificities. *Elsevier*, pages 4272–4294. DOI 10.1016/j.watres.2010.06.007.

Fenu, A., Roels, J., Wambecq, T., De Gussem, K., Thoeye, C., De Gueldre, G., and Van De Steene, B. (2010b). Energy audit of a full scale MBR system. *Desalination*, 262(1):121–128. DOI 10.1016/j.desal.2010.05.057.

Figoli, A. (2001). PhD Thesis: Synthesis of nanostructured mixed matrix membrane for facilitated gas separation. University of Twente, Netherlands. ISBN 90-365-1673-0.

Figoli, A., Hoinkis, J., Gabriele, B., De Luca, G., Galiano, F., and Deowan, S. (2015). Patent: Bicontinuous microemulsion polymerized coating for water treatment. Universita della Calabria, Italy. WO/2015/044335.

Flory, P. J. (1953). *Principles of Polymer Chemistry*. Cornell University Press, Ithaca, United States. ISBN 978-0-8014-0134-3, 1st edition.

Forbes, M. D. E. (1992). Time-Resolved Electron Paramagnetic Resonance Spectroscopy in the Q-Band Microwave Region. *Journal of Physics Chemistry*, 96:7836–7839. DOI 10.1524/zpch.1992.1.Part_2.063.

Fouassier, J. P. (1998). *Photoinitiated Polymerisation - Theory and Applications*. Rapra Technology Limited. ISBN 0889-3144, Shawbury, United Kingdom, 9 edition.

Fouassier, J.-P. and Merlin, A. (1980). Laser investigation of norrish type I photoscission in the photoinitiator irgacure (2,2-dimethoxy 2-phenyl-acetophenone). *Journal of Photochemistry*, 12(1):17–23. DOI 10.1016/0047–2670(80)85076–3.

Friha, I., Bradai, M., Johnson, D., Hilal, N., Loukil, S., Ben Amor, F., Feki, F., Han, J., Isoda, H., and Sayadi, S. (2015). Treatment of textile wastewater by submerged membrane bioreactor: In vitro bioassays for the assessment of stress response elicited by raw and reclaimed wastewater. *Journal of Environmental Management*, 160:184–192. DOI 10.1016/j.jenvman.2015.06.008.

Galiano, F. (2013). *Preparation and characterisation of polymerisable bicontious microemulsion membranes for water treatment application. ITM at UNICAL, Italy.* Phd thesis.

Galiano, F., Figoli, A., Deowan, S. A., Johnson, D., Altinkaya, S. A., Veltri, L., De Luca, G., Mancuso, R., Hilal, N., Gabriele, B., and Hoinkis, J. (2015). A step forward to a more efficient wastewater treatment by membrane surface modification via polymerizable bicontinuous microemulsion. *Journal of Membrane Science*, 482:103–114. DOI 10.1016/j.memsci.2015.02.019.

Gan, L., Li, T., Chew, C. H., and Teo, W. K. (1995). Microporous polymeric materials from polymerization of zwitterionic microemulsions. *Langmuir*, 11:3316–3320. DOI 10.1021/la00009a009.

Gan, L.-M. and Chew, C.-H. (1997). Microporous polymer composites from microemulsion polymerization. *Colloids and Surfaces A: Physicochemical and Engineering Aspects*, 123:681–693. DOI 10.1016/S0927–7757(96)03812–5.

Gan, L. M., Chow, P. Y., Liu, Z., Han, M., and Quek, C. H. (2005). The zwitterion effect in proton exchange membranes as synthesised by polymerisation of bicontinuous microemulsions. *The Royal Society of Chemistry*, (35):4459–4461. DOI 10.1039/b508035e.

Gao, B.-Y., Yue, Q.-Y., Wang, Y., and Zhou, W.-Z. (2007). Color removal from dye-containing wastewater by magnesium chloride. *Journal of Environmental Management*, 82(2):167–172. http://dx.doi.org/10.1016/j.jenvman.2005.

Gholami, M., Nasseri, S., Mesdaghinia, A., Vaezi, F., Mahvi, A., and Naddaffi, K. (2001). Dye Removal from Effluents of Textile Industries by ISO9888 Method and Mebrane Technology. *Iranian J. Publ. Health*, 30(1-2):73–80.

Gloeckner, P. (2008). *Radiation Curing, Coatings and Printing Inks, Technical Basics, Applications and Trouble Shooting*. Vincentz, Hannover, Germany. ISBN 978-3-86630-907-4.

Gregan, F., Oremusova, J., Remko, M., Gregan, J., and Mlynarciki, D. (1998). Stereoisomeric effect on antimicrobial activity of a series of quaternary ammonium salts. *Elsevier*, 53:41–48. DOI 10.1016/S0014–827X(97)00003–7.

Grelot, A., Grelier, P., Tazi-Pain, A., Lesjean, B., Brüss, U., and Grasmick, A. (2010). Performances and fouling control of a flat sheet membrane in a MBR pilot-plant. *Water Science & Technology*, 61(9):2185–2192. DOI 10.2166/wst.2010.127.

Groenenboom, C., Hageman, H. J., Overeem, T., and Weber, A. J. M. (1982). Photoinitiators and photoinitiation, 3. Comparison of the photodecompositions of a-methoxy- and a,a-dimethoxydeoxybenzoin in 1,1-diphenylethylene as model substrate. *Macromolecular Chemistry and Physics*, pages 281–292. DOI 10.1002/macp.1982.021830202.

H. Fischer R. Baer, R. H. I. V. M. W. (1990). 2,2-Dimethoxy-2-phenylacetophenone: photochemistry and free radical photofragmentation. *Journal Chemical Society*, pages 787–798.

Hai, F., Yamamoto, K., and Lee, C.-H. (2013). *Membrane Biological Reactors: Theory, Modeling, Design, Management and Applications to Wastewater Reuse*. IWA Publishing. ISBN 9781780401331, 1st edition.

Hartley, G. H. and Guillet, J. E. (1968). Photochemistry of Ketone Polymers. II. Studies of Model Compounds. *Macromolecules*, I(5):413–417. DOI 10.1021/ma60005a009.

Herold, D. (2011). Energy Efficient MBR Design: Rabigh Refinery, Saudi Arabia. http://www.sawea.org/pdf/Dirk_Herold.pdf (accessed September 15, 2016). In *Proceedings of the Water Arabia Conference*, Manama, Bahrain. Koch Membrane Systems.

Hoinkis, J., Deowan, S., Schmidt, S., Galiano, F., Figoli, A., and Drioli, E. (2014). Membrane Bioreactor (MBR) Process Using Commercial and Novel Low-Fouling Membranes for Treatment of Textile Dye Wastewater. In Canziani, R., Fatone, F., and Katsou, E., editors, *2nd IWA Specialized International Conference, ecoSTP2014, Eco Technologies for Wastewater Treatment, Technical, Environmental & Economic Challenges*, pages 160–163, Verona, Italy. IWA Publishing. ISBN 9788869250026.

Hoinkis, J. and Panten, V. (2008). Wastewater recycling in laundries—From pilot to large-scale plant, Chemical Engineering and Processing. 47(7):1159–1164. DOI 10.1016/j.cep.2007.12.010.

Holding, M. (1995). Molecular Weight Characterisation of Synthetic Polymers. Technical report, RAPRA Technology Limited Shawbury: Rapra review reports, Report 83.

Holman, S. R. and Ohlinger, K. N. (2007). An Evaluation of Fouling Potential and Methods to Control Fouling in Microfiltration Membranes for Secondary Wastewater Effluent. In *Proceedings of the Water Environment Federation, WEFTEC*, pages 6417–6444. Water Environment Federation. DOI 10.2175/193864707787223907.

Huang, R.-R., Hoinkis, J., Hu, Q., and Koch, F. (2009). Treatment of dyeing wastewater by hollow fiber membrane biological reactor. *Desalination and Water Treatment*, 11(1-3):288–293. DOI 10.5004/dwt.2009.863.

Huang, X., Gui, P., and Qian, Y. (2001). Effect of sludge retention time on microbial behaviour in a submerged membrane bioreactor. *Process Biochemistry*, 36(10):1001–1006. DOI 10.1016/S0032–9592(01)00135–2.

Idris, A., Zain, N. M., and Yusof, N. M. (2007). Characterization and performance of asymmetric polyethersulfone (PES) ultrafiltration membranes with polyethylene glycol of different molecular weights as additives. *Desalination*, 207(1-3):324–339. DOI 10.1016/j.desal.2006.08.008.

Isik, M. and Sponza, D. T. (2008). Anaerobic/ aerobic treatment of a simulated textile wastewater. *Separation and Purification Technology*, 60:64–72.

Jaegerman, P., Lendzian, F., Rist, G., and Moebius, K. (1987). Time-resolved ESR and endor during the photolysis of w ,w -dimethoxy- w -phenyl-acetophenone. *Chemical Physics Letters*, 140(6):615–619. DOI 10.1016/0009–2614(87)80498–0.

Jegatheesan, V., Pramanik, B. K., Chen, J., Navaratna, D., Chang, C.-Y., and Shu, L. (2016). Treatment of textile wastewater with membrane bioreactor: A critical review. *Bioresource Technology*, 204:202–212. DOI 10.1016/j.biortech.2016.01.006.

Jent, F., Paul, H., and Fischer, H. (1988). Two-Photon processes in ketone photochemistry observed by time-resolved ESR spectroscopy. *Chemical Physics Letters*, 146(3,4):315–319. DOI 10.1016/0009–2614(88)87451–7.

Joon, S.-H. (2016). *Membrane Bioreactor Processes-Principles and Applications*. CRC Press, Cornwall, Boca Raton. ISBN 978-1-4822-5583-6, 1st edition.

Judd, S. and Judd, C. (2007). *The MBR Book: Principles and Applications in Water and Wastewater Treatment*. Elsevier, London, United Kingdom. DOI 10.1016/B978-0-08-096682-3.10009-5, 1st edition.

Judd, S. and Judd, C. (2011). *The MBR Book (Second Edition) Principles and Applications of Membrane Bioreactors for Water and Wastewater Treatment*. Elsevier, London, United Kingdom. DOI 10.1016/B978-0-08-096682- 3.10007-1, 2nd edition.

Kaeselev, B., Kingshott, P., and Jonsson, G. (2002). Influence of the surface structure on the filtration performance of UV-modified PES membrane. *Desalination*, 146:265–271. DOI 10.1016/S0011–9164(02)00485–X.

Kant, R. (2012). Textile dyeing industry an environmental hazard. *Natural Science*, 4(1):22–26. DOI 10.4236/ns.2012.41004.

Khor, S. L., Sun, D. D., Hay, C. T., and Leckie, J. O. (2006). Comparison of Submerged MBR in different SRT conditions. *Water Practice and Technology*, 1(3):DOI 10.2166/wpt.2006.056.

Kim, K. J. and Fane, A. G. (1988). The performance of ultrafiltration membranes pretreated by polymers. In *International Membrane Technology Conference '88*, pages 229–249. DOI 10.1016/0011–9164(88)85057–4.

Kim, T. H., Park, C., Jang, J., and Kim, S. (2004). Comparison of disperse and reactive dye removals by chemical coagulation and Fenton oxidation. *Journal of Hazardous Materials*, 112(1-2):95–103. DOI http://dx.doi.org/10.1016/j.jhazmat.20.

Kneissl, M. and Rass, J. (2015). *III-Nitride Ultraviolet Emitters: Technology and Applications*. Springer, Berlin, Germany. DOI 10.1007/978-3-319-24100-5.

Koch-Membrane (2010). Membrane Classification. http://www.kochmembrane.com (accessed March 05, 2014).

Kochkodan, V., Johnson, D. J., and Hilal, N. (2014). Polymeric membranes : Surface modification for minimizing (bio) colloidal fouling. pages 116–140. DOI 10.1016/j.cis.2013.05.005.

Koleske, J. (2002). Radiation curing of coatings. In *ASTM International*, pages 35–48. ISBN 9780803120952.

Konkin, A., Roth, H.-K., Schroedner, M., Nazmutdinova, G., Aganov, A., Ida, T., and Garipov, R. (2003). Time-resolved EPR study of radicals from 2,2-dimethoxy-2-phenylacetophenone in ethylene glycol after flash photolysis. *Chemical Physics*, 287(3):377–389. DOI 10.1016/S0301–0104(02)01025–X.

Konsowa, A. H., Eloffy, M. G., and El-Taweel, Y. A. (2013). Treatment of dyeing wastewater using submerged membrane bioreactor. *Desalination and Water Treatment*, 51(4-6):37–41. DOI 10.1080/19443994.2012.699361.

Körbahti, B. K. and Tanyolac, A. (2009). Continuous electrochemical treatment of simulated industrial textile wastewater from industrial components in a tubular reactor. *Journal of Hazardous Materials*, 170:771–778.

Koreba, W. (2010). Aufbau und Inbetriebnahme eines Labor-Membranbioreaktors mit automatischer Datenerfassung und Steuerung, Master thesis, Sensor systems Technology, Karlsruhe University of Applied Science.

Kritikos, D., Xekoukoulotakis, N., Psillakis, E., and Mantzavinos, D. (2007). Photocatalytic degradation of reactive black 5 in aqueous solutions: Effect of operating conditions and coupling with ultrasound irradiation. 41(10):2236–2246. DOI 10.1016/j.watres.2007.01.048.

Leung, R. and Shah, D. O. (1987). Solubilization and phase equilibria of water-in-oil microemulsions. *Journal of Colloid and Interface Science*, 120(2):330–344. DOI 10.1016/0021–9797(87)90361–4.

Li, N. N., Fane, A. G., Ho, W. S. W., and Matsuura, T. (2011). *Advanced Membrane Technology and Applications*. John Wiley & Sons, New Jersey. ISBN 978-1-118-21154-0.

Li, T. D., Gan, L. M., Chew, C. H., Teo, W. K., and Gan, L. H. (1997). Hollow-fiber membranes coated with polymerizable bicontinuous microemulsions. *Journal of Membrane Science*, 133(2):177–187. DOI 10.1016/S0376–7388(97)00102–6.

Liu, C., Caothien, S., Hayes, J., Caohuy, T., and Otoyo, T. (2001). Membrane Cleaning: from Art to Science. http://www.pall.in/pdfs/Water- Treatment/mtc-paper.pdf (accessed August 25, 2016). In *Proceedings of Membrane Technology Conference*, Antonio, Texas.

Martin (2015). Martin-Membrane. http://www.martinmembrane. de/fileadmin/redakteur/downloads neu/MMS-Module-EN.pdf (accessed June 16, 2016).

Meinsberg (2014a). Conductivity sensor LTC 0.35/23 Manual Sensortechnik. http://www.meinsbergerelektroden. de/en/picture.php?pic=LTC0K35_23SMEK&alt=LTC 0,35/23 SMEK (accessed February 14, 2015).

Meinsberg (2014b). Oxygen sensor MF 39 Manual Sensortechnik. http://www.meinsberger-elektroden.de/en/picture.php?pic=EGA143SMEKX& alt=EGA 143 SMEK-X (accessed February 16, 2015).

Meinsberg (2014c). Oxygen Transmitter MV 3030 Manual Sensortechnik. http://www.meinsberger-elektroden.de/en/picture.php?pic=EGA143SMEKX&

alt=EGA 143 SMEK-X (accessed February 16, 2015). Technical report, Meinsberg GmbH, Waldheim, Germany. Technical report, Meinsberg GmbH, Waldheim, Germany.

Meinsberg (2014d). pH sensor EGA 143/PT1000 Manual Sensortechnik. http://www.meinsberger-elektroden.de/en/picture.php?pic=EGA143SMEKX& alt=EGA 143 SMEK-X (accessed February 16, 2015).

Merlin, A. and Fouassier, J. P. (1980). Mechanism of the methyl methacrylate polymerization photo-induced by benzoin derivatives. *Macromolecular Chemistry and Physics*, 181:1307–1319. DOI 10.1002/macp.1980.021810611.

Microdyn-Nadir-GmbH (2014). Submerged MBR Modules. http://www.microdynnadir. com/en/Products/BIO-CEL%C2%AE// (accessed March 14, 2015).

Mishra, G. and Tripathy, M. (1993). A Critical Review of the Treatments for De-colourization of Textile Effluent. *Colourage*, 40(10):35–38.

Moran, C., Hall, M. E., and Howell, R. (1997). Effects of sewage treatment on textile effluent. *Journal of the Society of Dyers and Colourists*, 113(10):272–274. DOI 10.1111/j.1478–4408.1997.tb01847.x.

Nady, N., Franssen, M., Zuilhof, H., Eldin, M., Boom, R., and Schroën, K. (2011). Modification methods for poly (arylsulfone) membranes : A mini-review focusing on surface modification. *Desalination*, 275:1–9. DOI 10.1016/j.desal.2011.03.010.

Pagga, U. and Brown, D. (1986). The degradation of dyestuffs: Part II Behaviour of dyestuffs in aerobic biodegradation tests. *Chemosphere*, 15(4):479–491. DOI 10.1016/0045–6535(86)90542–4.

Peinado, C., Bosch, P., Martin, V., and Corrales, T. (2006). Photoinitiated Polymerization in Bicontinious Microemulsions: Fluorescence Monitoring. *Journal of Polymer Science Part A Polymer Chemistry*, 44(18):5291–5303. DOI 10.1002/pola.21649.

PR Newswire (engl.) (2015). Membrane Bioreactor Market and MBR Systems. http://www.wallstreet-online.de/nachricht/7309652-membrane-bioreactormarket-and-mbr-systems-15-cagr-forecast-to-2018-2019-new-research-reports (accessed August 26,2016).

Rahimpour, A. (2011). UV photo-grafting of hydrophilic monomers onto the surface of nano-porous PES membranes for improving surface properties. *Desalination*, 265:93–101. DOI 10.1016/j.desal.2010.07.037.

Rondon, H., El-Cheikh, W., Boluarte, I. A. R., Chang, C.-Y., Bagshaw, S., Farago, L., Jegatheesan, V., and Shu, L. (2015). Application of enhanced membrane bioreactor (eMBR) to treat dye wastewater. *Bioresource Technology*, 183:78–85. DOI 10.1016/j.biortech.2015.01.110.

Saddoud, A., Ellouze, M., Dhouib, A., and Sayadi, S. (2007). Anaerobic membrane bioreactor treatment of domestic wastewater in Tunisia. *Desalination*, 207(1-3):205–215. DOI 10.1016/j.desal.2006.08.005.

Savitsky, A. N., Galander, M., and Moebius, K. (2001). W-band time-resolved electron paramagnetic resonance spectroscopy on transient organic radicals in solution. *Chemical Physics Letters*, 340:458–466. DOI 10.1016/S0009–2614(01)00438–9.

Schoeberl, P., Brik, M., Bertoni, M., Braun, R., and Fuchs, W. (2005). Optimization of operational parameters for a submerged membrane bioreactor treating dyehouse wastewater. *Separation and Purification Technology*, 44(1):61–68. DOI 10.1016/j.seppur.2004.12.004.

Schoeberl, P., Brik, M., Braun, R., and Fuchs, W. (2004). Treatment and recycling of textile wastewater - Case study and development of a recycling concept. *Desalination*, 171(2):173–183. DOI 10.1016/j.desal.2004.02.105.

Shieh, J. J., Chung, T. S., Wang, R., Srinivasan, M. P., and Paul, D. R. (2001). Gas separation performance of poly(4-vinylpyridine)/polyetherimide composite hollow fibers. *Journal of Membrane Science*, 182(1-2):111–123. DOI 10.1016/S0376–7388(00)00560–3.

Slomkowski, S., Alemán, J. V., Gilbert, R. G., Hess, M., Horie, K., Jones, R. G., Kubisa, P., Meisel, I., Mormann, W., Penczek, S., and Stepto, R. F. T. (2011). Terminology of polymers and polymerization processes in dispersed systems (IUPAC Recommendations 2011). *Pure Appl. Chem*, 83(12):2229–2259. DOI 10.1351/PAC–REC–10–06–03.

SpaceEnvironmentTechnologies (2014). ISO 21348 Definitions of Solar Irradiance Spectral Categories. http://www.spacewx.com/pdf/SET_21348_2004.pdf/ (accessed December 24, 2015).

Stephenson, T., Judd, S., Jefferson, B., and Brindle, K. (2000). Membrane Bioreactors for Wastewater Treatment. ISBN 9781900222075. *Journal of Membrane Science*.

Sun, F., Sun, B., Hu, J., He, Y., and Wu, W. (2015). Organics and nitrogen removal from textile auxiliaries wastewater with A2O-MBR in a pilot-scale. *Journal of Hazardous Materials*, 286:416–424. DOI 10.1016/j.jhazmat.2015.01.031.

Trozzolo, A. M. and Winslow, F. H. (1968). A Mechanism for the Oxidative Photodegradation of Polyethylene. *Macromolecules*, 1(1):98–100. DOI 10.1021/ma60001a019.

UN-Water (2006). Coping with water scarcity. http://www.unwater.org/downloads/waterscarcity.pdf (accessed August 19, 2014). Technical report, UN-WATER.

van Haandel, A. and van der Lubbe, J. (2012). *Handbook of Biological Wastewater Treatment*. London, United Kingdom. ISBN 9781780407753, 2 edition.

Venceslau, M. C., Stephenson, T., and Judd, S. J. (1994). Characterisation of textile wastewaters # a review. *Environmental Technology*, 15(10):917–929. DOI 10.1080/09593339409385500.

Vesley, G. (1986). Journal of Radiation Curing. *Journal of Radiation Curing*, 13(1):1–4. ISBN 0361–6428.

Vu, T., Schmidt, S., Deowan, S. A., Hoinkis, J., Figoli, A., and Galiano, F. (2015). Membrane bioreactor and promising application for textile industry in Vietnam. In *ScienceDirect*, pages 419–424. DOI 10.1016/j.procir.2016.01.083, Binh Duong New City, Vietnam.

Wang, L. S., Chow, P. Y., Tan, D. C. W., and Yang, Y. (2004). Nanostructured and Transparent Polymer Membranes with Thermosensitivity for Wound Dressing and Cell Grafting. *Advanced Materials*, 16:1790–1794. DOI 10.1002/adma.200400602.

Weiss, P. (1966). Photo induced Polymerization. *Pure and Applied Chemistry*, 15(3-4):587–600. DOI 10.1351/pac196715030587.

Wicks, Z., Jones, F., Pappas, S. P., and Wicks, D. A. (2007). *Organic Coatings: Science and Technology*. John Wiley & Sons, New Jersey, United States. ISBN 978-0-471-69806-7, 3rd edition.

Willmott, N., Guthrie, J., and Nelson, G. (1998). The biotechnology approach to colour removal from textile effluent. *JSDC*, 114:38–41.

Xing, C.-H., Tardieu, E., Qian, Y., and Wen, X.-H. (2000). Ultrafiltration membrane bioreactor for urban wastewater reclamation. *Journal of Membrane Science*, 177(1-2):73–82. DOI 10.1016/S0376–7388(00)00452–X.

Yan, F. and Texter, J. (2006). Capturing nanoscopic length scales and structures by polymerization in microemulsions. *The Royal Society of Chemistry*, 14(2):109–118. DOI 10.1039/b513914g.

Yigit, N. O., Uzal, N., Koseoglu, H., Harman, I., Yukseler, H., Yetis, U., Civelekoglu, G., and Kitis, M. (2009). Treatment of a denim producing textile industry wastewater using pilot-scale membrane bioreactor. *Desalination*, 240(1-3):143–150. DOI 10.1016/j.desal.2007.11.071.

You, S. J. and Teng, J. Y. (2009). Anaerobic decolorization bacteria for the treatment of azo dye in a sequential anaerobic and aerobic membrane bioreactor. *Journal of the Taiwan Institute of Chemical Engineers*, 40(5):500–504. DOI 10.1016/j.jtice.2009.01.007.

Yu, H.-Y., Hu, M.-X., Xu, Z.-K., Wang, J.-L., and Wang, S.-Y. (2005a). Surface modification of polypropylene microporous membranes to improve their antifouling property in MBR: NH3 plasma treatment. *Separation and Purification Technology*, 45(1):8–15. DOI 10.1016/j.seppur.2005.01.012.

Yu, H. Y., Liu, L. Q., Tang, Z. Q., Yan, M. G., Gu, J. S., and Wei, X. W. (2008). Mitigated membrane fouling in an SMBR by surface modification. *Journal of Membrane Science*, 310(1-2):409–417. DOI 10.1016/j.memsci.2007.11.017.

Yu, H. Y., Xie, Y. J., Hu, M. X., Wang, J. L., Wang, S. Y., and Xu, Z. K. (2005b). Surface modification of polypropylene microporous membrane to improve its antifouling property in MBR: CO2 plasma treatment. *Journal of Membrane Science*, 254(1-2):219–227. DOI 10.1016/j.memsci.2005.01.010.

Yu, H. Y., Xu, Z. K., Lei, H., Hu, M. X., and Yang, Q. (2007). Photoinduced graft polymerization of acrylamide on polypropylene microporous membranes for the improvement of antifouling characteristics in a submerged membrane-bioreactor. *Separation and Purification Technology*, 53(1):119–125. DOI 10.1016/j.seppur.2006.07.002.

Yun, M. A., Yeon, K. M., Park, J. S., Lee, C. H., Chun, J., and Lim, D. J. (2006). Characterization of biofilm structure and its effect on membrane permeability in MBR for dye wastewater treatment. *Water Research*, 40(1):45–52. DOI 10.1016/j.watres.2005.10.035.

Yusuff, R. and Sonibare, J. A. (2004). Characterization of textile industries effluents in Kaduna, Nigeria and pollutin implications. http://www.academia.edu/912996/Characterization_of_textile_industries_effluents_in_Kaduna_Nigeria_and_pollution_implications (accessed September 26, 2016). *Global Nest: Int. J6.3*, pages 212–221.

Zheng, X. and Liu, J. (2006). Dyeing and printing wastewater treatment using a membrane bioreactor with a gravity drain. *Desalination*, 190(1-3):277–286. DOI 10.1016/j.desal.2005.09.008.

Z.W. Wicks F.N. Jones, S. P. P. (1994). *Organic Coatings: Science and Technology, Volume II: Applications, Properties, and Performance*. John Wiley & Sons, New Jersey, United States. DOI 10.1002/recl.19951140111, 2nd edition.

A Affix

A.1 Maps and drawings
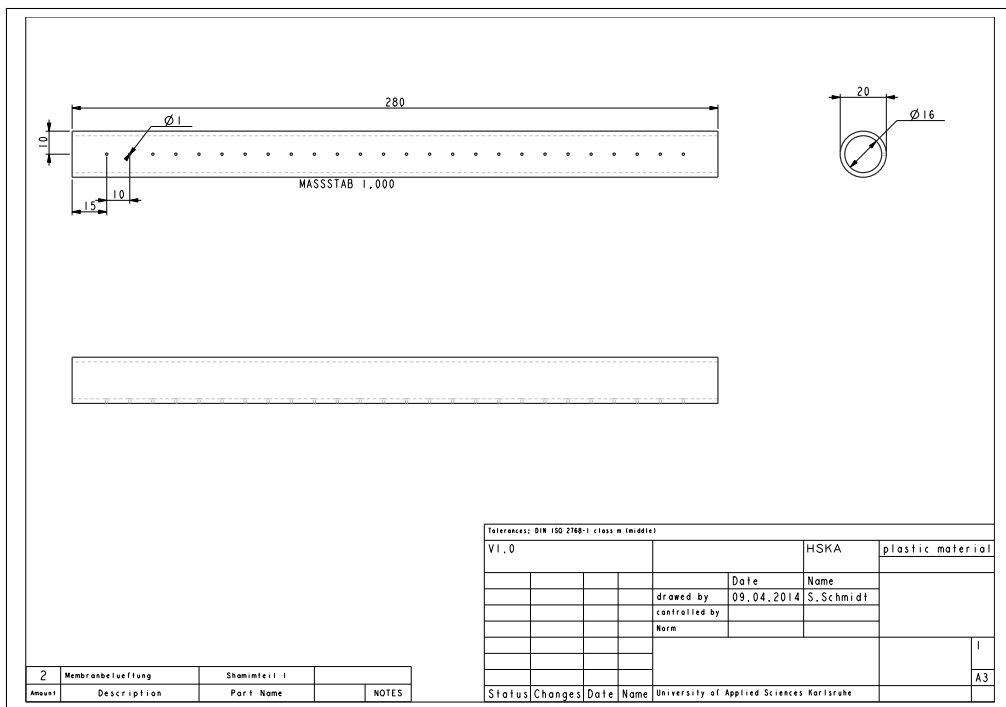
Figure A.1. Membrane aeration
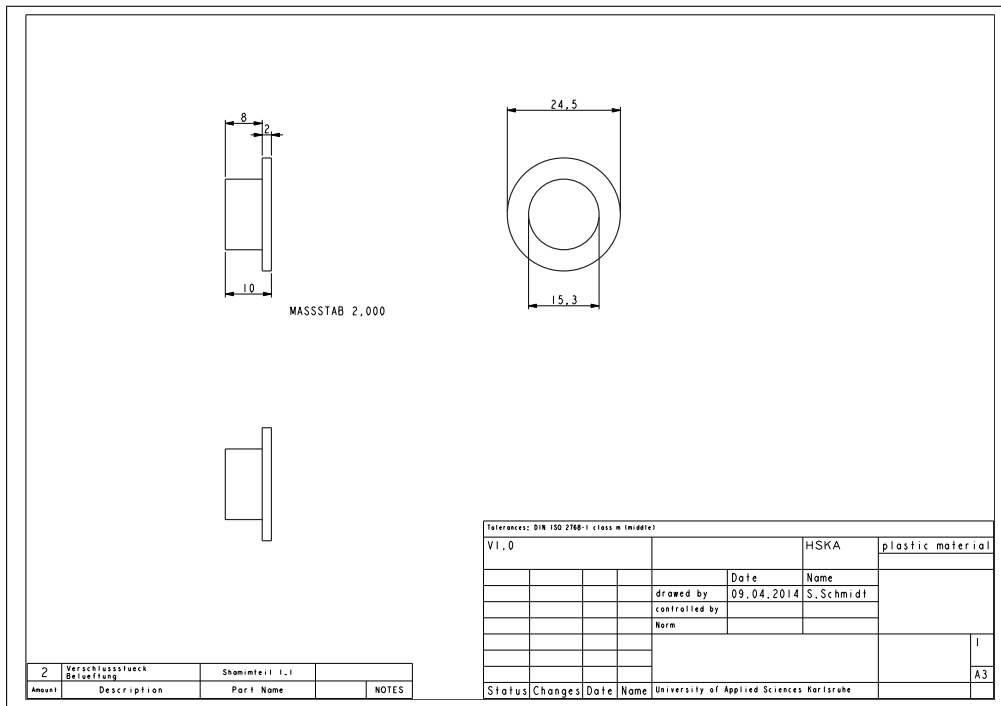
Figure A.2. Membrane aeration end piece
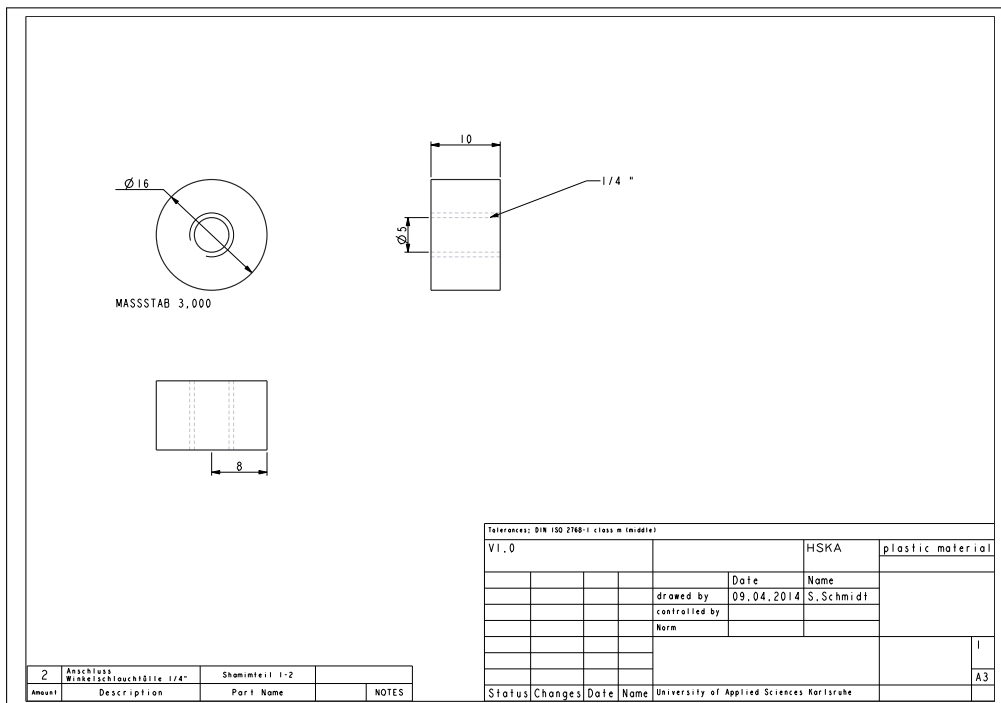
Figure A.3. Connection membrane aeration
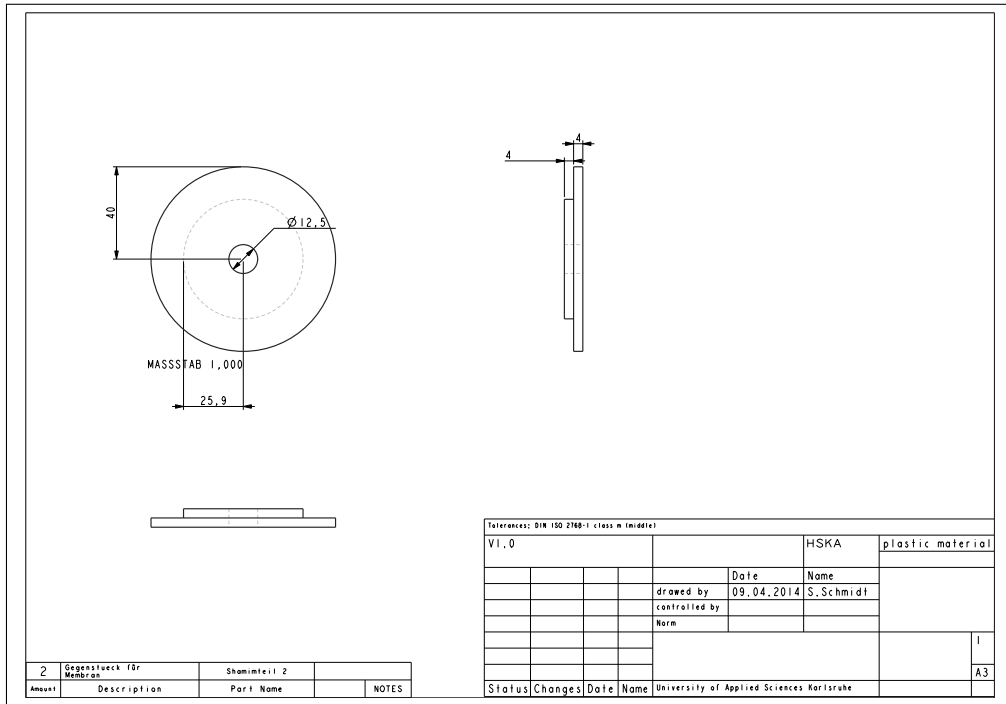
Figure A.4. Membrane holder
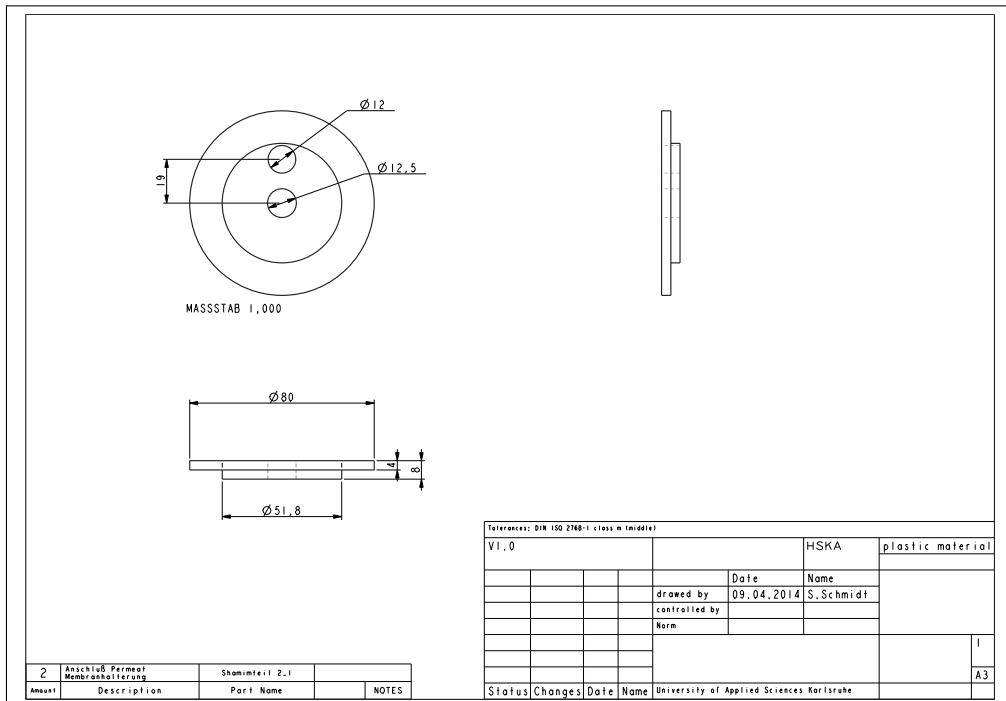
Figure A.5. Connection permeate line
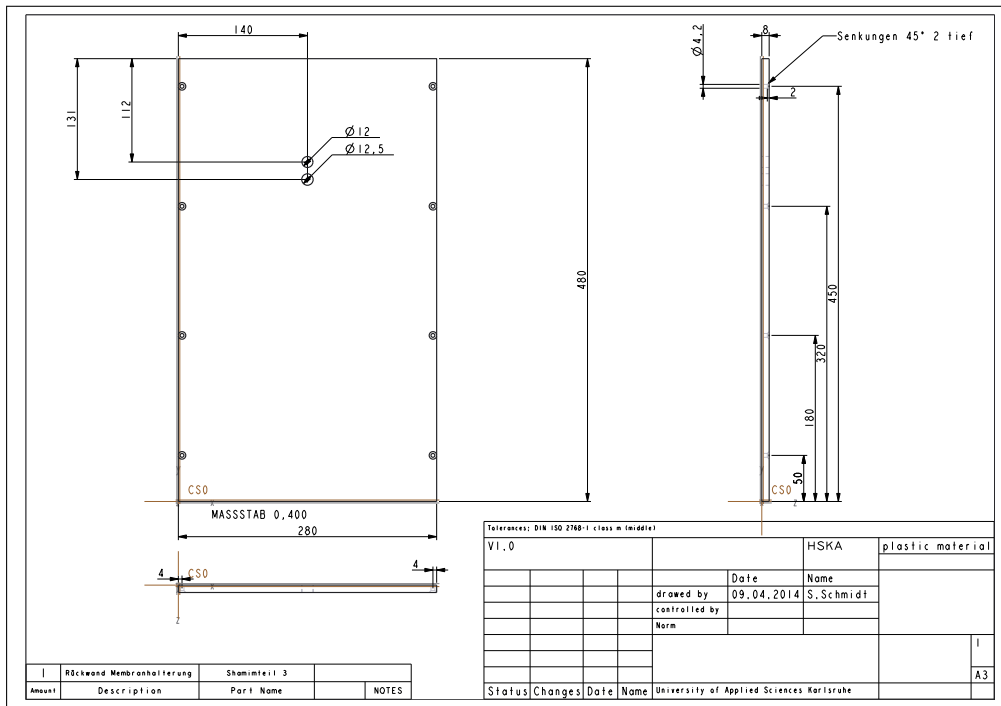
Figure A.6. Backside membrane holder
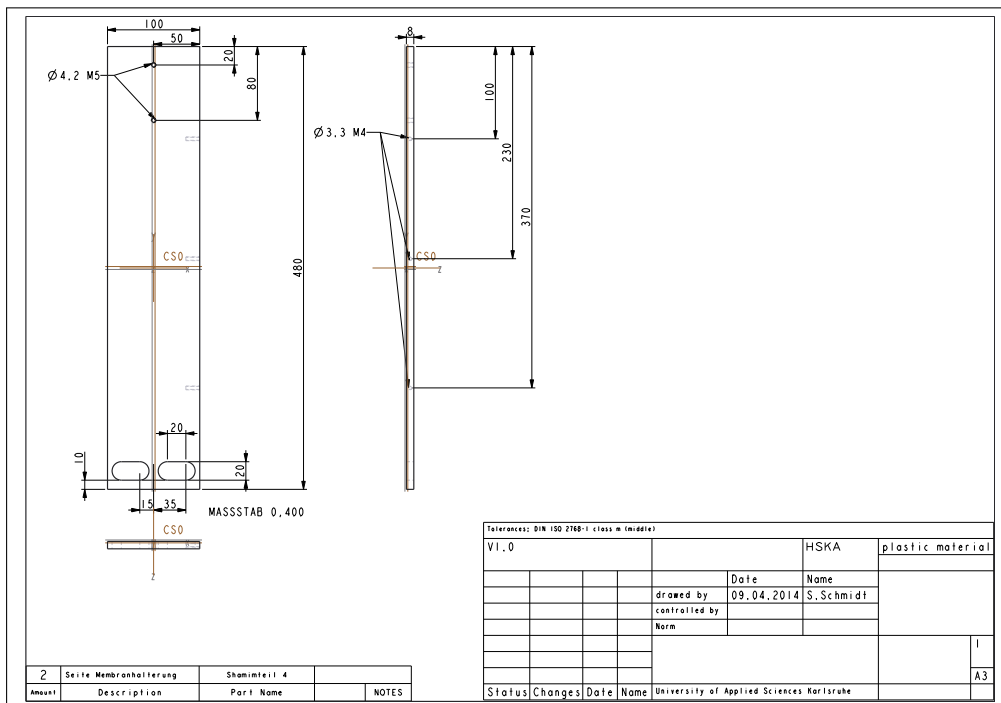
Figure A.7. side piece membrane holder
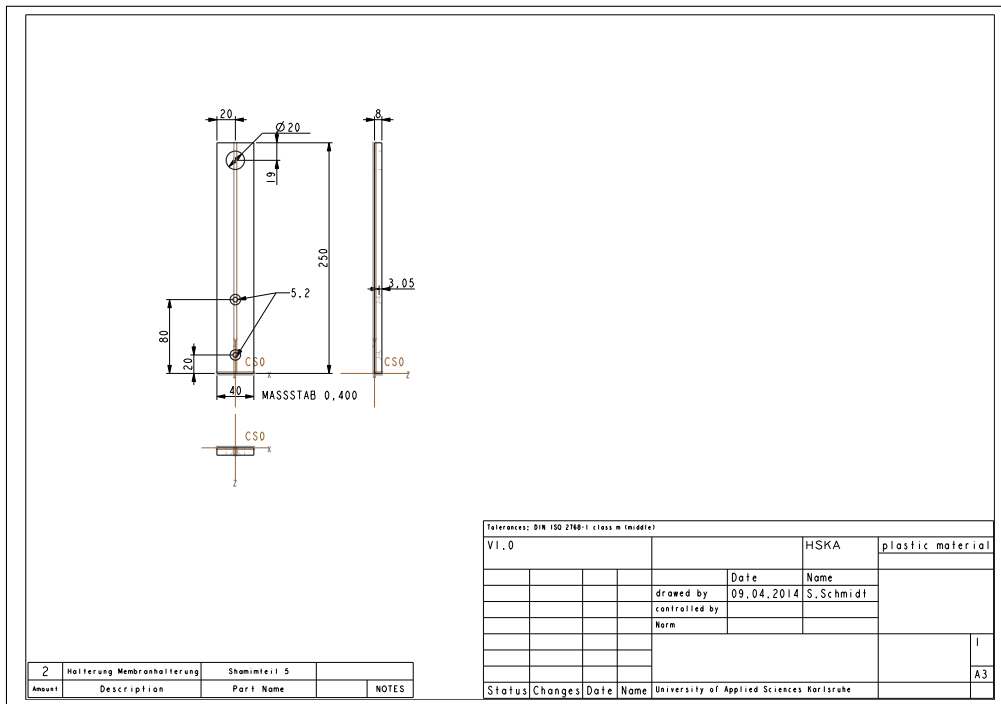
Figure A.8. Connection membrane holder
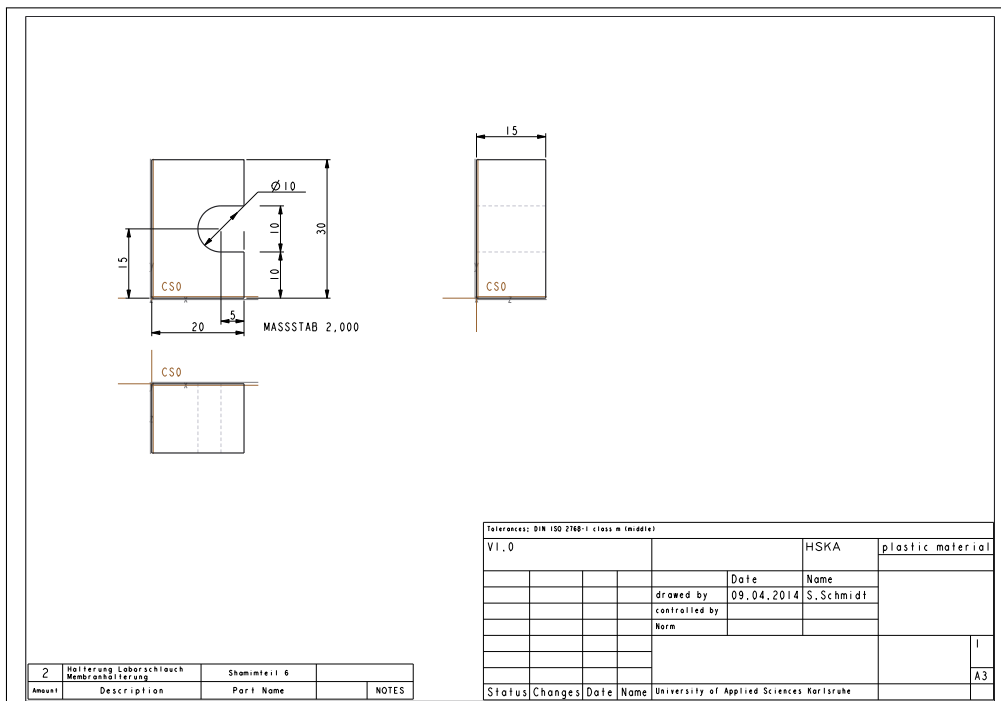
Figure A.9. Tube holder
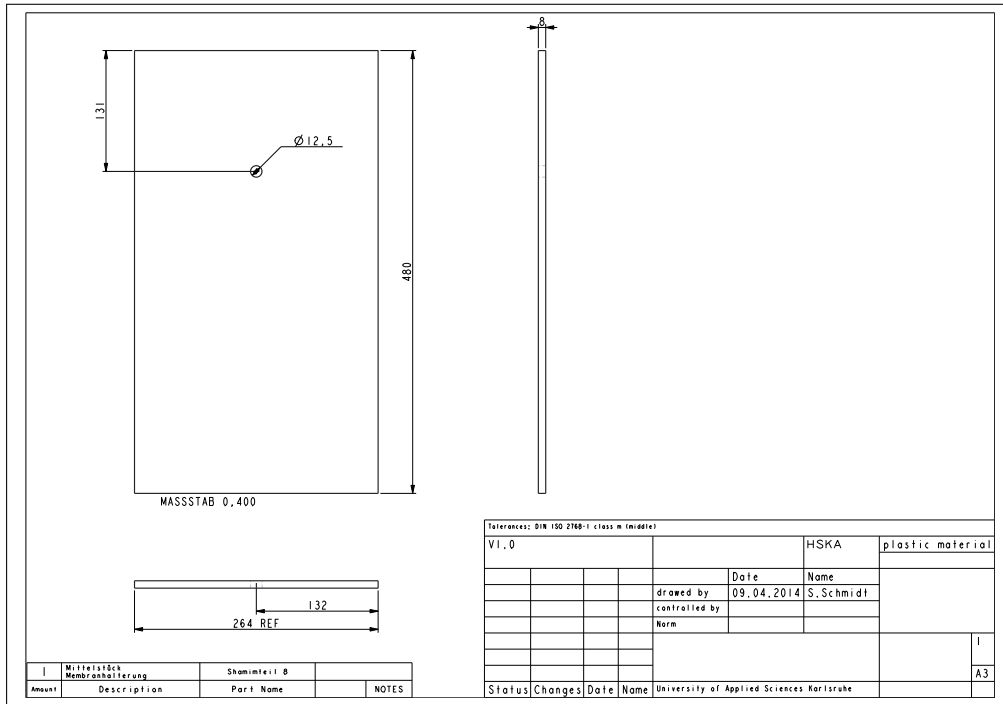
Figure A.10. Center wall

Figure A.11. Backside wall

Figure A.12. Sealing center screw

Figure A.13. Center screw

Figure A.14. M12 bolt

Figure A.15. Membrane sealing

Figure A.16. Reactor top

Figure A.17. Diffusor

A.2 TOC-reports

Figure A.18. TOC-report for checkup of theoreticl values p.1

TOC-Control L Report

Anal.: TN

Nr.	Fläche	Konz.	Inj. Vol.	At. Verd.	Ausg..	Kal.Kurve	Datum / Uhrzeit
1	1,526	1,784mg/L	50uL	1,000		Kall_TN_NEU.2013_10_28_09_15_34.cal	17.06.2014 11:51:36

MW Fläche   1,526
MW Konz.   1,784mg/L

Probe

Probenname: standard check TN
ProbenID: Unbenannt
Original: TOC+TN_Messung.met
Status   Fertig
Testergebnis

Typ	Anal.	Manuelle Verduennung	Ergebnis
Unbekannt	NPOC/TN	1,000	NPOC:0,9146mg/L TN:5,756mg/L

1. Det.

Anal.: NPOC

Nr.	Fläche	Konz.	Inj. Vol.	At. Verd.	Ausg..	Kal.Kurve	Datum / Uhrzeit
1	3,046	0,9146mg/L	50uL	1,000		Kall_TOC_100_11_12_2013.2013_12_11_09_16_05.cal	17.06.2014 12:11:33

MW Fläche   3,046
MW Konz.   0,9146mg/L

Anal.: TN

Nr.	Fläche	Konz.	Inj. Vol.	At. Verd.	Ausg..	Kal.Kurve	Datum / Uhrzeit
1	14,66	5,756mg/L	50uL	1,000		Kall_TN_NEU.2013_10_28_09_15_34.cal	17.06.2014 12:11:33

MW Fläche   14,66
MW Konz.   5,756mg/L

Probe

Probenname: standard tic
ProbenID: Unbenannt
Original: IC_Messung.met
Status   Fertig
Testergebnis

Figure A.19. TOC-report for checkup of theoreticl values p.2

TOC-Control L Report

System Administrator
PBM_TOC-L_Vu.tlx

Typ	Anal.	Manuelle Verduennung	Ergebnis
Unbekannt	IC	1,000	IC:55,95mg/L

1. Det.

Anal.: IC

Nr.	Fläche	Konz.	Inj. Vol.	At. Verd.	Ausg..	Kal.Kurve	Datum / Uhrzeit
1	1681	55,95mg/L	270uL	1,000		Kall_TIC_100.2013_09_10_08_54_33.cal	17.06.2014 12:24:32

MW Fläche   1681
MW Konz.   55,95mg/L

Probe

Probenname: red toc and tn
ProbenID: Unbenannt
Original: TOC+TN_Messung.met
Status   Fertig
Testergebnis

Typ	Anal.	Manuelle Verduennung	Ergebnis
Unbekannt	NPOC/TN	1,000	NPOC:18,73mg/L TN:2,189mg/L

1. Det.

Anal.: NPOC

Nr.	Fläche	Konz.	Inj. Vol.	At. Verd.	Ausg..	Kal.Kurve	Datum / Uhrzeit
1	84,64	18,73mg/L	50uL	1,000		Kall_TOC_100_11_12_2013.2013_12_11_09_16_05.cal	17.06.2014 12:36:08

MW Fläche   84,64
MW Konz.   18,73mg/L

Anal.: TN

Nr.	Fläche	Konz.	Inj. Vol.	At. Verd.	Ausg..	Kal.Kurve	Datum / Uhrzeit
1	2,864	2,189mg/L	50uL	1,000		Kall_TN_NEU.2013_10_28_09_15_34.cal	17.06.2014 12:36:08

MW Fläche   2,864
MW Konz.   2,189mg/L

Probe

Figure A.20. TOC-report for checkup of theoreticl values p.3

Figure A.21. TOC-report for checkup of theoreticl values p.4

TOC-Control L Report

Probe

Probenname:	blue tic
ProbenID:	Unbenannt
Original:	IC_Messung.met
Status	Fertig

Testergebnis

Typ	Anal.	Manuelle Verduennung	Ergebnis
Unbekannt	IC	1,000	IC:11,57mg/L

1. Det.

Anal.: IC

Nr.	Fläche	Konz.	Inj. Vol.	At. Verd.	Ausg.	Kal.Kurve	Datum / Uhrzeit
1	332,9	11,57mg/L	270uL	1,000		Kall_TIC_100.2013_09_10_08_54_33.cal	17.06.2014 14:40:07

MW Fläche	332,9
MW Konz.	11,57mg/L

Probe

Probenname:	albatex toc and tn
ProbenID:	Unbenannt
Original:	TOC+TN_Messung.met
Status	Fertig

Testergebnis

Typ	Anal.	Manuelle Verduennung	Ergebnis
Unbekannt	NPOC/TN	1,000	NPOC:15,50mg/L TN:1,323mg/L

1. Det.

Anal.: NPOC

Nr.	Fläche	Konz.	Inj. Vol.	At. Verd.	Ausg.	Kal.Kurve	Datum / Uhrzeit
1	69,85	15,50mg/L	50uL	1,000		Kall_TOC_100_11_12_2013.2013_12_11_09_16_05.cal	17.06.2014 15:02:15

MW Fläche	69,85
MW Konz.	15,50mg/L

Anal.: TN

Nr.	Fläche	Konz.	Inj. Vol.	At. Verd.	Ausg.	Kal.Kurve	Datum / Uhrzeit
1	0,000	1,323mg/L	50uL	1,000		Kall_TN_NEU.2013_10_28_09_15_34.cal	17.06.2014 15:02:15

Figure A.22. TOC-report for checkup of theoreticl values p.5

TOC-Control L Report

System Administrator
PBM_TOC-L_Vu.tlx

MW Fläche   0,000
MW Konz.   1,323mg/L.

Signal[mV]

Probe

Probenname: albatex tic
ProbenID: Unbenannt
Original: IC_Messung.met
Status   Fertig
Testergebnis

Typ	Anal.	Manuelle Verduennung	Ergebnis
Unbekannt	IC	1,000	IC:17,74mg/L

1. Det.

Anal.: IC

Nr.	Fläche	Konz.	Inj. Vol.	At. Verd.	Ausg..	Kal.Kurve	Datum / Uhrzeit
1	520,1	17,74mg/L	270uL	1,000		Kall_TIC_100.2013_09_10_08_54_33.cal	17.06.2014 15:09:09

MW Fläche   520,1
MW Konz.   17,74mg/L.

Signal[mV]

Probe

Probenname: glucose toc and tn
ProbenID: Unbenannt
Original: TOC+TN_Messung.met
Status   Fertig
Testergebnis

Typ	Anal.	Manuelle Verduennung	Ergebnis
Unbekannt	NPOC/TN	1,000	NPOC:266,7mg/L TN:1,323mg/L

1. Det.

Anal.: NPOC

Nr.	Fläche	Konz.	Inj. Vol.	At. Verd.	Ausg..	Kal.Kurve	Datum / Uhrzeit
1	1220	266,7mg/L	50uL	1,000		Kall_TOC_100_11_12_2013.2013_12_11_09_16_05.cal	17.06.2014 15:19:21

MW Fläche   1220
MW Konz.   266,7mg/L.

Signal[mV]

Anal.: TN

Figure A.23. TOC-report for checkup of theoreticl values p.6

Figure A.24. TOC-report for checkup of theoreticl values p.7

Figure A.25. TOC-report for checkup of theoreticl values p.8

TOC-Control L Report

Anal.: NPOC

Nr.	Fläche	Konz.	Inj. Vol.	At. Verd.	Ausg..	Kal.Kurve	Datum / Uhrzeit
1	6,068	1,575mg/L	50uL	1,000		Kall_TOC_100_11_12_2013.2013_12_11_09_16_05.cal	17.06.2014 15:59:34

MW Fläche   6,068
MW Konz.   1,575mg/L

Anal.: TN

Nr.	Fläche	Konz.	Inj. Vol.	At. Verd.	Ausg..	Kal.Kurve	Datum / Uhrzeit
1	147,9	46,05mg/L	50uL	1,000		Kall_TN_NEU.2013_10_28_09_15_34.cal	17.06.2014 15:59:34

MW Fläche   147,9
MW Konz.   46,05mg/L

Probe

Probenname: nitrat
ProbenID: Unbenannt
Original: TOC+TN_Messung.met
Status   Fertig
Testergebnis

Typ	Anal.	Manuelle Verduennung	Ergebnis
Unbekannt	NPOC/TN	1,000	NPOC:1,032mg/L TN:55,77mg/L

1. Det.

Anal.: NPOC

Nr.	Fläche	Konz.	Inj. Vol.	At. Verd.	Ausg..	Kal.Kurve	Datum / Uhrzeit
1	3,583	1,032mg/L	50uL	1,000		Kall_TOC_100_11_12_2013.2013_12_11_09_16_05.cal	17.06.2014 16:11:42

MW Fläche   3,583
MW Konz.   1,032mg/L

Anal.: TN

Nr.	Fläche	Konz.	Inj. Vol.	At. Verd.	Ausg..	Kal.Kurve	Datum / Uhrzeit
1	149,3	55,77mg/L	50uL	1,000		Kall_TN_100_6_12_2013.2013_12_06_08_34_29.cal	17.06.2014 16:11:42

Figure A.26. TOC-report for checkup of theoreticl values p.9

TOC-Control L Report

System Administrator
PBM_TOC-L_Vu.tlx

| MW Fläche | 149,3 |
| MW Konz. | 55,77mg/L |

Signal[mV]

Probe

Probenname:	Unbenannt
ProbenID:	Unbenannt
Original:	TOC+TN_Messung.met
Status	Fertig
Testergebnis	

Typ	Anal.	Manuelle Verduennung	Ergebnis
Unbekannt	NPOC/TN	1,000	NPOC:85,30mg/L TN:2,994mg/L

1. Det.

Anal.: NPOC

Nr.	Fläche	Konz.	Inj. Vol.	At. Verd.	Ausg..	Kal.Kurve	Datum / Uhrzeit
1	389,5	85,30mg/L	50uL	1,000		Kall_TOC_100_11_12_2013.2013_12_11_09_16_05.cal	17.06.2014 16:25:26

| MW Fläche | 389,5 |
| MW Konz. | 85,30mg/L |

Signal[mV]

Anal.: TN

Nr.	Fläche	Konz.	Inj. Vol.	At. Verd.	Ausg..	Kal.Kurve	Datum / Uhrzeit
1	5,525	2,994mg/L	50uL	1,000		Kall_TN_NEU.2013_10_28_09_15_34.cal	17.06.2014 16:25:26

| MW Fläche | 5,525 |
| MW Konz. | 2,994mg/L |

Signal[mV]

Probe

Probenname:	urea 50 mg
ProbenID:	Unbenannt
Original:	TOC+TN_Messung.met
Status	Fertig
Testergebnis	

Typ	Anal.	Manuelle Verduennung	Ergebnis
Unbekannt	NPOC/TN	1,000	NPOC:28,18mg/L TN:84,64mg/L

1. Det.

Anal.: NPOC

Figure A.27. TOC-report for checkup of theoreticl values p.10

A.3 Data sheets

Material Safety Data Sheet
acc. to OSHA and ANSI

Printing date 05/21/2009   Reviewed on 05/21/2009

1 Identification of substance:

Product details:

Product name: *Humic acid*

Stock number: 41747

Manufacturer/Supplier:
Alfa Aesar, A Johnson Matthey Company
Johnson Matthey Catalog Company, Inc.
30 Bond Street
Ward Hill, MA 01835-8099
Emergency Phone: (978) 521-6300
CHEMTREC: (800) 424-9300
Web Site: www.alfa.com

Information Department: Health, Safety and Environmental Department
Emergency information:
During normal hours the Health, Safety and Environmental Department. After normal hours call
Chemtrec at (800) 424-9300.

2 Composition/Data on components:

Chemical characterization:
Description: (CAS#)
Humic acid (CAS# 1415-93-6), 100%
Identification number(s):
EINECS Number: 215-809-6

3 Hazards identification

Hazard description: Not applicable
Information pertaining to particular dangers for man and environment Not applicable
Classification system
HMIS ratings (scale 0-4)
(Hazardous Materials Identification System)

HEALTH	1
FIRE	0
REACTIVITY	0

Health (acute effects) = 1
Flammability = 0
Reactivity = 0

GHS label elements Void

4 First aid measures

After inhalation
Supply fresh air. If required, provide artificial respiration. Keep patient warm.
Seek immediate medical advice.
After skin contact
Immediately wash with water and soap and rinse thoroughly.
Seek immediate medical advice.
After eye contact
Rinse opened eye for several minutes under running water. Then consult a doctor.
After swallowing Seek medical treatment.

5 Fire fighting measures

Suitable extinguishing agents
Carbon dioxide, extinguishing powder or water spray. Fight larger fires with water spray or
alcohol resistant foam.
Special hazards caused by the material, its products of combustion or resulting gases:
In case of fire, the following can be released:
Carbon monoxide and carbon dioxide
Protective equipment:
Wear self-contained respirator.
Wear fully protective impervious suit.

6 Accidental release measures

Person-related safety precautions:
Wear protective equipment. Keep unprotected persons away.
Ensure adequate ventilation
Measures for environmental protection:
Do not allow material to be released to the environment without proper governmental permits.
Measures for cleaning/collecting: Pick up mechanically.

USA

Figure A.28. MSDS humic acid p.1

Material Safety Data Sheet
acc. to OSHA and ANSI

Printing date 05/21/2009   *Reviewed on 05/21/2009*

Product name: Humic acid

(Contd. of page 1)

Additional information:
See Section 7 for information on safe handling
See Section 8 for information on personal protection equipment.
See Section 13 for disposal information.

7 Handling and storage

Handling
Information for safe handling:
Keep container tightly sealed.
Store in cool, dry place in tightly closed containers.
No special precautions are necessary if used correctly.
Information about protection against explosions and fires: *No special measures required.*

Storage
Requirements to be met by storerooms and receptacles: *No special requirements.*
Information about storage in one common storage facility: *Store away from oxidizing agents.*
Further information about storage conditions:
Keep container tightly sealed.
Store in cool, dry conditions in well sealed containers.

8 Exposure controls and personal protection

Additional information about design of technical systems:
Properly operating chemical fume hood designed for hazardous chemicals and having an average
face velocity of at least 100 feet per minute.

Components with limit values that require monitoring at the workplace: *Not required.*
Additional information: *No data*

Personal protective equipment
General protective and hygienic measures
The usual precautionary measures for handling chemicals should be followed.
Keep away from foodstuffs, beverages and feed.
Remove all soiled and contaminated clothing immediately.
Wash hands before breaks and at the end of work.
Breathing equipment: *Use suitable respirator when high concentrations are present.*
Protection of hands: *Impervious gloves*
Eye protection: *Safety glasses*
Body protection: *Protective work clothing.*

9 Physical and chemical properties:

General Information	
Form:	*Powder*
Color:	*Dark grey*
Odor:	*Not determined*

Change in condition	
Melting point/Melting range:	*Not determined*
Boiling point/Boiling range:	*Not determined*
Sublimation temperature / start:	*Not determined*

Flash point:	*Not applicable*
Flammability (solid, gaseous)	*Product is not flammable.*
Ignition temperature:	*Not determined*
Decomposition temperature:	*Not determined*
Danger of explosion:	*Product does not present an explosion hazard.*

Explosion limits:	
Lower:	*Not determined*
Upper:	*Not determined*

Vapor pressure:	*Not determined*
Density:	*Not determined*

Solubility in / Miscibility with	
Water:	*Slightly soluble*

— USA —

Figure A.29. MSDS humic acid p.2

Page 3/4

Material Safety Data Sheet
acc. to OSHA and ANSI

Printing date 05/21/2009   Reviewed on 05/21/2009

Product name: Humic acid

(Contd. of page 2)

10 Stability and reactivity

Thermal decomposition / conditions to be avoided:
Decomposition will not occur if used and stored according to specifications.
Materials to be avoided: Oxidizing agents
Dangerous reactions No dangerous reactions known
Dangerous products of decomposition: Carbon monoxide and carbon dioxide

11 Toxicological information

Acute toxicity:
Primary irritant effect:
on the skin: May cause irritation
on the eye: May cause irritation
Sensitization: No sensitizing effects known.
Subacute to chronic toxicity:
Other than potential irritation (see above), no information on illness or injury to humans
from acute or chronic exposure to this product is available.
Additional toxicological information:
To the best of our knowledge the acute and chronic toxicity of this substance is not fully
known.
No classification data on carcinogenic properties of this material is available from the EPA,
IARC, NTP, OSHA or ACGIH.

12 Ecological information:

General notes:
Do not allow undiluted product or large quantities of it to reach ground water, water course
or sewage system.
Do not allow material to be released to the environment without proper governmental permits.

13 Disposal considerations

Product:
Recommendation Consult state, local or national regulations to ensure proper disposal.

Uncleaned packagings:
Recommendation: Disposal must be made according to official regulations.

14 Transport information
Not a hazardous material for transportation.

DOT regulations:
Hazard class: None

Land transport ADR/RID (cross-border)
ADR/RID class: None

Maritime transport IMDG:
IMDG Class: None

Air transport ICAO-TI and IATA-DGR:
ICAO/IATA Class: None

Transport/Additional information: Not dangerous according to the above specifications.

15 Regulations

Product related hazard informations:
Observe the general safety regulations when handling chemicals

National regulations
All components of this product are listed in the U.S. Environmental Protection Agency Toxic
Substances Control Act Chemical substance Inventory.
All components of this product are listed on the Canadian Domestic Substances List (DSL).

Information about limitation of use: For use only by technically qualified individuals.

16 Other information:
Employers should use this information only as a supplement to other information gathered by
them, and should make independent judgement of suitability of this information to ensure
proper use and protect the health and safety of employees. This information is furnished

(Contd. on page 4)
— USA —

Figure A.30. MSDS humic acid p.3

Material Safety Data Sheet
acc. to OSHA and ANSI

Printing date 05/21/2009   Reviewed on 05/21/2009

Product name: Humic acid

(Contd. of page 3)

without warranty, and any use of the product not in conformance with this Material Safety
Data Sheet, or in combination with any other product or process, is the responsibility of the
user.

Department issuing MSDS: Health, Safety and Environmental Department.
Contact: Zachariah Holt
Abbreviations and acronyms:
ADR: Accord européen sur le transport des marchandises dangereuses par Route (European Agreement concerning the International
Carriage of Dangerous Goods by Road)
RID: Règlement international concernant le transport des marchandises dangereuses par chemin de fer (Regulations Concerning
the International Transport of Dangerous Goods by Rail)
IMDG: International Maritime Code for Dangerous Goods
DOT: US Department of Transportation
IATA: International Air Transport Association
IATA-DGR: Dangerous Goods Regulations by the "International Air Transport Association" (IATA)
ICAO: International Civil Aviation Organization
ICAO-TI: Technical Instructions by the "International Civil Aviation Organization" (ICAO)
GHS: Globally Harmonized System of Classification and Labelling of Chemicals
EINECS: European Inventory of Existing Commercial Chemical Substances
CAS: Chemical Abstracts Service (division of the American Chemical Society)
HMIS: Hazardous Materials Identification System (USA)

USA

Figure A.31. MSDS humic acid p.4

ALBATEX DBC *Seite: 6/8*

12. UMWELTBEZOGENE ANGABEN

| ALBATEX DBC | OECD 302B Inherent Biodegradability: Zahn-Wellens/EMPA Test | 0 % - 28 Tage | - | - |

Schlussfolgerung / Zusammenfassung	:	Wenig eliminierbar durch Adsorption an Klärschlamm Elimination aus dem Wasser durch Ausfällung oder Ausflockung möglich.		
BSB5	:	0	mgO2/g	
CSB	:	205	mgO2/g	
TOC	:	7.5	%	

Name des Produkts / Inhaltsstoffs	Aquatische Halbwertszeit	Photolyse	Biologische Abbaubarkeit
ALBATEX DBC	-	-	Nicht leicht

Andere schädliche Wirkungen	:	Keine besonderen Wirkungen oder Gefahren bekannt.
Organohalogengehalt	:	0 %
PBT	:	Nicht anwendbar.
vPvB	:	Nicht anwendbar.

Sonstige Angaben

Phosphorgehalt	:	1.5 % als organische Phosphonsäure
Stickstoffgehalt	:	0 %
	:	Metallgehalt unter den von der ETAD empfohlenen Limiten

13. HINWEISE ZUR ENTSORGUNG

Entsorgungsmethoden	:	Die Abfallerzeugung sollte nach Möglichkeit vermieden oder minimiert werden. Beachtliche Rückstandsmengen des Abfallprodukts sollten nicht über den Abwasserkanal entsorgt werden, sondern in einer geeigneten Abwasserbehandlungsanlage behandelt werden. Überschüsse und nicht zum Recyceln geeignete Produkte über ein anerkanntes Abfallbeseitigungsunternehmen entsorgen. Die Entsorgung dieses Produkts sowie seiner Lösungen und Nebenprodukte muss jederzeit unter Einhaltung der Umweltschutzanforderungen und Abfallbeseitigungsgesetze sowie den Anforderungen der örtlichen Behörden erfolgen. Verpackungsabfall sollte wiederverwertet werden. Verbrennung oder Deponierung sollte nur in Betracht gezogen werden, wenn Wiederverwertung nicht durchführbar ist. Abfälle und Behälter müssen in gesicherter Weise beseitigt werden. Leere Behälter und Auskleidungen können Produktrückstände enthalten. Vermeiden Sie die Verbreitung und das Abfließen von freigesetztem Material sowie den Kontakt mit dem Erdreich, Gewässern, Abflüssen und Abwasserleitungen.
Gefährliche Abfälle	:	Nach gegenwärtigem Kenntnisstand des Lieferanten ist dieses Produkt nicht als gefährlicher Abfall im Sinne der EU-Richtlinie 91/689/EWG zu betrachten.

14. ANGABEN ZUM TRANSPORT

Internationale Transportvorschriften

Rechtsvorschriften	UN-Nummer	Versandbezeichnung	Klassen	VG*	Etikett
ADR/RID-Klasse	Nicht anwendbar.		-	-	
ADN/ADNR-Klasse	Nicht anwendbar.		-	-	
IMDG-Klasse	Nicht anwendbar.		-	-	
IATA-Klasse			-	-	

Ausgabedatum/Überarbeitungsdatum	:	12 April 2011 *6/8*

Figure A.32. Albatex data sheet

Figure A.33. Irgacure 184 data sheet p.1

absorption spectrum

Irgacure® 184 concentration in acetonitrile

Application

Irgacure® 184 may be used for applications such as UV-curable clear coatings based on acrylates for paper, metal and plastic materials.

Irgacure® 184 is especially recommended when UV coatings are required to exhibit only minimal yellowing even after prolonged exposure to sunlight.

Yellowing of urethane-acrylate systems for outdoor applications directly exposed to sunlight may be further reduced by adding the hindered amine light stabilizer Tinuvin® 292.

recommended concentrations

The amount of Irgacure® 184 as supplied required for optimum performance should be determined in trials covering a concentration range.

film thickness 5 – 20 µm	2 – 4 %
film thickness 20 – 200 µm	1 – 3 %

Safety
When handling this product please comply with the advice and information given in the safety data sheet and observe protective and workplace hygiene measures adequate for handling chemicals.

Note
The data contained in this publication are based on our current knowledge and experience. In view of the many factors that may affect processing and application of our product, these data do not relieve processors from carrying out their own investigations and tests; neither do these data imply any guarantee of certain properties, nor the suitability of the product for a specific purpose. Any descriptions, drawings, photographs, data, proportions, weights, etc. given herein may change without prior information and do not constitute the agreed contractual quality of the product. The agreed contractual quality of the product results exclusively from the statements made in the product specification. It is the responsibility of the recipient of our product to ensure that any proprietary rights and existing laws and legislation are observed.

® = registered trademark, ™ = trademark of the BASF Group, unless otherwise noted

BASF SE
Pigments & Resins Europe
67056 Ludwigshafen, Germany
www.basf.com/resins
service-edc@basf.com

irgacure_I_184_ti_edc010510_lb_e_20121213.doc | EDC 010510-1212 E

Figure A.34. Irgacure 184 data sheet p.2

Technical Information

□ ▪ **BASF**
The Chemical Company
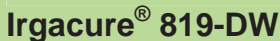
Irgacure® 819-DW

general

photoinitiator

Irgacure® 819-DW is a versatile photoinitiator for radical polymerization of unsaturated resins upon light exposure. It is especially suited for the curing of pigmented water-based dispersions (so-called polyurethane dispersions, PUDs, or acrylic dispersions), the daylight-curing of PUD-based clear coats and for use in combination with light stabilizers. Other possible uses include thick-section curing, emulsion-type and 100 % UV systems.

This product may settle, so please see special handling instructions typical for dispersions in the *storage* section below.

Irgacure® 819-DW is a dispersion of bis-acylphosphine oxide (BAPO) in water.

Properties

physical form

white to slightly yellow liquid (dispersion)

storage

Irgacure® 819-DW is sensitive to visible light and any exposure to sunlight should be avoided. Opened drums should be sealed after use to protect the product against light.

Irgacure® 819-DW should be stored at 5 – 35 °C (41 – 95 °F), if possible not exceeding 30 °C (86 °F) for a longer period of time. Otherwise, some sedimentation of the product at the bottom of the container may occur. Stirring for about 15 – 60 minutes (depending on the efficiency of the stirrer) at room temperature reverses sedimentation. Sometimes the product may gel. Agitating the product for a short time will return it to the fluid state.

typical properties
(no supply specification)

active (photoinitiator) content	~ 45 % (w/w)
density at 20 °C (68 °F)	~ 1.10 g/cm^3

EDC 003511 e, December 2012
supersedes EDC 003511 e, February 2011

page 1 of 3

Figure A.35. Irgacure 819DW data sheet p.1

absorption spectrum

Irgacure® 819-DW concentration in acetonitrile

Application

Irgacure® 819-DW may be used in UV-curable formulations for clear and for pigmented coatings on wood, metal, plastic, paper as well as for printing inks. For patent reasons, however, the use in dental applications is not allowed.

Irgacure® 819-DW was specifically developed for water-based UV-curable systems. It is very easily incorporated into water-based formulations and leads to stable dispersions. At low concentrations Irgacure® 819-DW exhibits an outstanding curing performance in highly opaque white and colored pigmented coatings or screen inks and leads to minimum yellowing after exposure to sufficient amounts of UV radiation. Additionally the outstanding absorption properties of Irgacure® 819-DW allow curing of thick sections.

Irgacure® 819-DW can be used in combination with other photoinitiators such as Irgacure® 500 or Darocur® 1173.

Its photo sensitivity at longer wavelengths allows Irgacure® 819-DW to be used in combinations with UV absorbers, e.g., Tinuvin® 1130. This makes it ideally suitable for weather-resistant UV-curable coatings.

Figure A.36. Irgacure 819DW data sheet p.2

recommended concentrations

The amount of Irgacure® 819-DW required for optimum performance should be determined in trials covering a concentration range.

water-based pigmented polyurethane dispersions (PUD)	0.5 – 1.0 % + 1.0 – 2.0 % Irgacure® 500
UV-stabilized clear PUD	0.4 – 0.6 % + 1.0 – 1.5 % Irgacure® 500
daylight-curing clear PUD	0.5 – 1.0 % + 0.5 – 1.0 % Irgacure® 500

as supplied

Figure A.37. Irgacure 819DW data sheet p.3

SIGMA-ALDRICH

SAFETY DATA SHEET

according to Regulation (EC) No. 1907/2006
Version 5.1 Revision Date 08.04.2014
Print Date 16.10.2014
GENERIC EU MSDS - NO COUNTRY SPECIFIC DATA - NO OEL DATA

SECTION 1: Identification of the substance/mixture and of the company/undertaking

1.1   Product identifiers
Product name   :   2,2-Dimethoxy-2-phenylacetophenone

Product Number   :   196118
Brand   :   Aldrich
REACH No.   :   A registration number is not available for this substance as the substance
                                     or its uses are exempted from registration, the annual tonnage does not
                                     require a registration or the registration is envisaged for a later
                                     registration deadline.
CAS-No.   :   24650-42-8

1.2   Relevant identified uses of the substance or mixture and uses advised against

Identified uses   :   Laboratory chemicals, Manufacture of substances

1.3   Details of the supplier of the safety data sheet

Company   :   Sigma-Aldrich Chemie GmbH
                                     Riedstrasse 2
                                     D-89555 STEINHEIM

Telephone   :   +49 89-6513-1444
Fax   :   +49 7329-97-2319
E-mail address   :   eurtechserv@sial.com

1.4   Emergency telephone number

Emergency Phone #   :   +49 7329-97-2323

SECTION 2: Hazards identification

2.1   Classification of the substance or mixture

Classification according to Regulation (EC) No 1272/2008
Skin sensitisation (Category 1), H317
Acute aquatic toxicity (Category 1), H400
Chronic aquatic toxicity (Category 1), H410

For the full text of the H-Statements mentioned in this Section, see Section 16.

Classification according to EU Directives 67/548/EEC or 1999/45/EC
Xi, N   Irritant, Dangerous for the   R43, R50/53
          environment

For the full text of the R-phrases mentioned in this Section, see Section 16.

2.2   Label elements

Labelling according Regulation (EC) No 1272/2008
Pictogram

Signal word   Warning

Hazard statement(s)
H317   May cause an allergic skin reaction.
H410   Very toxic to aquatic life with long lasting effects.

Aldrich **-** 196118   Page 1 of 7

Figure A.38. DMPA SDS p.1

Precautionary statement(s)
P273   Avoid release to the environment.
P280   Wear protective gloves.
P501   Dispose of contents/ container to an approved waste disposal plant.

Supplemental Hazard   none
Statements

2.3   Other hazards - none

SECTION 3: Composition/information on ingredients

3.1   Substances

Synonyms   :   Benzil α,α-dimethyl acetal
                                       α,α-Dimethoxy-α-phenylacetophenone

Formula   : $C_{16}H_{16}O_3$
Molecular Weight   :   256,3 g/mol
CAS-No.   :   24650-42-8
EC-No.   :   246-386-6

Hazardous ingredients according to Regulation (EC) No 1272/2008

Component		Classification	Concentration
2,2-Dimethoxy-1,2-diphenylethan-1-one			
CAS-No.	24650-42-8	Skin Sens. 1; Aquatic Acute 1; Aquatic Chronic 1; H317, H410	<= 100 %
EC-No.	246-386-6		

Hazardous ingredients according to Directive 1999/45/EC

Component		Classification	Concentration
2,2-Dimethoxy-1,2-diphenylethan-1-one			
CAS-No.	24650-42-8	Xi, N, R43 - R50/53	<= 100 %
EC-No.	246-386-6		

For the full text of the H-Statements and R-Phrases mentioned in this Section, see Section 16

SECTION 4: First aid measures

4.1   Description of first aid measures

General advice
Consult a physician. Show this safety data sheet to the doctor in attendance.

If inhaled
If breathed in, move person into fresh air. If not breathing, give artificial respiration. Consult a physician.

In case of skin contact
Wash off with soap and plenty of water. Consult a physician.

In case of eye contact
Flush eyes with water as a precaution.

If swallowed
Never give anything by mouth to an unconscious person. Rinse mouth with water. Consult a physician.

4.2   Most important symptoms and effects, both acute and delayed
The most important known symptoms and effects are described in the labelling (see section 2.2) and/or in section 11

4.3   Indication of any immediate medical attention and special treatment needed
no data available

Figure A.39. DMPA SDS p.2

SECTION 5: Firefighting measures

5.1   Extinguishing media

Suitable extinguishing media
Use water spray, alcohol-resistant foam, dry chemical or carbon dioxide.

5.2   Special hazards arising from the substance or mixture
Carbon oxides

5.3   Advice for firefighters
Wear self contained breathing apparatus for fire fighting if necessary.

5.4   Further information
no data available

SECTION 6: Accidental release measures

6.1   Personal precautions, protective equipment and emergency procedures
Use personal protective equipment. Avoid dust formation. Avoid breathing vapours, mist or gas. Ensure adequate ventilation. Avoid breathing dust.
For personal protection see section 8.

6.2   Environmental precautions
Prevent further leakage or spillage if safe to do so. Do not let product enter drains. Discharge into the environment must be avoided.

6.3   Methods and materials for containment and cleaning up
Pick up and arrange disposal without creating dust. Sweep up and shovel. Keep in suitable, closed containers for disposal.

6.4   Reference to other sections
For disposal see section 13.

SECTION 7: Handling and storage

7.1   Precautions for safe handling
Avoid contact with skin and eyes. Avoid formation of dust and aerosols.
Provide appropriate exhaust ventilation at places where dust is formed.
For precautions see section 2.2.

7.2   Conditions for safe storage, including any incompatibilities
Store in cool place. Keep container tightly closed in a dry and well-ventilated place.

Light sensitive.

7.3   Specific end use(s)
Apart from the uses mentioned in section 1.2 no other specific uses are stipulated

SECTION 8: Exposure controls/personal protection

8.1   Control parameters

Components with workplace control parameters

8.2   Exposure controls

Appropriate engineering controls
Handle in accordance with good industrial hygiene and safety practice. Wash hands before breaks and at the end of workday.

Personal protective equipment

Eye/face protection
Face shield and safety glasses Use equipment for eye protection tested and approved under appropriate government standards such as NIOSH (US) or EN 166(EU).

Figure A.40. DMPA SDS p.3

Skin protection
Handle with gloves. Gloves must be inspected prior to use. Use proper glove removal technique (without touching glove's outer surface) to avoid skin contact with this product. Dispose of contaminated gloves after use in accordance with applicable laws and good laboratory practices. Wash and dry hands.

The selected protective gloves have to satisfy the specifications of EU Directive 89/686/EEC and the standard EN 374 derived from it.

Body Protection
Complete suit protecting against chemicals, The type of protective equipment must be selected according to the concentration and amount of the dangerous substance at the specific workplace.

Respiratory protection
For nuisance exposures use type P95 (US) or type P1 (EU EN 143) particle respirator.For higher level protection use type OV/AG/P99 (US) or type ABEK-P2 (EU EN 143) respirator cartridges. Use respirators and components tested and approved under appropriate government standards such as NIOSH (US) or CEN (EU).

Control of environmental exposure
Prevent further leakage or spillage if safe to do so. Do not let product enter drains. Discharge into the environment must be avoided.

SECTION 9: Physical and chemical properties

9.1 **Information on basic physical and chemical properties**

a)	Appearance	Form: crystalline Colour: colourless
b)	Odour	no data available
c)	Odour Threshold	no data available
d)	pH	no data available
e)	Melting point/freezing point	Melting point/range: 67 - 70 °C - lit.
f)	Initial boiling point and boiling range	no data available
g)	Flash point	> 190 °C
h)	Evapouration rate	no data available
i)	Flammability (solid, gas)	no data available
j)	Upper/lower flammability or explosive limits	no data available
k)	Vapour pressure	no data available
l)	Vapour density	no data available
m)	Relative density	1,210 g/cm3
n)	Water solubility	no data available
o)	Partition coefficient: n-octanol/water	log Pow: 3,42
p)	Auto-ignition temperature	no data available
q)	Decomposition temperature	no data available
r)	Viscosity	no data available
s)	Explosive properties	no data available

Figure A.41. DMPA SDS p.4

t)   Oxidizing properties   no data available

9.2   Other safety information
no data available

SECTION 10: Stability and reactivity

10.1   Reactivity
no data available

10.2   Chemical stability
Stable under recommended storage conditions.

10.3   Possibility of hazardous reactions
no data available

10.4   Conditions to avoid
no data available

10.5   Incompatible materials
Strong acids, Strong oxidizing agents

10.6   Hazardous decomposition products
Other decomposition products - no data available
In the event of fire: see section 5

SECTION 11: Toxicological information

11.1   Information on toxicological effects

Acute toxicity
LD50 Oral - rat - > 6.000 mg/kg

LD50 Dermal - rat - > 7.000 mg/kg

Skin corrosion/irritation
Skin - rabbit
Result: No skin irritation

Serious eye damage/eye irritation
Eyes - rabbit
Result: No eye irritation

Respiratory or skin sensitisation
Causes photosensitivity. Exposure to light can result in allergic reactions resulting in dermatologic lesions,
which can vary from sunburnlike responses to edematous, vesiculated lesions, or bullae

Germ cell mutagenicity
Result: Not mutagenic in Ames Test.
Histidine reversion (Ames)

Carcinogenicity

IARC: No component of this product present at levels greater than or equal to 0.1% is identified as
             probable, possible or confirmed human carcinogen by IARC.

Reproductive toxicity
no data available

Specific target organ toxicity - single exposure
no data available

Specific target organ toxicity - repeated exposure
no data available

Aspiration hazard
no data available

Figure A.42. DMPA SDS p.5

Additional Information
RTECS: KM5775658

To the best of our knowledge, the chemical, physical, and toxicological properties have not been thoroughly investigated.

SECTION 12: Ecological information

12.1 Toxicity

Toxicity to fish	LC50 - Lepomis macrochirus (Bluegill) - 6 mg/l - 96,0 h
Toxicity to daphnia and other aquatic invertebrates	EC50 - Daphnia magna (Water flea) - 26 mg/l - 24 h

12.2 Persistence and degradability
no data available

12.3 Bioaccumulative potential
no data available

12.4 Mobility in soil
no data available

12.5 Results of PBT and vPvB assessment
PBT/vPvB assessment not available as chemical safety assessment not required/not conducted

12.6 Other adverse effects
Very toxic to aquatic life with long lasting effects.

SECTION 13: Disposal considerations

13.1 Waste treatment methods

Product
Offer surplus and non-recyclable solutions to a licensed disposal company. Dissolve or mix the material with a combustible solvent and burn in a chemical incinerator equipped with an afterburner and scrubber.

Contaminated packaging
Dispose of as unused product.

SECTION 14: Transport information

14.1 UN number
ADR/RID: 3077   IMDG: 3077   IATA: 3077

14.2 UN proper shipping name
ADR/RID: ENVIRONMENTALLY HAZARDOUS SUBSTANCE, SOLID, N.O.S. (2,2-Dimethoxy-1,2-diphenylethan-1-one)
IMDG: ENVIRONMENTALLY HAZARDOUS SUBSTANCE, SOLID, N.O.S. (2,2-Dimethoxy-1,2-diphenylethan-1-one)
IATA: Environmentally hazardous substance, solid, n.o.s. (2,2-Dimethoxy-1,2-diphenylethan-1-one)

14.3 Transport hazard class(es)
ADR/RID: 9   IMDG: 9   IATA: 9

14.4 Packaging group
ADR/RID: III   IMDG: III   IATA: III

14.5 Environmental hazards
ADR/RID: yes   IMDG Marine pollutant: yes   IATA: yes

14.6 Special precautions for user

Further information

Figure A.43. DMPA SDS p.6

EHS-Mark required (ADR 2.2.9.1.10, IMDG code 2.10.3) for single packagings and combination packagings containing inner packagings with Dangerous Goods > 5L for liquids or > 5kg for solids.

SECTION 15: Regulatory information

This safety datasheet complies with the requirements of Regulation (EC) No. 1907/2006.

15.1   Safety, health and environmental regulations/legislation specific for the substance or mixture

no data available

15.2   Chemical Safety Assessment
For this product a chemical safety assessment was not carried out

SECTION 16: Other information

Full text of H-Statements referred to under sections 2 and 3.

Aquatic Acute	Acute aquatic toxicity
Aquatic Chronic	Chronic aquatic toxicity
H317	May cause an allergic skin reaction.
H400	Very toxic to aquatic life.
H410	Very toxic to aquatic life with long lasting effects.
Skin Sens.	Skin sensitisation

Full text of R-phrases referred to under sections 2 and 3

N	Dangerous for the environment
Xi	Irritant
R43	May cause sensitisation by skin contact.
R50/53	Very toxic to aquatic organisms, may cause long-term adverse effects in the aquatic environment.

Further information

Figure A.44. DMPA SDS p.7

B Summary of publications, seminars and other activities

B.1 Articles

- Journal of Hazardous Materials, Pilot study on arsenic removal from groundwater using a small-scale reverse osmosis system– towards sustainable drinking water production, Stefan-André Schmidt, Ephraim Gukelberger, Mario Hermann, Florian Fiedler, Benjamin Großmann, Jan Hoinkis, Ashok Ghosh, Debashis Chatterjee, Jochen Bundschuh, accepted 03.06.2016, DOI 10.1016/ j.jhazmat.2016.06.005

- Journal of Membrane Science, UV-LED induced polymerisation of bicontinuous microemulsions - enhancing the antifouling properties of commercial membranes, S.A. Schmidt, X. Ye, F. Galiano, R. Kumar, R. Mancuso, E. Curcio, B. Gabriele, J. Hoinkis, A. Figoli, submission in progress

B.2 Book chapters and conference proceedings

- **Book chapter:** Membrane Technologies for Water Treatment, Removal of Fluoride and Uranium by Nanofiltration, S. Schmidt, Tiziana Marino, Catherine Aresipathi, S.A. Deowan, P.N. Pathak, P.K. Mohaptra, J. Hoinkis, A. Figoli, 2015, New York, CRC Press, ISBN 9781138027206.

- **Book chapter:** Impact of Climate Change on Socio-economic Conditions of Bangladesh, Chapter 10: Contribution to Climate Change Mitigation, Decentralized Small Scale Desalinator as Contribution to Climate Change Mitigation:

A Case Study , Dean Bianchi, S. Schmidt , S.A. Deowan, J. Hoinkis, Rafiqul Islam, pages 194-213, 2013, ISBN: 978-984-33-7883-5

- **Conference proceedings:** One Century of the Discovery of Arsenicosis in Latin America (1914-2014), Small-Scale Membrane-Based Desalinators: Developing a Viable Concept for Sustainable Arsenic Removal from Groundwater, Hoinkis J, Deowan S, Hermann M, Schmidt S, Gukelberger E, Fiedler F, Großmann B, Ghosh A, Chatterjee D, Bundschuh J, Buenos Aires-Argentina, Conference proceedings, CRC Press, ISBN: 978-113-800-1411

- **Conference proceedings:** 2nd IWA Specialized International Conference, ecoSTP2014, EcoTechnologies for Wastewater Treatment, Technical, Environmental & Economic Challenges, Membrane Bioreactor (MBR) Process Using Commercial and Novel Low-Fouling Membranes for Treatment of Textile Dye Wastewater, J. Hoinkis, S.A. Deowan, S. Schmidt, F. Galiano, A. Figoli, E. Drioli, Verona, Italy, 23-27 June 2014, Conference proceedings, p. 160-163, ISBN 9788869250026

- **Conference proceedings:** Understanding the Geological and Medical Interface of Arsenic, Arsenic Removal form Groundwater by Small-Scale Reverse Osmosis Unit in Rural Bihar, India, Hoinkis Jan, Hermann Mario, Schmidt Stefan, Gukelberger Ephraim, Ghosh Ashok, Chatterjee Debashis, Bundschuh, Jochen, Conference proceedings, Understanding the Geological and Medical Interface of Arsenic – Ng, Noller, Naidu, Bundschuh & Bhattacharya (eds) 2012 Taylor & Francis Group, London, pages 263-266, ISBN 978-0-415-63763-3

- **Conference proceedings:** Turning future research towards treatment and safe disposal of Arsenic-bearing wastes, Roundtable discussion, J. Hoinkis, S. Schmidt, Conference proceedings, One Century of the Discovery of Arsenicosis in Latin America (1914-2014), 2014, Buenos Aires, Argentina, 2014 Taylor & Francis Group, London, ISBN 978-1-138-00141-1, M. Litter, H. Nicolli, M. Meichtry

- **Conference proceedings:** One Century of the Discovery of Arsenicosis in Latin America (1914-2014), Developing a viable concept for sustainable arsenic removal from groundwater in remote area - findings of pilot trials in rural Bihar, India, Schmidt Stefan, Hermann Mario, Gukelberger Ephraim, Fiedler Florian,

Benjamin Großmann, Deowan Shamim Ahmed, Hoinkis Jan, Ghosh Ashok, Chatterjee Debashis, Bundschuh, Jochen, Conference proceedings, CRC Press, ISBN: 978-113-800-1411

- **Poster conference proceedings:** The 4th IWA Regional conference on Membrane technology, Novel nanostructured membranes for textile wastewater treatment, S. Schmidt, V.T. Luong, S.A. Deowan, F. Galiano, A. Figoli, J. Hoinkis, Ho Chi Minh City, Vietnam 3-6. December 2014, ISBN: 978-004-73-2950-0

- **Oral conference proceedings:** 13th Global Conference on Sustainable Manufacturing – Decoupling Growth from Resource Use, Membrane bioreactor and promising application for textile industry in Vietnam, Tan Vu. Luong, S. Schmidt, S.A. Deowan, J. Hoinkis, A. Figoli, F. Galiano, Vietnam, Elsevier, 2015, Binh Duong New City, Vietnam, pages 419-424, Volume 40, DOI 10.1016/j.procir.2016.01.083

B.3 Conferences

- **Oral talk and Chairmen by Stefan Schmidt:** 2nd International Conference on Desalination using membrane technology, Novel antifouling coating on Ultrafiltration membranes using UV light for polymerization for the treatment of textile dye water with an membrane bioreactor (MBR), Stefan-André Schmidt, Alberto Figoli, Bartolo Gabriele, Ephrem Curcio, Francesco Galiano, Jan Hoinkis, Xiaoyun Ye, Shamim Deowan, Singapore, 2015, Elsevier

- **Poster presented by Stefan Schmidt:** Euromembrane 2015, Novel coating using UV light for polymerization of a Polymerizable Bicontinuous Microemulsion (PBM) for the preparation of antifouling membranes, Schmidt Stefan, Galiano Francesco, Curcio Efrem, Ye Xiaoyun, Deowan Shamim, Gabriele Bartolo, Figoli Alberto, Hoinkis Jan, Aachen-Germany

- **Poster presented by Stefan Schmidt:** Poster event for 2nd year PhD 2015, UNICAL, Rende-Italy, Development of a UV-LED Based Polymerization Process for Membrane Bio-Reactor Application, S. Schmidt, A. Figoli, F. Galiano, B. Gabriele, E. Curcio, R. Molinari, J. Hoinkis

- **Poster presented by Stefan Schmidt:** XXXI EMS Summer School 2014 Innovative Membrane Systems, Application of the novel UV light polymerised membranes for Membrane Bio-Reactor, S. Schmidt, A. Figoli, F. Galiano, B. Gabriele, R. Mancuso, J. Hoinkis, 2014, Cetraro-Italy

- **Poster presented by Stefan Schmidt:** 1st year Poster Abstract of PhD, Application of the novel UV light polymerised membranes for Membrane Bio-reactor, S. Schmidt, A. Figoli, B. Gabriele, E. Curcio, R. Molinari, J. Hoinkis, 2014, UNICAL, Rende-Italy

- **Poster presented by Jan Hoinkis:** Fluoride Removal from Drinking Water: Health and Technology Implications, An interdisciplinary research workshop, Optimising renewable energy for desalination, Bianchi Dean, Schmidt Stefan, Hoinkis Jan, workshop in Arusha-Tanzania

- **Oral talk by Shamim Deowan:** Euromembrane 2015, Preparation and application of Novel Antifouling Membranes for Forward Osmosis (FO) Process in Concentrating of Textile Dye Wastewater, Deowan S, Islam R, Bucheri S, Galiano F, Mueller K, Schmidt S, Bouhadjar S, Hoinkis J, Gabriele B, Figoli A, Aachen-Germany

- **Oral talk by Krasimir Aleksandrov:** Fluoride Removal from Drinking Water: Health and Technology Implications, An interdisciplinary research workshop, Fluoride removal from groundwater by Nanofiltration, K. Aleksandrov, F. Fiedler, J. Hoinkis, S. Schmidt, Tengeru, Arusha, Tanzania, 2013

- **Poster presented by Stefan Schmidt:** One Century of the Discovery of Arsenicosis in Latin America (1914-2014), Developing a viable concept for sustainable arsenic removal from groundwater in remote area - findings of pilot trials in rural Bihar, India, Schmidt Stefan, Hermann Mario, Gukelberger Ephraim, Fiedler Florian, Benjamin Großmann, Deowan Shamim Ahmed, Hoinkis Jan, Ghosh Ashok, Chatterjee Debashis, Bundschuh, Jochen

B.4 Courses and seminars

- XXXI EMS Summer School 2014 Innovative Membrane Systems, Cetraro-Italy

- Technological Transfer, Prof. Jan Hoinkis, 2015

- Quantum mechanics approaches for membranes properties, Dr. De Luca Giorgio, 2015

- Lezioni di Chimica Organica Avanzata, Prof. Bartolo Gabriele, 2015

- Environmental Technologies, Prof. Jan Hoinkis, 2015

- MBR technologies and application, Prof. Jan Hoinkis, 2015

- Transfer technology, Prof. Jan Hoinkis, 2015

- Membrane preparation course, Dr Alberto Figoli, 2015

- Membrane preparation characterisation course, Dr Alberto Figoli 2015

B.5 Tutoring and supervising activity

- **Lecturing tutor:** Environmental technologies, 2015+2016

- **Supervising activity:** Master Thesis Luong Tan Vu 2014, Wastewater treatment using a novel pilot-scale Membrane Bioreactor

- **Supervising activity:** Project work Son Hong Mai 2014, Wastewater treatment using a pilot-scale Membrane Bioreactor

- **Supervising activity:** Master Thesis Luong Xiaoyun Ye 2015, Novel antifouling coating on ultrafiltration membrane using UV-light for polymerization for the treatment of textile dye water with a Membrane Bioreactor (MBR)

- **Supervising activity:** Master Thesis Rohit Kumar 2016, Improved UV light polymerisation of novel antifouling coating on PES membrane

C Acknowledgement

This work is dedicated to my wife Janina. Her patience and back-up were a huge anchor for me that gave me the strength to proceed even with challenges that seemed to be insurmountable.

I highly appreciate the support of my mentors Dr. Alberto Figoli, Prof. Bartolo Gabriele, Prof. Efrem Curcio, Prof. Raffaele Molinari and Prof. Jan Hoinkis. Their combined experience were a priceless source of information and inspiration.

Very special thanks go to Dr. Francesco Galiano. His know-how in various fields were a huge support for this work. In addition I am very thankful for his friendship.

Finally I want to thank my colleagues from the University of Applied Sciences Karlsruhe, Germany. The workshop staff Gerd Westermann, Jan Wernthal that supported me with the revamp of the MBR. Dr. Margaritha Alexandrova and Torsten Kuhlee for their high class work and source of information for several analysing methods.